

# Patterns in an Elastic Bar

Abdulmohsen Alruwaili

Department of Mathematics and Statistics  
University of Strathclyde  
Glasgow, UK

2020

The copyright of this thesis belongs to the author under the terms of the United Kingdom Copyright Acts as qualified by University of Strathclyde Regulation 3.50. Due acknowledgement must always be made of the use of any material contained in, or derived from, this thesis.

## Acknowledgements

I want to take a moment to thank everyone who has helped me reach this major step in my career. Achieving a PhD requires the effort of more than just one person, and I need to acknowledge those who have aided me in reaching the finish line.

First, thanks must go to my supervisors, Dr. Michael Grinfeld and Dr. Gabriel Barrenechea who have been assisting me in developing my skills and pushing my research forward. They have been unfailingly patient and have introduced me to new worlds and concepts within the field I would not have been able to access on my own.

I would also like to thank the Strathclyde community for welcoming me into the fold, especially those in my department office who have been a tremendous support structure throughout the entire process. Furthermore, my deepest gratitude is extended to Al-Jouf University, whose funding has graciously afforded me the opportunity to study here in Scotland.

## Abstract

We consider Yip's formulation of the Ericksen model for an elastic bar on an elastic foundation [63] which leads to the Euler-Lagrange equation for the functional

$$\mathcal{E}(u) = \int_0^1 (\gamma u_{xx}^2 + W(u_x) + \alpha u^2) dx, \quad x \in (0, 1),$$

with double Dirichlet boundary conditions. Here the potential  $W(p) = (|p| - 1)^2$ , is not differentiable at  $p = 0$ .

We define and prove existence and uniqueness of periodic solutions with any number  $n \geq 0$  of internal zeroes for all  $\alpha, \gamma > 0$  and discuss the existence of non-periodic solutions.

The Euler-Lagrange equation contains conditions that make it difficult to track, and then dropping one of them we obtain a weak formulation for this reduced problem, which we then prove it has a unique solution. Next, we use a combination of two numerical methods, namely the Finite Elements Method (FEM) to approximate the model and the Derivative Free Optimization (DFO) to find the location of the jump.

# Contents

Acknowledgements . . . . .	ii
Abstract . . . . .	iii
List of Figures . . . . .	viii
List of Tables . . . . .	xiv
<b>1 Introduction</b>	<b>1</b>
1.1 Solid Solid Phase transitions . . . . .	1
1.2 Microstructures . . . . .	2
1.3 One dimensional Non-Linear Elasticity . . . . .	3
1.3.1 Dynamic Version . . . . .	6
1.3.2 Boundary conditions . . . . .	6
1.4 Ericksen's Model . . . . .	6
1.5 Further work on Ericksen's Model . . . . .	8
1.5.1 Müller's problem . . . . .	9
1.5.2 Grinfeld and Lord's work . . . . .	10
1.5.3 Yip's work . . . . .	10
1.6 Other relevant work . . . . .	12

Contents

1.7	The Finite Element Method . . . . .	13
1.8	Mixed Finite Element Methods . . . . .	15
1.9	Thesis outline . . . . .	16
<b>2</b>	<b>Mathematical Background</b>	<b>18</b>
2.1	Calculus of Variations . . . . .	18
2.2	Euler Lagrange equation . . . . .	19
2.3	The Fredholm Alternative . . . . .	21
2.4	Functional analysis . . . . .	22
2.4.1	Examples of Hilbert spaces . . . . .	24
2.5	The Galerkin Method . . . . .	26
2.6	Formulation of a Finite Element Method . . . . .	27
<b>3</b>	<b>Stationary Solutions in Yip's Formulation of the Regularized Erick-</b>	
	<b>sen's Bar Model</b>	<b>31</b>
3.1	Introduction . . . . .	31
3.2	The Euler Lagrange Equation . . . . .	32
3.3	Periodic solutions . . . . .	36
3.3.1	Existence of $u_1$ symmetric solutions . . . . .	39
3.3.2	Existence of $u_k$ (periodic) solutions, $k > 1$ . . . . .	47
3.3.3	Existence of $u_1$ non-symmetric solutions . . . . .	54
3.4	Calculating the Energy . . . . .	58
3.4.1	Optimizing Energy . . . . .	63

Contents

3.5	Formula for the number of jumps and unknown parameters for solution of lap number $n \geq 2$ . . . . .	65
3.5.1	Periodic and Non Periodic Solutions with Lap number 3 . . . . .	69
3.5.2	Bifurcation . . . . .	72
3.6	Conclusion . . . . .	75
<b>4</b>	<b>Weak formulations for the Euler Lagrange equation</b>	<b>79</b>
4.1	Introduction . . . . .	79
4.2	Preliminaries . . . . .	80
4.3	A weak formulation for the Euler Lagrange equation omitting continuity at $c$ . . . . .	82
4.3.1	The Existence and Uniqueness of the Weak Formulation ( $S_2$ ) . . . . .	91
4.3.2	The Finite Element Method and Its Error Estimate . . . . .	97
4.4	A weak formulation for the Euler Lagrange Equation omitting the derivative condition . . . . .	100
4.4.1	The Existence and Uniqueness of the Weak Formulation . . . . .	102
4.4.2	The Finite Element Method and Its Error Estimate . . . . .	104
4.5	Conclusion . . . . .	108
<b>5</b>	<b>The Finite Element Method for the Model Problem</b>	<b>110</b>
5.1	Introduction . . . . .	110
5.2	The Finite Element Method (for the first weak formulation) . . . . .	111
5.2.1	A Numerical Experiment . . . . .	120
5.3	The Finite Element Method (for the second weak formulation) . . . . .	132

## Contents

5.3.1	A Numerical Experiment . . . . .	133
5.4	The Finite Element Method (Construct periodic solution of lap $> 2$ ) . .	137
5.4.1	A Numerical Experiment . . . . .	138
5.5	Derivative-Free Optimization . . . . .	140
5.5.1	The Algorithm . . . . .	140
5.5.2	Numerical results . . . . .	142
5.6	The Finite Element Method for a problem with non-constant parameters	147
5.6.1	A Numerical Experiment . . . . .	149
5.7	Conclusion . . . . .	152
<b>6</b>	<b>Conclusion and future work</b>	<b>154</b>
<b>A</b>	<b>MATLAB and MAPLE codes</b>	<b>158</b>
A.1	Matlab Code for The Finite Element Method for a problem with non-constant parameters . . . . .	158
A.2	Matlab Code for DFO . . . . .	160
A.3	Matlab Code for The Finite Element Method (for the first weak formulation) . . . . .	163
A.4	Matlab Code for The Finite Element Method (for the second weak formulation) . . . . .	167
A.5	MAPLE code for the Fredholm Alternative (with lap 2) . . . . .	169
A.6	MAPLE code for the Fredholm Alternative (with lap 3) . . . . .	173
A.7	Optimizing Energy (pseudo code) . . . . .	176
	<b>Bibliography</b>	<b>176</b>

# List of Figures

1.1	Log-lin pressure-temperature phase diagram of water [15]. . . . .	1
1.2	Martensitic microstructure (Chu and James, University of Minnesota) [48].	3
1.3	Linear vs. non-linear stress-strain relationship. . . . .	4
1.5	(a) energy density; (b) stress . . . . .	7
1.6	Examples of patterns of oscillations . . . . .	9
1.8	(a) energy density $W(P) = ( P  - 1)^2$ ; (b) stress . . . . .	11
2.1	Basis of $\varphi_i$ . . . . .	28
3.1	Example of a function with lap 2. . . . .	36
3.3	Examples of periodic solutions . . . . .	38
3.5	Location of the jump for different values of $\alpha$ and $\gamma$ . . . . .	42
3.6	Example of a symmetric solution where $\alpha = 10$ and $\gamma = 0.01$ . . . . .	47
3.7	Symmetric solution of lap 2 where $\alpha = 1, \gamma = 0.1$ . . . . .	52
3.8	Periodic solution of lap 3, $u_{2,1,0.1}$ . . . . .	53
3.10	Example of finding $u_3$ and $u_4$ where $\alpha = 1, \gamma = 0.1$ . . . . .	53
3.12	Example of finding $u_5$ and $u_6$ where $\alpha = 1, \gamma = 0.1$ . . . . .	54

List of Figures

3.13	Location of jumps where $\alpha = 190$ and $\gamma = 0.1$ . . . . .	55
3.15	Example of a non-symmetric solution of lap 2 when $\alpha = 190, \gamma = 0.1$ . and $c_1 = 0.5, c_2 = 0.36, c_3 = 0.63$ . . . . .	55
3.18	Example of symmetric and non-symmetric solutions of lap 2 for $1 - 4\alpha\gamma < 0$ . On the left we have the plot of $F_3(c)$ while on the right we have the solutions $u$ of the Euler-Lagrange equation that correspond to each $c$ with $F_3(c)$ . . . . .	56
3.20	Example of symmetric and non-symmetric solutions of lap 2 for $1 - 4\alpha\gamma < 0$ . On the left we have the plot of $F_3(c)$ while on the right we have the solutions $u$ of the Euler-Lagrange equation that correspond to each $c$ with $F_3(c)$ , where $\alpha = 139$ and $\gamma = 0.1$ . . . . .	57
3.21	Bifurcation curve ( $k = 1$ ). This is lowest connected component of $F'_3(\frac{1}{2}) = 0$ . Since $k = 1$ , we go from 1 to 3 solutions. In particular, below the bifurcation curve we have 1 solution and above the curve we have (at least) 3 solutions. . . . .	58
3.22	Curves where the energy of $u_i$ is equal to the energy of $u_{i+1}$ ( $i = 1, 2$ ). . . . .	64
3.23	Visual for lap number 4 ( $n = 4$ ). . . . .	66
3.24	Solution Plots for $\alpha = 2, \gamma = 0.01$ . On the left we have the plots of $F_1$ and $F_2$ and their 3 intersections. On the right we have the 3 corresponding solutions to these intersections. Notice the intersection at $(\frac{1}{4}, \frac{3}{4})$ on the left, which gives rise to a $p_3$ periodic solution on the right (middle graph). . . . .	71
3.25	Solution Plots for $\alpha = 1, \gamma = 0.1$ . Here we only have 1 intersection on the left and thus only a single corresponding solution to the EL equation on the right, namely the $p_3$ periodic one. . . . .	71
3.26	Solution Plots for $\alpha = 6, \gamma = 0.1$ . Here we only have 1 intersection on the left and thus only a single corresponding solution to the EL equation on the right, namely the periodic one. . . . .	72

List of Figures

3.27	Solution Plots for $\alpha = 40, \gamma = 0.1$ . On the left we have the plots of $F_1$ and $F_2$ and their 3 intersections. On the right we have the 3 corresponding solutions to these intersections. Notice the intersection at $(\frac{1}{4}, \frac{3}{4})$ on the left, which gives rise to a periodic solution on the right (middle graph).	72
3.29	Solution plots for $\alpha = 440$ and $\gamma = 0.02$ . On the top left we have the plots $F_1$ and $F_2$ and their 7 intersections. The other 4 plots correspond to these intersections. The first plot is the symmetric that correspond to $(\frac{1}{4}, \frac{3}{4})$ . The second and third plots represent the two pairs of non-periodic solutions. The fourth plot represents the two pairs of non-symmetric solutions (Each part of the pair is symmetric to the other part).	74
3.31	Solution plots for $\alpha = 362$ and $\gamma = 0.02$ . On the top left we have the plots $F_1$ and $F_2$ and their 5 intersections. The other 3 plots correspond to these intersections. The first plot is the symmetric that correspond to $(\frac{1}{4}, \frac{3}{4})$ . The second and third plots represents the two pairs of non-periodic solutions. (Each part of the pair is symmetric to the other part).	75
3.32	$(\alpha, \frac{1}{\gamma})$ plot of $E_{1,2}$ curve and the first bifurcation curve of lap 2.	77
3.33	Three bifurcation curves of lap 3.	77
5.1	The basis function $\varphi_i$	112
5.2	Basis of $H_h$	112
5.4	Basis of $\tilde{V}_h$ .	114
5.5	Exact symmetric solution when $\alpha = 93, \gamma = 0.05$ .	121
5.6	Numerical solution with $\alpha = 93, \gamma = 0.05$ and $N = 10$ .	122
5.7	Numerical solution with $\alpha = 93, \gamma = 0.05$ and $N = 40$ .	122
5.8	Numerical solution with $\alpha = 93, \gamma = 0.05$ and $N = 100$ .	123
5.9	Numerical solution with $\alpha = 93, \gamma = 0.05$ and $N = 1000$ .	123

List of Figures

5.10	Log-log plot of the error estimate of the energy $u$ for $\alpha = 93, \gamma = 0.05$ and $c = 0.5$ . The $x$ -axis represents $\log(N)$ while the $y$ -axis represents $\log  E - E_h $ . Notice the linear pattern. . . . .	125
5.11	Log-log plot of the error estimate of the energy $u$ for $\alpha = 93, \gamma = 0.05$ and $c = 0.5$ . The $x$ -axis represents $\log(N)$ while the $y$ -axis represents $\log  u - u_h _{\tilde{V}}$ . Notice the linear pattern. . . . .	126
5.12	Plot of a discontinuous graph for an incorrect location of the jump. Here $\alpha = 93$ and $\gamma = 0.05$ , but $c = 0.2$ as opposed to $c = 0.5$ (which would be the correct value). . . . .	126
5.13	Exact (non-symmetric) solutions . . . . .	127
5.14	Numerical (non-symmetric) solutions for $\alpha = 93, \gamma = 0.05$ and $N = 10$ . . . . .	128
5.15	Numerical (non-symmetric) solutions for $\alpha = 93, \gamma = 0.05$ and $N = 40$ . . . . .	128
5.16	Numerical (non-symmetric) solutions for $\alpha = 93, \gamma = 0.05$ and $N = 100$ . . . . .	129
5.17	Numerical (non-symmetric) solutions for $\alpha = 93, \gamma = 0.05$ and $N = 1000$ . . . . .	129
5.18	Log-log plot of the error estimate of the energy $u$ for $\alpha = 93, \gamma = 0.05$ and $c = 0.40214$ . The $x$ -axis represents $\log(N)$ while the $y$ -axis represents $\log  E - E_h $ . Notice the linear pattern. . . . .	130
5.19	Log-log plot of the error estimate of the energy $u$ for $\alpha = 93, \gamma = 0.05$ and $c = 0.40216$ . The $x$ -axis represents $\log(N)$ while the $y$ -axis represents $\log  u - u_h _{\tilde{V}}$ . Notice the linear pattern. . . . .	131
5.20	Numerical solution (for the second weak formulation) with $\alpha = 93, \gamma = 0.05$ and $N = 10$ . . . . .	133
5.21	Comparison of the solutions corresponding to the two weak formulations. The red graph on top corresponds to the first weak formulation, $\alpha = 91, \gamma = 0.05, c = 0.5$ and $N = 10$ . . . . .	133

List of Figures

5.22 Comparison of the solutions corresponding to the two weak formulations.  
 The red graph on top corresponds to the first weak formulation,  $\alpha = 91, \gamma = 0.05, c = 0.5$  and  $N = 40$ . . . . . 134

5.23 Comparison of the solutions corresponding to the two weak formulations.  
 The red graph on top corresponds to the first weak formulation,  $\alpha = 91, \gamma = 0.05, c = 0.5$  and  $N = 100$ . . . . . 134

5.24 Comparison of the solutions corresponding to the two weak formulations.  
 The red graph on top corresponds to the first weak formulation,  $\alpha = 91, \gamma = 0.05, c = 0.5$  and  $N = 1000$ . . . . . 134

5.25 Log-log plot of the error estimate of the energy  $u$  for  $\alpha = 93, \gamma = 0.05$  and  $c = 0.5$ . The  $x$ -axis represents  $\log(N)$  while the  $y$ -axis represents  $\log |E - E_h|$ . Notice the linear pattern. . . . . 135

5.26 Log-log plot of the error estimate of the energy  $u$  for  $\alpha = 93, \gamma = 0.05$ . The  $x$ -axis represents  $\log(N)$  while the  $y$ -axis represents  $\log |u - u_h|_{\tilde{V}}$ . Notice the linear pattern. . . . . 136

5.27 symmetric periodic solution of lap 3, where  $\alpha = 1, \gamma = 0.1, c_1 = \frac{1}{4}$  and  $c_2 = \frac{3}{4}$ . . . . . 138

5.28 symmetric periodic solution of lap 4, where  $\alpha = 1, \gamma = 0.1, c_1 = \frac{1}{6}$   $c_2 = \frac{1}{2}$ , and  $c_3 = \frac{5}{6}$ . . . . . 138

5.29 symmetric periodic solution of lap 5, where  $\alpha = 1, \gamma = 0.1, c_1 = \frac{1}{8}$   $c_2 = \frac{3}{8}, c_3 = \frac{5}{8}$  and  $c_4 = \frac{7}{8}$ . . . . . 139

5.30 symmetric periodic solution of lap 6, where  $\alpha = 1, \gamma = 0.1, c_1 = \frac{1}{10}$   $c_2 = \frac{3}{10}, c_3 = \frac{1}{2}, c_4 = \frac{7}{10}$  and  $c_5 = \frac{9}{10}$ . . . . . 139

5.31 symmetric periodic solution of lap 7, where  $\alpha = 1, \gamma = 0.1, c_1 = \frac{1}{12}$   $c_2 = \frac{1}{4}, c_3 = \frac{5}{12}, c_4 = \frac{7}{12}, c_5 = \frac{3}{4}$  and  $c_6 = \frac{11}{12}$ . . . . . 139

List of Figures

5.33 Successive iterations of DFO plotting solutions with a new location of the jump in each step where  $\alpha = 1, \gamma = 0.1, N = 1000$  and the starting points are  $c_1 = 0.2, c_2 = 0.4, c_3 = 0.9$ . . . . . 142

5.34 Log-log plot of the error estimate of the energy  $u$  for  $E = 0.8935833875$  and  $c = 0.5$ . The  $x$ -axis represents  $\log(N)$  while the  $y$ -axis represents  $\log|E - E_{DFO}|$ . Notice the linear pattern. . . . . 143

5.35 Log-log plot of the error estimate of the energy  $u$  for  $E = 0.917355785$  and  $c = 0.3743602663$ . The  $x$ -axis represents  $\log(N)$  while the  $y$ -axis represents  $\log|E - E_{DFO}|$ . Notice the linear pattern. . . . . 144

5.36 Comparison to numerical solutions with constant parameters when  $N = 10$ . Here we have  $1 \leq x + 1 \leq 2$  for all  $x \in [0, 1]$ . . . . . 149

5.37 Comparison to numerical solutions with constant parameters when  $N = 20$ . Here we have  $1 \leq x + 1 \leq 2$  for all  $x \in [0, 1]$ . . . . . 150

5.38 Comparison to numerical solutions with constant parameters when  $N = 40$ . Here we have  $1 \leq x + 1 \leq 2$  for all  $x \in [0, 1]$ . . . . . 150

5.39 Comparison to numerical solutions with constant parameters when  $N = 80$ . Here we have  $1 \leq x + 1 \leq 2$  for all  $x \in [0, 1]$ . . . . . 150

5.40 Comparison to numerical solutions with constant parameters when  $N = 160$ . Here we have  $1 \leq x + 1 \leq 2$  for all  $x \in [0, 1]$ . . . . . 151

5.41 Comparison to numerical solutions with constant parameters when  $N = 1000$ . Here we have  $1 \leq x + 1 \leq 2$  for all  $x \in [0, 1]$ . . . . . 151

# List of Tables

3.1	Comparing energy for different values of $\alpha$ and for fixed $\gamma = 0.05$ . . . . .	62
3.2	Comparing energy for different values of $\alpha$ and for fixed $\gamma = 0.014$ . . . . .	62
5.1	FEM numerical solutions for $c = 0.5$ and various $N$ , and the exact energy is $E = 0.9083414738$ . . . . .	124
5.2	Errors generated for $\alpha = 93$ and $\gamma = 0.05$ and various $N$ . . . . .	125
5.3	FEM numerical solutions for $\alpha = 91, \gamma = 0.05, c = 0.40214$ and various $N$ , and the exact energy is $E = 0.9081601666$ . . . . .	130
5.4	Errors generated for $\alpha = 93$ and $\gamma = 0.05, c = 0.40216$ and various $N$ . . . . .	131
5.5	FEM numerical solutions for $c = 0.5$ and various $N$ , and the exact energy is $E = 0.9083414738$ . . . . .	135
5.6	Errors generated for $\alpha = 93$ and $\gamma = 0.05$ and various $N$ . . . . .	136
5.7	Errors generated by the different formulations for various parameter pairs $(\alpha, \gamma)$ and $N = 500$ . . . . .	137
5.8	DFO numerical prediction for $c = 0.5$ and $E = 0.8935833875$ . . . . .	143
5.9	DFO numerical prediction for $c = 0.3743602663$ and $E = 0.917355785$ . . . . .	144
5.10	Full DFO process with detailed iterations when $(\alpha, \gamma) = (190, 0.1)$ and $N = 1000$ and where the exact $c = 0.3623549804$ . . . . .	145

List of Tables

5.11 Full DFO process with detailed iterations when $(\alpha, \gamma) = (1, 0.1)$ and $N = 1000$ and where the exact $c = 0.5$ . . . . .	145
5.12 Full DFO process with detailed iterations when $(\alpha, \gamma) = (33, 0.01)$ and $N = 1000$ and where the exact $c = 0.5$ . . . . .	145
5.13 DFO predictions as a function of $h = \frac{1}{N}$ where $(\alpha, \gamma) = (60, 0.1)$ and the exact values are $c = 0.5$ and $E = 0.8891382917$ . . . . .	146
5.14 DFO numerical prediction for for various parameter pairs $(\alpha, \gamma)$ and $N = 5000$ . . . . .	146
5.15 Numerical values (according to FEM) for energies corresponding to the solution with $\alpha(x) = x + 1$ and $c = 0.5$ for various values of $N$ . On the left of the table we calculate the difference between successive levels of Energy in a logarithmic scale. . . . .	152

# Chapter 1

## Introduction

### 1.1 Solid Solid Phase transitions

Our work is motivated by the study of solid-solid transformations. Those transformations occur when we have transition from one solid state to a different solid state [16]. As an example, ice has 18 different known solid states that range from amorphous ice, all the way up to what is known as square ice [15]. Some of these transition can be viewed graphically in the following Log-lin pressure-temperature phase diagram of water:

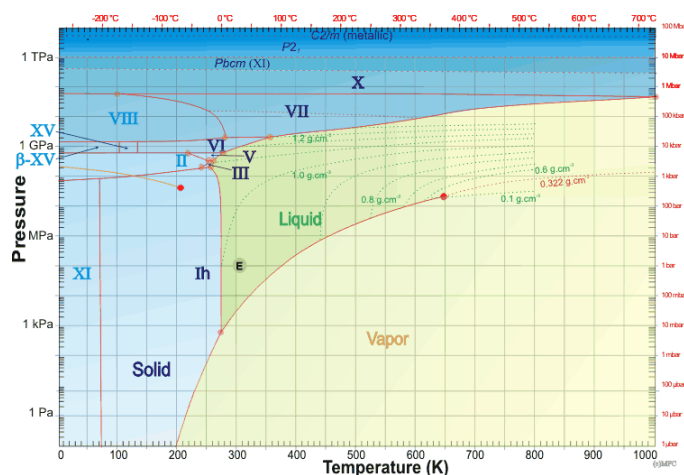


Figure 1.1: Log-lin pressure-temperature phase diagram of water [15].

## 1.2 Microstructures

Traditionally, a microstructure is any structure between the macroscopic scale (i.e. objects big enough to observe with naked eye) and the atomic scale (i.e. the size that even microscopes fail to detect) [48].

According to Müller [48], microstructures are important since they affect the way material behaves in the macroscopic world. Thus scientists are incentivized to build model that both describe them properly and predict their behaviour.

In particular, one may use variational models which when optimized highly resemble certain configurations of the microstructures. Examples of such models appear in solid-solid phase transformations of elastic material, usually alloys (see Figure 1.2). [48].

When it heats up, iron undergoes phase alteration in the sequence  $\alpha \rightarrow \beta \rightarrow \gamma \rightarrow \delta$ . Iron's stable phase at ambient temperature is called  $\alpha$  iron. Iron converts to the  $\beta$  phase when it heats to  $790^\circ\text{C}$ . Furthermore, when iron heats to  $910^\circ\text{C}$ , it converts to  $\gamma$  iron. At  $1400^\circ\text{C}$ , iron achieves the final solid-state change on heating, namely,  $\gamma \rightarrow \delta$ . There is a close association between the  $\gamma \rightarrow \alpha$  change on temperature reduction and what is known as martensitic transformation. [49]

More specifically, we are interested in a group of solid-solid phase transformations known by the name of Martensitic transformations (named after Adolf Martens), where the structure of material (lattice) changes suddenly at certain temperature levels. In particular, we can identify two extreme phases. The phase associated with high temperature is called Austenite while the phase associated with low-temperature is called Martensite [7, 20].

Mathematically, these two different phases are associated with the two different “bottoms” of the double well potential. In other words, as the strain oscillates from  $-1$  to  $+1$ , the equilibrium states do as well and we transition between the two phases described above (Martensite to Austenite and vice versa).

The microstructure features of the martensitic phase transformation can be observed

in pictures like the one following in Figure 1.2

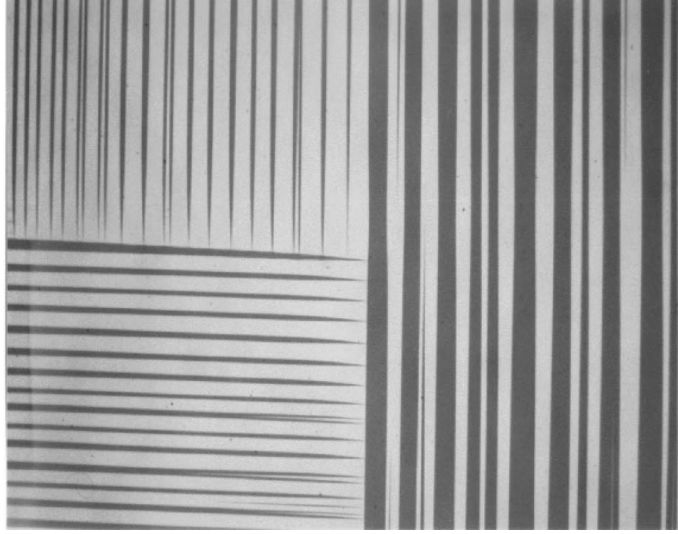


**Figure 1.2:** Martensitic microstructure (Chu and James, University of Minnesota) [48].

### 1.3 One dimensional Non-Linear Elasticity

Let us consider a piece of material that undergoes a certain deformation. More formally, if  $\Omega$  represents the location (domain) of all particles in the reference (non-deformed) configuration, the deformation can be thought of as a smooth mapping  $R : \Omega \rightarrow \mathbb{R}^3$  [52].

For each  $x \in \Omega$  we let the displacement of  $x$  be  $u(x) = R(x) - x$ , i.e. the vector change of a particle originally in position  $x$ , after the deformation. Here, we are interested in one dimensional domain, like 1-dimensional rods, and in particular  $\Omega = [0, 1]$ . There, the amount of deformation applied to a point  $x \in \Omega$  is measured by the strain  $\epsilon$ , which is the percentage of change with respect to the initial location [43].

$$\epsilon = \frac{du}{dx} = u_x. \quad (1.3.1)$$

Next, we define the stress  $\sigma$ , which is generally thought of as the amount of force applied per unit area, as a function of strain. Namely:

$$\sigma(x) = \sigma(\epsilon(x)) = \sigma(u_x(x)),$$

## CHAPTER ONE

where  $\sigma$  is generally a non-linear smooth function [41]. For simplicity, we will often write:  $\sigma = \sigma(\epsilon)$ .

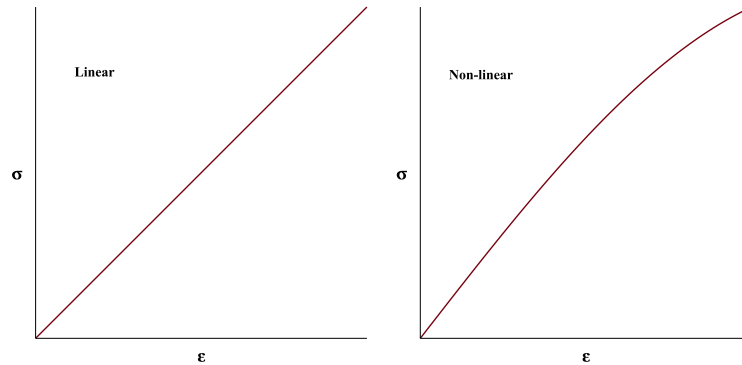


**Figure 1.3:** Linear vs. non-linear stress-strain relationship.

We know from physics that we have an equation of motion. Starting with Newton's Second Law:

$$F_{tot} = m a, \quad (1.3.2)$$

where,  $F_{tot}$  are all forces applied to a particle,  $a$  is acceleration of the particle and  $m$  is mass of the particle. Let us concentrate in a small region of a rod. Let  $b$  be the average force per unit volume. Using (1.3.2), we get the 1-dimensional equation of motion [43]:

$$\frac{d\sigma}{dx} + b = \rho a. \quad (1.3.3)$$

where  $\rho$  is the density of the material and it is connected to the mass  $m$  via the formula  $dm = \rho dv$  (with  $dv$  being the infinitesimal volume of the object).

Now, if we let  $a = 0$  (still object) and  $\sigma = \sigma(u_x)$ , we get the Navier's first equation of motion:

$$\frac{d}{dx}(\sigma(u_x)) + b = 0.$$

In practice, the body force  $b$  is usually negligible, so we can assume  $b \approx 0$ . This leads

## CHAPTER ONE

to the first formulation of the problem, namely [43]:

$$\frac{d}{dx}(\sigma(u_x)) = 0 \quad (1.3.4)$$

which turns out to be the Euler Lagrange equation of the following functional

$$E(u_x) = \int_0^1 W(u_x) dx. \quad (1.3.5)$$

To see this, start by defining stress via the following relation:

$$\sigma(u_x) = W'(u_x). \quad (1.3.6)$$

From there, consider the Euler-Lagrange equation of (1.3.5) which is given by:

$$\begin{aligned} \frac{\partial W(u_x)}{\partial u} - \frac{d}{dx} \frac{\partial W(u_x)}{\partial u_x} &= 0 \\ \Rightarrow \frac{d}{dx} W'(u_x) &= [W'(u_x)]_x = 0 \\ \Rightarrow \sigma(u_x)_x &= 0. \end{aligned}$$

On top of the above two main formulations of the problem (1.3.5) and (1.3.4), we have a third one, namely the variational formulation. Starting with (1.3.4) and multiplying it on both sides by an arbitrary smooth function  $v : [0, 1] \rightarrow \mathbb{R}$  satisfying  $v(0) = v(1) = 0$

$$\sigma(u_x)_x v(x) = 0.$$

By taking the integral and using integration by parts we get

$$\int_0^1 \sigma(u_x) v'(x) dx = 0 \quad \text{for all smooth } v : [0, 1] \rightarrow \mathbb{R}. \quad (1.3.7)$$

## CHAPTER ONE

### 1.3.1 Dynamic Version

The three formulations above are all time invariant. We can include time in our model by allowing

$$a = \frac{d^2 u}{dt^2} = u_{tt} \quad (\text{i})$$

in the Navier's equation (1.3.3).

$$(\sigma'(u_x)) u_{xx} = \rho a. \quad (\text{ii})$$

By (i) and (ii) we get the time dependent version of our first formulation above

$$(\sigma'(u_x)) u_{xx} = \rho u_{tt}. \quad (1.3.8)$$

### 1.3.2 Boundary conditions

Naturally, all of the PDE's described above are subject to boundary conditions, those depend on the context and restrictions of our model. For example we can have

- Dirichlet boundary conditions (time invariant):  $u(0) = u(1) = 0$
- Dirichlet boundary conditions (time dependent):

$$\begin{cases} u(0, t) = u(1, t) = 0 & \forall 0 \leq t \leq T \\ u(x, 0) = u(x, T) = 0 & \forall 0 \leq x \leq 1 \end{cases}$$

For more detailed analysis see [5], [50].

## 1.4 Ericksen's Model

Ericksen was the first one to study equilibria on a non-linear elastic bar attached to an elastic foundation. In his original paper [32] in 1975 Ericksen viewed the bar as a

## CHAPTER ONE

one-dimensional solid on the interval  $[0, 1]$ . The function  $u : [0, 1] \rightarrow \mathbb{R}$  represents the displacement of the bar at the point  $x \in [0, 1]$ , and the study of equilibria reduces to the following problem:

$$\text{minimize } E(u_x) = \int_0^1 W(u_x) dx, \quad (1.4.1)$$

subject to

$$u(0) = 0, \quad u(1) = \beta$$

where  $\beta$  is the total strain imposed on the bar and  $W(u_x)$  is the free energy density or the double-well potential function with two minima/zeros at  $u_x = \pm 1$ .

If  $W(u_x)$  is convex, the above problem has a unique solution, which would make for an unsatisfactory model as it would not account for phase transitions in solids. In order to resolve this issue, Ericksen proposed a non-convex energy density function, given by:

$$W(u_x) = \frac{1}{4}[(u_x)^2 - 1]^2. \quad (1.4.2)$$

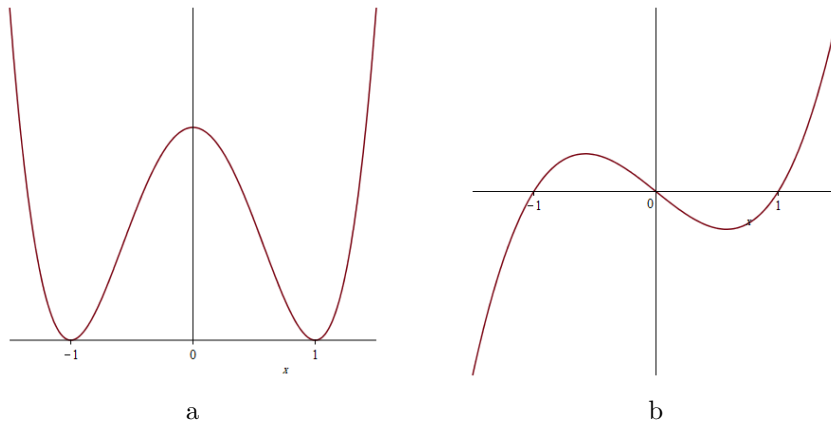


**Figure 1.5:** (a) energy density; (b) stress

Ericksen proved that for every  $-1 \leq \beta \leq 1$ , the minimization problem above has

## CHAPTER ONE

multiple solutions. In particular,  $u$  which alternates between the states  $u_x = \pm 1$  is a solution [13, 55, 59].

### 1.5 Further work on Ericksen's Model

Later on, Ball et.al. [4] in 1991 using Young's prior work in 1980 [64], Added the term  $\alpha u^2$ . That is,  $\alpha$  models the stiffness of the material namely the resistance of the bar to change when subjected to external influences [6, 59]. More specifically, we assume a linear relationship between the displacement and the force  $F$  associated with stiffness (Hook's Law):

$$F(u) = \alpha u. \tag{1.5.1}$$

We then know that the potential energy (PE) due to stiffness is given by:

$$PE = \int_0^u F(s) ds = \int_0^u \alpha s ds = \frac{1}{2} \alpha u^2.$$

Adding the above potential energy (elastic foundation) to the energy functional model produces [60]:

$$E(u_x) = \int_0^1 [W(u_x) + \alpha u^2] dx. \tag{1.5.2}$$

Here,  $u(x)$  is the lateral displacement of the bar and  $\alpha$  measures how strongly the bar is welded to the foundation [40]. In other words, the introduction of the  $\alpha u^2$  term allows for the strain ( $u_x$ ) to be near the bottom of the wells only if the displacements  $u(x)$  are small which requires fine oscillations [55].

Unfortunately, the above model does not fully capture the essence of the microstructure either as in that case  $E(u)$  produces minimizing sequences of displacement functions with increasingly faster oscillations between  $u_x \approx \pm 1$ . The idea is that such displace-

## CHAPTER ONE

ments try to achieve  $u_x = \pm 1$  and  $u \approx 0$  simultaneously. This results in a sawtooth pattern in which the states  $u_x = \pm 1$  show up at a ratio of approximately 1 : 1. At the limit infimum of the functional over such minimizing sequence is zero. In other words, we can construct an infinite family of functions  $u_i(x)$  each of which smoothly oscillates  $i$  times from  $(u_i)_x(x) = 1$  to  $(u_i)_x(x) = -1$ . So we can create an infinite sequence of  $u_i$  so that each  $u_i$  has an increasing number of oscillations around zero while  $E(u_i)$  gets closer and closer to zero without reaching it [47, 59, 61].

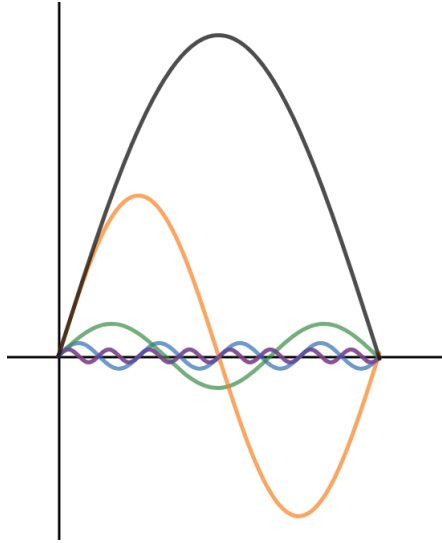


**Figure 1.6:** Examples of patterns of oscillations

**Note:** when  $\alpha = 1$ , (1.5.2) is called "tacking problem" and known from the time of Bolza and Young [9, 48].

### 1.5.1 Müller's problem

To resolve this issue of increasing the number of oscillations, Müller [47] in 1993 proposed the inclusion of the surface energy density  $\gamma u_{xx}^2$  that penalizes oscillations (i.e. abrupt changes in  $u_x$ ). This leads to the following model:

$$\text{minimize } E(u_x) = \int_0^1 [\gamma u_{xx}^2 + (W(u_x)) + \alpha u^2] dx \quad (1.5.3)$$

## CHAPTER ONE

where

$$W(u_x) = (u_x^2 - 1)^2.$$

The main result of Müller's paper is the following theorem:

**Theorem 1.** *For a small enough  $\gamma$  and fixed  $\alpha = 1$ , a global minimizer is always periodic.*

Moreover, Müller formulated a conjecture about local minimizers.

**Conjecture 2.** *All Local minimizers of  $E_2$  are periodic.*

where

$$E_2 = \frac{1}{2} \int_0^1 [u_t^2 + \gamma u_{xx}^2 + 2W(u_x) + \frac{\alpha}{2} u^2] dx.$$

### 1.5.2 Grinfeld and Lord's work

Later on in 2008 Grinfeld and Lord [40] used bifurcation analysis to give evidence for Müller's Conjecture 2. In particular they studied the symmetry of the local minimizers of  $E_2$  and described in detail the structure of the primary branch connections.

Moreover, Grinfeld and Lord formulated a conjecture for Müller's problem based on numerical observations.

**Conjecture 3.** *If  $\alpha > k^2\pi^2$ , there are no equilibria with less than  $k - 1$  internal zeroes.*

Conjecture 3 says that if  $\alpha$  is sufficiently large ( $\alpha > k^2\pi^2$  where  $k$  is an integer) then the Euler Lagrange equation has no solution with less than  $(k - 1)$  internal zeros. In particular, when  $\alpha$  is large, then there should not be any solution with no internal zeros.

### 1.5.3 Yip's work

A few years earlier in 2006, Yip [63] considered (1.5.3) but with  $W(u_x) = (|u_x| - 1)^2$  which has a discontinuous first derivative (see Figure 1.8).

CHAPTER ONE

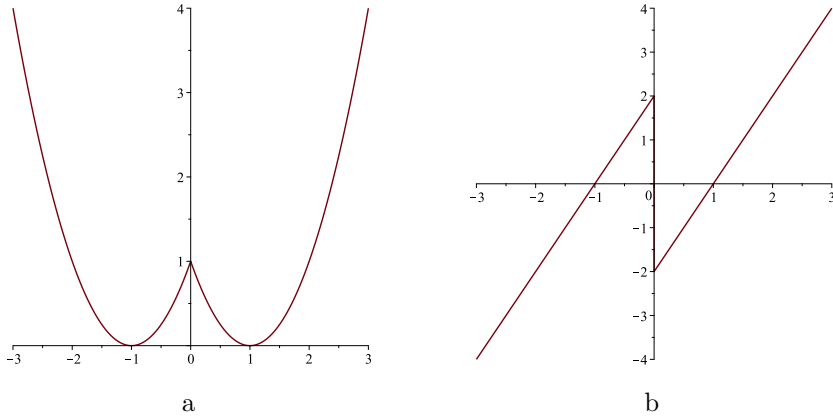


**Figure 1.8:** (a) energy density  $W(P) = (|P| - 1)^2$ ; (b) stress

The functional above (1.5.3) yields the following Euler-Lagrange equation which can be solved explicitly:

$$\gamma u_{xxxx} - u_{xx} + \alpha u = 0 \tag{1.5.4}$$

where the above is defined in the intervals where  $u_x \neq 0$ . At the points  $c_1, c_2, \dots, c_n$  where  $u_x = 0$  and  $u_x$  changes signs, we have a jump condition for  $u_{xxx}$ . We say that  $u \in \mathcal{Z}$  if all the above are true and  $u \in C^2 [0, 1]$ .

Yip [63] considered solutions of (1.5.3) in the following sense:

**Definition 1.5.1.** *A function  $u \in \mathcal{Z}$  is called a solution of (1.5.4) if the following hold for all  $i$ :*

$$\gamma u_{xxxx} - u_{xx} + \alpha u = 0 \quad \text{on } (c_i, c_{i+1}); \tag{1.5.5}$$

$$u_x(c_i) = 0 \text{ and } u_x \geq 0 \text{ (or } u_x \leq 0) \text{ for all } x \in (c_i, c_{i+1}); \tag{1.5.6}$$

$$[\gamma u_{xxx}](c_i) (= [\frac{1}{2}W'(u_x)](c_i)) = -2\text{sgn}^*(u_{xx}(c_i)); \tag{1.5.7}$$

$$u_x(0) = u_x(1) = 0, \quad \gamma u_{xxx}(0) = -\text{sgn}^*(u_{xx}(0)), \quad \gamma u_{xxx}(1) = \text{sgn}^*(u_{xx}(1)). \tag{1.5.8}$$

## CHAPTER ONE

Where the bracket notation  $[f](x) = f(x^+) - f(x^-)$ , and the star notation

$$2\text{sgn}^*(u_{xx}(c_i)) = \text{sgn}(u_x(c_i^+)) - \text{sgn}(u_x(c_i^-)).$$

The main result of Yip's paper is the following theorem [63]:

**Theorem 4.** *For a small enough  $\gamma$  and fixed  $\alpha = 1$ , all local minimizers are always periodic.*

### 1.6 Other relevant work

As we already saw, the phase transitions of solid solid transformations reveal a fine layered microstructure. Starting with Ericksen in 1975, scientists have tried to theoretically model such phenomena and made considerable progress for more than 40 years [37].

As mentioned earlier, the standard approach in the literature is to find minimizers of an energy functional, modeled by non-convex elastic strain energy which usually represented by some form of a double well potential. In his pivotal work Ericksen [32] showed the existence of non-unique minimizers in the case of a 1-dimensional elastic bar with a non-monotone stress-strain relation [37].

Ball et.al. [4] proposed a time dependent process as a candidate for modelling microstructures dynamically:

$$u_{tt} = (W'(u_x) + \beta u_{tx})_x - \alpha u \tag{1.6.1}$$

with Dirichlet boundary conditions  $u(0, t) = u(1, t) = 0$  and  $W'(u_x) = \frac{1}{4}(u_x - 1)^2$ . Friesecke and McLeod [36] proved that (1.6.1) has an uncountable family of steady states that are unstable but locally asymptotically stable.

Truskinovsky and Zanzotto [59] attempted to regularize Ericksen's model, essentially by adding both a surface energy term (scaled with a constant  $\alpha$ ) and an elastic foundation

## CHAPTER ONE

term (scaled with a constant  $\beta$ ) due to the loading device, in order to resolve the issue of the global minimum producing an arbitrary number of discontinuities in strain. They also used  $W(z) = (|z| - 1)^2$  as their double well potential. Also, Kohn and Müller worked on a two-dimensional model [44, 45].

Last but not least, Ren and Truskinovsky [55] were able to construct a simple one-dimensional model to account for formation and growth of globally stable finite scale microstructure. They achieved it by adding the usual surface energy and the oscillation-forcing (foundation) terms (to Ericksen's original energy functional) with the exception that the foundation term is non-local and has a negative definite kernel. Also Ren and Wei [56, 57] considered non-local versions of the foundation term while Brandon and Rogers [9] considered a non-local regularization of the problem (non-local surface energy).

### 1.7 The Finite Element Method

Many of the problems described above have an equivalent variational formulation, which in its simplest form looks like the following: Find  $u \in [0, 1] \rightarrow \mathbb{R}$  satisfying the boundary conditions s.t:

$$\int_0^1 \sigma(u_x) v'(x) dx = 0 \quad \text{for all smooth } v : [0, 1] \rightarrow \mathbb{R}$$

(see section (1.2) for more details).

Ideally, we would like to have exact solutions under all circumstances, as well as closed form formulas to describe them. Unfortunately, this is not always feasible and not all models like the above one are easy to be solved analytically. Whether we are dealing with the inevitable complexity of the model or the innate difficulty of the problem itself. An example of the former would be the direct correlation between calculations and the lap number, where the lap number is the number of intervals of monotonicity, (as the lap number increase, so do the calculations) while an example of the latter is

## CHAPTER ONE

the fact that we have no prior knowledge of the location of the jump. To circumvent these issues people have resorted to several numerical methods such as Finite Elements Method (FEM) to solve the problem.

However, even those numerical approaches have several issues to overcome. Efficiency is one of them, since the finite element method approaches used to model simple microstructures require a lot of unknowns [48]. In addition to that the computational challenges of minimization in a non-convex setting are not only significant but also can not be resolved by resorting to their corresponding analytical result [14].

Historically, the Finite Element Method was developed in 1942 by Richard L. Courant who included it in his paper on variational methods [27]. Despite the fact, that the method was not used for almost two decades after that [53], it was revived again by engineers in the late 50's as a way of approximating solutions to equations in structural engineering. Over the next couple of decades the method was studied extensively by mathematicians who realized that it is a great general technique for finding numerical solutions to PDE's. Since then it has been established itself as a stable method for these types of problems [42].

Authors have made considerable progress on the FEM. In particular, more relevant to our work, the first finite element approach to the one-dimensional setting was done by Collins, Kinderlehrer and Luskin who noticed in [23] that variational problems which involve double well potentials do not have a minimizer. Instead, they have minimizing sequences which can have oscillations.

Since the above problems show up in certain classes of solid crystals, they gave a rigorous justification for the use of numerical methods to model these behaviors. Collins and Luskin continued to use numerical methods to approximate these models, this time to estimate the error [24] as did Chipot who investigated the patterns of the minimizing sequences as well [17].

Chipot and Collins, also used further numerical methods to analyze the minimizing sequences and to estimate the deformation as it approximates a measure [18]. Moreover,

## CHAPTER ONE

Gremaud estimated the rate of convergence of the approximated gradient deformation, again using a finite element method [39]. Last but not least, Chipot, Collins and Kinderlehrer used piecewise linear elements to approximate the continuous version of a problem that involves multiple wells [19].

### 1.8 Mixed Finite Element Methods

In our work, we use many of the ideas presented above, tailored to suit the needs of our specific problem. In particular, we are dealing with a fourth order PDE, which can be rewritten as an appropriate system of two second order differential equations which we then proceed to solve using numerical methods. This process is known as the mixed element method.

To illustrate how this method works we give an example of a much simpler problem, namely the Poisson's equation.

Say we are interested in solving  $-\Delta u = f$  in some space  $\Omega$  with boundary conditions  $u = 0$  on  $\partial\Omega$  (where  $\Delta$  is the Laplace operator).

We can reduce the order of the above equation, by considering the following equivalent system

$$\left\{ \begin{array}{l} \sigma = \nabla u \\ -\nabla \cdot \sigma = f \quad \text{in } \Omega \\ u = 0 \quad \text{on } \partial\Omega. \end{array} \right. \quad \begin{array}{l} (1.8.1) \\ (1.8.2) \\ (1.8.3) \end{array}$$

Now, in order to get a weak formulation (see Section 2.4) we multiply (1.8.1) and (1.8.2) by the test functions  $\tau$  (vector-valued) and  $v$  (scalar) and integrate over  $\Omega$ . Finally we use integration by parts (and the boundary condition) to get the following:

$$\int_{\Omega} \sigma \cdot \tau \, dx + \int_{\Omega} u(\nabla \cdot \tau) \, dx = 0 \quad \forall \tau. \quad (1.8.4)$$

## CHAPTER ONE

Similarly, but without integration by parts we get:

$$\int_{\Omega} (\nabla \cdot \sigma) v \, dx = - \int_{\Omega} f v \, dx \quad \forall v. \quad (1.8.5)$$

This leads to the following system: namely, find a pair  $(\sigma, u)$  that satisfies (1.8.4) and (1.8.5) where the test functions  $\tau, v$  range over appropriate spaces. For more details and examples one can consult [1, 8, 33].

Notice that we did not integrate the second equation by parts. This is in order to obtain a symmetric bilinear form. In other words, if we add the two equations together we get a bilinear form acting on the trial and test functions  $(\sigma, u)$  and  $(\tau, v)$  which is symmetric: Find  $(\sigma, u)$  such that

$$B((\sigma, u), (\tau, v)) := \int_{\Omega} \sigma \cdot \tau \, dx + \int_{\Omega} u(\nabla \cdot \tau) \, dx + \int_{\Omega} (\nabla \cdot \sigma) v \, dx = - \int_{\Omega} f v \, dx \quad \forall (\tau, v).$$

The literature of the Mixed Finite Element Method is large and authors have made a tremendous amount of work since the seventies. For example, one can consult [3, 11, 12, 34], and for more recent references [2, 38, 58, 62]. However, we will not give a detailed description of Mixed Finite Element Methods because, as can be seen later, the bilinear form associated to our problem is elliptic. This gives a freedom to choose any Finite Element spaces for our variables, contrary to most Mixed methods where the Finite Element spaces for all the variables need to be correctly balanced in order to be able to prove stability and convergence.

### 1.9 Thesis outline

The thesis is organised as follows. Chapter 2 introduces our mathematical background and the framework which we will employ. Chapters 3, 4 and 5 contain the major research ideas of the thesis. In summary we study a specific energy functional based on Ericksen's model [32] for an elastic bar which is attached to an elastic foundation. The

## CHAPTER ONE

formula includes Müller's term which penalizes oscillations. As for of the double-well potential, we use Yip's selection, namely  $W(p) = (|p| - 1)^2$  in order to make explicit calculations. We allow for a stiffness parameter  $\alpha > 0$  which will help us better study bifurcations and thus answer a conjecture first posed by Grinfeld and Lord.

In Chapter 3 we show the existence and uniqueness of both periodic and non-periodic solutions for positive  $\alpha > 0$  and small  $\gamma > 0$ . We consider separate cases depending on how many times the displacement function  $u$  changes monotonicity. In particular, we solve the problem explicitly, when  $u$  changes monotonicity once or twice. On top of that, we provide a recursive formula for the energy functional  $E(u_n)$  of the more complex periodic solutions  $u_n$ , as a function of the simplest periodic solution  $u_1$ . We conclude all of the above, by summarizing our findings in a single but descriptive graph.

In chapter 4, we use ideas from functional analysis, in order to find some convenient weak formulations which are equivalent to our corresponding Euler-Lagrange equation, which we then show that can be solved uniquely. One important result in this chapter is that this unique solution still exists even if we restrict ourselves to appropriate solution subspaces, by using the Finite Element Method approach. We can then show that both weak formulations have unique solutions within those subspaces for any given mesh. More importantly, we give an error estimate which guarantees that the unique solution of the subspace can be arbitrary close to the unique solution of the original space, as we refine the mesh.

Chapter 5 uses Chapter 4 as a foundational setup and it introduces the specific numerical methods used in this thesis. In particular, we show that two well known methods, namely the Finite Element Method and the Derivative-Free Optimization method, can be used in combination with one another in order to produce arbitrarily good approximations to the exact solution of the EL equation. The accuracy of these calculations was verified by comparing them the results produced by these two methods (FEM and DFO) to those given by MAPLE from the exact solutions. Lastly, the chapter would not be complete without the presence of several numerical plots of these approximations as well as tables of their corresponding energies for progressively finer mesh.

## Chapter 2

# Mathematical Background

### 2.1 Calculus of Variations

The core of our work is based on Calculus of Variations (CoV), the field of mathematics that tries to understand how small changes (aka variations or perturbations) in a function, which acts as an input of certain functional, affect the mentioned functional. Here, a functional is simply a mapping from a class of functions to the real numbers. That is, a functional takes a function as an input and produces a real number as an output. Typically, and in our case too, functionals are expressed as definite integrals that utilize various orders of derivatives. For example, in our work we use the following functional:

$$E(u) = \int_0^1 [\gamma u_{xx}^2 + W(u_x) + \alpha u^2] dx.$$

The goal of calculus of variation is mainly to optimize (maximize or minimize) the functional using concepts such as the Euler-Lagrange equation ( [29], [28]).

**Remark 1.** *All theorems and results in this chapter are provided with references but without proofs.*

## 2.2 Euler Lagrange equation

The Euler Lagrange equation is a partial differential equation whose solutions are the candidate functions for which the functional is optimized. In particular, to find a function that extremizes the functional

$$I(u) = \int_{x_1}^{x_2} L(x, u(x), u_x(x)) dx,$$

we have the following theorem

**Theorem 5.** *The function  $u = u(x)$  that extremizes the functional  $I$  necessarily satisfies the Euler-Lagrange equation on  $[x_1, x_2]$ :*

$$\frac{\partial L}{\partial u} - \frac{d}{dx} \left( \frac{\partial L}{\partial u_x} \right) = 0.$$

*Proof.* See [46], Theorem 1. □

As an example, the Euler-Lagrange equation can be used to prove that the shortest distance between two points on a Euclidean plane is a straight line. Let,

$$L(u) = \sqrt{1 + u'^2},$$

where  $u \in C^\infty$ ,  $u : \mathbb{R} \rightarrow \mathbb{R}$ . Then the Euler-Lagrange equation will be

$$\frac{\partial L}{\partial u} - \frac{d}{dx} \left( \frac{u'}{\sqrt{1 + u'^2}} \right) = 0,$$

which means the inside is a constant function:  $\frac{u'}{\sqrt{1 + u'^2}} = C_1$ . Solving for  $u'$ , we also get  $u' = C_2$  (constant) and hence  $y = Cx + D$  (straight line).

In general if

$$I(u) = \int_{x_1}^{x_2} L(x, u(x), u_x(x), u_{xx}(x), u_{xxx}(x), \dots) dx,$$

## CHAPTER TWO

then the Euler Lagrange equation will be

$$\frac{\partial L}{\partial u} - \frac{d}{dx} \left( \frac{\partial L}{\partial u_x} \right) + \frac{d^2}{dx^2} \left( \frac{\partial L}{\partial u_{xx}} \right) - \frac{d^3}{dx^3} \left( \frac{\partial L}{\partial u_{xxx}} \right) + \dots = 0.$$

In our case we only deal with derivatives up to second order so the Euler Lagrange equation is given by

$$\frac{\partial L}{\partial u} - \frac{d}{dx} \left( \frac{\partial L}{\partial u_x} \right) + \frac{d^2}{dx^2} \left( \frac{\partial L}{\partial u_{xx}} \right) = 0.$$

Next we present a more involved example, which is also the main topic of our work. Start with the Euler-Lagrange equation

$$\frac{\partial L}{\partial u} - \frac{d}{dx} \left( \frac{\partial L}{\partial u_x} \right) + \frac{d^2}{dx^2} \left( \frac{\partial L}{\partial u_{xx}} \right) = 0,$$

where  $L = L(x, u, u_x, u_{xx}) = \gamma u_{xx}^2(x) + W(u_x) + \alpha u^2$ .

Calculating all partial derivatives of  $L$ , we get

$$\frac{\partial L}{\partial u} = 2\alpha u, \quad \frac{d}{dx} \frac{\partial L}{\partial u_x} = W''(u_x) u_{xx} \quad \text{and} \quad \frac{d^2}{dx^2} \frac{\partial L}{\partial u_{xx}} = 2\gamma u_{xxxx}.$$

Putting it all together we get :

$$\alpha u - \frac{W''}{2}(u_x) u_{xx} + \gamma u_{xxxx} = 0. \tag{2.2.1}$$

**Definition 2.2.1.** We say that the functional  $E(u)$  has a minimum at  $u = u_0$  with a functional space  $\mathcal{V}$ , if its first variation  $\partial E(u) = 0$  at  $u = u_0$  and its second variation  $\partial^2 E(u) = 0$  is strongly positive at  $u = u_0$  (that is  $\partial^2 E(u) \geq k\|u\|^2$  for some  $k > 0$  and all  $u \in \mathcal{V}$ ). We say that  $u_0$  is a local minimizer of  $E(u)$ .

We can also weaken the above definition by introducing the notion of weak local minimizers.

**Definition 2.2.2.** A function  $u_0 \in \mathcal{V}$  is called a  $\mathcal{V}$ -local minimizer of  $E$ , if there is a  $\sigma > 0$  such that  $E(u_0) \leq E(u)$  for all  $u \in \mathcal{V}$  with  $0 < \|u - u_0\| < \sigma$ .

## CHAPTER TWO

**Definition 2.2.3.** We say that  $u_0 \in \mathcal{V}$  is a global minimizer of  $E(u)$  if  $E(u_0) \leq E(u)$  for all  $u \in \mathcal{V}$ .

**Remark 2.** A necessary (but not sufficient) condition for a local extremum  $u_0$ , is that it satisfies the Euler-Lagrange equation. This means that investigating the solutions of the EL reveals the possible candidates. Note that, like in regular calculus, a critical point (solution the the Euler-Lagrange equation), may be either a (local) minimum, a (local) maximum or even a saddle point. In our context a (local) maximum would be a critical point  $u$  with strongly negative second variation, while a saddle point will be a critical point  $u$  which is neither (local) minimum or maximum.

### 2.3 The Fredholm Alternative

In our work, we will also need the following theorem from Linear algebra.

**Theorem 6.** Let  $A \in \mathbb{R}^{n \times m}$ ,  $x \in \mathbb{R}^{m \times 1}$ ,  $b \in \mathbb{R}^{n \times 1}$ ,  $y \in \mathbb{R}^{n \times 1}$ . The linear system  $Ax = b$  has a solution  $x$  if and only if  $y^T b = 0$  for all  $y$  such that  $y \in \ker(A^T)$  and  $A^T y = 0$ .

*Proof.* See [51], Theorem 5.45. □

As an example let  $A = \begin{bmatrix} 1 & 2 \\ 0 & 1 \\ 2 & 4 \end{bmatrix}$ ,  $b = \begin{bmatrix} 4 \\ 1 \\ 8 \end{bmatrix}$ .

Now we need to know if there is  $x = \begin{bmatrix} x_1 \\ x_2 \end{bmatrix}$  such that  $Ax = b$ ? Towards that, we use Theorem 6 as follows:

$$A^T y = 0 \Rightarrow \begin{bmatrix} 1 & 0 & 2 \\ 2 & 1 & 4 \end{bmatrix} \begin{bmatrix} y_1 \\ y_2 \\ y_3 \end{bmatrix} = \begin{bmatrix} 0 \\ 0 \end{bmatrix},$$

a simple calculation gives us  $y = \begin{bmatrix} -2 \\ 0 \\ 1 \end{bmatrix} y_3 \in \ker(A^T)$ . We want  $y^T b = 0$ . A

direct calculation shows that  $y^T b = \begin{bmatrix} -2y_3 & 0 & y_3 \end{bmatrix} \begin{bmatrix} 4 \\ 1 \\ 8 \end{bmatrix} = 0$ . Since  $y^T b = 0$ , the

Fredholm alternative condition is satisfied and thus  $Ax = b$  has a unique solution  $x$ .

## 2.4 Functional analysis

In this section, we introduce the framework in which our problem can be formulated. We will need a generalization of the classical derivative, known as the weak derivative. To set up the stage, we need the following definitions which can be found among the following references, [10, 26, 30].

Let us recall the following definitions

**Definition 2.4.1.** *Let  $V$  be a real vector space and  $L : V \rightarrow \mathbb{R}$ . We say that  $L$  is linear if*

$$L(\alpha u + \beta v) = \alpha L(u) + \beta L(v) \quad \forall u, v \in V, \forall \alpha, \beta \in \mathbb{R}.$$

**Definition 2.4.2.** *Let  $V$  be a vector space and  $A : V \times V \rightarrow \mathbb{R}$ . We say that  $A$  is bilinear if*

$$A(\alpha u_1 + \beta u_2, v) = \alpha A(u_1, v) + \beta A(u_2, v) \quad \forall u_1, u_2 \in V, \forall \alpha, \beta \in \mathbb{R}.$$

$$A(u, \alpha v_1 + \beta v_2) = \alpha A(u, v_1) + \beta A(u, v_2) \quad \forall v_1, v_2 \in V, \forall \alpha, \beta \in \mathbb{R}.$$

We are also interested in a specific form of a bilinear function called inner product, traditionally denoted by  $(\cdot, \cdot)$ .

**Definition 2.4.3.** *We say that the bilinear function  $(\cdot, \cdot) : V \times V \rightarrow \mathbb{R}$  is an inner*

## CHAPTER TWO

product if it is symmetric and positive definite. I.e.

$$\begin{aligned}(u, v) &= (v, u) \quad \forall u, v \in V \\ (u, u) &> 0 \quad \forall u \in V \text{ with } u \neq 0.\end{aligned}$$

The inner product naturally gives rise to the norm, typically denoted by  $\|\cdot\|$ .

**Definition 2.4.4.** Let  $V$  be a real vector space. If  $(\cdot, \cdot)$  is an inner product on  $V \times V$  we define  $\|\cdot\| : V \rightarrow \mathbb{R}$  as follows:

$$\|u\| = \sqrt{(u, u)} \quad \forall u \in V.$$

Then,  $\|\cdot\|$  is a norm in  $V$ .

We should also mention an important relationship between the inner product and the norm:

**Lemma 1.** (Cauchy-Schwarz inequality). Let  $V$  be a vector space,  $(\cdot, \cdot)$  be an inner product on  $V$  and  $\|\cdot\|$  be the associated norm. We have

$$|\langle u, v \rangle| \leq \|u\| \cdot \|v\| \quad \forall u, v \in V.$$

*Proof.* See [65], Proposition 2. □

We are finally ready to define Hilbert spaces, one of the most common types of spaces used in this work.

**Definition 2.4.5.** Let  $\mathbb{H}$  be a vector space with inner product  $(\cdot, \cdot)$  and associated norm  $\|\cdot\|$ . We say  $\mathbb{H}$  is Hilbert if  $\mathbb{H}$  is complete, that is if  $\|u_n - u_m\| \rightarrow 0$  as  $m, n \rightarrow \infty$ , there exists  $u \in \mathbb{H}$  such that  $\|u_n - u\| \rightarrow 0$ .

Since we are mostly interested in a particular type of Hilbert spaces, namely Sobolev spaces, we will introduce first the idea of distributions which are fundamental in their description.

## CHAPTER TWO

**Definition 2.4.6.** *The support of a function  $\phi : \mathbb{R} \rightarrow \mathbb{R}$  defined as*

$$\text{supp}(\phi) = \overline{\{x \in \mathbb{R} : \phi(x) \neq 0\}}.$$

**Definition 2.4.7.** *The space of compactly supported infinitely smooth functions is defined as follows:*

$$\mathcal{D}(a, b) = \{\phi \in C^\infty(a, b), \text{supp}(\phi) \text{ is compact and } \text{supp}(\phi) \subseteq (a, b)\}.$$

**Definition 2.4.8** (distributions). *The space of distribution over  $(a, b)$  is defined as follows*

$$\mathcal{D}'(a, b) = \{T : \mathcal{D}(a, b) \rightarrow \mathbb{R}, T \text{ is a linear and continuous}\}.$$

**Remark 3.**  $\langle \cdot, \cdot \rangle_{(a, b)}$  will denote the duality pairing between  $\mathcal{D}'(a, b)$  and  $\mathcal{D}(a, b)$ . This is, whenever  $f$  and  $g$  are regular enough we have

$$\langle f, g \rangle_{(a, b)} = \int_b^a f(x) g(x) dx.$$

**Definition 2.4.9.** *For a distribution  $u \in \mathcal{D}'(a, b)$ , we say  $v \in \mathcal{D}'(a, b)$  is its weak derivative if*

$$\langle u, \varphi' \rangle_{(a, b)} = -\langle v, \varphi \rangle_{(a, b)},$$

for all  $\varphi \in \mathcal{D}(a, b)$ .

### 2.4.1 Examples of Hilbert spaces

The following are all real Hilbert spaces:

- $L^2(0, 1) = \{f : (0, 1) \rightarrow \mathbb{R} : \int_0^1 f^2(x) dx < \infty\}.$

Its inner product is defined as

$$(f, g) = \int_0^1 f(x) g(x) dx.$$

## CHAPTER TWO

- $H^1(a, b) = \{v \in L^2(a, b) : v' \in L^2(a, b)\}$

where the inner product is defined as

$$(f, g)_{H^1} = \int_a^b f(x)g(x)dx + \int_a^b f'(x)g'(x)dx.$$

- $H^2(a, b) = \{v \in L^2(a, b) : v', v'' \in L^2(a, b)\}$

where the inner product is defined as

$$(f, g)_{H^2} = \int_a^b f(x)g(x)dx + \int_a^b f'(x)g'(x)dx + \int_a^b f''(x)g''(x)dx.$$

- $H_0^1(a, b) = \{v \in H^1(a, b) : v(a) = v(b) = 0\}$

where the inner product is defined as

$$(f, g)_{H_0^1} = \int_a^b f'(x)g'(x)dx.$$

We will also make use of the following result, (known as Sobolev's embedding theorem) which states that all functions in  $H_0^1$  are continuous:

**Theorem 7. (Sobolev's embedding theorem).**  $H_0^1(a, b) \subset C^0[a, b]$  and there exists a constant  $C > 0$  such that

$$\|u\|_{C^0} \leq C\|u\|_{H_0^1}.$$

*Proof.* See [10], Theorem 8.8. □

Also,

**Theorem 8. (Poincaré Inequality).** There exists  $C > 0$  such that

$$\|v\|_{L^2(a, b)} \leq C|v|_{H_0^1(a, b)} \quad \forall v \in H_0^1(a, b).$$

*Proof.* See [10], Theorem 8.13. □

## 2.5 The Galerkin Method

The Finite Element Methods used in this work are a special case of what is known as the Galerkin method, which is a way of finding numerical approximations to the following problem on a Hilbert space  $V$ : Find  $u \in V$  such that

$$A(u, v) = f(v) \quad \forall v \in V,$$

where  $A(u, v)$  is a bilinear form and  $f$  is a bounded linear functional on  $V$ .

In particular, Galerkin contribution was to change the (infinite dimensional) solution space  $V$ , by finding a finite dimensional subspace  $V_h \subset V$  of dimension  $h$  and solve the approximate problem: Find  $u_h \in V_h$  such that

$$A(u_h, v_h) = f(v_h) \quad \forall v_h \in V_h.$$

The above allows us to numerically approximate the solution to the original problem. The key idea behind this method, is what is known as Galerkin orthogonality which means that the error term  $\epsilon_h = u_h - u$  is orthogonal to the subspace  $V_h$ . In other words

$$A(\epsilon_h, v_h) = A(u_h - u, v_h) = A(u_h, v_h) - A(u, v_h) = f(v_h) - f(v_h) = 0.$$

It is well established that the Lax-Milgram theorem is one of the basic components of the method, since it can produce uniqueness of solutions to the (weak formulations) of the Euler Lagrange equation. Moreover, Cea's lemma provides us with an error estimate between the actual solution and the approximation produced by the FEM [22, 33].

**Theorem 9** (Lax-Milgram theorem). *Let  $\mathbb{H}$  be a vector space with inner product  $(\cdot, \cdot)$  and associated norm  $\|\cdot\|$ . Let also  $L : \mathbb{H} \rightarrow \mathbb{R}$  be linear and  $A : \mathbb{H} \times \mathbb{H} \rightarrow \mathbb{R}$  be bilinear with :*

1.  $\exists \gamma > 0$  s.t.  $|A(u, v)| \leq \gamma \|u\| \cdot \|v\| \quad \forall u, v \in \mathbb{H}$  (continuity of  $A$ ).
2.  $\exists \alpha > 0$  s.t.  $A(u, u) \geq \alpha \|u\|^2 \quad \forall u \in \mathbb{H}$  (ellipticity of  $A$ ).

## CHAPTER TWO

3.  $\exists \beta > 0$  s.t.  $|L(u)| \leq \lambda \|u\| \quad \forall u \in \mathbb{H}$  (continuity of  $L$ ).

Then there exists a unique  $u \in \mathbb{H}$  s.t.  $A(u, v) = L(v) \quad \forall v \in \mathbb{H}$ .

*Proof.* See [22], Theorem 198. □

**Lemma 2** (Cea's lemma). *Let  $\mathbb{H}$  be a vector space with inner product  $(\cdot, \cdot)$  and associated norm  $\|\cdot\|$ . Let also  $L : \mathbb{H} \rightarrow \mathbb{R}$  be linear and  $A : \mathbb{H} \times \mathbb{H} \rightarrow \mathbb{R}$  be bilinear. Finally, let  $\mathbb{H}_h$  be a finite dimensional subspace of  $\mathbb{H}$ . Moreover, let  $u$  is such that  $A(u, v) = L(v) \quad \forall v \in \mathbb{H}$  and  $u_h$  is such that  $A(u_h, v_h) = L(v_h) \quad \forall v_h \in \mathbb{H}_h$ . Then  $\|u - u_h\|_{\mathbb{H}} \leq \frac{\gamma}{\alpha} \|u - v_h\|_{\mathbb{H}} \quad \forall v_h \in \mathbb{H}_h$ , where  $\alpha, \gamma$  are the constant given by 1. and 2. of the Lax-Milgram.*

*Proof.* See [22], Lemma 201. □

## 2.6 Formulation of a Finite Element Method

Suppose we are interested in solving the following problem, for  $f \in L^2(0, 1)$ , which is called the Poisson problem.

$$\begin{aligned} -u''(x) &= f(x) \quad \text{in } (0, 1), \\ u(0) &= u(1) = 0. \end{aligned} \tag{S}$$

The above problem (S) is equivalent to solving:

Find  $u \in H_0^1(0, 1)$  s.t

$$(u', v') = (f, v) \quad \forall v \in H_0^1(0, 1). \tag{W}$$

Since  $f \in L^2(0, 1)$ , then  $u''$  exists and is continuous. For more details of the proof see [42].

## CHAPTER TWO

The above equivalence is important, because we can now solve  $(W)$  instead of  $(S)$ . We divide the interval  $[0, 1]$  as follows

$$0 = x_0 < x_1 < x_2 < \dots < x_{N-1} < x_N = 1$$

with  $h = \frac{1}{N} = (x_k - x_{k-1})$  for  $k = 1, \dots, N$ . This is, we divide  $[0, 1]$  into equidistant points. Over this partition we define a basis function for the space of continuous, piecewise linear functions. Let

$$\mathbb{V}_h = \{v \in H_0^1(0, 1), v \text{ is linear on each } [x_{i-1}, x_i]\}.$$

The main idea of the FEM is to find an approximation solution of the form  $v(x) = \sum_{i=1}^N \xi_i \varphi_i(x)$ , where

$$\varphi_i(x_j) = \begin{cases} 1 & j = i \\ 0 & \text{otherwise} \end{cases}$$

is a continuous, piece-wise linear function and  $\xi_i$ 's are constants to be determined. To determine the constants we will write a MATLAB code.

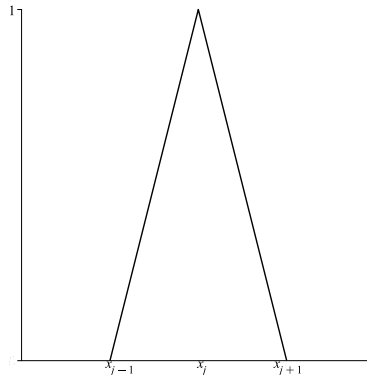


**Figure 2.1:** Basis of  $\varphi_i$

The finite element method reads as follow: Find  $u_h \in \mathbb{V}_h$  s.t

$$(u'_h, v'_h) = (f_h, v_h) \quad \forall v_h \in \mathbb{V}_h. \quad (F).$$

We will show that  $(F)$  can be written as a linear system. We look for approximation

## CHAPTER TWO

for  $u_h$  in the form

$$u_h(x) = \sum_{i=1}^N \xi_i \varphi_i(x).$$

As a result, by using bilinearity we can express all inner products of the form  $(u'_n, \varphi'_m)$  as a linear combination of the products of the form  $(\varphi'_i, \varphi'_m)$ . By repeating this process for every  $m \in \{1, 2, \dots, N\}$  we can write  $F$  as the following matrix equation  $\mathbb{A} \mathbf{X} = \mathbf{b}$ , where

$$\mathbb{A} = \begin{bmatrix} (\varphi'_1, \varphi'_1) & (\varphi'_1, \varphi'_2) & \dots & \dots & (\varphi'_1, \varphi'_N) \\ (\varphi'_2, \varphi'_1) & (\varphi'_2, \varphi'_2) & \dots & \dots & (\varphi'_2, \varphi'_N) \\ \vdots & \vdots & \vdots & \vdots & \vdots \\ (\varphi'_N, \varphi'_1) & (\varphi'_N, \varphi'_2) & \dots & \dots & (\varphi'_N, \varphi'_N) \end{bmatrix}, \mathbf{b} = \begin{bmatrix} b_1 \\ b_2 \\ \vdots \\ b_N \end{bmatrix} = \begin{bmatrix} (f, \varphi_1) \\ (f, \varphi_2) \\ \vdots \\ (f, \varphi_N) \end{bmatrix},$$

where we know all the entries of  $\mathbb{A}$  and  $\mathbf{b}$ . The method concludes by calculating the coefficient  $\mathbf{X} = [\zeta_1, \zeta_2, \dots, \zeta_N]^T \in \mathbb{R}^N$ , which is the unknown in our system, and thus the value we are solving for.

Notice that the matrix  $\mathbb{A}$  is sparse (most entries of the matrix are zero). More precisely:

$$(\varphi'_i, \varphi'_m) = \begin{cases} \frac{2}{h} & i = m, \\ \frac{-1}{h} & |i - m| = 1, \\ 0 & \text{otherwise.} \end{cases}$$

For example, with  $m = 5$  we have

$$\frac{1}{h} \begin{bmatrix} 2 & -1 & 0 & 0 & 0 \\ -1 & 2 & -1 & 0 & 0 \\ 0 & -1 & 2 & -1 & 0 \\ 0 & 0 & -1 & 2 & -1 \\ 0 & 0 & 0 & -1 & 2 \end{bmatrix} \begin{bmatrix} \xi_1 \\ \xi_2 \\ \xi_3 \\ \xi_4 \\ \xi_5 \end{bmatrix} = \begin{bmatrix} b_1 \\ b_2 \\ b_3 \\ b_4 \\ b_5 \end{bmatrix}.$$

As we will see in Chapter 4, any solution produced by the FEM approximates the exact solution within a small error. Coupled with the fact that the algorithm itself boils down to a Gauss-Jordan elimination, we have ourselves a method which is both accurate and

## CHAPTER TWO

computationally efficient. For more details see [21, 33, 42].

## Chapter 3

# Stationary Solutions in Yip's Formulation of the Regularized Ericksen's Bar Model

### 3.1 Introduction

In what follows we will study a specific energy functional of Ericksen's model [32] for an elastic bar which is attached to an elastic foundation. We include Müller's term of the surface energy density component  $\gamma u_{xx}^2$  that penalizes oscillations. Also, we include Yip's selection of the double-well potential  $W(p) = (|p| - 1)^2$  in order to make explicit calculations. Last but not least, in our context we allow for a stiffness parameter  $\alpha > 0$  which will help us better study bifurcations and thus ultimately answer a conjecture first posed by Grinfeld and Lord.

All in all we will work on the following functional:

$$E(u) = \int_0^1 [\gamma u_{xx}^2 + W(u_x) + \alpha u^2] dx, \quad (3.1.1)$$

## CHAPTER THREE

where  $u : [0, 1] \rightarrow \mathbb{R}$  can be thought of as the displacement function (see Section 1.3). We will also be assuming Dirichlet boundary conditions, namely  $u(0) = u(1) = 0$  and  $u_{xx}(0) = u_{xx}(1) = 0$ .

With that context in mind, Grinfeld and Lord's conjecture becomes:

**Conjecture 10.** *For the above formulation, for large  $\alpha$ , there are no solutions without internal zeroes.*

This chapter analyzes the existence and uniqueness of periodic and non-periodic solutions for different values of the parameters  $\alpha > 0$  and  $\gamma > 0$ . We consider separate cases depending on how many times the displacement function  $u$  changes monotonicity. In particular, we solve the problem explicitly, when  $u$  changes monotonicity once or twice, and also give recursive formulas for  $E(u)$  when  $u$  is more complex. Finally, we conclude the chapter with a pictorial summary of our finding.

### 3.2 The Euler Lagrange Equation

The Euler-Lagrange equation of our functional is given by:

$$\frac{\partial L}{\partial u} - \frac{d}{dx} \frac{\partial L}{\partial u_x} + \frac{d^2}{dx^2} \frac{\partial L}{\partial u_{xx}} = 0,$$

where  $L = L(x, u, u_x, u_{xx}) = \gamma u_{xx}^2(x) + W(u_x) + \alpha u^2$ .

Calculating all partial derivatives of  $L$ , we get:

$$\frac{\partial L}{\partial u} = \alpha u, \quad \frac{d}{dx} \frac{\partial L}{\partial u_x} = W''(u_x) u_{xx} \quad \text{and} \quad \frac{d^2}{dx^2} \frac{\partial L}{\partial u_{xx}} = \gamma u_{xxxx}.$$

Putting it all together we get :

$$\alpha u - \frac{W''}{2}(u_x) u_{xx} + \gamma u_{xxxx} = 0, \tag{3.2.1}$$

since  $W(u_x) = (|u_x| - 1)^2$ , we have  $W''(u_x) = 2$ , except for when  $u_x = 0$  (in which

## CHAPTER THREE

case we have a “jump”). In the interval of monotonicity, the Euler Lagrange equation becomes

$$\gamma u_{xxxx} - u_{xx} + \alpha u = 0. \quad (3.2.2)$$

In other words, the above is only valid in the intervals where  $u_x \neq 0$  and thus  $W'' = 2$ , while at the points  $c_1, c_2, \dots, c_n$  where  $u_x = 0$  and change signs, we have a jump condition for  $u_{xxx}$ . More formally, we have the following definition (due to [63]) for the space on the functions that satisfy these properties.

**Definition 3.2.1.** *A function  $u$  is said to belong to class  $\mathcal{Z}$  if  $u \in C^2([0, 1])$  and  $[0, 1]$  can be partitioned into a finite number of intervals  $\{[c_i, c_{i+1}] : i = 0, 1, \dots, N-1\}$  for some positive integer  $N$  and  $c_i$ 's :  $0 = c_0 < c_1 < \dots < c_{N-1} < c_N = 1$  such that*

1.  *$u$  is monotone ( $u_x \geq 0$  or  $u_x \leq 0$ ) in each of the segment  $(c_i, c_{i+1})$  and the sign of  $u_x$  alternates between adjacent segments, i.e.  $u_x$  changes sign across the  $c_i$ 's;*
2. *the zeros of  $u_x$  are isolated. In particular,  $u_x$  is not identically zero in any interval.*

The Euler Lagrange equation above (3.2.2) is linear, which means that its general solution depends on its characteristic polynomial

$$\gamma r^4 - r^2 + \alpha = 0.$$

It is easy to see the solutions of the above polynomial are given by:

$$\pm \sqrt{\frac{1 + \sqrt{1 - 4\alpha\gamma}}{2\gamma}} \stackrel{\text{def}}{=} \pm\Lambda, \quad \pm \sqrt{\frac{1 - \sqrt{1 - 4\alpha\gamma}}{2\gamma}} \stackrel{\text{def}}{=} \pm\lambda.$$

This means that within the intervals where  $u$  maintains monotonicity the solution  $u(x)$  of the Euler Lagrange equation should have one of the following 3 forms depending on the relationship between  $\alpha$  and  $\gamma$ .

CHAPTER THREE

- Case 1:  $1 - 4\alpha\gamma > 0$ :

$$u(x) = A e^{\Lambda x} + B e^{-\Lambda x} + C e^{\lambda x} + D e^{-\lambda x}.$$

- Case 2:  $1 - 4\alpha\gamma = 0$ : (Then  $\Lambda = \lambda = d = \sqrt{\frac{1}{2\gamma}}$ )

$$u(x) = A e^{dx} + B x e^{dx} + C e^{-dx} + D x e^{-dx}.$$

- Case 3:  $1 - 4\alpha\gamma < 0$ :

$$u(x) = A e^{tx} \cos(\omega x) + B e^{tx} \sin(\omega x) + C e^{-tx} \cos(\omega x) + D e^{-tx} \sin(\omega x),$$

where

$$t = \sqrt{\frac{\sqrt{4\alpha\gamma} + 1}{4\gamma}}, \quad \omega = \sqrt{\frac{\sqrt{4\alpha\gamma} - 1}{4\gamma}}.$$

We calculate  $t, \omega$  as follows: we know that the 4 roots of the characteristic polynomial,  $r^4 - \frac{r^2}{\gamma} + \frac{\alpha}{\gamma} = 0$  are  $r = \pm t \pm \omega i$ . Hence

$$0 = (r - t - \omega i)(r + t - \omega i)(r - t + \omega i)(r + t + \omega i) = r^4 - \frac{r^2}{\gamma} + \frac{\alpha}{\gamma}.$$

Therefore,

$$\begin{aligned} [r^2 - (t + i\omega)^2][r^2 - (t - i\omega)^2] &= r^4 - \frac{r^2}{\gamma} + \frac{\alpha}{\gamma}, \\ r^4 - r^2[2t^2 - 2\omega^2] + (t^2 + \omega^2)^2 &= r^4 - \frac{r^2}{\gamma} + \frac{\alpha}{\gamma}, \end{aligned}$$

and hence

$$t^2 - \omega^2 = \frac{1}{\gamma}, \quad t^2 + \omega^2 = \sqrt{\frac{\alpha}{\gamma}}.$$

Adding the two equations above together, we get:

$$2t^2 = \frac{1}{\gamma} + \sqrt{\frac{\alpha}{\gamma}} \quad \Rightarrow \quad t = \sqrt{\frac{\sqrt{4\alpha\gamma} + 1}{4\gamma}},$$

## CHAPTER THREE

and subtracting them we get:

$$2\omega^2 = \sqrt{\frac{\alpha}{\gamma}} - \frac{1}{\gamma} \quad \Rightarrow \quad \omega = \sqrt{\frac{\sqrt{4\alpha\gamma} - 1}{4\gamma}}.$$

We define solutions of (3.2.2) using a modification of a definition used by Yip [63] to account for our imposed Dirichlet Boundary conditions, namely:

**Definition 3.2.2.** *A function  $u \in \mathcal{Z}$  is called a solution of (3.2.2) if the following hold for all  $i$ :*

$$\gamma u_{xxxx} - u_{xx} + \alpha u = 0 \quad \text{on } (c_i, c_{i+1}) \text{ for } i = 0, 1, \dots, n; \quad (3.2.3)$$

$$u_x(c_i) = 0 \text{ and } u_x \geq 0 \text{ (or } u_x \leq 0) \text{ for all } x \in (c_i, c_{i+1}); \quad (3.2.4)$$

$$[\gamma u_{xxx}](c_i) (= [\frac{1}{2}W'(u_x)](c_i)) = -2\text{sgn}^*(u_{xx}(c_i)); \quad (3.2.5)$$

$$u(0) = u(1) = 0, \quad \gamma u_{xx}(0) = \gamma u_{xx}(1) = 0. \quad (3.2.6)$$

Where we are using the same bracket notation for jump as in Yip [63], namely,

$$[f](x) = f(x^+) - f(x^-).$$

We are also using the star notation [63],  $2\text{sgn}^*(u_{xx}(c_i)) = \text{sgn}(u_x(c_i^+)) - \text{sgn}(u_x(c_i^-))$ .

Here,

$$\begin{aligned} \gamma [u_{xxx}(c_1^+) - u_{xxx}(c_1^-)] &= -2\text{sgn}^*(u_{xx}(c_1)) \\ &= -(\text{sgn}(u_x(c_1^+)) - \text{sgn}(u_x(c_1^-))) = -(-1 - 1) = 2. \end{aligned}$$

The reason why the second equality on (3.2.5) is true, is as follows:

we observe that after we integrate both sides of the Euler Lagrange equation (3.2.1) we get

$$\gamma u_{xxx} = \frac{W'(u_x)}{2} - \int_0^x \alpha u(y) dy + C. \quad (3.2.7)$$

## CHAPTER THREE

Using the bracket notation, we obtain:

$$\begin{aligned} [\gamma u_{xxx}] &= \frac{W'(u_x)(c)}{2} + \int_0^{c_1^+} u(y)dy + C - \frac{W'(u_x)(c)}{2} - \int_0^{c_1^-} u(y)dy - C, \\ &= \frac{1}{2}W'(u_x)(c_1^+) - \frac{1}{2}W'(u_x)(c_1^-) (= [\frac{1}{2}W'(u_x)(c)]), \end{aligned}$$

since  $W'(u_x) = 2(|u_x| - 1)$ ,

$$\frac{1}{2}2[u_x(c_1^+) + 1] - \frac{1}{2}2[u_x(c_1^-) - 1] = u_x(c_1^+) + 1 - u_x(c_1^-) + 1.$$

Now by (3.2.4) and by continuity of  $u_x$ ,

$$\operatorname{sgn}(u_x(c_1^-)) - \operatorname{sgn}(u_x(c_1^+)) = -(\operatorname{sgn}(u_x(c_1^+)) - \operatorname{sgn}(u_x(c_1^-))) = -2\operatorname{sgn}^*(u_{xx}(c_1)).$$

Next we will define periodic solutions.

### 3.3 Periodic solutions

**Definition 3.3.1.** *Let  $f : [0, 1] \rightarrow \mathbb{R}$  be a continuous function. We define the lap number of  $f$ , as the number of intervals of monotonicity of  $f$ .*

For example: function with lap number 2 is first increasing and then decreasing, or the other way around.

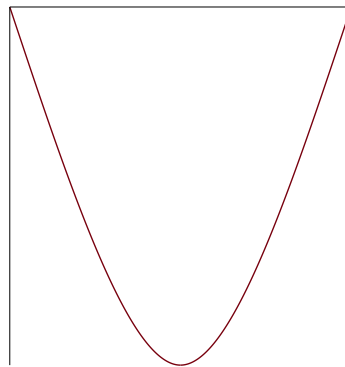


**Figure 3.1:** Example of a function with lap 2.

## CHAPTER THREE

Now, going back to equation (3.2.2), we see that in the simplest case we have only a single jump in  $u_{xxx}$ . This means that  $0 = c_0 < c_1 < c_2 = 1$  and thus any such solution would be of lap of 2.

We now define three levels of periodicity. We start with the classic definition.

**Definition 3.3.2.** A function  $f : \mathbb{R} \rightarrow \mathbb{R}$  is said to be  $P_1$ -periodic if  $\exists T > 0$  such that  $\forall x, x + T \in \mathbb{R} \quad f(x + T) = f(x)$ .

**Remark 4.** If  $f(0) = f(1)$  then for  $T = 1$  we have that  $f(0 + T) = f(0 + 1) = f(1) = f(0)$ , and thus  $f$  is  $P_1$ -periodic. In particular, if  $f(0) = f(1) = 0$ ,  $f$  is  $P_1$ -periodic.

Next we work inside  $P_1$  and allow for oscillations to occur.

**Definition 3.3.3.** A function  $f : [0, 1] \rightarrow \mathbb{R}$  is said to be  $P_2$ -periodic if  $\exists n > 1$  and  $\exists F : [0, 1] \rightarrow \mathbb{R}$  with  $F(0) = F(1) = 0, F > 0$  or  $F < 0$  on  $(0, 1)$  s.t.

$$f(x) = \text{Osc}_n F(x) \quad \forall x \in [0, 1],$$

where

$$f(x) = \text{Osc}_n F(x) = \begin{cases} F(nx) & x \in [0, \frac{1}{n}], \\ -F(n(x - \frac{1}{n})) & x \in [\frac{1}{n}, \frac{2}{n}], \\ \vdots & \\ (-1)^{n-1} F(n(x - \frac{n-1}{n})) & x \in [\frac{n-1}{n}, 1]. \end{cases}$$

**Remark 5.** An  $F$  like the one in the definition (3.3.3) (i.e.  $F(0) = F(1) = 0, F > 0$  or  $F < 0$  on  $(0, 1)$ ) acts as a building block for solutions for higher lap number (see Section 3.3.2 for more details).

Lastly, we give a definition of periodicity that also involves symmetry.

**Definition 3.3.4.** A function  $f : [0, 1] \rightarrow \mathbb{R}$  is said to be  $P_3$ -periodic (symmetric) if  $\exists n > 1$  and  $\exists F : [0, 1] \rightarrow \mathbb{R}$  with  $F(0) = F(1) = 0, F > 0$  or  $F < 0$  on

CHAPTER THREE

$(0, 1), F(x) = F(1 - x) \forall x \in [0, 1]$  such that

$$f(x) = \text{Osc}_n F(x) \quad \forall x \in [0, 1],$$

where  $\text{Osc}_n F(x)$  is defined exactly as in Definition 3.3.3.

**Remark 6.** An  $F$  like the one in the Definition (3.3.4) (i.e.  $F(0) = F(1) = 0, F > 0$  or  $F < 0$  on  $(0, 1), F(x) = F(1 - x) \forall x \in [0, 1]$ ) is a symmetric building block for symmetric solutions for higher lap number.

**Remark 7.**  $P_3 \subset P_2 \subset P_1$ .

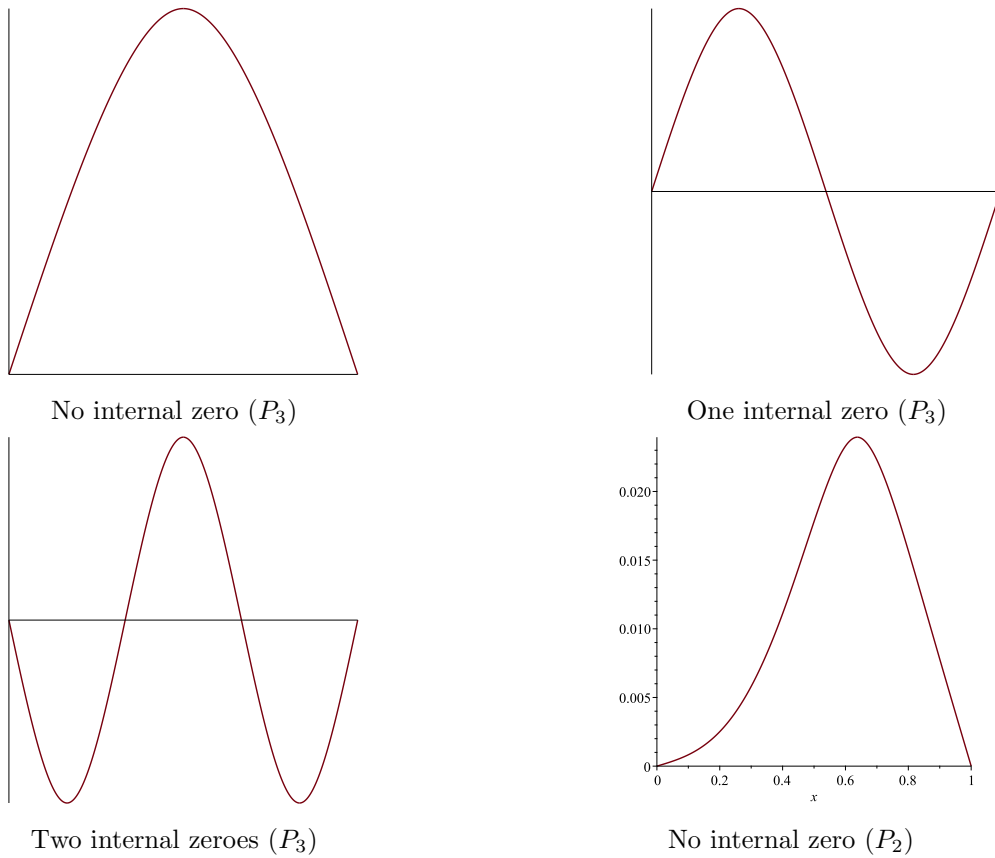


**Figure 3.3:** Examples of periodic solutions

Let  $k \geq 1$ . We denote by  $u_k$  a symmetric periodic solutions with  $k - 1$  internal zeros.

### 3.3.1 Existence of $u_1$ symmetric solutions

Let  $u_{1,\alpha,\gamma}(x)$  be the solution of the Euler-Lagrange equation with lap number 2. We have the following Theorem.

**Theorem 11.** *For all  $\gamma > 0$  and  $\alpha > 0$  there exists a unique (up to sign) symmetric solution  $u_{1,\alpha,\gamma}(x)$ .*

*Proof.* First, assume case1, namely  $1 - 4\alpha\gamma > 0$ :

We have 9 equations in total that describe a  $u \in \mathcal{Z}$  with lap 2. Namely, four equations from the boundary conditions  $u(0) = u(1) = 0$ ,  $u_{xx}(0) = u_{xx}(1) = 0$ , four equations due to continuity conditions  $u(c_1^-) = u(c_1^+)$ ,  $u_{xx}(c_1^-) = u_{xx}(c_1^+)$ ,  $u_x(c_1^-) = 0$ ,  $u_x(c_1^+) = 0$ , and finally we have one equation due to the jump  $u_{xxx}(c_1^+) - u_{xxx}(c_1^-) = \frac{2}{\gamma}$ .

By our work on Section 3.2, we also know that there should be two “segments” of solutions, one for  $x < c_1$  and one for  $x > c_1$ . More precisely:

$$\begin{cases} A_1 e^{\Lambda x} + A_2 e^{-\Lambda x} + A_3 e^{\lambda x} + A_4 e^{-\lambda x} & \text{on } [0, c_1), \\ A_5 e^{\Lambda x} + A_6 e^{-\Lambda x} + A_7 e^{\lambda x} + A_8 e^{-\lambda x} & \text{on } (c_1, 1]. \end{cases}$$

This leads to 9 unknowns total, 4 from the first segment and 4 from the second segment. We also have an additional unknown  $c_1$  for the location of the jump which we will treat as a constant, until we figure out its precise value and replace it into the equations. This naturally leads to a  $9 \times 8$  Matrix  $M$  where each row represents the exponential terms next to the unknown coefficients  $A_i$ . In other words we have a matrix equation  $M X = B$  where  $X = [A_1, A_2, \dots, A_8]^T$  and  $B = [\frac{2}{\gamma}, 0, \dots, 0]^T$ . In particular, each restriction corresponds to an equation, as seen by the following calculations:

- $u_{xxx}(c^+) - u_{xxx}(c^-) = \frac{2}{\gamma} \Leftrightarrow A_1 \Lambda^3 e^{\Lambda c} - A_2 \Lambda^3 e^{-\Lambda c} + A_3 \lambda^3 e^{\lambda c} - A_4 \lambda^3 e^{-\lambda c} - A_5 \Lambda^3 e^{\Lambda c} + A_6 \Lambda^3 e^{-\Lambda c} - A_7 \lambda^3 e^{\lambda c} + A_8 \lambda^3 e^{-\lambda c} = \frac{2}{\gamma}$ .
- $u_{xx}(c^-) - u_{xx}(c^+) = 0 \Leftrightarrow A_1 \Lambda^2 e^{\Lambda c} + A_2 \Lambda^2 e^{-\Lambda c} + A_3 \lambda^2 e^{\lambda c} + A_4 \lambda^2 e^{-\lambda c} - A_5 \Lambda^2 e^{\Lambda c} - A_6 \Lambda^2 e^{-\Lambda c} - A_7 \lambda^2 e^{\lambda c} - A_8 \lambda^2 e^{-\lambda c} = 0$ .
- $u_x(c^-) - u_x(c^+) = 0 \Leftrightarrow A_1 e^{\Lambda c} + A_2 e^{-\Lambda c} + A_3 e^{\lambda c} + A_4 e^{-\lambda c} - A_5 e^{\Lambda c} - A_6 e^{-\Lambda c} - A_7 e^{\lambda c} - A_8 e^{-\lambda c} = 0$ .

## CHAPTER THREE

- $u(1) = 0 \Leftrightarrow A_5 e^\Lambda + A_6 e^{-\Lambda} + A_7 e^\lambda + A_8 e^{-\lambda} = 0.$
- $u_x(c^-) = 0 \Leftrightarrow A_1 \Lambda e^{\Lambda c} A_2 - \Lambda e^{-\Lambda c} + A_3 \lambda e^{\lambda c} A_4 - \lambda e^{-\lambda c} = 0.$
- $u_{xx}(1) = 0 \Leftrightarrow A_5 \Lambda^2 e^\Lambda + A_6 \Lambda^2 e^{-\Lambda} + A_7 \lambda^2 e^\lambda + A_8 \lambda^2 e^{-\lambda} = 0.$
- $u_{xx}(0) = 0 \Leftrightarrow A_1 \Lambda^2 + A_2 \Lambda^2 + A_3 \lambda^2 + A_4 \lambda^2 = 0.$
- $u_x(c^+) = 0 \Leftrightarrow A_5 \Lambda e^{\Lambda c} A_6 - \Lambda e^{-\Lambda c} + A_7 \lambda e^{\lambda c} A_8 - \lambda e^{-\lambda c} = 0.$
- $u(0) = 0 \Leftrightarrow A_1 + A_2 + A_3 + A_4 = 0.$

By the Fredholm Alternative (see Section 2.3), we know that the equation  $MX = B$  has a solution iff  $B \perp \mathcal{N}(M^T)$  (This means,  $X$  is a solution for  $MX = B$  iff for all  $y \in \mathbb{R}^9$  s.t.  $M^T y = 0$  we have  $y^T B = 0$ ). Using the Fredholm alternative approach, all we have to do is find a basis for the kernel of  $M^T$  and make sure it is perpendicular to the vector  $B$ . This will yield an equation (having  $c_1$  as the only unknown) which can then solve for  $c_1$ .

Luckily we have a few things working in our favor to simplify our calculations: The vector  $B$  is mostly zero except for one entry ( $\frac{2}{\gamma}$ ), the nullspace of the ( $M^T$ ) has dimension 1 (i.e. is small) and notice also that each object (matrix, vector) is a function of  $c_1$ . Now we can use MAPLE for all the calculations, see Appendix A.5.

The 9 conditions give us the following 9 equations which they can be neatly represented as the equation  $MX = B$  where  $X = [A_1, A_2, \dots, A_8]^T$ ,  $B = [\frac{2}{\gamma}, 0, \dots, 0]^T$  and the matrix  $M$  is given by:

$$M = \begin{bmatrix} \Lambda^3 e^{\Lambda c} & -\Lambda^3 e^{-\Lambda c} & \lambda^3 e^{\lambda c} & -\lambda^3 e^{-\lambda c} & -\Lambda^3 e^{\Lambda c} & \Lambda^3 e^{-\Lambda c} & -\lambda^3 e^{\lambda c} & \lambda^3 e^{-\lambda c} \\ \Lambda^2 e^{\Lambda c} & \Lambda^2 e^{-\Lambda c} & \lambda^2 e^{\lambda c} & \lambda^2 e^{-\lambda c} & -\Lambda^2 e^{\Lambda c} & -\Lambda^2 e^{-\Lambda c} & -\lambda^2 e^{\lambda c} & -\lambda^2 e^{-\lambda c} \\ e^{\Lambda c} & e^{-\Lambda c} & e^{\lambda c} & e^{-\lambda c} & -e^{\Lambda c} & -e^{-\Lambda c} & -e^{\lambda c} & -e^{-\lambda c} \\ 0 & 0 & 0 & 0 & e^\Lambda & e^{-\Lambda} & e^\lambda & e^{-\lambda} \\ 0 & 0 & 0 & 0 & \Lambda^2 e^\Lambda & \Lambda^2 e^{-\Lambda} & \lambda^2 e^\lambda & \lambda^2 e^{-\lambda} \\ 0 & 0 & 0 & 0 & \Lambda e^{\Lambda c} & -\Lambda e^{-\Lambda c} & \lambda e^{\lambda c} & -\lambda e^{-\lambda c} \\ \Lambda e^{\Lambda c} & -\Lambda e^{-\Lambda c} & \lambda e^{\lambda c} & -\lambda e^{-\lambda c} & 0 & 0 & 0 & 0 \\ \Lambda^2 & \Lambda^2 & \lambda^2 & \lambda^2 & 0 & 0 & 0 & 0 \\ 1 & 1 & 1 & 1 & 0 & 0 & 0 & 0 \end{bmatrix}.$$

Maple shows that the nullspace of  $M^T$  is one-dimensional for all  $c_1$ , as shown by its

CHAPTER THREE

reduced row echelon form depicted below, which only has 1 row of zeroes.

$$\begin{bmatrix} 1 & 0 & 0 & 0 & 0 & 0 & 0 & 0 & 0 \\ 0 & 1 & 0 & 0 & 0 & 0 & 0 & 0 & 0 \\ 0 & 0 & 1 & 0 & 0 & 0 & 0 & 0 & 0 \\ 0 & 0 & 0 & 1 & 0 & 0 & 0 & 0 & 0 \\ 0 & 0 & 0 & 0 & 1 & 0 & 0 & 0 & 0 \\ 0 & 0 & 0 & 0 & 0 & 1 & 0 & 0 & 0 \\ 0 & 0 & 0 & 0 & 0 & 0 & 1 & 0 & 0 \\ 0 & 0 & 0 & 0 & 0 & 0 & 0 & 1 & 0 \\ 0 & 0 & 0 & 0 & 0 & 0 & 0 & 0 & 1 \\ 0 & 0 & 0 & 0 & 0 & 0 & 0 & 0 & 0 \end{bmatrix}.$$

A basis for the null space  $\mathcal{N}(M^T)$  is given by  $y = [y_1, y_2, y_3, y_4, y_5, y_6, y_7, y_8, 1]^T \in \mathbb{R}^9$ , where  $y_1 = \frac{F}{D}$ , with

$$F = \begin{cases} e^{(2c-1)\Lambda-\lambda} - e^{(2c-1)\lambda-\Lambda} - e^{-2\Lambda c+\Lambda-\lambda} + e^{(2c-1)\lambda+\Lambda} \\ +e^{-2c\lambda-\Lambda+\lambda} - e^{(2c-1)\Lambda+\lambda} - e^{-2c\lambda+\Lambda+\lambda} + e^{-2\Lambda c+\Lambda+\lambda}, \end{cases}$$

and

$$D = \begin{cases} 2\Lambda(\Lambda e^{(c-1)\lambda-\Lambda} - \Lambda e^{(c-1)\lambda+\Lambda} + \Lambda e^{-c\lambda-\Lambda+\lambda} - \Lambda e^{-c\lambda+\Lambda+\lambda} \\ +\lambda e^{(c-1)\Lambda+\lambda} - \lambda e^{(c-1)\Lambda-\lambda} + \lambda e^{-c\Lambda+\Lambda+\lambda} - \lambda e^{-c\Lambda+\Lambda-\lambda}). \end{cases}$$

**Note:** As the following calculation illustrates the other values of  $y$  (namely  $y_i$  for  $i \geq 2$ ) do not matter since they are multiplied by the zeroes of the vector  $B$ .

By Fredholm Alternative we want that  $\langle Y, B \rangle = 0$ , which means

$$\langle [y_1, y_2, y_3, y_4, y_5, y_6, y_7, y_8, y_9], [\frac{2}{\gamma}, 0, 0, 0, 0, 0, 0, 0, 0] \rangle = 0,$$

and thus

$$y_1 \cdot \frac{2}{\gamma} = 0 \Rightarrow \frac{F}{D} \cdot \frac{2}{\gamma} = 0 \Rightarrow \frac{2F}{\gamma D} = 0 \Rightarrow F = 0.$$

CHAPTER THREE

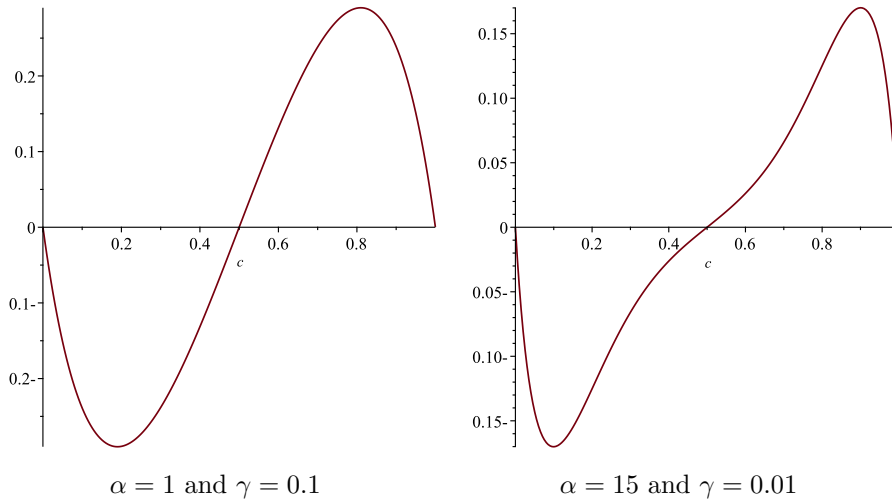


**Figure 3.5:** Location of the jump for different values of  $\alpha$  and  $\gamma$ .

**Remark 8.** We can rewrite  $F(c)$  as term of the sinh function

$$F(c) = \sinh[(2c - 1)\lambda] \sinh(\Lambda) - \sinh[(2c - 1)\Lambda] \sinh(\lambda) = 0. \quad (3.3.1)$$

First of all, we observe that  $F(0) = F(1) = F(\frac{1}{2}) = 0$ . We will show that these are the only possible roots regardless of  $\alpha$  and  $\gamma$  (provided that  $1 - 4\alpha\gamma > 0$ ).

For simplicity, let  $a = 2c - 1$ . Then we notice that  $F(c) \geq 0$  if and only if

$$\sinh[(a)\Lambda] \sinh(\lambda) - \sinh[(a)\lambda] \sinh(\Lambda) \geq 0,$$

dividing by  $[\sinh(\lambda) \sinh(\Lambda)]$ , we get

$$\frac{\sinh(a\Lambda)}{\sinh(\Lambda)} \geq \frac{\sinh(a\lambda)}{\sinh(\lambda)}.$$

Let

$$F_a(x) = \frac{\sinh(ax)}{\sinh(x)},$$

since  $\lambda \leq \Lambda$  it is enough to show that  $F_a(x)$  is increasing.

We need a proposition as proved in [54]:

## CHAPTER THREE

**Proposition 1.** [54] Suppose that  $f(a^+) = g(a^+) = 0$  or  $f(a^-) = g(a^-) = 0$ . (Then  $g$  is non-zero and does not change sign on  $(a, b)$ , since  $g'$  is so.)

(1) If  $\frac{f'}{g'}$  is increasing on  $(a, b)$  then  $(\frac{f}{g})' > 0$  on  $(a, b)$ .

(2) If  $\frac{f'}{g'}$  is decreasing on  $(a, b)$  then  $(\frac{f}{g})' < 0$  on  $(a, b)$ .

Now, using the above proposition, it is enough to show that  $\frac{f'}{g'}$  is increasing where  $f(x) = \sinh(ax)$  and  $g(x) = \sinh(x)$ . Notice that:

- $f$  and  $g$  are differentiable on  $(0, 1)$ ,
- $g' = \cosh(x) = \frac{e^x + e^{-x}}{2} > 0$  on  $(0, 1)$ ,
- $f(0^+) = g(0^+) = 0$ .

We will now show that  $\frac{f'}{g'}$  is monotonic on  $(0, 1)$ . Let  $h_a = \frac{f'}{g'}$ , where

$$\begin{cases} f' = [\sinh(ax)]' = a \cosh(ax) \\ g' = [\sinh(x)]' = \cosh(x) \end{cases}, \quad -1 < a < 1.$$

So,

$$h_a(x) = \frac{a \cosh(ax)}{\cosh(x)} = \frac{a \left( \frac{e^{ax} + e^{-ax}}{2} \right)}{\frac{e^x + e^{-x}}{2}} = a \frac{e^{ax} + e^{-ax}}{e^x + e^{-x}}.$$

Our goal is to show that  $h_a(x)$  is monotonic on  $(0, 1)$  by showing that  $h'_a(x) > 0$  or  $h'_a(x) < 0$ . Towards that goal we have the following calculations:

$$\begin{aligned} h'_a(x) &= a \frac{(e^{ax} + e^{-ax})'(e^x + e^{-x}) - (e^{ax} + e^{-ax})(e^x + e^{-x})'}{(e^x + e^{-x})^2}, \\ &= \frac{a [(1-a)[e^{-x(a+1)} - e^{x(a+1)}] + (a+1)[e^{-x(1-a)} - e^{x(1-a)}]}{(e^x + e^{-x})^2}, \end{aligned}$$

which is negative since  $x \geq 0$ ,  $1+a \geq 0$ ,  $1-a \geq 0$  and  $e^x$  is increasing.

- If  $0 < a < 1$ , we have  $h'_a < 0$  which means  $h_a = \frac{f'}{g'}$  is decreasing, then by Proposition 1 we know that  $(\frac{f}{g})' < 0$ , so  $F_a = \frac{f}{g}$  is decreasing. We conclude that  $F_a(\Lambda) < F_a(\lambda)$ .

## CHAPTER THREE

- Similarly, if  $-1 < a < 1$ , then  $h'_a > 0$  which means  $h_a = \frac{f'}{g}$  is increasing. By Proposition 1 we know that  $(\frac{f}{g})' > 0$  and thus,  $F_a = \frac{f}{g}$  is increasing. We conclude that  $F_a(\Lambda) > F_a(\lambda)$ .

Hence the only time that  $F(c) = 0$  is exactly when  $F_a(\Lambda) = F_a(\lambda)$  which happens when  $a = 0$ , so that  $c = \frac{1}{2}$ , or  $a = \pm 1$ . We proved that  $F(0) = F(1) = F(\frac{1}{2}) = 0$  are the only possible roots regardless of  $\alpha$  and  $\gamma$ .

For case 2 when  $1 - 4\alpha\gamma = 0$ : The 9 conditions give us 9 equations which they can be represented in the following matrix equation  $MX = B$  where  $X = [A_1, A_2, \dots, A_8]^T$ ,  $B = [\frac{2}{\gamma}, 0, \dots, 0]^T$  and

$$M = \begin{bmatrix} -d^3e^{dc} & -3d^2e^{dc} - cd^3e^{dc} & d^3e^{-dc} & -3d^2e^{-dc} + cd^3e^{-dc} & d^3e^{dc} & 3d^2e^{dc} + cd^3e^{dc} & -d^3e^{-dc} & 3d^2e^{-dc} - cd^3e^{-dc} \\ d^2 & 2d & d^2 & -2d & 0 & 0 & 0 & 0 \\ de^{dc} & e^{dc} + cde^{dc} & -de^{-dc} & e^{-dc} - cde^{-dc} & 0 & 0 & 0 & 0 \\ 0 & 0 & 0 & 0 & e^d & e^d & e^{-d} & e^{-d} \\ 0 & 0 & 0 & 0 & d^2e^d & 2de^d + d^2e^d & d^2e^{-d} & -2de^{-d} + d^2e^{-d} \\ 0 & 0 & 0 & 0 & de^{dc} & e^{dc} + cde^{dc} & -de^{-dc} & e^{-dc} - cde^{-dc} \\ e^{dc} & ce^{dc} & e^{-dc} & ce^{-dc} & -e^{dc} & -ce^{dc} & -e^{-dc} & -ce^{-dc} \\ d^2e^{dc} & 2de^{dc} + cd^2e^{dc} & d^2e^{-dc} & -2de^{-dc} + cd^2e^{-dc} & -d^2e^{dc} & -2de^{dc} - cd^2e^{dc} & -d^2e^{-dc} & 2de^{-dc} - cd^2e^{-dc} \\ 1 & 0 & 1 & 0 & 0 & 0 & 0 & 0 \end{bmatrix}.$$

A similar approach to what we did above leads to the following equations when  $1 - 4\alpha\gamma = 0$ :

$$F_2(c) = (c - 1) \sinh(2dc) - c \sinh(2d(c - 1)) = 0.$$

So we have that  $F_2(c) = 0$  iff  $c = 0, \frac{1}{2}$  or  $1$ .

Now for  $F_3(c)$  when  $1 - 4\alpha\gamma < 0$ : We can calculate  $F_3$  either through the Fredholm Alternative or by using  $F_1(c)$  directly. Specifically, we know that  $\Lambda = t + i\omega$ , and  $\lambda = t - i\omega$ . We also know Euler's identity:

$$e^{i\theta} = \cos(\theta) + i \sin(\theta) \Rightarrow e^{2i\omega c} = \cos(2\omega c) + i \sin(2\omega c).$$

## CHAPTER THREE

We can use the above and replace the values of  $\Lambda$  and  $\lambda$  in  $F_1(c)$ . After some straightforward algebra and a few convenient cancellations we get:

$$\begin{aligned} F_3(c) &= 2i [e^{2t(c-1)} \sin(2\omega c) - e^{-2t(c-1)} \sin(2\omega c) + e^{2ct} \sin(2\omega(c-1)) - e^{-2ct} \sin(2\omega(c-1))] = 0, \\ &= \sin(2\omega c) [e^{2t(c-1)} - e^{-2t(c-1)}] - \sin(2\omega(c-1)) [e^{2ct} - e^{-2ct}] = 0, \\ &= \sin(2\omega c) \sinh(2t(c-1)) - \sin(2\omega(c-1)) \sinh(2tc) = 0. \end{aligned}$$

For the third case we have other roots that lead to non-symmetric solutions. These alternative locations for the jump occur for certain pairs of  $(\alpha, \gamma)$ . Of course, it is still true regardless of  $\alpha$  and  $\gamma$  that  $F_3(\frac{1}{2}) = 0$ , so we always have a symmetric solution. We investigate these non-symmetric solutions in section (3.3.3) below.  $\square$

**Remark 9** (Justification of symmetric solution when  $c = \frac{1}{2}$ ).

For  $u$  to be symmetric at  $c = \frac{1}{2}$ , we need  $u(\frac{1}{2} - x) = u(\frac{1}{2} + x) \quad \forall x \in [0, \frac{1}{2}]$ , which is the same as:

$$\begin{aligned} A_1 e^{\Lambda(\frac{1}{2}-x)} + A_2 e^{-\Lambda(\frac{1}{2}-x)} + A_3 e^{\lambda(\frac{1}{2}-x)} + A_4 e^{-\lambda(\frac{1}{2}-x)} &= A_5 e^{\Lambda(\frac{1}{2}+x)} + A_6 e^{-\Lambda(\frac{1}{2}+x)} + A_7 e^{\lambda(\frac{1}{2}+x)} + A_8 e^{-\lambda(\frac{1}{2}+x)}, \\ A_2 e^{-\frac{\Lambda}{2}} e^{\Lambda x} + A_1 e^{\frac{\Lambda}{2}} e^{-\Lambda x} + A_4 e^{-\frac{\lambda}{2}} e^{\lambda x} + A_3 e^{\frac{\lambda}{2}} e^{-\lambda x} &= A_5 e^{-\frac{\Lambda}{2}} e^{\Lambda x} + A_6 e^{\frac{\Lambda}{2}} e^{-\Lambda x} + A_7 e^{-\frac{\lambda}{2}} e^{\lambda x} + A_8 e^{\frac{\lambda}{2}} e^{-\lambda x}. \end{aligned}$$

Since the above is true for all  $x \in [0, \frac{1}{2}]$ , it holds if and only if

1.  $A_2 e^{-\frac{\Lambda}{2}} = A_5 e^{\frac{\Lambda}{2}} \Rightarrow \frac{A_2}{A_5} = e^{\Lambda}$ .
2.  $A_1 e^{\frac{\Lambda}{2}} = A_6 e^{-\frac{\Lambda}{2}} \Rightarrow \frac{A_1}{A_6} = e^{\Lambda}$ .
3.  $A_4 e^{-\frac{\lambda}{2}} = A_7 e^{\frac{\lambda}{2}} \Rightarrow \frac{A_4}{A_7} = e^{\lambda}$ .
4.  $A_3 e^{\frac{\lambda}{2}} = A_8 e^{-\frac{\lambda}{2}} \Rightarrow \frac{A_3}{A_8} = e^{\lambda}$ .

The calculation above yields a necessary and sufficient condition for  $u$  to be symmetric around  $c = \frac{1}{2}$ . In other words,  $u$  is symmetric if and only if the 4 ratios described above are satisfied. A quick calculation (using MAPLE, see Appendix A.5) shows that this is indeed the case, i.e. the 4 ratios are satisfied. We conclude that the solution is symmetric and only symmetric at  $c = \frac{1}{2}$ .

**Remark 10.** Conjecture 10 says that if  $\alpha$  is sufficiently large ( $\alpha > k^2 \pi^2$  where  $k$  is an integer) then the EL has no solution with less than  $(k-1)$  internal zero. In particular,

### CHAPTER THREE

when  $\alpha$  is large, all solutions have internal zeros. But the theorem above contradicts that fact, since we know that there should be a solution without internal zeroes regardless of how large  $\alpha$  is. This disproves conjecture 10 and shows that the Müller problem [47] and the Yip problem [63] are very different.

Now let us go back to case 1 where  $1 - 4\alpha\gamma > 0$ . we have shown that  $c = \frac{1}{2}$  is always a solution to (3.3.1) which in turn means that there is always a solution to the Euler Lagrange equation that has a jump at  $c = \frac{1}{2}$ . In particular we can plug in this value of  $c$  to the matrix  $M$  from above and get:

$$\begin{bmatrix} -\Lambda^3 e^{\Lambda/2} & \Lambda^3 e^{-\Lambda/2} & -\lambda^3 e^{\lambda/2} & \lambda^3 e^{-\lambda/2} & \Lambda^3 e^{\Lambda/2} & -\Lambda^3 e^{-\Lambda/2} & \lambda^3 e^{\lambda/2} & -\lambda^3 e^{-\lambda/2} \\ 1 & 1 & 1 & 1 & 0 & 0 & 0 & 0 \\ \Lambda^2 & \Lambda^2 & \lambda^2 & \lambda^2 & 0 & 0 & 0 & 0 \\ \Lambda e^{\Lambda/2} & -\Lambda e^{-\Lambda/2} & \lambda e^{\lambda/2} & -\lambda e^{-\lambda/2} & 0 & 0 & 0 & 0 \\ 0 & 0 & 0 & 0 & e^\Lambda & e^{-\Lambda} & e^\lambda & e^{-\lambda} \\ 0 & 0 & 0 & 0 & \Lambda^2 e^\Lambda & \Lambda^2 e^{-\Lambda} & \lambda^2 e^\lambda & \lambda^2 e^{-\lambda} \\ 0 & 0 & 0 & 0 & \Lambda e^{\Lambda/2} & -\Lambda e^{-\Lambda/2} & \lambda e^{\lambda/2} & -\lambda e^{-\lambda/2} \\ \Lambda^2 e^{\Lambda/2} & \Lambda^2 e^{-\Lambda/2} & \lambda^2 e^{\lambda/2} & \lambda^2 e^{-\lambda/2} & -\Lambda^2 e^{\Lambda/2} & -\Lambda^2 e^{-\Lambda/2} & -\lambda^2 e^{\lambda/2} & -\lambda^2 e^{-\lambda/2} \\ e^{\Lambda/2} & e^{-\Lambda/2} & e^{\lambda/2} & e^{-\lambda/2} & -e^{\Lambda/2} & -e^{-\Lambda/2} & -e^{\lambda/2} & -e^{-\lambda/2} \end{bmatrix}.$$

From there, we can use  $MX = B$  and solve for  $X$ , where  $X = [x_1, x_2, x_3, x_4, x_5, x_6, x_7, x_8]^T$ . For example, for  $\alpha = 10$  and  $\gamma = 0.01$  we have

$$X(10, 0.01) = \begin{bmatrix} -0.0012342496 \\ 0.0012342496 \\ 0.0693587456 \\ -0.0693587452 \\ 0.0000001001 \\ -15.2161800696 \\ -0.0024161742 \\ 1.9910135560 \end{bmatrix},$$

## CHAPTER THREE

which gives us the following graph

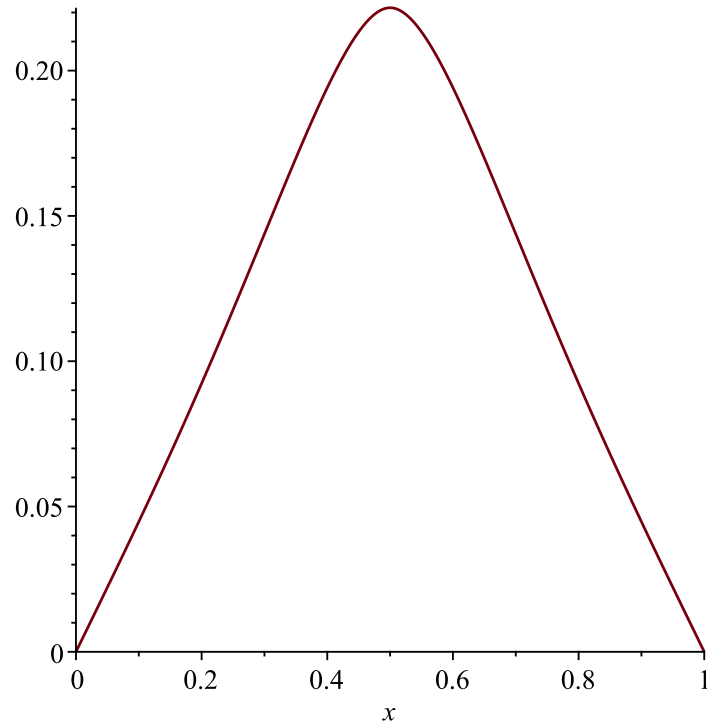


**Figure 3.6:** Example of a symmetric solution where  $\alpha = 10$  and  $\gamma = 0.01$ .

**Remark 11.** Notice that the solution  $u$  in Figure 3.6, has no internal zeroes. This is relevant, because as we will see in the next sections we can use that solution as a “building block” to create more solutions with higher lap number and internal zeroes.

### 3.3.2 Existence of $u_k$ (periodic) solutions, $k > 1$

Let  $\alpha > 0$ ,  $\gamma > 0$ . Now that we have a solution  $u_{1,\alpha,\gamma}$  of the Euler-Lagrange equation with lap number 2, we can use it to construct more complex solutions to the Euler-Lagrange equation with higher lap numbers.

It turns out that we can use  $u_1$  as a building block (and in a unique way) to formulate solutions of higher order. In particular, we can scale and construct multiple copies of  $u_1$  for different values of the parameters  $\alpha$  and  $\gamma$ .

## CHAPTER THREE

Let  $u_{n,\alpha,\gamma}(x)$  be the following expression:

$$u_{n,\alpha,\gamma} = \frac{1}{n} \sum_{k=0}^{n-1} (-1)^k u_{1,\alpha',\gamma'} \left( n \left( x - \frac{k}{n} \right) \right) \chi_{\left[ \frac{k}{n}, \frac{k+1}{n} \right]}, \quad (3.3.2)$$

where  $\alpha' = f(\alpha, n)$ ,  $\gamma' = g(\gamma, n)$  and  $u_{1,\alpha',\gamma'}$  is a solution of the Euler-Lagrange equation of lap 2 and parameters  $\alpha', \gamma'$ .

The expression above is the unique solution of lap number  $n+1$  ( $n-1$  internal zeroes). We therefore have the following Theorem.

**Theorem 12.** *Let  $\alpha > 0$  and  $\gamma > 0$ ,  $\alpha' = \frac{\alpha}{n^2}$ ,  $\gamma' = \gamma n^2$ . For those values  $u_{n,\alpha,\gamma}(x)$  is the unique (up to reflection) periodic solution to the Euler-Lagrange equation of  $n-1$  internal zeroes (lap number  $n+1$ ).*

*Proof.* Let  $\gamma > 0$  and  $\alpha > 0$ ,  $\alpha' = \frac{\alpha}{n^2}$ ,  $\gamma' = \gamma n^2$ . We will show that the  $u_{n,\alpha,\gamma}$  defined above (3.3.2) is the unique periodic solution we are looking for. By construction,  $u_{n,\alpha,\gamma}$  is periodic. We will show the following:

- $u_{n,\alpha,\gamma}$  defined above is a solution of the Euler-Lagrange equation (3.2.2).
- $u_{n,\alpha,\gamma}$  satisfies the boundary conditions  $u(0) = u(1) = 0$ ,  $u_{xx}(0) = u_{xx}(1) = 0$ .
- $u_{n,\alpha,\gamma}$  satisfies the jump condition  $u_{xxx}(c_1^+) - u_{xxx}(c_1^-) = \frac{2}{\gamma}$ .
- $u_{n,\alpha,\gamma}$  clearly satisfies the other conditions too ( $u(c_1^-) = u(c_1^+)$ ,  $u_{xx}(c_1^-) = u_{xx}(c_1^+)$ ,  $u_x(c_1^-) = 0$ ,  $u_x(c_1^+) = 0$ ).
- $u_{n,\alpha,\gamma}$  is unique (i.e. there are no other periodic solution of the Euler-Lagrange equation).

First we show that (3.3.2) is a solution of the Euler-Lagrange equation. Towards that, let  $x \in [0, 1]$ . There exists  $k < n$  such that  $x \in \left[ \frac{k}{n}, \frac{k+1}{n} \right]$ . By its definition,  $u_{n,\alpha,\gamma}$  satisfies the Euler-Lagrange equation if and only if:

$$\gamma [(-1)^k u_{1,\alpha',\gamma'} \left( n \left( x - \frac{k}{n} \right) \right)]_{xxx} - [(-1)^k u_{1,\alpha',\gamma'} \left( n \left( x - \frac{k}{n} \right) \right)]_{xx} + \alpha (-1)^k u_{1,\alpha',\gamma'} \left( n \left( x - \frac{k}{n} \right) \right) = 0,$$

### CHAPTER THREE

$$\cancel{(-1)^k} \gamma n^4 [u_{1,\alpha',\gamma'}]_{xxxx} \left(n\left(x - \frac{k}{n}\right)\right) - \cancel{(-1)^k} n^2 [u_{1,\alpha',\gamma'}]_{xx} \left(n\left(x - \frac{k}{n}\right)\right) + \cancel{(-1)^k} \alpha u_{1,\alpha',\gamma'} \left(n\left(x - \frac{k}{n}\right)\right) = 0. \quad (3.3.3)$$

For convenience, let's do the following change of variables. Let

$$y = n\left(x - \frac{k}{n}\right). \quad (3.3.4)$$

But we know  $\frac{k}{n} < x < \frac{k+1}{n}$  which means  $0 < x - \frac{k}{n} < \frac{1}{n}$  and using (3.3.4) we get  $0 < y < 1$ . Now we can rewrite (3.3.3) as

$$\gamma n^4 [u_{1,\alpha',\gamma'}]_{xxxx}(y) - n^2 [u_{1,\alpha',\gamma'}]_{xx}(y) + \alpha u_{1,\alpha',\gamma'}(y) = 0 \quad \forall y \in [0, 1],$$

dividing by  $n^2$  we get

$$\gamma n^2 [u_{1,\alpha',\gamma'}]_{xxxx}(y) - [u_{1,\alpha',\gamma'}]_{xx}(y) + \frac{\alpha}{n^2} u_{1,\alpha',\gamma'}(y) = 0.$$

Since we know that  $\alpha' = \frac{\alpha}{n^2}$  and  $\gamma' = \gamma n^2$ , the above becomes

$$\gamma' [u_{1,\alpha',\gamma'}]_{xxxx}(y) - [u_{1,\alpha',\gamma'}]_{xx}(y) + \alpha' u_{1,\alpha',\gamma'}(y) = 0 \quad (y \in (0, 1)),$$

which is of course a true statement since  $u_{1,\alpha',\gamma'}$  is a solution to the Euler-Lagrange equation with parameters  $\alpha', \gamma'$ .

Next, we will show that  $u_{n,\alpha,\gamma}$  satisfies the jump condition, namely

$$[u_{n,\alpha,\gamma}]_{xxx} = \frac{2}{\gamma},$$

applying that into (3.3.2) and using the chain rule and the fact that  $u_1$  satisfies the jump condition, we get

$$n^2 \frac{2}{\gamma n^2} = \frac{2}{\gamma} \Leftrightarrow n^2 \frac{2}{\gamma'} = \frac{2}{\gamma} \Leftrightarrow \gamma' = \gamma n^2,$$

which is a true statement. Thus the jump condition holds too.

### CHAPTER THREE

Thirdly, we show that  $u_{n,\alpha,\gamma}$  satisfies the boundary conditions. Clearly,

$$u_{n,\alpha,\gamma}(0) \stackrel{(k=0)}{=} \frac{1}{n}(-1)^0 u_{1,\alpha',\gamma'}(n(0 - \frac{0}{n})) = \frac{1}{n}(-1)^0 \cancel{u_{1,\alpha',\gamma'}(0)} = 0,$$

(because  $u_{1,\alpha',\gamma'}$  satisfies the boundary conditions). Similarly,

$$u_{n,\alpha,\gamma}(1) \stackrel{(k=n-1)}{=} \frac{1}{n}(-1)^{n-1} u_{1,\alpha',\gamma'}(n(1 - \frac{n-1}{n})) = \frac{1}{n}(-1)^{n-1} \cancel{u_{1,\alpha',\gamma'}(1)} = 0.$$

For notational simplicity let  $u = u_{n,\alpha,\gamma}$ ,  $v = u_{1,\alpha',\gamma'}$ . We have

$$u_{xx}(0) \stackrel{(k=0)}{=} \frac{1}{n}(-1)^0 n^2 v_{xx}(n(0 - \frac{0}{n})) = n \cancel{v_{xx}(0)} = 0.$$

We also have

$$u_{xx}(1) \stackrel{(k=n-1)}{=} \frac{1}{n}(-1)^{n-1} n^2 v_{xx}(n(1 - \frac{n-1}{n})) = n(-1)^{n-1} \cancel{v_{xx}(1)} = 0.$$

Moreover, we need to prove that  $u_{xx}(\frac{1}{n}) = 0$ . Let  $v$  be a periodic solution. We know that  $v$  is odd around  $x = \frac{1}{n}$  which means

$$v(\frac{1}{n} + \epsilon) = -v(\frac{1}{n} - \epsilon),$$

using Taylor expansion, we get

$$v(\frac{1}{n}) + \epsilon v_x(\frac{1}{n}) + \frac{\epsilon^2}{2} v_{xx}(\frac{1}{n}) + \dots = -(v(\frac{1}{n}) - \epsilon v_x(\frac{1}{n}) + \frac{\epsilon^2}{2} v_{xx}(\frac{1}{n}) \dots),$$

after a few convenient cancellations we arrive at:

$$\epsilon^2 v_{xx}(\frac{1}{n}) + \frac{2\epsilon^4}{4!} v_{xxxx}(\frac{1}{n}) + \dots = 0.$$

Since the above is a polynomial expression of  $\epsilon > 0$  (and true for all  $\epsilon > 0$ ), we conclude that:

$$v_{xx}(\frac{1}{n}) = v_{xxxx}(\frac{1}{n}) = \dots = 0.$$

## CHAPTER THREE

In particular  $v_{xx}(\frac{1}{n}) = 0$ .

Also, by construction and since  $u_{1,\alpha',\gamma'}$  is a solution,  $u_{n,\alpha,\gamma}$  satisfies all the continuity conditions.

Lastly, we prove uniqueness. Towards that, let  $u_{n,\alpha,\gamma}^1$  and  $u_{n,\alpha,\gamma}^2$  be two periodic solutions with  $n - 1$  internal zeroes. That is

$$u_{n,\alpha,\gamma}^1 = \frac{1}{n} \sum_{k=0}^{n-1} (-1)^k u^1(n(x - \frac{k}{n})) \chi_{[\frac{k}{n}, \frac{k+1}{n}]},$$

$$u_{n,\alpha,\gamma}^2 = \frac{1}{n} \sum_{k=0}^{n-1} (-1)^k u^2(n(x - \frac{k}{n})) \chi_{[\frac{k}{n}, \frac{k+1}{n}]}$$

where  $u^1$  and  $u^2$  are two symmetric functions of no internal zeroes.

By the work above we know that  $u^1 = u_{1,\alpha',\gamma'}^1, u^2 = u_{1,\alpha',\gamma'}^2$  are solutions of the Euler-Lagrange equation for  $\alpha' = \frac{\alpha}{n^2}$  and  $\gamma' = \gamma n^2$ . However, by Theorem 11 (uniqueness of solution of lap number 2 for a fixed pair  $(\alpha', \gamma')$ ) we must have  $u^1 = u^2$ . Thus,  $u_{n,\alpha,\gamma}^1 = u_{n,\alpha,\gamma}^2$  which completes the proof of uniqueness. □

**Remark 12.** *The proof above states that a periodic solution  $u_{n,\alpha,\gamma}$  is uniquely determined by the solution  $u_{1,\frac{\alpha}{n^2},\gamma n^2}$ . It should be clear that the converse is also true, namely given  $u_{1,\alpha,\gamma}$  be the periodic solution of lap 2,  $u_{n,\alpha n^2,\frac{\gamma}{n^2}}$  is the unique periodic solution of lap  $n + 1$  for  $\alpha' = \alpha n^2$  and  $\gamma' = \frac{\gamma}{n^2}$ .*

*In other words, there is 1 - 1 correspondence between  $u_{1,\alpha_1,\gamma_1}$  and  $u_{n,\alpha_2,\gamma_2}$  with  $(\alpha_2, \gamma_2) = (\alpha_1 n^2, \frac{\gamma_1}{n^2})$  ( or equivalently  $(\alpha_1, \gamma_1) = (\frac{\alpha_2}{n^2}, \gamma_2 n^2)$ ). This correspondence combined with the fact that every periodic solution can be written as  $u_{n,\alpha,\gamma}$  (for appropriate,  $\alpha > 0, \gamma > 0$  and  $n \in \mathbb{N}$ ) provides us with a complete characterization of all periodic solutions.*

Below, we present some concrete examples. For instance, let  $\alpha = 1$  and  $\gamma = 0.1$ . We can calculate the location of the jump  $c = 0.5$ . Then,  $u_{1,\alpha,\gamma} = u_{1,1,0.1} = u_1$  is given by

## CHAPTER THREE

the following two segments:

$$u_1^l(x) = \begin{cases} -0.09300746171 e^{2.978755335x} + 0.09300746171 e^{-2.978755335x} \\ +0.5313995522 e^{1.061610406x} - 0.5313995522 e^{-1.061610406x} \end{cases}, \quad 0 \leq x \leq 0.5,$$

$$u_2^r(x) = \begin{cases} 0.004729996162 e^{2.978755335x} - 1.828836151 e^{-2.978755335x} \\ -0.1838102153 e^{1.061610406x} + 1.536288311 e^{-1.061610406x}. \end{cases}, \quad 0.5 \leq x \leq 1.$$

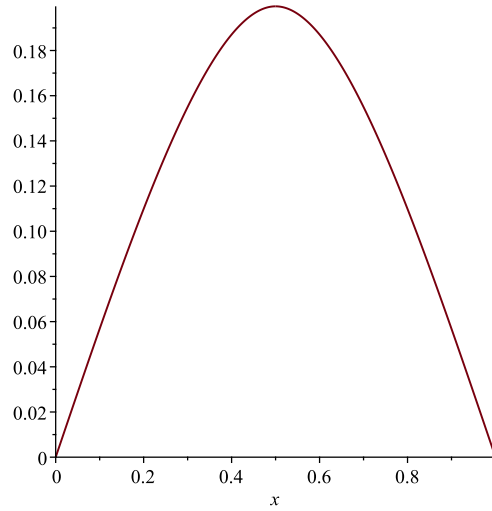


**Figure 3.7:** Symmetric solution of lap 2 where  $\alpha = 1, \gamma = 0.1$ .

We can also calculate  $u_{1, \frac{1}{2^2}, 0.1(2^2)}$  in a similar way. This will be important for the calculation of  $u_{2,1,0.1}$  which depends on  $u_{1, \frac{1}{4}, 0.4}$ . In particular, for  $\alpha = 1, \gamma = 0.1, \alpha' = \frac{\alpha}{2^2}, \gamma' = \gamma 2^2$ , we have:

$$u_{2,\alpha,\gamma} = \frac{1}{2} \left[ u_{1,\alpha',\gamma'}(2x)\chi_{[0,\frac{1}{2}]} - u_{1,\alpha',\gamma'}[2(x - \frac{1}{2})]\chi_{[\frac{1}{2},1]} \right],$$

and its graph is given by:

CHAPTER THREE

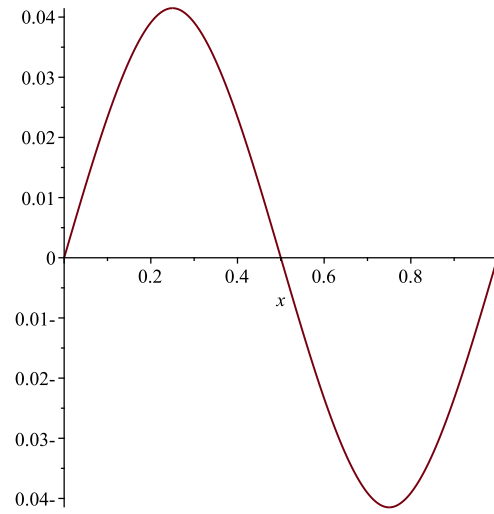


**Figure 3.8:** Periodic solution of lap 3,  $u_{2,1,0.1}$

Similarly,  $u_3, u_4, u_5$  and  $u_6$  are given by the following expressions and graphs.

$$u_{3,\alpha,\gamma} = \frac{1}{3} \left[ u_{1,\alpha',\gamma'}(3x)\chi_{[0,\frac{1}{3}]} - u_{1,\alpha',\gamma'}\left[3\left(x - \frac{1}{3}\right)\right]\chi_{[\frac{1}{3},\frac{2}{3}]} + u_{1,\alpha',\gamma'}\left[3\left(x - \frac{2}{3}\right)\right]\chi_{[\frac{2}{3},1]} \right],$$

$$u_{4,\alpha,\gamma} = \frac{1}{4} \left[ u_{1,\alpha',\gamma'}(4x)\chi_{[0,\frac{1}{4}]} - u_{1,\alpha',\gamma'}\left[4\left(x - \frac{1}{4}\right)\right]\chi_{[\frac{1}{4},\frac{2}{4}]} + u_{1,\alpha',\gamma'}\left[4\left(x - \frac{2}{4}\right)\right]\chi_{[\frac{2}{4},\frac{3}{4}]} - u_{1,\alpha',\gamma'}\left[4\left(x - \frac{3}{4}\right)\right]\chi_{[\frac{3}{4},1]} \right].$$

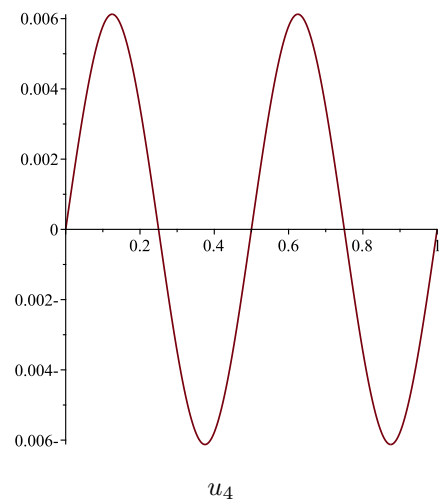
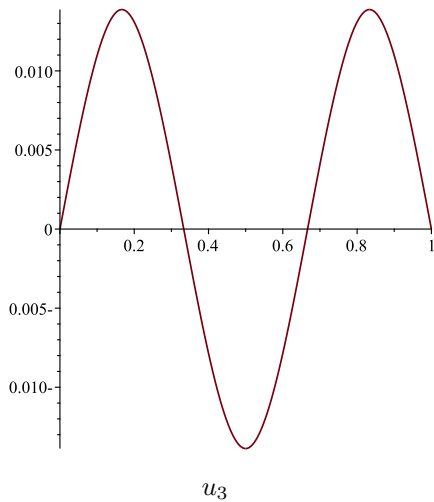


**Figure 3.10:** Example of finding  $u_3$  and  $u_4$  where  $\alpha = 1, \gamma = 0.1$ .

## CHAPTER THREE

$$u_{5,\alpha,\gamma} = \frac{1}{5} \left[ u_{1,\alpha',\gamma'}(5x)\chi_{[0,\frac{1}{5}]} - u_{1,\alpha',\gamma'}[5(x - \frac{1}{5})]\chi_{[\frac{1}{5},\frac{2}{5}]} + u_{1,\alpha',\gamma'}[5(x - \frac{2}{5})]\chi_{[\frac{2}{5},\frac{3}{5}]} - u_{1,\alpha',\gamma'}[5(x - \frac{3}{5})]\chi_{[\frac{3}{5},\frac{4}{5}]} + u_{1,\alpha',\gamma'}[5(x - \frac{4}{5})]\chi_{[\frac{4}{5},1]} \right],$$

$$u_{6,\alpha,\gamma} = \frac{1}{6} \left[ u_{1,\alpha',\gamma'}(6x)\chi_{[0,\frac{1}{6}]} - u_{1,\alpha',\gamma'}[6(x - \frac{1}{6})]\chi_{[\frac{1}{6},\frac{2}{6}]} + u_{1,\alpha',\gamma'}[6(x - \frac{2}{6})]\chi_{[\frac{2}{6},\frac{3}{6}]} - u_{1,\alpha',\gamma'}[6(x - \frac{3}{6})]\chi_{[\frac{3}{6},\frac{4}{6}]} + u_{1,\alpha',\gamma'}[6(x - \frac{4}{6})]\chi_{[\frac{4}{6},\frac{5}{6}]} - u_{1,\alpha',\gamma'}[6(x - \frac{5}{6})]\chi_{[\frac{5}{6},1]} \right].$$

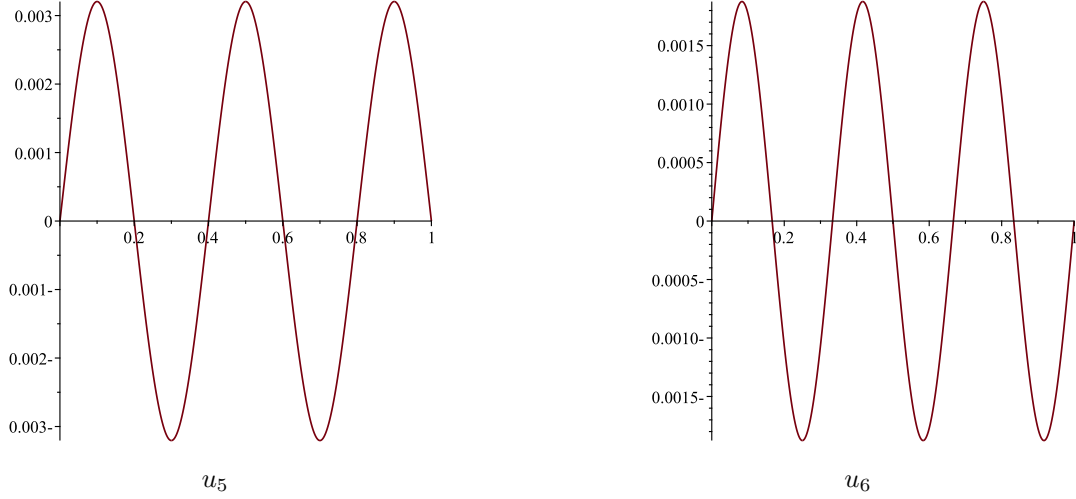


**Figure 3.12:** Example of finding  $u_5$  and  $u_6$  where  $\alpha = 1$ ,  $\gamma = 0.1$ .

### 3.3.3 Existence of $u_1$ non-symmetric solutions

Now let's go back to case 3 from Section 3.2 Namely, when  $1 - 4\alpha\gamma < 0$ . In section 3.3 we found that

$$F_3(c) = \sin(2\omega c) \sinh(2t(c-1)) - \sin(2\omega(c-1)) \sinh(2tc) = 0. \quad (3.3.5)$$

We already know that  $F_3(0) = F_3(\frac{1}{2}) = F_3(1) = 0$ , but for certain pairs of  $(\alpha, \gamma)$  we have  $F_3(c) = 0$  where  $c \neq 0, c \neq \frac{1}{2}, c \neq 1$ . For example when  $\alpha = 190, \gamma = 0.1$ , we have three solutions. One is a symmetric solution at  $c_1 = 0.5$  and two are non-symmetric solutions where  $c_2 = 0.3623549804$  and  $c_3 = 0.6376450198$  (see figures below).

CHAPTER THREE

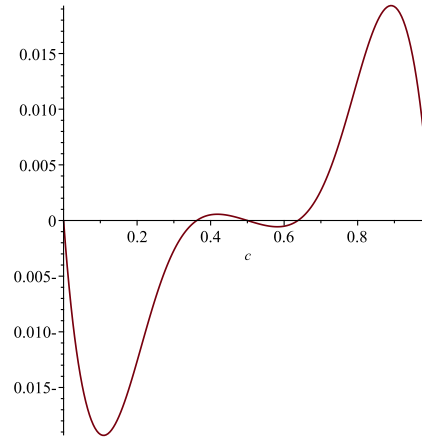


**Figure 3.13:** Location of jumps where  $\alpha = 190$  and  $\gamma = 0.1$ .

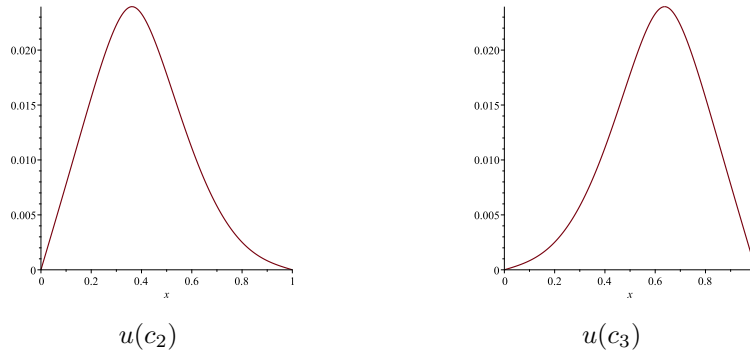


**Figure 3.15:** Example of a non-symmetric solution of lap 2 when  $\alpha = 190, \gamma = 0.1$ . and  $c_1 = 0.5, c_2 = 0.36, c_3 = 0.63$

In the example above, notice that  $c_2 + c_1 = 1$ . This is not a coincidence. In fact,  $F_3(1 - x) = -F_3(x)$  which means that if  $x = c$  a root of  $F_3$ , so is  $x = 1 - c$ . ( $F_3(c) = 0 \Leftrightarrow F_3(1 - c) = -F_3(c) = 0$ ). To see this let

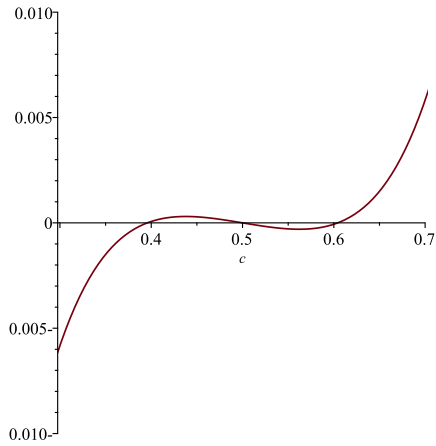
$$\begin{aligned}
 F_3(c) &= \sin(2\omega(1 - x)) \sinh(2t(1 - x - 1)) - \sin(2\omega(1 - x - 1)) \sinh(2t(1 - x)), \\
 &= \sin(2\omega(1 - x)) \sinh(-2t x) - \sin(-2\omega x) \sinh(2t(1 - x)), \\
 &= \sin(2\omega(x - 1)) \sinh(2t x) - \sin(2\omega x) \sinh(2t(x - 1)), \\
 &= -F_3(x).
 \end{aligned}$$

Moreover, if  $F_3(c) = F_3(1 - c) = 0$  ( $c \neq 0, c \neq 1, c \neq \frac{1}{2}$ ) then the corresponding solution with jumps at  $x_1 = c, x_2 = 1 - c$  are symmetric to one another.

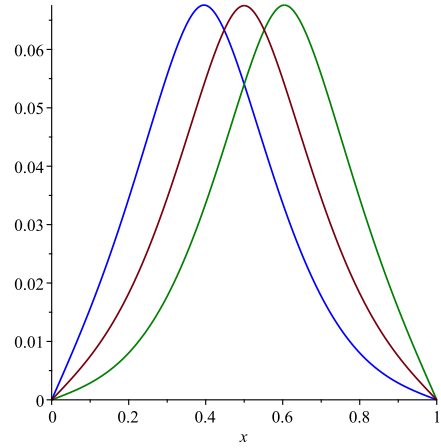
CHAPTER THREE

In particular, if  $u$  and  $v$  are such a pair of non-symmetric solutions, it can be easily shown that,  $u(1-x) = v(x) \quad \forall x \in [0, 1]$  which means that the solutions are reflections of one another around the line  $x = \frac{1}{2}$ .

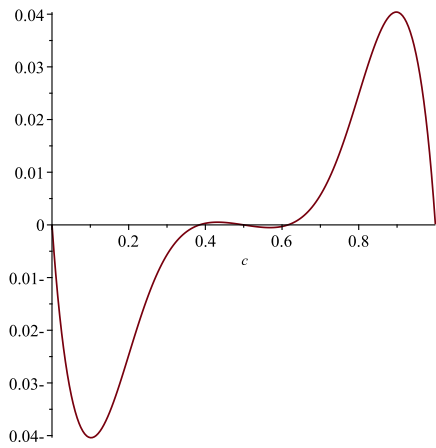
Below are more examples with different values of  $\alpha$  and  $\gamma$ :



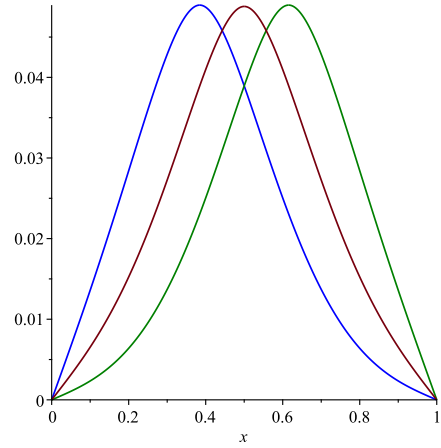
$\alpha = 67$  and  $\gamma = 0.02$



$\alpha = 67$  and  $\gamma = 0.02$



$\alpha = 90$  and  $\gamma = 0.04$



$\alpha = 90$  and  $\gamma = 0.04$

**Figure 3.18:** Example of symmetric and non-symmetric solutions of lap 2 for  $1 - 4\alpha\gamma < 0$ . On the left we have the plot of  $F_3(c)$  while on the right we have the solutions  $u$  of the Euler-Lagrange equation that correspond to each  $c$  with  $F_3(c)$ .

CHAPTER THREE

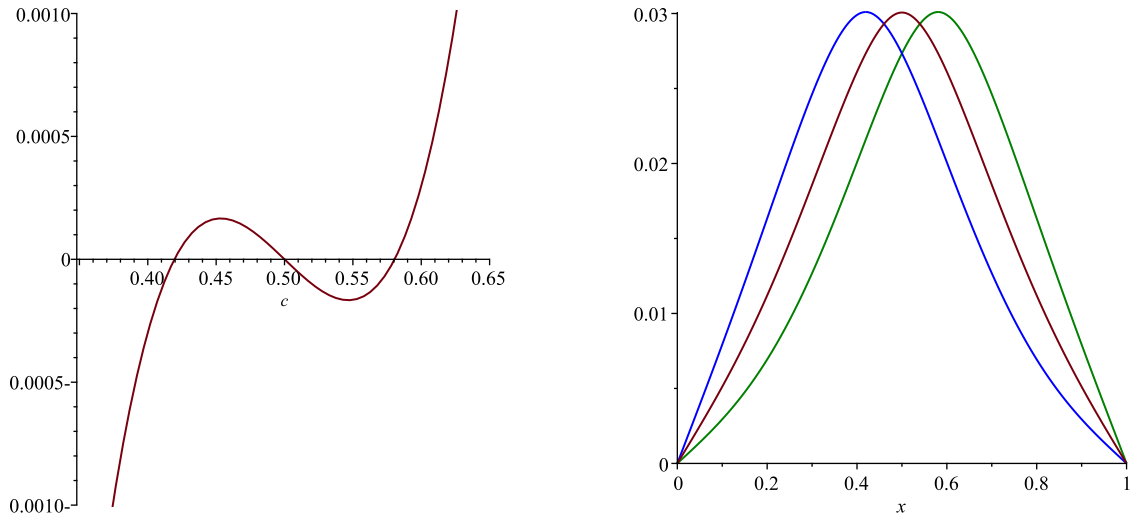


**Figure 3.20:** Example of symmetric and non-symmetric solutions of lap 2 for  $1 - 4\alpha\gamma < 0$ . On the left we have the plot of  $F_3(c)$  while on the right we have the solutions  $u$  of the Euler-Lagrange equation that correspond to each  $c$  with  $F_3(c)$ , where  $\alpha = 139$  and  $\gamma = 0.1$ .

AS we can see from Figures 3.18-3.20, the closer the other two roots are at  $\frac{1}{2}$  the “flatter” the  $F_3$  at  $c = \frac{1}{2}$ . In other words, to find the bifurcation curve, we would need to calculate the exact values of  $\alpha$  and  $\gamma$  for which  $F'_3(\frac{1}{2}) = 0$ .

More generally, to find any bifurcation curve on the  $(\alpha, \frac{1}{\gamma})$  plane, we need to solve the following equation  $F'_3(c) = 0$ .

$$F'_3(c) = 2\omega \cos(2\omega c) \sinh(2t(c-1)) + 2\sin(2\omega c)t \cosh(2t(c-1)) \\ - 2\omega \cos(2\omega(c-1)) \sinh(2ct) - 2\sin(2\omega(c-1))t \cosh(2ct).$$

Note that the  $\alpha$  and  $\gamma$  for which  $F'_3(\frac{1}{2}) = 0$  do not form a continuous graph on the  $(\alpha, \frac{1}{\gamma})$ . Instead they form several connected curves the lowest of which is given in the following graph, Figure 3.21. These bifurcation curves represent the critical values of the  $(\alpha, \frac{1}{\gamma})$  pair which form a threshold between  $2k - 1$  and  $2k + 1$  solutions of the Euler Lagrange equation. In particular, the lowest of those curve ( $k = 1$ ) represents the bifurcation from 1 to 3 solutions respectively.

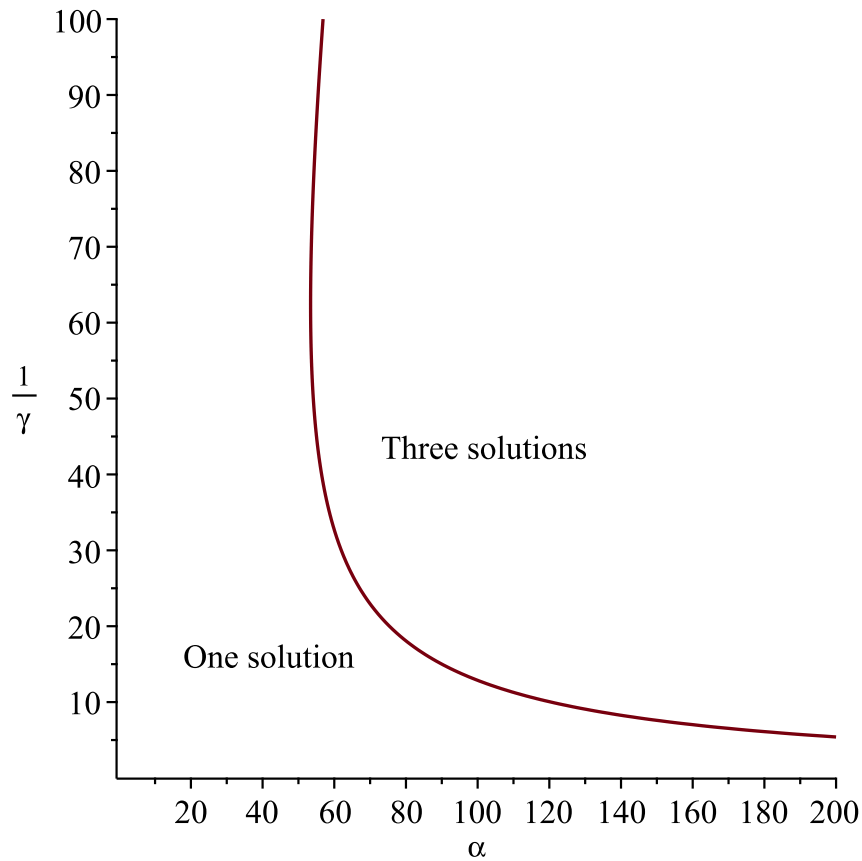


**Figure 3.21:** Bifurcation curve ( $k = 1$ ). This is lowest connected component of  $F'_3(\frac{1}{2}) = 0$ . Since  $k = 1$ , we go from 1 to 3 solutions. In particular, below the bifurcation curve we have 1 solution and above the curve we have (at least) 3 solutions.

**Remark 13.** *Figure 3.21 illustrates that the bifurcation curve, tends to the “north-east”. More formally, we make the conjecture that if  $\alpha \rightarrow \infty$  then  $\frac{1}{\gamma} \rightarrow 0$  (on the bottom) and  $\frac{1}{\gamma} \rightarrow \infty$  (on the top).*

### 3.4 Calculating the Energy

In the previous section we constructed periodic solutions with lap number  $n + 1$ ,  $n > 1$  ( $u_{n,\alpha,\gamma}$ ), explicitly from solutions of lap number 2 ( $u_{1,\alpha',\gamma'}$ ) where  $\alpha' = \frac{\alpha}{n^2}$  and  $\gamma' = n^2\gamma$ , which we used as building blocks. Since we are interested in minimizers of the energy functional, it would be useful to express the energy of higher lap periodic solutions as a function of the energy of symmetric solutions with lap 2 (see Definitions 3.3.2 - 3.3.4).

## CHAPTER THREE

Moreover, since non-symmetric solutions are reflection to one another, they must have the same energy. This is confirmed by a simple change of variable.

However, the main question is, which of these solutions are the minimizers (local or global) to our original energy functional. We can address that question as follows. First, we need to decide on the parameters  $\alpha$  and  $\gamma$ . From there, we can utilize the energy formula (and its corresponding reduction to lap 2 solutions) to calculate the energies of all symmetric-periodic solutions for those parameters. Finally, we can separately calculate the energy of the non-symmetric solutions directly and compare them to the energies of the symmetric ones. The solution with the smallest energy will be our minimizer.

We start this sections with an important Lemma that provides us with a formula for the energy of periodic solutions of arbitrary lap number as a function of symmetric solutions with lap number 2. We finish the section by summarizing the nature of all minimizers for various parameter values.

The construction in Theorem 12 is very useful because it gives us an explicit relation between  $u_{n,\alpha,\gamma}$  and  $u_{1,\alpha',\gamma'}$ . This relation translates to energies. In particular, we have

**Lemma 3.** *Let  $u_{1,\alpha',\gamma'}$  be the unique symmetric solution of lap 2. Let  $u_{n,\alpha,\gamma}$  be the unique periodic solution given by (3.3.2). Then*

$$E(u_{n,\alpha,\gamma}) = \gamma' \int_0^1 (u_{1,\alpha',\gamma'}^2)_{xx}(y) dy + \int_0^1 W(u_{1,\alpha',\gamma'})_x(y) dy + \alpha' \int_0^1 u_{1,\alpha',\gamma'}^2(y) dy,$$

where  $\alpha' = \frac{\alpha}{n^2}$  and  $\gamma' = n^2\gamma$ .

*Proof.* For simplicity let:

$$\bar{u}_1 = \bar{u}_{1,\alpha',\gamma'}(x) = \frac{1}{n} u_{1,\gamma',\alpha'}(nx).$$

CHAPTER THREE

We observe that by the chain rule, the  $n$  cancels out since

$$(\bar{u}_1)_x = \frac{n}{n}(u_{1,\alpha',\gamma'})_x(nx) = (u_{1,\alpha',\gamma'})_x(nx),$$

which means that the  $W(u_x)$  term does not change. We also have:

$$(\bar{u}_1)_{xx} = \frac{n^2}{n}(u_{1,\alpha',\gamma'})_{xx}(nx) = n(u_{1,\alpha',\gamma'})_{xx}(nx).$$

Thus a simple change of variables  $y = nx$  leads to:

$$E(u_n) = n E(\bar{u}_1) = \gamma n^2 \int_0^1 [(u_{1,\alpha',\gamma'}^2)_{xx}(y)] dy + \int_0^1 W(u_{1,\alpha',\gamma'})_x(y) dy + \frac{\alpha}{n^2} \int_0^1 u_{1,\alpha',\gamma'}^2(y) dy.$$

**Claim 1.**

$$E(u_{n,\alpha,\gamma})(x) = n E(\bar{u}_1).$$

By (3.3.2) we have that  $u_{n,\alpha,\gamma}$  is the sum of  $n$  identical (up to reflection) functions with non-overlapping support. Then

$$\begin{aligned} E(u_n) &= E_{[0, \frac{1}{n}]}(\frac{1}{n}u_{1,\alpha',\gamma'}(nx)) + E_{[\frac{1}{n}, \frac{2}{n}]}(\frac{1}{n}u_{1,\alpha',\gamma'}(nx)) + \cdots + E_{[\frac{n-1}{n}, 1]}(\frac{1}{n}u_{1,\alpha',\gamma'}(nx)), \\ &= \sum_0^{n-1} E_{[\frac{k}{n}, \frac{k+1}{n}]}(\frac{1}{n}u_{1,\alpha',\gamma'}(nx)) = \sum_0^{n-1} E_{[0, \frac{1}{n}]}(\frac{1}{n}u_{1,\alpha',\gamma'}(nx)) = n E_{[0, \frac{1}{n}]}(\frac{1}{n}u_{1,\alpha',\gamma'}(nx)). \end{aligned}$$

□

Lemma 1 shows that  $E_{n,\alpha,\gamma}$  depends on 3 integrals over  $u_{1,\alpha',\gamma'}$ . In particular, let

$$\begin{cases} A = A(n, \alpha, \gamma) = \int_0^1 (u_{1,\alpha',\gamma'})_{xx}^2(x) dx = \int_0^1 (u_{1, \frac{\alpha}{n^2}, \gamma n^2})_{xx}^2(x) dx, \\ B = B(n, \alpha, \gamma) = \int_0^1 (u_{1,\alpha',\gamma'})^2(x) dx = \int_0^1 (u_{1, \frac{\alpha}{n^2}, \gamma n^2})^2(x) dx, \\ C = C(n, \alpha, \gamma) = \int_0^1 W(u_{1,\alpha',\gamma'})_x(x) dx = \int_0^1 W(u_{1, \frac{\alpha}{n^2}, \gamma n^2})_x(x) dx. \end{cases}$$

### CHAPTER THREE

It is clear that  $A, B, C \geq 0$ . Moreover, we can now write

$$E(u_{n,\alpha,\gamma}) = \gamma n^2 A + \frac{\alpha}{n^2} B + C. \quad (3.4.1)$$

For example: for  $n = 2$ ,

$$E(u_{2,\alpha,\gamma}) = 4\gamma A(2, \alpha, \gamma) + \frac{\alpha}{4} B(2, \alpha, \gamma) + C(2, \alpha, \gamma).$$

Now we will provide an example of how to calculate  $E(u_{2,\alpha,\gamma})$  using our formula above. Let's calculate the energy of  $u_{2,\alpha,\gamma} = u_{2,3,0.04}$ . Since  $\alpha = 3, \gamma = 0.04$ , then we are in case 1 and where  $c = \frac{1}{2}$  and  $u_{1,\frac{\alpha}{n^2},\gamma n^2} = u_{1,\frac{3}{4},0.16}$  is given by the following two segments:

$$u_1^l(x) = \begin{cases} -0.1707370889 e^{2.319152764 x} + 0.1707370889 e^{-2.319152764 x} \\ + 0.6685576813 e^{0.9335579537 x} - 0.6685576813 e^{-0.9335579537 x} \end{cases}, \quad 0 \leq x \leq 0.5,$$

$$u_1^r(x) = \begin{cases} 0.01679316765 e^{2.319152764 x} - 1.735893672 e^{-2.319152764 x} \\ - 0.2628450576 e^{0.9335579537 x} + 1.700505146 e^{-0.9335579537 x} \end{cases}, \quad 0.5 \leq x \leq 1.$$

Since we have a formula to calculate the energy (3.4.1), now we can find all the integrals  $A, B$  and  $C$  from Maple.

$$A = \int_0^c (u_{1,\alpha',\gamma'}^l(x))_{xx}^2 dx + \int_c^1 (u_{1,\alpha',\gamma'}^r(x))_{xx}^2 dx = 1.17651,$$

$$B = \int_0^c (u_{1,\alpha',\gamma'}^l(x))^2 dx + \int_c^1 (u_{1,\alpha',\gamma'}^r(x))^2 dx = 0.0116542,$$

$$C = \int_0^c (|u_{1,\alpha',\gamma'}^l(x)| - 1)^2 dx + \int_c^1 (|u_{1,\alpha',\gamma'}^r(x)| - 1)^2 dx = 0.490641.$$

Substituting  $A, B$  and  $C$  into (3.4.1), we get

$$E(u_2) = 0.16 (1.17651) + \frac{3}{4} (0.0116542) + 0.490641 = 0.68762507.$$

CHAPTER THREE

Also, in the tables below we calculate and compare energies between symmetric and non-symmetric solutions of lap number 2 for various pairs of  $(\alpha, \gamma)$ . To avoid confusion, we use the notation  $u_2^{sym}$  for symmetric solutions and  $u_2^{ns}$  for non-symmetric solutions. Whenever non-symmetric solutions do not exist, we indicate it by the use of a omission bar (-).

$\alpha$	$\frac{1}{\gamma}$	$u_2^{sym}$	$u_2^{ns}$
20	20	0.7502426453	-
30	20	0.8020312120	-
40	20	0.8350022830	-
50	20	0.8578708898	-
60	20	0.8746881896	-
70	20	0.8875933104	-
80	20	0.8978224256	0.8978043655
90	20	0.9061397819	0.9060042690
100	20	0.9130433379	0.9127488553
110	20	0.9188714895	0.9184161969

**Table 3.1:** Comparing energy for different values of  $\alpha$  and for fixed  $\gamma = 0.05$ .

$\alpha$	$\frac{1}{\gamma}$	$u_2^{sym}$	$u_2^{ns}$
10	70	0.5750154659	-
20	70	0.6971554736	-
30	70	0.7608044123	-
40	70	0.8001248766	-
50	70	0.8269823351	-
60	70	0.8465882904	0.8465375704
70	70	0.8615934478	0.8613718782
80	70	0.8734900073	0.8730892445
90	70	0.8831831920	0.8826307680
100	70	0.8912546608	0.8901272498

**Table 3.2:** Comparing energy for different values of  $\alpha$  and for fixed  $\gamma = 0.014$ .

It is worth noting here that Yip in [63] showed that all local minimizers are periodic. Although, the tables above indicate the existence of non-periodic solutions with lower energy (than the corresponding periodic ones) this does not contradict Yip's conclusion as he only considered cases with  $\alpha = 1$ , all of which lie below the first bifurcation curve and thus  $u_1$ , is necessarily a local or global minimizer (depending on the value of  $\gamma$ ).

## CHAPTER THREE

We can summarize these behaviours of the lap 2 solutions in the next section.

### 3.4.1 Optimizing Energy

Our work above gives us a direct way to calculate the energy of all periodic solutions (with any amount of internal zeroes) as function of the symmetric solution with no internal zeroes. Also, we can calculate the energy of the non-symmetric solutions (with lap 2) directly. Now we will find the periodic solutions which are local/global minimizers for our functional  $E$ .

On the  $(\alpha, \frac{1}{\gamma})$  plane we plot the curve  $E_{1,2}$  corresponding to  $E(u_1) = E(u_2)$ , where  $u_1, u_2$  are the solutions with no and one internal zeroes respectively. In general, we calculate  $E_{i,j}$  by solving the equation  $E(u_i) = E(u_j)$  using MAPLE and in particular curve fitting. More specifically, since we know the energy formula  $E(u_i) = E(u_i, \alpha, \gamma)$  for a given  $i, \alpha, \gamma$ , we can incrementally change the values of  $\alpha$  and  $\gamma$  until we find several pairs  $(\alpha, \frac{1}{\gamma})$  for which  $E(u_i) = E(u_j)$ . These (finitely many) pairs approximate the curve  $(\alpha, \frac{1}{\gamma})$  (see Appendix A.7). Also, let  $F'_3(\frac{1}{2}) = 0$  be the bifurcation curve (see Section 3.3.3).

We make the following observations, see Figure 3.32.

**Remark 14.** *The  $E_{1,2}$  energy curve is always below the bifurcation curve. Moreover:*

- (i) *For a point  $(\alpha, \frac{1}{\gamma})$  below the  $E_{1,2}$  energy curve,  $u_1$  is the global minimizer.*
- (ii) *For a point  $(\alpha, \frac{1}{\gamma})$  above the  $E_{1,2}$  energy curve but below the bifurcation curve,  $u_1$  is a local but not a global minimizer.*
- (iii) *For a point  $(\alpha, \frac{1}{\gamma})$  above the bifurcation curve,  $u_1$  is not a minimizer.*

The numerical illustration of the above remark is as follows:

Firstly, MAPLE reveals that  $E_{1,2}$  energy curve is below the first bifurcation curve.

- (i) Now, we know that  $E_{1,2}$  is the only place that  $E_1 = E_2$ . That is, the only location on the  $(\alpha, \frac{1}{\gamma})$  plane that  $E_1 - E_2$  changes sign. With that in mind, we can choose

CHAPTER THREE

any point below the curve and calculate the sign of the quantity  $E_1 - E_2$ . In particular, we choose  $(1, 10)$  and we find that  $E_1 - E_2 < 0$  and thus  $E_1 < E_2$ . A similar approach, using higher energy curves  $E_{2,3}, E_{3,4}$ , etc shows that for any point below the  $E_{1,2}$  curve we have that  $E_1 < E_2 < E_3 < E_4, \dots$

Moreover, in that region,  $u_1, u_2, u_3, u_4$ , are the only solution to the EL equation and thus the only candidates for the global minimizer. Additionally, the increasing pattern of the energies lead us to conclude that  $u_1$  is a global minimizer.

We make the following conjecture

**Conjecture 13.** *The graphs of  $E_{i,j}$ ,  $j \geq i$  are ordered as follows:*

*$E_{i',j'}$  is above  $E_{i,j}$  if and only if  $j' > j$  or  $j' = j$  and  $i' > i$ .*

The picture of the first few curves where pairs of energies are equal is as follows:

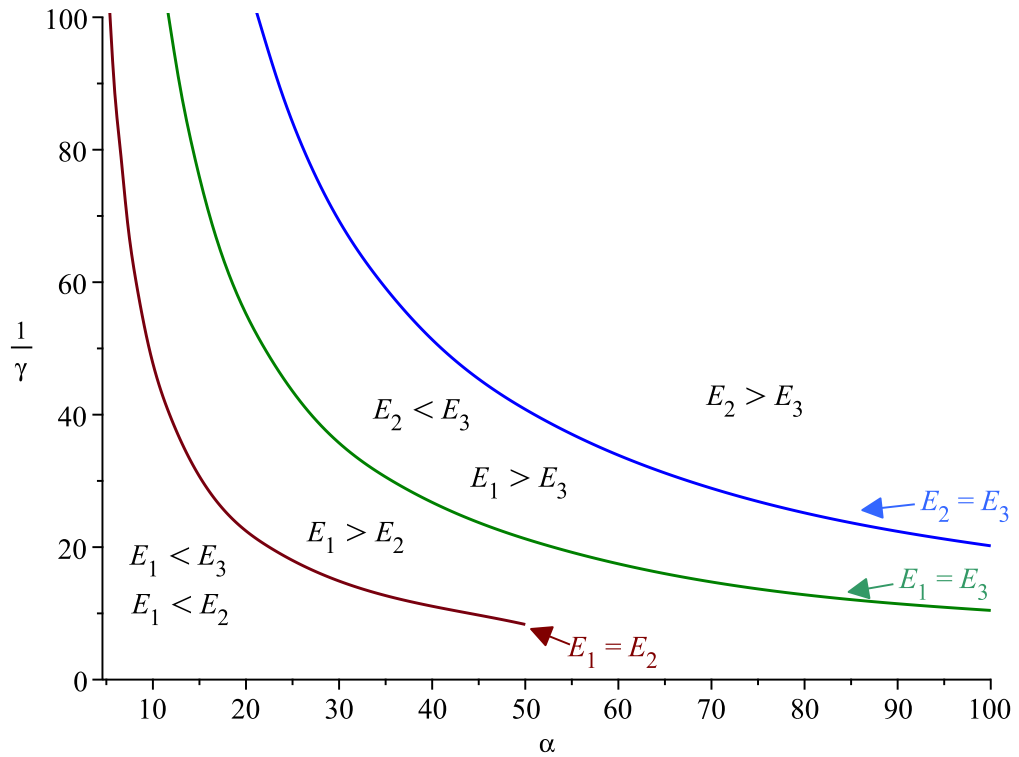


**Figure 3.22:** Curves where the energy of  $u_i$  is equal to the energy of  $u_{i+1}$  ( $i = 1, 2$ ).

(ii) A similar point calculation like the one above reveals that above  $E_{1,2}$  curve,

## CHAPTER THREE

$E_1 > E_2$ . But since we are also below the bifurcation curve, only the (periodic)  $u_1, u_2, u_3, \dots$  are the solutions of the EL equation. But since  $E_1 > E_2$ ,  $u_1$  can not be a global minimizer.

- (iii) Above the bifurcation curve, we also have non-symmetric solutions to the EL equation. In particular,  $u_1$  bifurcates to two non-symmetric solutions  $w_1, w_2$  such that  $E(w_1) = E(w_2) < E(u_1)$ . This means that  $u_1$  is no longer a local minimizer.

### 3.5 Formula for the number of jumps and unknown parameters for solution of lap number $n \geq 2$

So far we have been working on solutions with lap number 2. However, we are also interested in solutions of an arbitrary lap number  $n \geq 2$ . In general, any solution with lap number  $n$ , has  $n - 1$  jumps,  $0 < c_1 < c_2 < \dots < c_{n-1} < 1$ . Each interval of monotonicity  $(c_i, c_{i+1})$  gives rise to an Euler-Lagrange equation with 4 unknown coefficients. Thus we have a total of  $4n$  unknown coefficients. Together with the  $n - 1$  unknown locations of the jumps we have a total of  $p = 5n - 1$  unknowns. On the other hand, each  $c_i$  gives rise to 4 continuity conditions (one for the regular continuity, two for the first derivative and one for the second derivative) and one jump condition. This makes for  $5 \times (n - 1) = 5n - 5$  "interior" conditions. Moreover, we have 4 more boundary (Dirichlet) conditions for a total of  $q = 5n - 1$  restrictions. This brings the total amount of restrictions to match the number of unknowns.

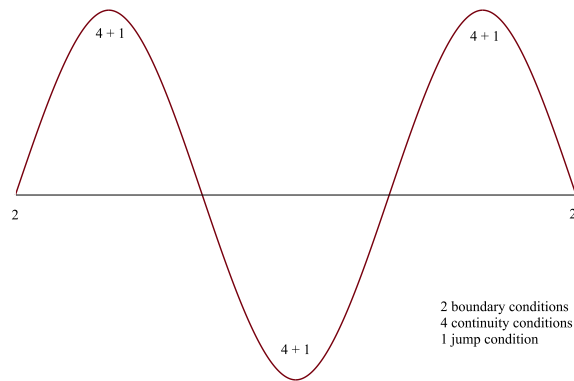


**Figure 3.23:** Visual for lap number 4 ( $n = 4$ ).

However, since we do not know the  $n - 1$  locations of the jumps ahead of time, we should split the number of unknowns  $p$  into two parts:  $p_1$ , the  $4n$  unknown coefficients and  $p_2$ , the  $n - 1$  unknown locations of the jumps. Clearly,  $p = p_1 + p_2$  like we saw earlier. Next, we can define the restriction matrix  $M \in \mathbb{R}^{q \times p_1}$  as a function of the locations of the jumps, like we did in Section 3.3.1. Following the same process as in section 3.3.1, we can consider the  $p_1 \times q$  matrix  $M^T$  and apply the Fredholm alternative, which will result to an equation of the form  $F(c_1, c_2, \dots, c_{n-1}) = 0$ . The latter includes the  $n - 1$  locations of the jumps as unknowns, which we can then solve using MAPLE. After we do, the  $p_2$  locations of the jumps will now be known and thus we can plug them into the matrix  $M$ , which in turn will allow us to calculate the remaining  $p_1$  unknown coefficients via a simple Gauss-Jordan elimination from  $MX = B$  (where  $X$  is the vector of  $p_1$  coefficients and  $B$  is the constant vector of size  $q$  obtained by the right hand side of the  $q$  restrictions. I.e  $B$  is mostly zeroes, except for the jump conditions which is  $\pm \frac{2}{\gamma}$ ).

In the general case of lap  $n > 2$  we can write  $M$  as an upper triangular block matrix

## CHAPTER THREE

that has the following form:

$$M(n) = \begin{bmatrix} M_1 & * & * & * \\ 0 & M_2 & * & * \\ & & \ddots & \\ 0 & 0 & \dots & M_{n-1} \\ \hline & & & L \end{bmatrix}.$$

In particular, we have

$$M_1 = \begin{bmatrix} 1 & 1 & 1 & 1 \\ \Lambda^2 & \Lambda^2 & \lambda^2 & \lambda^2 \\ \Lambda e^{\Lambda c_1} & -\Lambda e^{-\Lambda c_1} & \lambda e^{\lambda c_1} & -\lambda e^{-\lambda c_1} \\ \Lambda^3 e^{\Lambda c_1} & -\Lambda^3 e^{-\Lambda c_1} & \lambda^3 e^{\lambda c_1} & -\lambda^3 e^{-\lambda c_1} \end{bmatrix} \in \mathbb{R}^{4 \times 4},$$

$$M_{i+1} = \begin{bmatrix} \Lambda e^{\Lambda c_i} & -\Lambda e^{-\Lambda c_i} & \lambda e^{\lambda c_i} & -\lambda e^{-\lambda c_i} \\ \Lambda e^{\Lambda c_{i+1}} & -\Lambda e^{-\Lambda c_{i+1}} & \lambda e^{\lambda c_{i+1}} & -\lambda e^{-\lambda c_{i+1}} \\ e^{\Lambda c_{i+1}} & e^{-\Lambda c_{i+1}} & e^{\lambda c_{i+1}} & e^{-\lambda c_{i+1}} \\ \Lambda^2 e^{\Lambda c_{i+1}} & \Lambda^2 e^{-\Lambda c_{i+1}} & \lambda^2 e^{\lambda c_{i+1}} & \lambda^2 e^{-\lambda c_{i+1}} \end{bmatrix} \in \mathbb{R}^{4 \times 4} \quad \forall 1 \leq i \leq n-3,$$

and

$$M_{n-1} = \begin{bmatrix} \Lambda e^{\Lambda c_{n-2}} & -\Lambda e^{-\Lambda c_{n-2}} & \lambda e^{\lambda c_{n-2}} & -\lambda e^{-\lambda c_{n-2}} & 0 & 0 & 0 & 0 \\ \Lambda e^{\Lambda c_{n-1}} & -\Lambda e^{-\Lambda c_{n-1}} & \lambda e^{\lambda c_{n-1}} & -\lambda e^{-\lambda c_{n-1}} & 0 & 0 & 0 & 0 \\ e^{\Lambda c_{n-1}} & e^{-\Lambda c_{n-1}} & e^{\lambda c_{n-1}} & e^{-\lambda c_{n-1}} & -e^{\Lambda c_{n-1}} & -e^{-\Lambda c_{n-1}} & -e^{\lambda c_{n-1}} & -e^{-\lambda c_{n-1}} \\ \Lambda^2 e^{\Lambda c_{n-1}} & \Lambda^2 e^{-\Lambda c_{n-1}} & \lambda^2 e^{\lambda c_{n-1}} & \lambda^2 e^{-\lambda c_{n-1}} & -\Lambda^2 e^{\Lambda c_{n-1}} & -\Lambda^2 e^{-\Lambda c_{n-1}} & -\lambda^2 e^{\lambda c_{n-1}} & -\lambda^2 e^{-\lambda c_{n-1}} \\ \Lambda^3 e^{\Lambda c_{n-1}} & -\Lambda^3 e^{-\Lambda c_{n-1}} & \lambda^3 e^{\lambda c_{n-1}} & -\lambda^3 e^{-\lambda c_{n-1}} & -\Lambda^3 e^{\Lambda c_{n-1}} & \Lambda^3 e^{-\Lambda c_{n-1}} & -\lambda^3 e^{\lambda c_{n-1}} & \lambda^3 e^{-\lambda c_{n-1}} \\ 0 & 0 & 0 & 0 & \Lambda e^{\Lambda c_{n-1}} & -\Lambda e^{-\Lambda c_{n-1}} & \lambda e^{\lambda c_{n-1}} & -\lambda e^{-\lambda c_{n-1}} \\ 0 & 0 & 0 & 0 & e^{\Lambda} & e^{-\Lambda} & e^{\lambda} & e^{-\lambda} \\ 0 & 0 & 0 & 0 & \Lambda^2 e^{\Lambda} & \Lambda^2 e^{-\Lambda} & \lambda^2 e^{\lambda} & \lambda^2 e^{-\lambda} \end{bmatrix} \in \mathbb{R}^{8 \times 8}.$$

Finally,  $L \in \mathbb{R}^{(n-1) \times (5n-1)}$  is the matrix of the “leftover” rows.

## CHAPTER THREE

As an example, the full matrix corresponding to lap 4 is given by:

$$\begin{bmatrix} 1 & 1 & 1 & 1 & 0 & 0 & 0 & 0 & 0 & 0 & 0 & 0 & 0 & 0 & 0 & 0 \\ \Lambda^2 & \Lambda^2 & \lambda^2 & \lambda^2 & 0 & 0 & 0 & 0 & 0 & 0 & 0 & 0 & 0 & 0 & 0 & 0 \\ \Lambda e^{\Lambda c l} & -\Lambda e^{-\Lambda c l} & \lambda e^{\lambda c l} & -\lambda e^{-\lambda c l} & 0 & 0 & 0 & 0 & 0 & 0 & 0 & 0 & 0 & 0 & 0 & 0 \\ \Lambda^3 e^{\Lambda c l} & -\Lambda^3 e^{-\Lambda c l} & \lambda^3 e^{\lambda c l} & -\lambda^3 e^{-\lambda c l} & -\Lambda^3 e^{\Lambda c l} & \Lambda^3 e^{-\Lambda c l} & -\lambda^3 e^{\lambda c l} & \lambda^3 e^{-\lambda c l} & 0 & 0 & 0 & 0 & 0 & 0 & 0 & 0 \\ \hline 0 & 0 & 0 & 0 & \Lambda e^{\Lambda c l} & -\Lambda e^{-\Lambda c l} & \lambda e^{\lambda c l} & -\lambda e^{-\lambda c l} & 0 & 0 & 0 & 0 & 0 & 0 & 0 & 0 \\ 0 & 0 & 0 & 0 & \Lambda e^{\Lambda c 2} & -\Lambda e^{-\Lambda c 2} & \lambda e^{\lambda c 2} & -\lambda e^{-\lambda c 2} & 0 & 0 & 0 & 0 & 0 & 0 & 0 & 0 \\ 0 & 0 & 0 & 0 & e^{\Lambda c 2} & e^{-\Lambda c 2} & e^{\lambda c 2} & e^{-\lambda c 2} & -e^{\Lambda c 2} & -e^{-\Lambda c 2} & -e^{\lambda c 2} & -e^{-\lambda c 2} & 0 & 0 & 0 & 0 \\ 0 & 0 & 0 & 0 & \Lambda^2 e^{\Lambda c 2} & \Lambda^2 e^{-\Lambda c 2} & \lambda^2 e^{\lambda c 2} & \lambda^2 e^{-\lambda c 2} & -\Lambda^2 e^{\Lambda c 2} & -\Lambda^2 e^{-\Lambda c 2} & -\lambda^2 e^{\lambda c 2} & -\lambda^2 e^{-\lambda c 2} & 0 & 0 & 0 & 0 \\ \hline 0 & 0 & 0 & 0 & 0 & 0 & 0 & 0 & \Lambda e^{\Lambda c 2} & -\Lambda e^{-\Lambda c 2} & \lambda e^{\lambda c 2} & -\lambda e^{-\lambda c 2} & 0 & 0 & 0 & 0 \\ 0 & 0 & 0 & 0 & 0 & 0 & 0 & 0 & \Lambda e^{\Lambda c 3} & -\Lambda e^{-\Lambda c 3} & \lambda e^{\lambda c 3} & -\lambda e^{-\lambda c 3} & 0 & 0 & 0 & 0 \\ 0 & 0 & 0 & 0 & 0 & 0 & 0 & 0 & e^{\Lambda c 3} & e^{-\Lambda c 3} & e^{\lambda c 3} & e^{-\lambda c 3} & -e^{\Lambda c 3} & -e^{-\Lambda c 3} & -e^{\lambda c 3} & -e^{-\lambda c 3} \\ 0 & 0 & 0 & 0 & 0 & 0 & 0 & 0 & \Lambda^2 e^{\Lambda c 3} & \Lambda^2 e^{-\Lambda c 3} & \lambda^2 e^{\lambda c 3} & \lambda^2 e^{-\lambda c 3} & -\Lambda^2 e^{\Lambda c 3} & -\Lambda^2 e^{-\Lambda c 3} & -\lambda^2 e^{\lambda c 3} & -\lambda^2 e^{-\lambda c 3} \\ 0 & 0 & 0 & 0 & 0 & 0 & 0 & 0 & \Lambda^3 e^{\Lambda c 3} & -\Lambda^3 e^{-\Lambda c 3} & \lambda^3 e^{\lambda c 3} & -\lambda^3 e^{-\lambda c 3} & -\Lambda^3 e^{\Lambda c 3} & \Lambda^3 e^{-\Lambda c 3} & -\lambda^3 e^{\lambda c 3} & \lambda^3 e^{-\lambda c 3} \\ 0 & 0 & 0 & 0 & 0 & 0 & 0 & 0 & 0 & 0 & 0 & 0 & \Lambda e^{\Lambda c 3} & -\Lambda e^{-\Lambda c 3} & \lambda e^{\lambda c 3} & -\lambda e^{-\lambda c 3} \\ 0 & 0 & 0 & 0 & 0 & 0 & 0 & 0 & 0 & 0 & 0 & 0 & e^{\Lambda} & e^{-\Lambda} & e^{\lambda} & e^{-\lambda} \\ 0 & 0 & 0 & 0 & 0 & 0 & 0 & 0 & 0 & 0 & 0 & 0 & \Lambda^2 e^{\Lambda} & \Lambda^2 e^{-\Lambda} & e^{\lambda} & e^{-\lambda} \\ \hline 0 & 0 & 0 & 0 & \Lambda^3 e^{\Lambda c 2} & -\Lambda^3 e^{-\Lambda c 2} & \lambda^3 e^{\lambda c 2} & -\lambda^3 e^{-\lambda c 2} & -\Lambda^3 e^{\Lambda c 2} & \Lambda^3 e^{-\Lambda c 2} & -\lambda^3 e^{\lambda c 2} & \lambda^3 e^{-\lambda c 2} & 0 & 0 & 0 & 0 \\ \Lambda^2 e^{\Lambda c l} & \Lambda^2 e^{-\Lambda c l} & \lambda^2 e^{\lambda c l} & \lambda^2 e^{-\lambda c l} & -\Lambda^2 e^{\Lambda c l} & -\Lambda^2 e^{-\Lambda c l} & -\lambda^2 e^{\lambda c l} & -\lambda^2 e^{-\lambda c l} & 0 & 0 & 0 & 0 & 0 & 0 & 0 & 0 \\ e^{\Lambda c l} & e^{-\Lambda c l} & e^{\lambda c l} & e^{-\lambda c l} & -e^{\Lambda c l} & -e^{-\Lambda c l} & -e^{\lambda c l} & -e^{-\lambda c l} & 0 & 0 & 0 & 0 & 0 & 0 & 0 & 0 \end{bmatrix}$$

Let the above  $M(n)$  be the standard representation of matrix  $M$  with lap  $n$ . We have the following useful theorem:

**Theorem 14.** *Let  $M \in \mathbb{R}^{(5n-1) \times 4n}$  be the matrix corresponding to lap  $n$  such that  $MX = B$ . We have that  $\text{rank}(M) = 4n$  and  $\dim(\mathcal{N}(M^T)) = n - 1$ .*

*Proof.* First we can write  $M$  in the standard form  $M(n)$  (rearranging rows if necessary). Since  $M(n)$  is an upper triangular block matrix, we know that

$$\text{rank}(M) = \text{rank}(M(n)) = \sum_{i=1}^{n-1} \text{rank}(M_i).$$

A simple Gauss-Jordan elimination shows that:

$$\begin{cases} \text{rank}(M_1) = 4, \\ \text{rank}(M_{i+1}) = 4, \forall 1 \leq i \leq n-3, \\ \text{rank}(M_{n-1}) = 8, \end{cases}$$

## CHAPTER THREE

Thus  $\text{rank}(M) = \sum_{i=1}^{n-1} \text{rank}(M_i) = (n-2) \times 4 + 8 = 4n$ .

We also know  $\text{rank}(M^T) = \text{rank}(M) = 4n$ . By the rank-nullity theorem

$$\dim(\mathcal{N}(M^T)) = 5n - 1 - \text{rank}(M^T) = n - 1.$$

□

In what follows, we show how this process works for lap number 3.

### 3.5.1 Periodic and Non Periodic Solutions with Lap number 3

For lap number 3 we have  $p_1 = 4 \times 3 = 12$  coefficient unknowns ( $A_1, \dots, A_{12}$ ),  $p_2 = 3 - 1 = 2$  unknown locations of the jumps ( $c_1, c_2$ ) and  $q = (5 \times 3) - 1 = 14$  total restrictions ( $4 \times 2$  continuity restrictions, 2 jump restrictions and 4 boundary conditions) which are the following:

$$\begin{cases} u_1(0) = 0, & u_{1,x}(c_1^-) = 0, & u_{1,xx}(0) = 0, & u_{2,x}(c_1) = 0, \\ u_{2,x}(c_2) = 0, & u_{3,x}(c_2) = 0, & u_3(1) = 0, & u_{3,xx}(1) = 0, \\ u_1(c_1) = u_2(c_1), & u_{1,xx}(c_1) = u_{2,xx}(c_1), & u_2(c_2) = u_3(c_2), & u_{2,xx}(c_2) = u_{3,xx}(c_2), \\ u_{1,xxx}(c_1^+) - u_{2,xxx}(c_1^-) = \frac{2}{\gamma}, & u_{2,xxx}(c_2^+) - u_{3,xxx}(c_2^-) = \frac{-2}{\gamma}, \end{cases}$$

where  $u_i$  is the  $i^{\text{th}}$  segment of the Euler-Lagrange equation,  $i = 1, 2, 3$ .

First, let us work on the case 1, namely the one where the parameters satisfy the inequality  $1 - 4\alpha\gamma > 0$ . Following the procedure we described above, we start by only considering the  $p_1 = 12$  coefficient unknowns as well as all the  $q = 14$  restrictions. This gives rise to a  $14 \times 12$  matrix  $M$ , whose rows are determined by the 14 restriction conditions and  $B$  is the constant vector of size 14 obtained by the right hand side of the 14 restrictions. In other words  $MX = B$  where  $X = [A_1, A_2, \dots, A_{12}]^T$ ,

CHAPTER THREE

$B = [\frac{2}{\gamma}, \frac{-2}{\gamma}, 0, \dots, 0]^T$  and  $M$  is given by the following:

$$M = \begin{bmatrix} 1 & 1 & 1 & 1 & 0 & 0 & 0 & 0 & 0 & 0 & 0 & 0 \\ \Lambda^2 & \Lambda^2 & \lambda^2 & \lambda^2 & 0 & 0 & 0 & 0 & 0 & 0 & 0 & 0 \\ \Lambda e^{\Lambda c_1} & -\Lambda e^{-\Lambda c_1} & \lambda e^{\lambda c_1} & -\lambda e^{-\lambda c_1} & 0 & 0 & 0 & 0 & 0 & 0 & 0 & 0 \\ \Lambda^3 e^{\Lambda c_1} & -\Lambda^3 e^{-\Lambda c_1} & \lambda^3 e^{\lambda c_1} & -\lambda^3 e^{-\lambda c_1} & -\Lambda^3 e^{\Lambda c_1} & \Lambda^3 e^{-\Lambda c_1} & -\lambda^3 e^{\lambda c_1} & \lambda^3 e^{-\lambda c_1} & 0 & 0 & 0 & 0 \\ 0 & 0 & 0 & 0 & \Lambda e^{\Lambda c_1} & -\Lambda e^{-\Lambda c_1} & \lambda e^{\lambda c_1} & -\lambda e^{-\lambda c_1} & 0 & 0 & 0 & 0 \\ 0 & 0 & 0 & 0 & \Lambda e^{\Lambda c_2} & -\Lambda e^{-\Lambda c_2} & \lambda e^{\lambda c_2} & -\lambda e^{-\lambda c_2} & 0 & 0 & 0 & 0 \\ 0 & 0 & 0 & 0 & e^{\Lambda c_2} & e^{-\Lambda c_2} & e^{\lambda c_2} & e^{-\lambda c_2} & -e^{\Lambda c_2} & -e^{-\Lambda c_2} & -e^{\lambda c_2} & -e^{-\lambda c_2} \\ 0 & 0 & 0 & 0 & \Lambda^2 e^{\Lambda c_2} & \Lambda^2 e^{-\Lambda c_2} & \lambda^2 e^{\lambda c_2} & \lambda^2 e^{-\lambda c_2} & -\Lambda^2 e^{\Lambda c_2} & -\Lambda^2 e^{-\Lambda c_2} & -\lambda^2 e^{\lambda c_2} & -\lambda^2 e^{-\lambda c_2} \\ 0 & 0 & 0 & 0 & \Lambda^3 e^{\Lambda c_2} & -\Lambda^3 e^{-\Lambda c_2} & \lambda^3 e^{\lambda c_2} & -\lambda^3 e^{-\lambda c_2} & -\Lambda^3 e^{\Lambda c_2} & \Lambda^3 e^{-\Lambda c_2} & -\lambda^3 e^{\lambda c_2} & \lambda^3 e^{-\lambda c_2} \\ 0 & 0 & 0 & 0 & 0 & 0 & 0 & 0 & \Lambda e^{\Lambda c_2} & -\Lambda e^{-\Lambda c_2} & \lambda e^{\lambda c_2} & -\lambda e^{-\lambda c_2} \\ 0 & 0 & 0 & 0 & 0 & 0 & 0 & 0 & e^{\Lambda} & e^{-\Lambda} & e^{\lambda} & e^{-\lambda} \\ 0 & 0 & 0 & 0 & 0 & 0 & 0 & 0 & \Lambda^2 e^{\Lambda} & \Lambda^2 e^{-\Lambda} & \lambda^2 e^{\lambda} & \lambda^2 e^{-\lambda} \\ \Lambda^2 e^{\Lambda c_1} & \Lambda^2 e^{-\Lambda c_1} & \lambda^2 e^{\lambda c_1} & \lambda^2 e^{-\lambda c_1} & -\Lambda^2 e^{\Lambda c_1} & -\Lambda^2 e^{-\Lambda c_1} & -\lambda^2 e^{\lambda c_1} & -\lambda^2 e^{-\lambda c_1} & 0 & 0 & 0 & 0 \\ e^{\Lambda c_1} & e^{-\Lambda c_1} & e^{\lambda c_1} & e^{-\lambda c_1} & -e^{\Lambda c_1} & -e^{-\Lambda c_1} & -e^{\lambda c_1} & -e^{-\lambda c_1} & 0 & 0 & 0 & 0 \end{bmatrix}$$

For example  $u_1(0) = 0$  leads to the equation:  $A_1 + A_2 + A_3 + A_4 = 0$  and thus the row of  $M$  is  $[1, 1, 1, 1, 0, 0, 0, 0, 0, 0, 0, 0]$ .

Maple shows that the nullspace of  $M^T$  is two-dimensional (see Appendix A.6), since its reduced row echelon form is full rank(12) (also see Theorem 14). This means that we can find two vectors  $y_1 = [a_1, a_2, \dots, a_{14}]^T$  and  $y_2 = [a'_1, a'_2, \dots, a'_{14}]^T$  in  $\mathcal{N}(M^T)$ . By the Fredholm alternative (see Section 2.3) we have  $\langle y_1, B \rangle = \langle y_2, B \rangle = 0$ . Since  $B = [\frac{2}{\gamma}, \frac{-2}{\gamma}, 0, \dots, 0]$ , we have that:

$$\left. \begin{aligned} a_1\left(\frac{2}{\gamma}\right) - a_2\left(\frac{2}{\gamma}\right) &= 0 \\ a'_1\left(\frac{2}{\gamma}\right) - a'_2\left(\frac{2}{\gamma}\right) &= 0 \end{aligned} \right\} \begin{aligned} a_1 - a_2 &= 0. \\ a'_1 - a'_2 &= 0. \end{aligned}$$

Since each  $a_1, a_2, a'_1$  and  $a'_2$  are functions of the jumps  $c_1$  and  $c_2$ , we can solve the above system to find the jumps, see Appendix A.6. Symbolically, we can express the system above as follows:

$$\begin{cases} F_1(c_1, c_2) = 0, \\ F_2(c_1, c_2) = 0. \end{cases}$$

### CHAPTER THREE

However, here we do present a few explicit graphical examples of their curves. We start with some fixed values of the parameter pair  $(\alpha, \gamma)$  and then we plot the  $F_1, F_2$  curves on the  $(c_1, c_2)$  plane. Of course, the locations where these two curves intersect are exactly the solutions to our system and thus the locations of the jumps  $c_1$  and  $c_2$ . Naturally, each of these intersections (jump pair) gives rise to a unique solution to the Euler-Lagrange equation. To illustrate the connection we add an extra plot (on the  $(x, u)$  plane) with the solutions that correspond to the intersections.

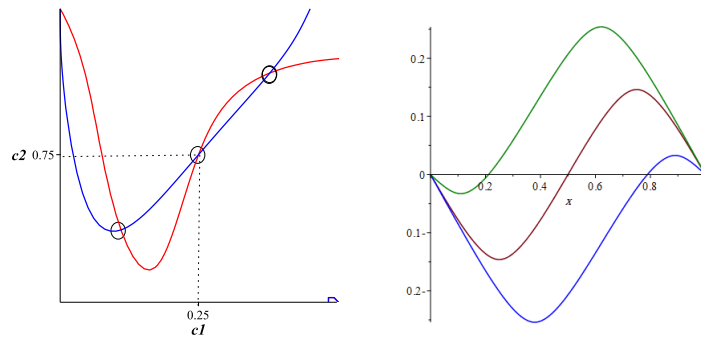


**Figure 3.24:** Solution Plots for  $\alpha = 2, \gamma = 0.01$ . On the left we have the plots of  $F_1$  and  $F_2$  and their 3 intersections. On the right we have the 3 corresponding solutions to these intersections. Notice the intersection at  $(\frac{1}{4}, \frac{3}{4})$  on the left, which gives rise to a  $p_3$  periodic solution on the right (middle graph).

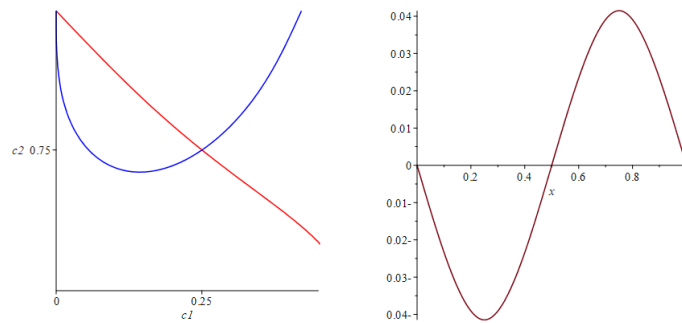


**Figure 3.25:** Solution Plots for  $\alpha = 1, \gamma = 0.1$ . Here we only have 1 intersection on the left and thus only a single corresponding solution to the EL equation on the right, namely the  $p_3$  periodic one.

So far, we only talked about solutions when  $1 - 4\alpha\gamma > 0$ . The process for the other two cases (namely,  $1 - 4\alpha\gamma < 0, 1 - 4\alpha\gamma = 0$ ) is identical, with the only difference being the change in  $\lambda$  and  $\Lambda$ . This will effect the numerical values of  $M$  (but not its structure)

## CHAPTER THREE

as well as the expressions of  $F_1$  and  $F_2$ . Below are a few sample solutions in the case  $1 - 4\alpha\gamma < 0$ :

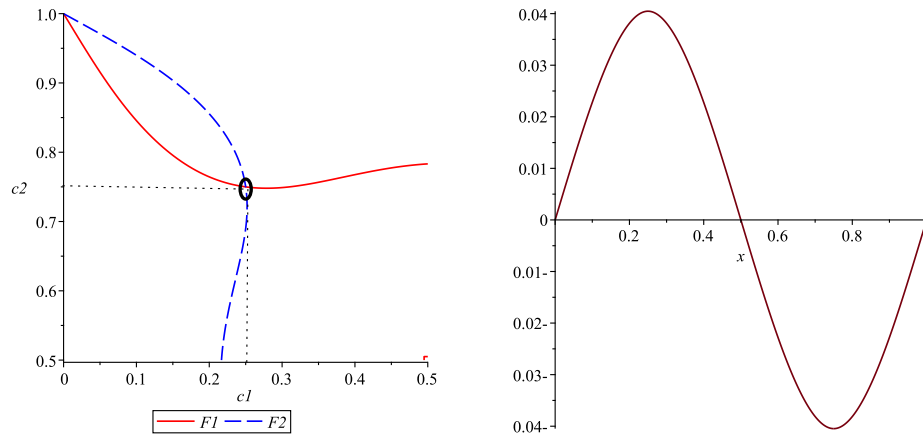


**Figure 3.26:** Solution Plots for  $\alpha = 6, \gamma = 0.1$ . Here we only have 1 intersection on the left and thus only a single corresponding solution to the EL equation on the right, namely the periodic one.

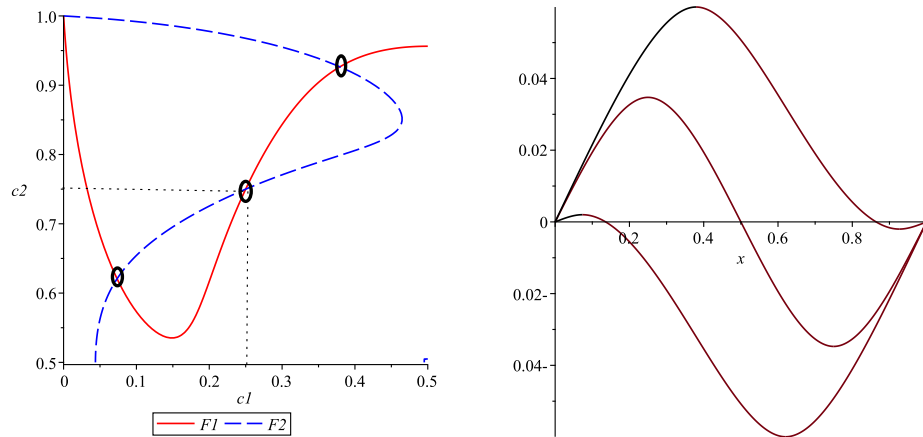


**Figure 3.27:** Solution Plots for  $\alpha = 40, \gamma = 0.1$ . On the left we have the plots of  $F_1$  and  $F_2$  and their 3 intersections. On the right we have the 3 corresponding solutions to these intersections. Notice the intersection at  $(\frac{1}{4}, \frac{3}{4})$  on the left, which gives rise to a periodic solution on the right (middle graph).

### 3.5.2 Bifurcation

Next we investigate the first three bifurcation curves in the  $(\alpha, \frac{1}{\gamma})$  plane. In other words, we want to understand how the change of parameters effects the total numbers of solutions to the Euler-Lagrange equation (3.2.2). We approximated all other these

## CHAPTER THREE

bifurcation curves by estimating the “thresholds” where we go from a lower to a higher number of solutions using MAPLE and straightforward curve-fitting. In particular, for various values of  $\alpha$  we let  $\gamma$  change incrementally until we observe an increase in the number of solutions to the Euler Lagrange equation. This yields several “bifurcation” points  $(\alpha, \frac{1}{\gamma})$  which we can then connect to each other to get the approximation to the bifurcation curve, see Appendix A.6.

The first few bifurcations can be shown in Figure 3.33. We observed two main types of pitchfork bifurcations, those that give rise to two new non-periodic solutions (see  $p_1$  and  $p_2$  in Figure 3.33) and those that give rise to two new non-symmetric solutions (see  $s_1$  in Figure 3.33).

Notably, the first bifurcation  $p_1$  (i.e. the first time we observe more solutions than just the periodic one) is of the first type. Namely, it gives rise to the first non-periodic solutions. In other words, below the curve  $p_1$  we only have a unique (necessarily periodic) solution while above  $p_1$  we have more than 1 solutions.

The other interesting bifurcation curve is  $s_1$ , namely the first time we observe non-symmetric solutions. In other words, below  $s_1$  we only have symmetric solutions while above  $s_1$  non-symmetric solutions appear.

To illustrate this progression, we selected a point within two regions and plotted all solutions, as illustrated below.

CHAPTER THREE

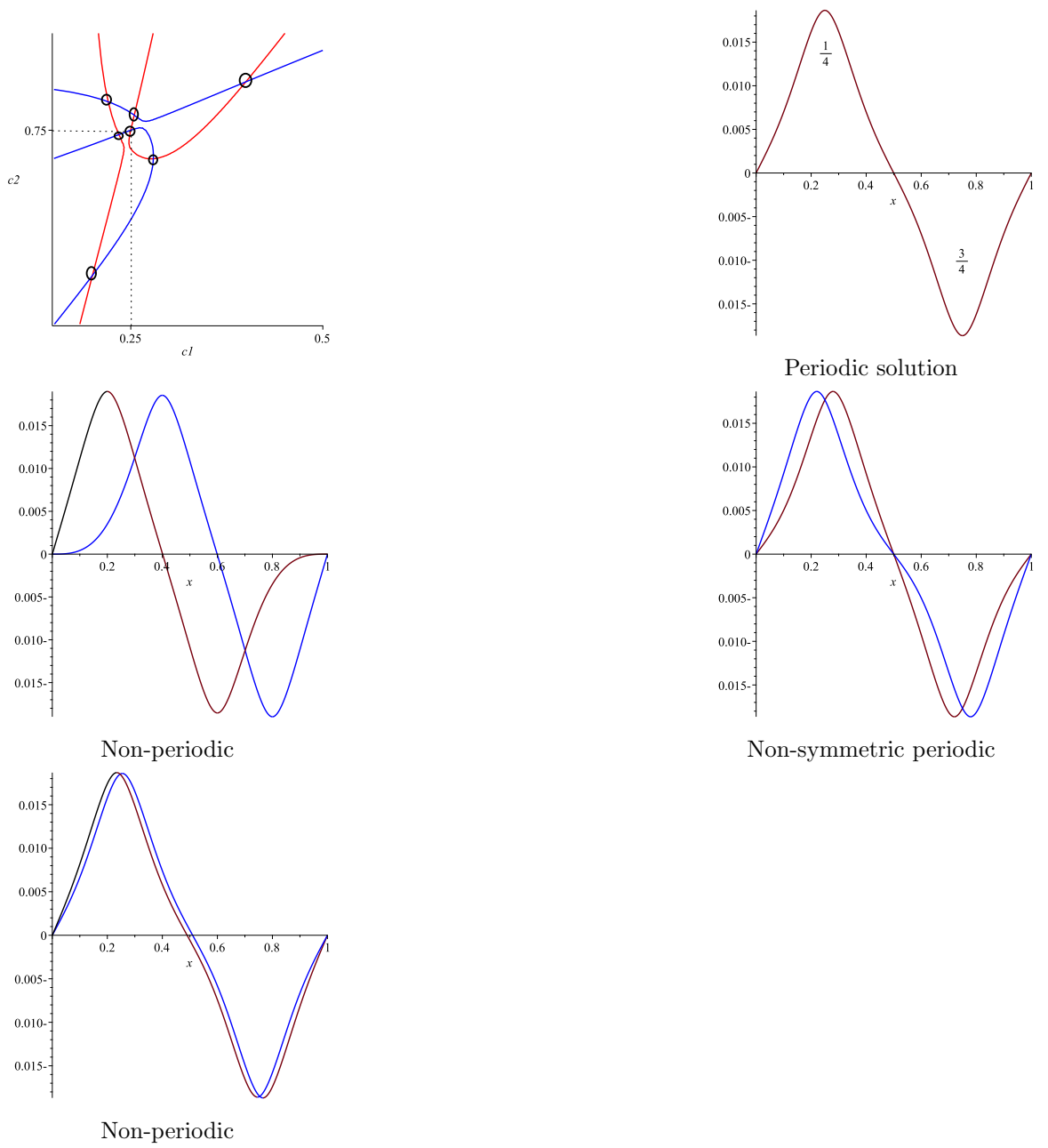


**Figure 3.29:** Solution plots for  $\alpha = 440$  and  $\gamma = 0.02$ . On the top left we have the plots  $F_1$  and  $F_2$  and their 7 intersections. The other 4 plots correspond to these intersections. The first plot is the symmetric that correspond to  $(\frac{1}{4}, \frac{3}{4})$ . The second and third plots represent the two pairs of non-periodic solutions. The fourth plot represents the two pairs of non-symmetric solutions (Each part of the pair is symmetric to the other part).

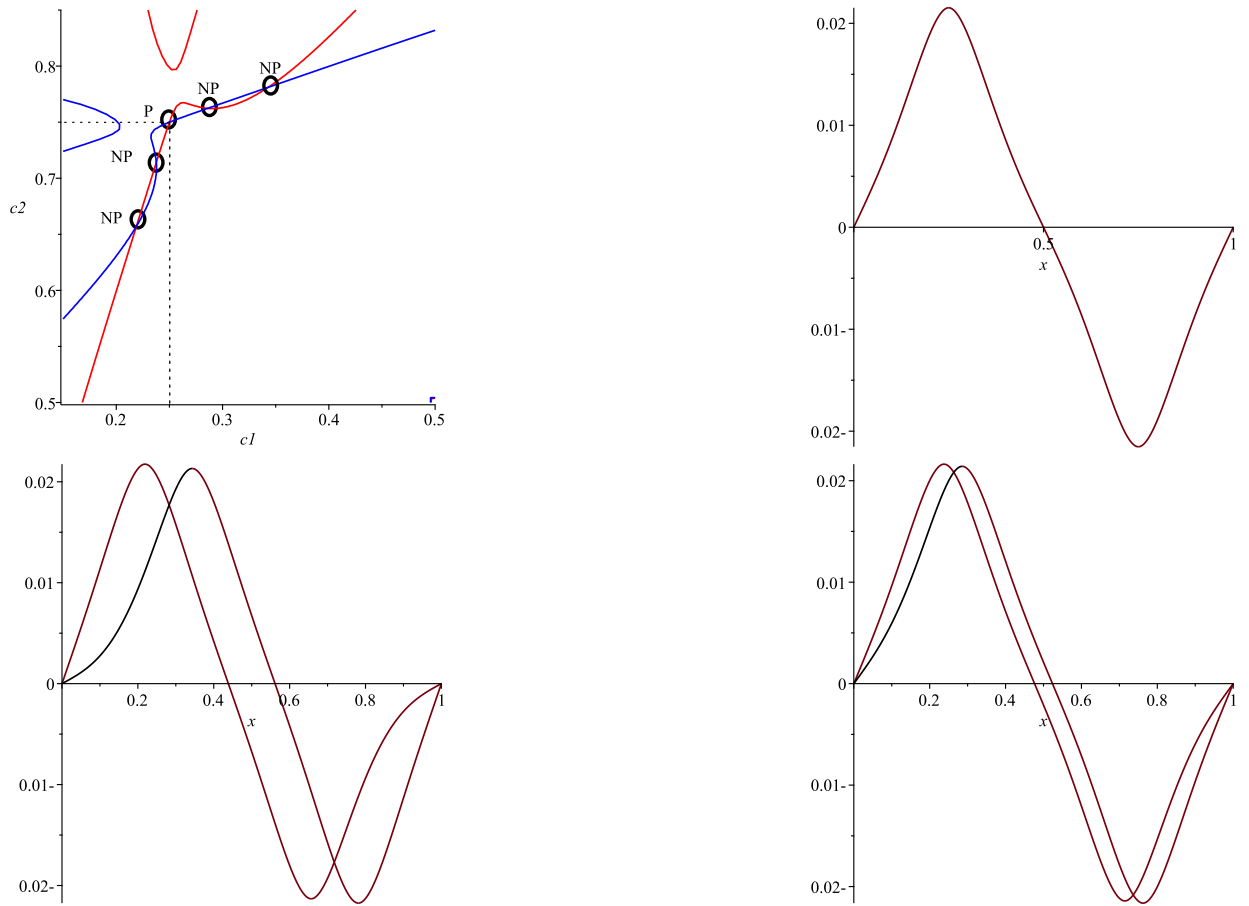


**Figure 3.31:** Solution plots for  $\alpha = 362$  and  $\gamma = 0.02$ . On the top left we have the plots  $F_1$  and  $F_2$  and their 5 intersections. The other 3 plots correspond to these intersections. The first plot is the symmetric that correspond to  $(\frac{1}{4}, \frac{3}{4})$ . The second and third plots represents the two pairs of non-periodic solutions. (Each part of the pair is symmetric to the other part).

In conclusion, we have shown that the solutions to the EL follow a nice progression from periodic to non-periodic to non-symmetric, adding arbitrarily more as  $\alpha$  and  $\frac{1}{\gamma}$  go to infinity. We conjecture that these bifurcation curves continue to appear indefinitely. Whether or not this is indeed the case is an open question at this point.

### 3.6 Conclusion

In this work, we started with Grinfeld and Lord's conjecture for Müller's problem. We then reformulated it to match Yip's problem (see Conjecture 10). Our main results can

## CHAPTER THREE

be summarized as follows:

We started with an energy functional that matches Yip's formulation and Müller's boundary conditions (see Definition (3.2.2)). The functional naturally gives rise to an Euler-Lagrange equation which we then proceed to solve.

It turns out that given initial parameters  $\alpha, \gamma$ , there is a unique symmetric solution of lap 2 (See Theorem 11). Moreover, every other symmetric solution can be expressed using solutions of lap 2 (See Theorem 12).

Theorem 11 and Theorem 12 were enough to disprove the conjecture, and show that Müller's problem and Yip's problem are very different, because the latter framework guarantees the existence of solutions of lap number 2 (for each  $\alpha$  and  $\gamma$ ) which in turn guarantees the existence of solutions with no internal zeroes.

We also showed that non-symmetric solutions exist and they come in pairs which are symmetric with one another. Next, we identified bifurcation curves (for solution with lap 2) and particularly the locus of pitchfork bifurcation.

Furthermore, we evaluated the energies at each solution and also found a formula to calculate energies of higher lap number from a lap number 2.

We can summarize most our work (for solution of lap 2) in Figure 3.32, where the  $\Gamma$  is the curve  $1 - 4\alpha\gamma = 0$  (see Section 3.2). Above the bifurcation curve, we have 3 solutions (of lap 2) two of which are non-symmetric. Below the  $E_{1,2}$  curve,  $u_1$  is a global minimizer. Above the bifurcation curve,  $u_1$  is not a minimizer and between the  $E_{1,2}$  and the bifurcation curve,  $u_1$  is a local minimizer.

CHAPTER THREE

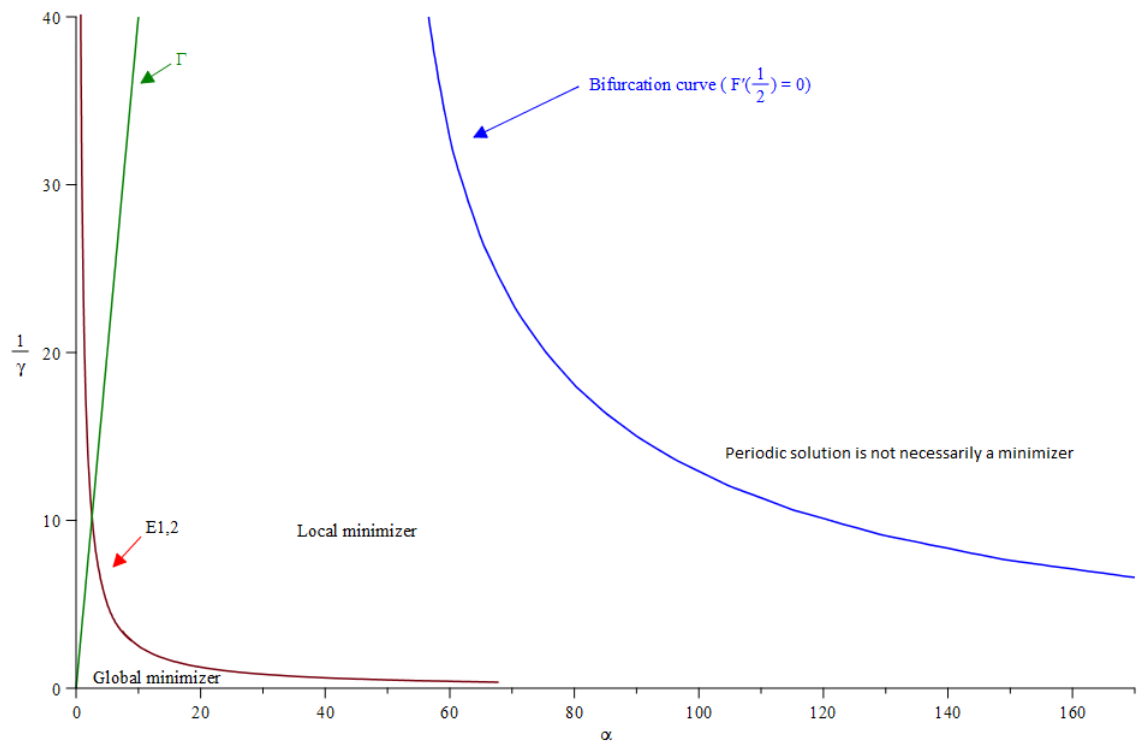


**Figure 3.32:**  $(\alpha, \frac{1}{\gamma})$  plot of  $E_{1,2}$  curve and the first bifurcation curve of lap 2.

Furthermore, we used MAPLE to investigate the bifurcation diagrams of solutions of lap 3. We can summarize our work (of lap 3) in the following picture.

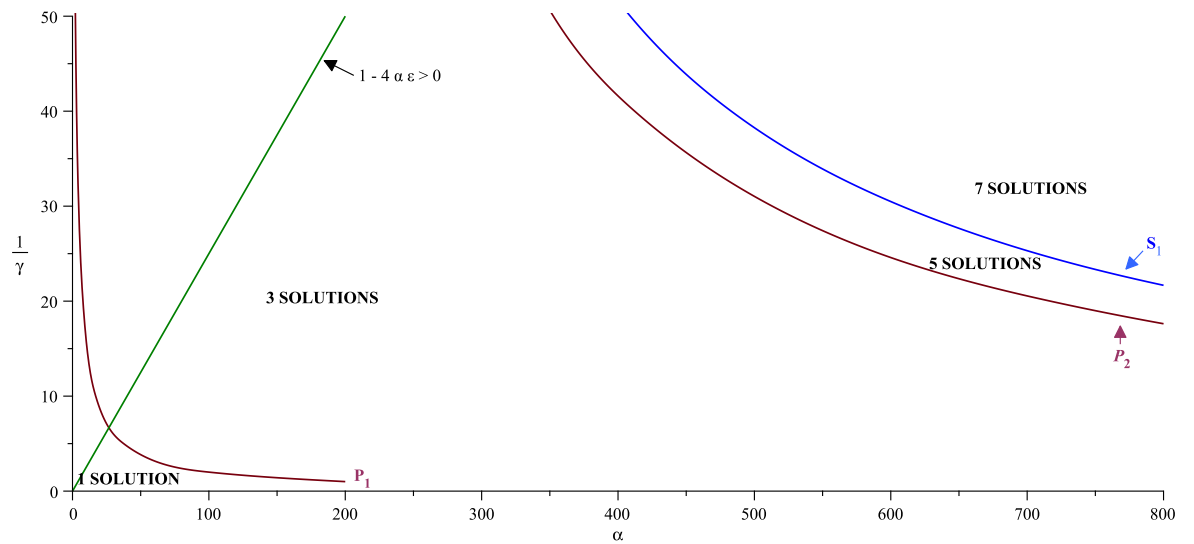


**Figure 3.33:** Three bifurcation curves of lap 3.

## CHAPTER THREE

Our research revealed two types of bifurcation curves, one that gives rise to a fresh pair of non-periodic solutions ( $p$ -curves) and one that gives rise to a fresh pair of non-symmetric solutions ( $s_1$ -curve).

The first bifurcation curve  $p_1$  (i.e. the first time we observe more solutions than just the periodic one) is of the first type. Namely, it gives rise to the first non-periodic solutions. In other words, below the curve  $p_1$  we only have a unique (necessarily periodic) solution while above  $p_1$  we have more than 1 solutions.

The other interesting bifurcation curve is  $s_1$ , namely the first time we observe non-symmetric solutions. In other words, below  $s_1$  we only have symmetric solutions while above  $s_1$  non-symmetric solutions appear (see Section 3.5.1).

Finally, for Figures 3.32 and 3.33, we make the conjecture that if  $\alpha \rightarrow \infty$  then  $\frac{1}{\gamma} \rightarrow 0$  (on the bottom) and  $\frac{1}{\gamma} \rightarrow \infty$  (on the top). More formally, we can parametrize the curve  $r$  using a parameter  $\tau$ . That is, we can write  $r(\tau) = (\alpha(\tau), \gamma(\tau))$ . Moreover we have  $\alpha(\tau) \rightarrow \infty$  whenever  $\tau \rightarrow \pm\infty$  while we also have that  $\gamma(\tau) \rightarrow 0$  whenever  $\tau \rightarrow -\infty$  and  $\gamma(\tau) \rightarrow \infty$  whenever  $\tau \rightarrow \infty$ .

## Chapter 4

# Weak formulations for the Euler Lagrange equation

### 4.1 Introduction

In order to establish the minimizers of the original functional (3.1.1), we would first need to solve the corresponding Euler-Lagrange equation (3.2.2). Ideally, we would like to find closed form theoretical solutions (i.e. exact solutions) but since this is not always possible, we resort to a numerical approximation instead.

The reason why exact solution is not always feasible is due to the fact that we are dealing with the innate difficulty of a very complicated model. For instance, there is a direct correlation between the amount of calculations and the lap number. As the lap number increases, so do the calculations. In particular, we can depend on software like MAPLE so long the lap number remains low. Otherwise, if we have several jumps the theoretical calculation are virtually impossible to work out even with the help of MAPLE. Similarly, the calculations become sometimes impossible when the parameters  $(\alpha, \gamma)$  depend on  $x$ . Another conceptual issue we are facing is that we have no a priori knowledge for the location of the jump(s) which means that the domain of our function is adjustable and not a priori defined which means that the intervals of monotonicity

## CHAPTER FOUR

vary and not specified until we know the value of  $c$ . As we will see later in Chapter 5, this issue will be tackled as follows: we first present a numerical method for a fixed (known) location of the jump  $c$ , and this is then coupled to an optimisation method that seeks the location of the jump  $c$ . Hence, it is a good idea to explore numerical methods.

In particular, we will be working with lap number 2 which is the simplest case. However, before we move to concrete numerical models, we will first establish the theoretical background behind them. The goal of this chapter is to present an equivalent (weak) formulation of the corresponding Euler-Lagrange equation, and the proof of its solvability. This will work as our foundational setup for the specific numerical methods we will use later.

An added benefit of these methods is that they allow us to find solutions in more generalized models (for example, when  $\alpha$  depends on  $x$ ). These are settings where no theoretical framework for solving the ODEs explicitly on a domain of monotonicity is known.

### 4.2 Preliminaries

The Euler Lagrange equation for lap number 2 is given by: Find  $u$  such that

$$\gamma u_{xxxx} - u_{xx} + \alpha u = 0 \quad \text{in } (0, c) \cup (c, 1) \quad (4.2.1)$$

with double Dirichlet boundary conditions, 4 continuity conditions, and one jump condition:

$$\left\{ \begin{array}{l} u(0) = u(1) = 0, u_{xx}(0) = u_{xx}(1) = 0, \\ u(c^-) = u(c^+), u_{xx}(c^-) = u_{xx}(c^+), \\ u_x(c^-) = 0, u_x(c^+) = 0, \\ u_{xxx}(c^+) - u_{xxx}(c^-) = \frac{2}{\gamma}. \end{array} \right. \quad (4.2.2)$$

## CHAPTER FOUR

As we already saw in Chapter 3, (4.2.1) and (4.2.2) lead to a system of 9 equations and 9 unknowns,  $c$  being one of them. This can be tackled directly using the Fredholm Alternative method.

A different approach is to establish an equivalence of the above system with a weak formulation. This latter formulation which can be solved using numerical methods, such as the Finite Element Method, would function as a convenient alternative to the Euler-Lagrange equation. Since the two formulations are equivalent, an approximation of the solution to the weak formulation will also be an approximation of the Euler-Lagrange equation.

Our first hurdle to overcome is that the definition of such formulation requires prior knowledge of  $c$  (the location of the jump), which means we need to fix it a priori. Naturally, by fixing  $c$  we are reducing the number of unknowns to 8 while we still have 9 constraints. This means that for all but the correct value of  $c$ , we would have a singular system and no solutions. To rectify this issue and restore the balance, we can choose to remove one of the restrictions. That way our system will always have a unique solution (as we show in Lemma 4 and Lemma 6). Of course, that solution may or may not satisfy the condition we have omitted. However, when it does, we know that the initial choice for  $c$  was the correct one, as it would now satisfy all of 9 restrictions (not just 8 of them).

For example, we may choose to drop the continuity condition for  $u$ , namely  $u(c^-) = u(c^+)$ . In this case, then for each value of  $c$  the Finite Element Method would produce a different numerical approximation for  $u$ , which will likely have a discontinuity at  $c$ . We are next left with the question of finding the location of  $c$ . For this, we use an optimization method called Derivative-Free Optimization (DFO). The outcomes of this process will provide an approximate location of the jump, and an approximation of  $u$  which is continuous at jump. That way we can guarantee that the produced numerical approximation  $u$  (derived by FEM) will also be continuous at  $c$ , for the reasons we described above. In principle, there is nothing special about dropping this specific condition (i.e. continuity of  $u$  at  $c$ ) and we may elect to drop any of the 3 continuity conditions or even

## CHAPTER FOUR

the jump condition. As a matter of fact, dropping the  $u'(c^-) = u'(c^+) = 0$  condition, leads to a simpler theoretical model as the solution space will be significantly simplified.

In this chapter, we will consider omitting two conditions (one at a time), namely  $u(c^-) = u(c^+)$  and  $u'(c^-) = u'(c^+) = 0$ , as well as the corresponding equivalence of the resulting, less restricted, Euler-Lagrange equation with a weak formulation. In each case, we will show that the weak formulation has a solution which is unique. Finally, we will show how such a solution can be found numerically using the Finite Element Method, and we will precisely estimate its error from the corresponding exact solution of the Euler Lagrange equation.

### 4.3 A weak formulation for the Euler Lagrange equation omitting continuity at $c$

In this section we will drop the continuity condition  $u(c^-) = u(c^+)$  from (4.2.2). Then, introducing  $w = u''$  as an extra unknown, the Euler-Lagrange equation (4.2.1) can be written as the following system of a second order ordinary differential equations

$$\left. \begin{array}{l} w - u'' = 0 \\ \gamma w'' - w + \alpha u = 0 \end{array} \right\} \text{ on } x \in (0, c) \cup (c, 1) : \quad (4.3.1)$$

with the following conditions:

- Dirchlet boundary conditions:  $u(0) = u(1) = w(0) = w(1) = 0$ ,
- three continuity conditions:  $w(c^-) = w(c^+)$ ,  $u'(c^-) = 0$ ,  $u'(c^+) = 0$ ,
- one jump condition:  $w'(c^+) - w'(c^-) = \frac{2}{\gamma}$ .

We will look for a solution pair  $(u, w) \in (\tilde{V}, H_0^1(0, 1))$  of the above system (4.3.1) and its subsequent 8 restrictions, where (see Definitions 2.4.7-2.4.8 and Subsection 2.4.1)

$$H_0^1(0, 1) = \{v \in H^1(0, 1) : v(0) = v(1) = 0\},$$

CHAPTER FOUR

$$\tilde{V} = \{v : v|_{(0,c)} \in H^1(0,c), v|_{(c,1)} \in H^1(c,1), v(0) = v(1) = 0\}.$$

**Remark 15.** •  $\langle \cdot, \cdot \rangle_{(a,b)}$  will denote the duality pairing between  $\mathcal{D}'(a,b)$  and  $\mathcal{D}(a,b)$ .

This is, whenever  $f$  and  $g$  are regular enough we have

$$\langle f, g \rangle_{(a,b)} = \int_b^a f(x) g(x) dx.$$

- All derivatives in this chapter are considered in the distributional sense (i.e. in the weak sense). For example, for  $w \in \mathcal{D}'(a,b)$  we define  $w' \in \mathcal{D}'(a,b)$  as

$$\langle w', \phi \rangle_{(a,b)} = -\langle w, \phi' \rangle_{(a,b)} \quad \forall \phi \in \mathcal{D}(a,b).$$

We can extend this to  $\mathcal{D}^j w$ , the  $j^{\text{th}}$  derivative, as

$$\langle \mathcal{D}^j w, \phi \rangle_{(a,b)} = (-1)^j \langle w, \phi^j \rangle_{(a,b)} \quad \forall \phi \in \mathcal{D}(a,b).$$

The next result gives a weak formulation for the system (4.3.1).

**Lemma 4.** We consider the following two systems of equations:

$$(S_1) \left\{ \begin{array}{ll} u'' = w & \text{on } (0,c) \cup (c,1) & (S_{1a}) \\ \gamma w'' - w + \alpha u = 0 & \text{on } (0,c) \cup (c,1) & (S_{1b}) \\ u(0) = u(1) = 0, w(0) = w(1) = 0, \\ w(c^-) = w(c^+), \\ u_x(c^-) = 0, u_x(c^+) = 0, \\ w'(c^+) - w'(c^-) = \frac{2}{\gamma}, \end{array} \right.$$

CHAPTER FOUR

and: Find  $u \in \tilde{V}$  and  $w \in H_0^1(0,1)$  such that

$$(S_2) \begin{cases} \int_0^1 w(x)v(x) dx + \int_0^1 u'(x)v'(x) dx = 0 \quad \forall v \in \tilde{V}, & (S_{2a}) \\ \gamma \int_0^1 w'(x)z'(x) dx + \int_0^1 w(x)z(x) dx - \alpha \int_0^1 u(x)z(x) dx = 2z(c) \quad \forall z \in H_0^1(0,1). & (S_{2b}) \end{cases}$$

Under the above definitions the systems  $S_1$  and  $S_2$  are equivalent, this is, the pair  $(u, w)$  solves  $S_1$  if and only if  $(u, w)$  solves  $S_2$ .

**Remark 16.** *The arguments given in this proof are standard in the Finite Element literature. In particular, they have been adapted from [42] or [33].*

*Proof.* First, we will show that  $S_1 \Rightarrow S_2$ . From  $(S_{1a})$  we get that, since  $w \in L^2(0,1)$ ,  $u'' \in L^2(0,c)$  and  $u'' \in L^2(c,1)$ . We multiply then  $(S_{1a})$  by  $v \in \tilde{V}$ , integrate over  $(0,c)$  and  $(c,1)$ , and add the resulting equations to get:

$$\Rightarrow \int_0^1 wv - \int_0^c u''v - \int_c^1 u''v = 0.$$

Proceeding as in ([10], pp. 225 – 226), that is, applying Green's formula ([10], p. 296) we get

$$\int_0^1 w(x)v(x) dx + \int_0^c u'(x)v'(x) dx - \left[ u'(x)v(x) \right]_0^c + \int_c^1 u'(x)v'(x) dx - \left[ u'(x)v(x) \right]_c^1 = 0.$$

CHAPTER FOUR

Using the boundary conditions and  $u'(c^-) = u'(c^+) = 0$ , we get

$$\begin{aligned}
 & \int_0^1 w(x)v(x) dx + \int_0^c u'(x)v'(x) dx - \left[ \cancel{u'(c^-)}v(c^-) - u'(0)v(0) \right] \\
 & + \int_c^1 u'(x)v'(x) dx - \left[ u'(1)v(1) - \cancel{u'(c^+)}v(c^+) \right] = 0 \\
 \Rightarrow & \int_0^1 w(x)v(x) dx + \int_0^c u'(x)v'(x) dx + \int_c^1 u'(x)v'(x) dx = 0 \\
 \Rightarrow & \int_0^1 w(x)v(x) + \int_0^1 u'(x)v'(x) dx = 0,
 \end{aligned}$$

so,  $u$  and  $w$  satisfy

$$\int_0^1 w(x)v(x) dx + \int_0^1 u'(x)v'(x) dx = 0 \quad \forall v \in \tilde{V},$$

which is  $(S_{2a})$ .

For  $(S_{1b})$  we proceed in a similar way. We multiply  $(S_{1b})$  by  $z \in H_0^1(0, 1)$  and integrate over  $(0, 1)$  to get

$$\int_0^1 w''(x)z(x) dx - \int_0^1 w(x)z(x) dx + \alpha \int_0^1 u(x)z(x) dx = 0. \quad (4.3.2)$$

The only term that need attention is the first one. Proceeding as before we get

$$\begin{aligned}
 \int_0^1 w''(x)z(x) dx &= \int_0^{c^-} w''(x)z(x) dx + \int_{c^+}^1 w''(x)z(x) dx \\
 &= - \int_0^{c^-} w'(x)z'(x) dx + \left[ w'(x)z(x) \right]_0^{c^-} - \int_{c^+}^1 w'(x)z'(x) dx + \left[ w'(x)z(x) \right]_{c^+}^1.
 \end{aligned}$$

CHAPTER FOUR

Hence

$$\begin{aligned}
 \int_0^1 w''(x) z(x) dx &= - \int_0^c w'(x) z'(x) dx + \left[ w'(c^-) z(c^-) - w'(0) z(0) \right] \\
 &\quad - \int_c^1 w'(x) z'(x) dx + \left[ w'(1) z(1) - w'(c^+) z(c^+) \right], \\
 &= - \int_0^c w'(x) z'(x) dx - \int_c^1 w'(x) z'(x) dx + \left[ w'(c^-) z(c) - w'(c^+) z(c) \right], \quad (4.3.3)
 \end{aligned}$$

where we have used that  $z(c^-) = z(c^+) = z(c)$ , (since  $H_0^1 \subseteq C^0(0, 1)$ , see [10]). Finally, using the jump condition  $w'(c^+) - w'(c^-) = \frac{2}{\gamma}$ , (4.3.3) becomes

$$\begin{aligned}
 \int_0^1 w''(x) z(x) dx &= - \int_0^c w'(x) z'(x) dx - \int_c^1 w'(x) z'(x) dx - \frac{2}{\gamma} z(c) \\
 &= - \int_0^1 w'(x) z'(x) dx - \frac{2}{\gamma} z(c). \quad (4.3.4)
 \end{aligned}$$

So, replacing (4.3.4) in (4.3.2) we arrive at the following equation for  $w$ :

$$\gamma \int_0^1 w'(x) z'(x) dx + \int_0^1 w(x) z(x) dx - \alpha \int_0^1 u(x) z(x) dx = 2 z(c) \quad \forall z \in H_0^1(0, 1), \quad (4.3.5)$$

which is  $(S_{2b})$ .

Thus,  $(S_2)$  is a weak formulation for  $(S_1)$ , and any solution of  $(S_1)$  solves  $(S_2)$ .

Next we will show that  $S_2 \Rightarrow S_1$ .

CHAPTER FOUR

Let  $(u, w)$  be a solution of  $(S_2)$ . Then, for all  $z_1 \in H_0^1(0, c)$  we consider the function

$$\tilde{Z} = \begin{cases} z_1 & \text{in } (0, c) \\ 0 & \text{in } (c, 1). \end{cases},$$

then  $\tilde{Z} \in H_0^1(0, 1)$ . For  $(S_{2b})$  we have

$$\begin{aligned} & \int_0^1 (\gamma w'(x) \tilde{Z}'(x) + w(x) \tilde{Z}(x) - \alpha u(x) \tilde{Z}(x)) dx = 0 \\ \Rightarrow & \int_0^c \gamma w'(x) z_1'(x) dx + w(x) z_1(x) dx - \alpha u(x) z_1(x) dx = 0, \end{aligned} \quad (4.3.6)$$

for all  $z_1 \in H_0^1(0, c)$ . Next, since

$$\int_0^c w'(x) \phi'(x) dx = -\langle w'', \phi \rangle_{(0,c)} \quad \forall \phi \in \mathcal{D}(0, c),$$

(4.3.6) implies

$$\langle -\gamma w'' + w - \alpha u, \phi \rangle_{(0,c)} = 0,$$

for all  $\phi \in \mathcal{D}(0, c)$ . Thus

$$-\gamma w'' + w - \alpha u \quad \text{in } \mathcal{D}'(0, c).$$

But,  $w - \alpha u \in L^2(0, c)$ , and then

$$w'' = \frac{1}{\gamma}(w - \alpha u) \in L^2(0, c),$$

which implies that  $w \in H^2(0, c)$ .

Proceeding in exactly the same way we get

$$w'' = \frac{1}{\gamma}(w - \alpha u) \in L^2(c, 1)$$

CHAPTER FOUR

which implies that  $w \in H^2(c, 1)$ , and also

$$-\gamma w'' + w - \alpha u = 0 \quad \text{in } (0, c) \text{ and } (c, 1),$$

which shows that  $(u, w)$  solves  $(S_{1b})$ . Now, since  $w \in H_0^1(0, 1)$ , then  $w \in C^0(0, 1)$  (using the Sobolev's embedding theorem (see [10], Theorem 8.8), and then  $w(c^-) = w(c^+)$ .

We next verify the jump condition. Since we can take any  $z \in H_0^1(0, 1)$ , let  $z \in H_0^1(0, 1)$  such that  $z(c) = 1$ . By  $(S_{2b})$  we have

$$\gamma \int_0^1 w'(x) z'(x) dx + \int_0^1 w(x) z(x) dx - \alpha \int_0^1 u(x) z(x) dx = 2z(c) \quad \forall z \in H_0^1(0, 1).$$

Let us work inside  $\int_0^1 w'(x) z'(x) dx$ :

$$\int_0^c w'(x) z'(x) dx = - \int_0^c w''(x) z(x) dx + w'(c^-) z(c),$$

where we used integration by parts. Similarly,

$$\int_c^1 w'(x) z'(x) dx = - \int_c^1 w''(x) z(x) dx + w'(c^+) z(c).$$

Then

$$\int_0^1 w'(x) z'(x) dx = \int_0^1 w''(x) z(x) dx + (w'(c^+) - w'(c^-)) z(c).$$

Substituting into  $(S_{2b})$  we arrive at

$$\gamma \left[ \int_0^1 w''(x) z(x) dx + (w'(c^+) - w'(c^-)) z(c) \right] + \int_0^1 w(x) z(x) dx - \alpha \int_0^1 u(x) z(x) dx = 2z(c),$$

CHAPTER FOUR

and

$$\int_0^1 (\gamma w''(x) - w(x) + \alpha u(x)) z(x) dx + \gamma \left[ w'(c^+) - w'(c^-) \right] z(c) = 2z(c). \quad (4.3.7)$$

Therefore, since  $w'' - w + \alpha = 0$  in  $(0, c) \cup (c, 1)$ , and  $z(c) = 1$ , (4.3.7) implies

$$\left[ w'(c^+) - w'(c^-) \right] = \frac{2}{\gamma}.$$

So far we recovered the boundary conditions, the jump condition and the continuity of the second derivative. It only remains to show that  $(u, w)$  satisfies  $(S_{1a})$ . Let  $v \in H_0^1(0, c)$  and define

$$\tilde{v} = \begin{cases} v & \text{in } (0, c) \\ 0 & \text{in } \tilde{V}. \end{cases} \quad \Rightarrow \tilde{v} \in H_0^1(0, 1)$$

Then, since  $(u, w)$  solves  $(S_{2a})$  we get

$$\begin{aligned} & \int_0^1 u'(x) \tilde{v}'(x) + w(x) \tilde{v}(x) dx = 0 \\ \Rightarrow & \int_0^c u'(x) v'(x) + w(x) v(x) dx = 0 \quad \forall v \in H_0^1(0, c), \end{aligned}$$

and then

$$\begin{aligned} & \langle -u'', \phi \rangle_{(0,c)} + \langle w, \phi \rangle_{(0,c)} \\ & = \langle u', \phi' \rangle_{(0,c)} + \langle w, \phi \rangle_{(0,c)} = 0 \quad \forall \phi \in \mathcal{D}(0, c). \end{aligned}$$

Thus,

$$u'' - w = 0 \quad \text{in } \mathcal{D}'(0, c)$$

## CHAPTER FOUR

which, again, implies that  $u'' \in L^2(0, c)$ , and

$$u'' - w = 0 \quad \text{a.e. in } (0, c).$$

Analogously we can show that

$$u'' - w = 0 \quad \text{a.e. in } (c, 1).$$

The only remaining condition to satisfy is  $u'(c^-) = u'(c^+) = 0$ . First, since  $u \in H^2(0, c)$  and  $u \in H^2(c, 1)$ , then  $u'(c^-)$  and  $u'(c^+)$  are well-defined. Let  $\hat{v} \in \tilde{V}$  s.t.  $\hat{v}|_{(c,1)} = 0$ ,  $\hat{v}(c^-) = 1$ . Then, from  $(S_{2a})$  we get

$$\int_0^c w(x)\hat{v}(x) dx - \int_0^c u'(x)\hat{v}'(x) dx = 0$$

and then, integrating by parts

$$\int_0^c (w(x) - u''(x))\hat{v}(x) + u'(c^-)\hat{v}(1) = 0$$

But  $w - u'' = 0$  a.e. in  $(0, c)$  and  $\hat{v}(1) = 1$ , and we thus conclude that  $u'(c^-) = 0$ .

In a completely analogous way we see that  $u'(c^+) = 0$ . □

**Remark 17.** *The weak form  $(S_2)$  appears as a result of introducing the extra variable  $w = u''$  into the problem. This process of replacing a high order differential equation by a system of low order equations leads to a particular class of Finite Element Methods, namely Mixed Finite Element Methods. Examples of such methods can be found in [33], or the very extensive review [8].*

*We will not give a detailed description of Mixed Finite Element Methods because, as we will show in the next section, the bilinear form associated to  $(S_2)$  is elliptic. This gives a freedom to choose any Finite Element spaces for  $u$  and  $w$ , contrary to most Mixed methods where the Finite Element spaces for all the variables need to be correctly*

## CHAPTER FOUR

*balanced.*

Lemma 4 allows us to find a solution to the (less restricted) Euler-Lagrange equation  $(S_1)$ , indirectly by finding a solution to the weak formulation  $(S_2)$  instead, provided that such a solution exists. As we will see next, not only such a solution always exists and it is a unique, but also we can directly apply numerical methods to approximate it, namely the Finite Element method (FEM).

### 4.3.1 The Existence and Uniqueness of the Weak Formulation $(S_2)$

Next, we prove the existence and uniqueness of solution of the weak formulation described above. First, let us recall the following important definition.

- $\tilde{V} = \{v : v|_{(0,c)} \in H^1(0,c), v|_{(c,1)} \in H^1(c,1), v(0) = v(1) = 0\}$ ,  
provided with an inner product defined by

$$\langle f, g \rangle_{\tilde{V}} = \int_0^c f'(x)g'(x)dx + \int_c^1 f'(x)g'(x)dx. \quad (4.3.8)$$

**Lemma 5.**  $\tilde{V}$  is a complete (and thus Hilbert) space.

*Proof.* To show (4.3.8) satisfies an inner product, the only property we need to prove is positive definiteness:

$$\langle f, f \rangle_{\tilde{V}} = \int_0^c [f']^2 + \int_c^1 [f']^2 \geq 0.$$

Next, if  $f \in \tilde{V}$  is s.t.

$$\langle f, f \rangle_{\tilde{V}} = 0 \Rightarrow [f']^2|_{(0,c)} = [f']^2|_{(c,1)} = 0 \Rightarrow f'(x) = 0 \forall x \text{ on } (0,1) \setminus \{c\}.$$

Then,  $f(x) = c_1$  in  $(0,c)$  and  $f(x) = c_2$  in  $(c,1)$ , but,  $f(0) = 0$  and  $f(1) = 0$  which implies that  $c_1 = c_2 = 0$ .

## CHAPTER FOUR

Now to prove the completeness, let  $f_n \in \tilde{V}$  be a Cauchy sequence and let

$$g_n = f_n |_{(0,c)} \in H^1(0,c).$$

Clearly  $g_n \in H^1(0,c)$  is also a Cauchy. But  $H^1(0,c)$  is a Hilbert space and thus complete. So there exists  $g \in H^1(0,c)$  such that  $g_n \rightarrow g$  in  $H^1(0,c)$ . Moreover, since

$$g_n(0) = f_n(0) = 0 \quad \forall n \in \mathbb{N},$$

also,  $g_n \in C([0,c])$ , again from Sobolev's embedding theorem convergence in  $H_0^1(0,1)$  imply convergence in  $C^0[0,c]$ , we have that

$$g(0) = \lim g_n(0) = 0.$$

Similarly, for  $h_n = f_n |_{(c,1)} \in H^1(c,1)$ , there exists  $h \in H^1(c,1)$  with  $h(1) = 0$  such that  $h_n \rightarrow h$  in  $H^1(c,1)$ . Let

$$f(x) = \begin{cases} g(x) & \text{when } x \in [0,c), \\ h(x) & \text{when } x \in (c,1]. \end{cases}$$

Clearly  $f \in \tilde{V}$ , and

$$\begin{aligned} \|f_n - f\|_{\tilde{V}}^2 &\leq \|f_n |_{(0,c)} - f |_{(0,c)}\|_{H^1(0,c)}^2 + \|f_n |_{(c,1)} - f |_{(c,1)}\|_{H^1(c,1)}^2 \\ &= \|g_n - g\|_{H^1(0,c)}^2 + \|h_n - h\|_{H^1(c,1)}^2 \rightarrow 0. \end{aligned}$$

Thus,  $\tilde{V}$  is complete and therefore a Hilbert space. □

We also know that if  $H_1$  and  $H_2$  are Hilbert spaces then

$$H_1 \times H_2 = \{(f, g) : f \in H_1, g \in H_2\}$$

## CHAPTER FOUR

is a Hilbert space [31].

**Corollary 1.** *The space  $\mathbf{H} = \tilde{V} \times H_0^1(0,1)$  is a Hilbert space with a scalar product:*

$$\begin{aligned} \langle (f_1, g_1), (f_2, g_2) \rangle_{\mathbf{H}} &= \langle f_1, f_2 \rangle_{\tilde{V}} + \langle g_1, g_2 \rangle_{H_0^1(0,1)} \\ &= \int_0^c f_1'(x) f_2'(x) dx + \int_c^1 f_1'(x) f_2'(x) dx + \int_0^1 g_1'(x) g_2'(x) dx. \end{aligned}$$

with induced norm  $\|(v, w)\|_{\mathbf{H}} = \left[ (v, w), (v, w) \right]_{\mathbf{H}}^{1/2}$ .

Next we define bilinear and linear functionals respectively:

1. Define  $A : \mathbf{H} \times \mathbf{H} \rightarrow \mathbb{R}$  by

$$\begin{aligned} (u, w), (v, z) \rightarrow A((u, w), (v, z)) &= \int_0^1 u'(x) v'(x) dx + \int_0^1 w(x) v(x) dx - \int_0^1 u(x) z(x) dx \\ &+ \frac{\gamma}{\alpha} \int_0^1 w'(x) z'(x) dx + \frac{1}{\alpha} \int_0^1 w(x) z(x) dx. \end{aligned} \tag{4.3.9}$$

Then  $A$  is a bilinear.

2. Define  $L : \mathbf{H} \rightarrow \mathbb{R}$  by

$$(v, z) \rightarrow L((v, z)) = \frac{2}{\alpha} z(c). \tag{4.3.10}$$

Then  $L$  is a linear functional.

With those notations, problem  $(S_2)$  becomes : Find  $(u, w) \in \mathbf{H}$  such that for all  $(v, z) \in \mathbf{H}$ ,

$$A((u, w), (v, z)) = L((v, z)). \tag{4.3.11}$$

We have the following theorem:

**Theorem 15.** *There exists a unique  $(u, w) \in \mathbf{H}$ , solution of (4.3.11).*

## CHAPTER FOUR

*Proof.* By Lax-Milgram theorem [33], to prove (4.3.11) has a unique solution, it is enough to show:

1.  $L$  is continuous:

$$\exists k_1 > 0 \quad \text{s.t.} \quad |L(v, z)| \leq k_1 \|(v, z)\|_{\mathbf{H}}, \quad \forall (v, z) \in \mathbf{H},$$

2.  $A$  is continuous:

$$\exists k_2 > 0 \quad \text{s.t.} \quad |A((v, z), (u, w))| \leq k_2 \|(v, z)\|_{\mathbf{H}} \|(u, w)\|_{\mathbf{H}}, \quad \forall (v, z), (u, w) \in \mathbf{H},$$

3.  $A$  is elliptic:

$$\exists k_3 > 0 \quad \text{s.t.} \quad |A((v, z), (v, z))| \geq k_3 \|(v, z)\|_{\mathbf{H}}^2 \quad \forall (v, z) \in \mathbf{H}.$$

Now we will prove the previous three conditions. First for  $L$  is continuous:

Let  $(v, z) \in \mathbf{H}$ . Since  $z \in H_0^1(a, b) \subseteq C^0([a, b])$  there exists  $t \in (0, 1)$  such that

$$|z(x)| \leq |z(t)| \quad \forall x \in [0, 1].$$

Using the Sobolev's embedding theorem this implies, in particular, that

$$|L(v, z)| = \frac{2}{\gamma} |z(c)| \leq \frac{2}{\gamma} |z(t)| = \frac{2}{\gamma} \|z\|_{C^0([0,1])} \leq \frac{C}{\gamma} \|z\|_{H_0^1(0,1)} \leq \frac{C}{\gamma} \|(v, z)\|_{\mathbf{H}}.$$

Second, we prove that  $A$  is continuous. Let  $(u, w), (v, z) \in \mathbf{H}$ . Then

$$|A((u, w), (v, z))| \leq \int_0^1 |u', v'| + \int_0^1 |w, v| + \int_0^1 |u, z| + \frac{\gamma}{\alpha} \int_0^1 |w', z'| + \frac{1}{\alpha} \int_0^1 |w, z|,$$

## CHAPTER FOUR

and using the Cauchy-Schwarz inequality, we get

$$|A((u, w), (v, z))| \leq \|u'\|_{L^2(0,1)} \|v'\|_{L^2(0,1)} + \|w\|_{L^2(0,1)} \|v\|_{L^2(0,1)} + \|u\|_{L^2(0,1)} \|z\|_{L^2(0,1)} \\ + \frac{\gamma}{\alpha} \|w'\|_{L^2(0,1)} \|z'\|_{L^2(0,1)} + \frac{1}{\alpha} \|w\|_{L^2(0,1)} \|z\|_{L^2(0,1)}.$$

We know that by definition

$$\begin{cases} \|w'\|_{L^2(0,1)} = \|w\|_{H_0^1(0,1)}, \\ \|z'\|_{L^2(0,1)} = \|z\|_{H_0^1(0,1)}. \end{cases}$$

Similarly,

$$\begin{cases} \|u'\|_{L^2(0,1)} = \|u\|_{\tilde{V}}, \\ \|v'\|_{L^2(0,1)} = \|v\|_{\tilde{V}}. \end{cases}$$

Now using the Poincaré Inequality [33], we know that there exists  $C > 0$  s.t.

$$\|w\|_{L^2(0,1)}^2 \leq C \|w\|_{H_0^1(0,1)}^2.$$

A similar argument shows that  $\|z\|_{L^2(0,1)} \leq C \|z\|_{\tilde{V}}$ . Putting all together, we get

$$|A((u, w), (v, z))| \leq \|u\|_{\tilde{V}} \|v\|_{\tilde{V}} + \|w\|_{H_0^1(0,1)} \|v\|_{\tilde{V}} + \|u\|_{\tilde{V}} \|z\|_{H_0^1(0,1)} \\ + \frac{\gamma}{\alpha} \|w\|_{H_0^1(0,1)} \|z\|_{H_0^1(0,1)} + \frac{1}{\alpha} \|w\|_{H_0^1(0,1)} \|z\|_{H_0^1(0,1)} \\ \leq \max \left\{ 1, \frac{\gamma+1}{\alpha} \right\} \left[ \|u\|_{\tilde{V}} \|v\|_{\tilde{V}} + \|w\|_{H_0^1(0,1)} \|v\|_{\tilde{V}} \right. \\ \left. + \|u\|_{\tilde{V}} \|z\|_{H_0^1(0,1)} + \|w\|_{H_0^1(0,1)} \|z\|_{H_0^1(0,1)} \right]$$

CHAPTER FOUR

$$\begin{aligned}
&= \max \left\{ 1, \frac{\gamma+1}{\alpha} \right\} \left[ (\|u\|_{\tilde{V}} + \|w\|_{H_0^1(0,1)}) (\|v\|_{\tilde{V}} + \|z\|_{H_0^1(0,1)}) \right] \\
&\leq 2 \max \left\{ 1, \frac{\gamma+1}{\alpha} \right\} \sqrt{\|u\|_{\tilde{V}}^2 + \|w\|_{H_0^1(0,1)}^2} \sqrt{\|v\|_{\tilde{V}}^2 + \|z\|_{H_0^1(0,1)}^2},
\end{aligned}$$

where we used the fact that if  $a, b > 0$  then  $a + b \leq \sqrt{2} \sqrt{a^2 + b^2}$ . Recall

$$\|(u, w)\|_{\mathbf{H}}^2 = \int_0^c (u')^2 + \int_c^1 (u')^2 + \int_0^1 (w')^2 = \|u\|_{\tilde{V}}^2 + \|w\|_{H_0^1}^2. \quad (4.3.12)$$

Similarly,

$$\|(v, z)\|_{\mathbf{H}}^2 = \|v\|_{\tilde{V}}^2 + \|z\|_{H_0^1}^2. \quad (4.3.13)$$

Let  $k_2 = 2 \max \left\{ 1, \frac{\gamma+1}{\alpha} \right\}$ . Thus

$$\begin{aligned}
|A((u, w), (v, z))| &\leq k_2 \sqrt{\|u\|_{\tilde{V}}^2 + \|w\|_{H_0^1(0,1)}^2} \sqrt{\|v\|_{\tilde{V}}^2 + \|z\|_{H_0^1(0,1)}^2} \\
&\leq k_2 \|(u, w)\|_{\mathbf{H}} \|(v, z)\|_{\mathbf{H}}
\end{aligned}$$

Thirdly, we prove that  $A$  is elliptic. By its definition, and the fact that  $\|z\|_{L^2(0,1)}^2 \geq 0$ , it follows that

$$\begin{aligned}
A((v, z), (v, z)) &= \langle v', v' \rangle + \cancel{\langle z, v \rangle} - \cancel{\langle v, z \rangle} + \frac{\gamma}{\alpha} \langle z', z' \rangle + \frac{1}{\alpha} \langle z, z \rangle \\
&= \|v\|_{\tilde{V}}^2 + \frac{\gamma}{\alpha} \|z\|_{H_0^1(0,1)}^2 + \frac{1}{\alpha} \|z\|_{L^2(0,1)}^2 \\
&\geq \|v\|_{\tilde{V}}^2 + \frac{\gamma}{\alpha} \|z\|_{H_0^1(0,1)}^2 \\
&\geq \min \left\{ 1, \frac{1}{\alpha} \right\} \|(v, z)\|_{\mathbf{H}}^2.
\end{aligned}$$

Thus  $A$  is elliptic.

So, we have checked the hypothesis of Lax-Milgram's lemma, and then problem (4.3.11)

## CHAPTER FOUR

has a unique solution  $(u, w) \in \mathbf{H}$ . □

### 4.3.2 The Finite Element Method and Its Error Estimate

Next, we produce a similar result for a subspace of  $\mathbf{H}$ . First, we divide the interval  $[0, 1]$  as follows

$$0 = x_0 < x_1 < x_2 < \dots < x_{N-1} < x_N = 1$$

with  $h = \frac{1}{N} = (x_k - x_{k-1})$  for  $k = 1, \dots, N$ . This is, we divide  $[0, 1]$  into equidistant points. If the jump is located at  $c \in (0, 1)$  then there exists a unique  $j \in \{0, \dots, N\}$  such that

$$x_{j-1} \leq c < x_j.$$

Now we introduce the following subspace:

$$\mathbf{H}_h = \tilde{V}_h \times H_h \subseteq \mathbf{H} = \tilde{V} \times H_0^1(0, 1),$$

where

$$H_h = \{v_h \in C^0([0, 1]) = v_h|_{(x_i, x_{i+1})} \in \mathbb{P}_1, v_h(0) = v_h(1) = 0\},$$

and

$$\tilde{V}_h = \{v_h|_{(0,c)} \in C^0([0, c]), v_h|_{(c,1)} \in C^0([c, 1]) : v_h|_{(0,c)} \in \mathbb{P}_1^h[0, c], v_h|_{(c,1)} \in \mathbb{P}_1^h[c, 1],$$

$$v_h(0) = v_h(1) = 0\}.$$

and  $\mathbb{P}_1^h[a, b]$  is the class of piecewise linear functions on the partition  $[a = y_0 < y_1 < \dots < y_n = b]$  with  $y_{i+1} - y_i = h$  with possibly on exception of the first or last segment which should be clear from the context. Also, the method should still work for  $\mathbb{P}_2$  (piecewise parabolic functions) or higher  $\mathbb{P}_i$ 's as we would be adding extra degree of freedom, the basis functions should be adjusted accordingly.

Note that we did not use the Discontinuous Galerkin method, because even when we consider the space  $\tilde{V}$  (which consists of functions discontinuous at  $x = c$ ), we

## CHAPTER FOUR

really are working on each of the continuous segments separately. The Discontinuous Galerkin method refers to using a space of totally discontinuous finite element method, supplemented by appropriate term to enhance stability.

The Finite Element Method consists of finding  $(u_h, w_h) \in \tilde{V}_h \times H_h$  s.t.

$$A((u_h, w_h), (v_h, z_h)) = L((v_h, z_h)) \quad \forall (v_h, z_h) \in \tilde{V}_h \times H_h. \quad (4.3.14)$$

As an immediate consequence of Theorem 15 we also have a similar theorem when we restrict ourselves to the subspace  $\mathbf{H}_h \subseteq \mathbf{H}$

**Theorem 16.** *There exists a unique  $(u_h, w_h) \in \mathbf{H}_h$ , solution of (4.3.14).*

*Proof.* Since  $\tilde{V}_h \times H_h \subseteq \tilde{V} \times H_0^1(0, 1)$ , then  $A$  is elliptic and continuous in this space as well. Also,  $L$  is continuous in  $\tilde{V}_h \times H_h$ .  $\square$

Next we evaluate the error of the solution produced by the Finite element method introduced above. We have the following theorem

**Theorem 17.** *Let  $(u, w)$  be a solution of (4.3.11) which satisfies  $u|_{0,c} \in H^2(0, c)$ ,  $u|_{c,1} \in H^2(c, 1)$  and  $w \in H^2(0, c)$  and  $w \in H^2(c, 1)$ . Then, there exists  $C > 0$  independent of  $h$  such that*

$$\|(u - u_h, w - w_h)\|_{\mathbf{H}} \leq Ch \left\{ \sqrt{|u|_{H^2(0,c)}^2 + |u|_{H^2(c,1)}^2} + \sqrt{|w|_{H^2(0,c)}^2 + |w|_{H^2(c,1)}^2} \right\}.$$

*Proof.* Let  $(u, w) \in \tilde{V} \times H_0^1$  be the unique solution of (4.3.11). Let  $(u_h, w_h) \in \tilde{V}_h \times H_h$  be the unique solution of (4.3.14). Thus

$$A((u, w), (v_h, z_h)) = L((v_h, z_h)),$$

$$A((u_h, w_h), (v_h, z_h)) = L((v_h, z_h)),$$

and then

$$A((u, w), (v_h, z_h)) = A((u_h, w_h), (v_h, z_h)), \quad \forall (v_h, z_h) \in \tilde{V}_h \times H_h.$$

## CHAPTER FOUR

The bilinearity of  $A$  implies the following ‘‘Galerkin orthogonality’’

$$A((u - u_h, w - w_h), (v_h, z_h)) = 0 \quad \forall (v_h, z_h) \in \mathbf{H}_h. \quad (4.3.15)$$

But we know that  $A$  is elliptic and continuous. Then, using (4.3.15) we get

$$\begin{aligned} k_3 \|(u - u_h, w - w_h)\|_{\mathbf{H}}^2 &\leq A((u - u_h, w - w_h), (u - u_h, w - w_h)) \\ &= A((u - u_h, w - w_h), (u, w)) - A((u - u_h, w - w_h), (u_h, w_h)) \\ &\stackrel{(4.3.15)}{=} A((u - u_h, w - w_h), (u, w)) \\ &= A((u - u_h, w - w_h), (u, w)) - A((u - u_h, w - w_h), (v_h, z_h)) \\ &= A((u - u_h, w - w_h), (u - v_h, w - z_h)) \\ &\leq k_2 \|(u - u_h, w - w_h)\|_{\mathbf{H}} \|(u - v_h, w - z_h)\|_{\mathbf{H}}, \quad \forall (v_h, z_h) \in \mathbf{H}_h, \end{aligned}$$

where we used the fact that  $A$  is continuous. Dividing by  $\|(u - u_h, w - w_h)\|_{\mathbf{H}}$  we conclude that:

$$\|(u - u_h, w - w_h)\|_{\mathbf{H}} \leq \frac{k_2}{k_3} \|(u - v_h, w - z_h)\|_{\mathbf{H}} \quad \forall (v_h, z_h) \in \mathbf{H}_h \quad (4.3.16)$$

The above implies that

$$\|(u - u_h, w - w_h)\|_{\mathbf{H}} \leq \frac{k_2}{k_3} \inf_{(v_h, z_h) \in \mathbf{H}_h} \|(u - v_h, w - z_h)\|_{\mathbf{H}}.$$

In particular, we choose

$$\begin{cases} v_h = \tilde{i}_h(u), \\ z_h = i_h(w), \end{cases}$$

where  $\tilde{i}_h(u)$  and  $i_h(w)$  are defined as

$$\begin{cases} \tilde{i}_h(u) = \sum_{i=1}^{N+2} \xi_i \psi_i(x), \\ i_h(w) = \sum_{i=1}^N \zeta_i \varphi_i(x), \end{cases}$$

## CHAPTER FOUR

where the  $\psi_i$  and  $\varphi_i$  are basis functions of the corresponding  $\tilde{V}_h$  and  $H_h$  respectively and the discrepancy in the number of summands is a result of the allowed discontinuities at  $c$  in the first  $\tilde{V}_h$ . For more details see Chapter 5.

These interpolates satisfy the bounds (see [42])

$$\|u - \tilde{i}_h(u)\|_{\tilde{V}} \leq Ch \sqrt{|u|_{H^2(0,c)}^2 + |u|_{H^2(c,1)}^2}$$

and

$$\|w - i_h(w)\|_{H_0^1(0,1)} \leq Ch \sqrt{|w|_{H^2(0,c)}^2 + |w|_{H^2(c,1)}^2}.$$

The above proves that

$$\begin{aligned} \|(u - u_h, w - w_h)\|_{\mathbf{H}} &\leq Ch (\|u - \tilde{i}_h(u)\|_{\tilde{V}} + \|w - i_h(w)\|_{H_0^1(0,1)}) \\ &\leq Ch \left[ \sqrt{|w|_{H^2(0,c)}^2 + |w|_{H^2(c,1)}^2} + \sqrt{|u|_{H^2(0,c)}^2 + |u|_{H^2(c,1)}^2} \right]. \end{aligned}$$

□

**Remark 18.** *Clearly the right hand side goes to zero when  $h$  tends to zero, this is when the mesh gets refined.*

### 4.4 A weak formulation for the Euler Lagrange Equation omitting the derivative condition

In this section we will drop the derivative condition  $u'(c^-) = 0$ . Without the derivative condition the Euler-Lagrange equation (4.2.1) can be written as the following system of second order ordinary differential equations

$$\left. \begin{aligned} w - u'' &= 0 \\ \gamma w'' - w + \alpha u &= 0 \end{aligned} \right\} \text{in } (0, c) \cup (c, 1) \quad (4.4.1)$$

## CHAPTER FOUR

with the following conditions:

- Dirchlet boundary conditions:  $u(0) = u(1) = w(0) = w(1) = 0$ ,
- three continuity conditions:  $w(c^-) = w(c^+)$ ,  $u'(c^-) = u'(c^+)$ ,  $u(c^-) = u(c^+)$ ,
- one jump condition:  $w(c^+) - w(c^-) = \frac{2}{\gamma}$ .

Notice that the  $u'(c^-) = 0$  condition has been now replaced by  $u(c^-) = u(c^+)$ . Unlike the previous case we seek for a solution  $u, w \in H_0^1(0, 1)$  where only  $w$  was in  $H_0^1(0, 1)$  while  $u$  was in  $\tilde{V}$ , here we seek a solution where both  $u, w \in H_0^1(0, 1)$ . The next result gives a weak formulation for the system (4.4.1).

**Lemma 6.** *We consider the following two systems of equations:*

$$(S'_1) \begin{cases} u'' = w & (S'_{1a}) \\ \gamma w'' - w + \alpha u = 0 & (S'_{1b}) \\ u(0) = u(1) = 0, w(0) = w(1) = 0, \\ u_x(c^-) = u_x(c^+), u(c^-) = u(c^+), \\ w(c^-) = w(c^+), w'(c^+) - w'(c^-) = \frac{2}{\gamma}. \end{cases}$$

and: Find  $u, w \in H_0^1(0, 1)$  such that

$$(S'_2) \begin{cases} \int_0^1 w(x)v(x) dx + \int_0^1 u'(x)v'(x) dx = 0 \quad \forall v \in H_0^1(0, 1), & (S'_{2a}) \\ \gamma \int_0^1 w'(x)z'(x) dx + \int_0^1 w(x)z(x) dx - \alpha \int_0^1 u(x)z(x) dx = 2z(c) \quad \forall z \in H_0^1(0, 1). & (S'_{2b}) \end{cases}$$

Under the above definitions the systems  $(S'_1)$  and  $(S'_2)$  are equivalent, this is, the pair  $(u, w)$  solves  $(S'_1)$  if and only if  $(u, w)$  solves  $(S'_2)$ .

*Proof.* The proof is similar to the ones in the previous section (see proof of Lemma 4) except for the following:

## CHAPTER FOUR

First, we will show that  $(S'_1) \Rightarrow (S'_2)$ . We start with  $(S'_{1a})$  and multiply it by  $v \in H_0^1(0, 1)$  to get

$$\int_0^1 w(x)v(x) dx - \langle u'', v \rangle_{(0,1)} = 0.$$

By the definition of the weak derivative, we have

$$\int_0^1 w(x)v(x) dx + \int_0^1 u'(x)v'(x) dx = 0,$$

which is  $(S'_{2a})$ .

The other difference is in proving  $(S'_2) \Rightarrow (S'_1)$ . Hence  $(S'_{2a})$  implies

$$\langle w, v \rangle_{(0,1)} - \langle u'', v \rangle_{(0,1)} = 0$$

for all  $v \in \mathcal{D}(0, 1)$ . Notice that by definition of the weak derivative we get

$$\langle w - u'', v \rangle_{(0,1)} = 0 \quad \forall v \in \mathcal{D}(0, 1).$$

So,  $w - u'' = 0$  which means  $u'' = w \in L^2(0, 1)$ , and so  $u \in H^2(0, 1)$ . Thus  $u' \in H^1(0, 1) \subseteq C^0(0, 1)$ , which implies that  $u'(c^+) = u'(c^-)$ . Finally, by the definition of  $H_0^1(0, 1)$  and the fact that  $u, w \in H_0^1(0, 1)$ , we immediately have that  $u(0) = u(1) = w(0) = w(1) = 0$  and  $u(c^-) = u(c^+)$ ,  $w(c^-) = w(c^+)$ .

□

### 4.4.1 The Existence and Uniqueness of the Weak Formulation

Next, we prove the existence and uniqueness for the weak formulation  $S'_2$  defined above. The major difference is that  $u$  belongs to  $H_0^1(0, 1)$  rather than  $\tilde{V}$ . This leads to the following relevant facts.

**Corollary 2.** *The space  $\mathbf{H}_2 = H_0^1(0, 1) \times H_0^1(0, 1)$  is a Hilbert space with a scalar*

## CHAPTER FOUR

*product:*

$$\begin{aligned} \langle (f_1, g_1), (f_2, g_2) \rangle_{\mathbf{H}_2} &= \langle f_1, f_2 \rangle_{H_0^1(0,1)} + \langle g_1, g_2 \rangle_{H_0^1(0,1)} \\ &= \int_0^1 f_1'(x) f_2'(x) dx + \int_0^1 g_1'(x) g_2'(x) dx, \end{aligned}$$

with induced norm  $\|(v, w)\|_{\mathbf{H}_2} = \sqrt{\langle (v, w), (v, w) \rangle_{\mathbf{H}_2}}$ .

Next we update the bilinear functional  $A_2$  and the linear  $L_2$  accordingly:

1. Define  $A_2 : \mathbf{H}_2 \times \mathbf{H}_2 \rightarrow \mathbb{R}$  by

$$\begin{aligned} (u, w), (v, z) \rightarrow A_2((u, w), (v, z)) &= \int_0^1 u'(x) v'(x) dx + \int_0^1 w(x) v(x) dx \\ &- \int_0^1 z(x) u(x) dx + \frac{\gamma}{\alpha} \int_0^1 w'(x) v'(x) dx + \frac{1}{\alpha} \int_0^1 w(x) z(x) dx. \end{aligned} \quad (4.4.2)$$

2. Define  $L_2 : \mathbf{H}_2 \rightarrow \mathbb{R}$  by

$$(v, z) \rightarrow L_2((v, z)) = \frac{2}{\alpha} z(c). \quad (4.4.3)$$

Now our problem  $(S'_2)$  becomes : Find  $(u, w) \in \mathbf{H}_2$  such that for all  $(v, z) \in \mathbf{H}_2$ ,

$$A_2((u, w), (v, z)) = L_2((v, z)). \quad (4.4.4)$$

We have the following theorem:

**Theorem 18.** *There exists a unique  $(u, w) \in \mathbf{H}_2$ , solution of (4.4.4).*

*Proof.* The proof is exactly the same as before, except that  $\mathbf{H}$  is replaced by  $\mathbf{H}_2$  and (4.3.12) is replaced by

$$\|(u, w)\|_{\mathbf{H}_2}^2 = \int_0^1 (u')^2 + \int_0^1 (w')^2 = \|u\|^2 + \|w\|^2.$$

## CHAPTER FOUR

In particular, by the Lax-Milgram theorem (see [22], [42]), as in Theorem 15, we need to prove that  $A_2$  is continuous and elliptic and  $L_2$  is continuous.

Now we will prove the previous three conditions. First for  $L_2$  is continuous:

Let  $(v, z) \in \mathbf{H}_2$ . Since  $z \in H_0^1(a, b) \subseteq C^0(a, b)$  there exists  $\tilde{t} \in (0, 1)$  such that

$$|z(x)| \leq |z(\tilde{t})| \quad \forall x \in [0, 1].$$

Using the Sobolev's embedding theorem this implies, in particular, that

$$|L_2(v, z)| = \frac{2}{\gamma} |z(c)| \leq \frac{2}{\gamma} |z(\tilde{t})| = \frac{2}{\gamma} \|z\|_{C^0([0,1])} \leq \frac{C}{\gamma} \|z\|_{H_0^1(0,1)} \leq \frac{C}{\gamma} \|(v, z)\|_{\mathbf{H}_2}.$$

Second, we prove that  $A_2$  is continuous: like in Theorem 15, we get

$$|A_2((u, w), (v, z))| \leq 2 \max \left\{ 1, \frac{\gamma + 1}{\alpha} \right\} \sqrt{\|u\|_{H_0^1(0,1)}^2 + \|w\|_{H_0^1(0,1)}^2} \sqrt{\|v\|_{H_0^1(0,1)}^2 + \|z\|_{H_0^1(0,1)}^2}.$$

Thirdly, we prove that  $A_2$  is elliptic. Similarly, like in Theorem 15, it follows that

$$A_2((v, w), (v, z)) \geq \min \left\{ 1, \frac{1}{\alpha} \right\} \|(v, z)\|_{\mathbf{H}_2}^2.$$

Thus  $A_2$  is elliptic.

Hence, the proof is finished by applying the Lax-Milgram theorem.  $\square$

### 4.4.2 The Finite Element Method and Its Error Estimate

Next, we produce a similar result for the following subspace:

$$(\mathbf{H}_2)_h = H_h \times H_h \subseteq \mathbf{H}_2 = H_0^1(0, 1) \times H_0^1(0, 1)$$

where

$$H_h = \{v_h \in C^0([0, 1]) = v_h \mid_{(x_i, x_{i+1})} \in \mathbb{P}_1, v_h(0) = v_h(1) = 0\}.$$

## CHAPTER FOUR

The Finite Element Method is to find  $(u_h, w_h) \in H_h \times H_h$  such that

$$A_2((u_h, w_h), (v_h, z_h)) = L_2((v_h, z_h)) \quad \forall (v_h, z_h) \in H_h \times H_h. \quad (4.4.5)$$

Again, as an immediate consequence of Theorem 18 we also have a similar theorem when we restrict ourselves to the subspace  $(\mathbf{H}_2)_h \subseteq \mathbf{H}_2$

**Theorem 19.** *There exists a unique  $(u_h, w_h) \in (\mathbf{H}_2)_h$ , solution of (4.4.5).*

*Proof.* Since  $H_h \times H_h \subseteq H_0^1(0, 1) \times H_0^1(0, 1)$ , then  $A_2$  is elliptic and continuous in this space as well. Also,  $L_2$  is continuous in  $H_h \times H_h$ .  $\square$

Next we evaluate the error of the solution produced by the Finite element method introduced above.

**Remark 19.** *From the proof of Lemma 6, we showed that  $u \in H^2(0, 1), w \in H^2(0, c), w \in H^2(c, 1)$ .*

We have the following theorem

**Theorem 20.** *Let  $(u, w)$  be a solution of (4.4.4) satisfies  $u \in H^2(0, 1)$  and  $w \in H^2(0, c)$  and  $w \in H^2(c, 1)$ . Then, there exists  $C > 0$  such that*

$$\|(u - u_h, w - w_h)\|_{\mathbf{H}} \leq Ch \left\{ \sqrt{|u|_{H^2(0,1)}^2} + \sqrt{|w|_{H^2(0,c)}^2 + |w|_{H^2(c,1)}^2} \right\}.$$

*Proof.* Let  $(u, w) \in H_0^1(0, 1) \times H_0^1(0, 1)$  be the unique solution of (4.4.4). Let  $(u_h, w_h) \in H_h \times H_h$  be the unique solution of (4.4.5). Thus

$$A_2((u, w), (v_h, z_h)) = L_2((v_h, z_h)),$$

$$A_2((u_h, w_h), (v_h, z_h)) = L_2((v_h, z_h)),$$

and then

$$A_2((u, w), (v_h, z_h)) = A_2((u_h, w_h), (v_h, z_h)) \quad \forall (v_h, z_h) \in H_h \times H_h.$$

## CHAPTER FOUR

The bilinearity of  $A_2$  implies the following ‘‘Galerkin orthogonality’’

$$A_2((u - u_h, w - w_h), (v_h, z_h)) = 0 \quad \forall (v_h, z_h) \in (\mathbf{H}_2)_h. \quad (4.4.6)$$

But we know that  $A_2$  is elliptic and continuous. Then, for all  $(v_h, z_h) \in (\mathbf{H}_2)_h$ , using (4.4.6) we have

$$\begin{aligned} k_3 \|(u - u_h, w - w_h)\|_{\mathbf{H}_2}^2 &\leq A_2((u - u_h, w - w_h), (u - u_h, w - w_h)) \\ &= A_2((u - u_h, w - w_h), (u - v_h, w - z_h)) \\ &\leq k_2 \|(u - u_h, w - w_h)\|_{\mathbf{H}_2} \|(u - v_h, w - z_h)\|_{\mathbf{H}_2}, \end{aligned}$$

where we used the fact that  $A_2$  is continuous. Dividing by  $\|(u - u_h, w - w_h)\|_{\mathbf{H}_2}$ , we conclude that:

$$\|(u - u_h, w - w_h)\|_{\mathbf{H}_2} \leq \frac{k_2}{k_3} \|(u - v_h, w - z_h)\|_{\mathbf{H}_2} \quad \forall (v_h, z_h) \in (\mathbf{H}_2)_h. \quad (4.4.7)$$

The above implies that

$$\|(u - u_h, w - w_h)\|_{\mathbf{H}_2} \leq \frac{k_2}{k_3} \inf_{(v_h, z_h) \in (\mathbf{H}_2)_h} \|(u - v_h, w - z_h)\|_{\mathbf{H}_2}.$$

In particular, we choose

$$\begin{cases} v_h = i_h(u), \\ z_h = i_h(w), \end{cases}$$

where  $i_h(u)$  and  $i_h(w)$  are defined as

$$\begin{cases} i_h(u) = \sum_{i=1}^N \xi_i \varphi_i(x), \\ i_h(w) = \sum_{i=1}^N \zeta_i \varphi_i(x). \end{cases}$$

## CHAPTER FOUR

These interpolates satisfy the bounds [42]

$$\begin{aligned} \|u - i_h(v)\|_{H_0^1(0,1)} &\leq C h \|v\|_{H^2(0,1)} \quad \forall v \in H^2(0,1) \\ \|w - i_h(v)\|_{H_0^1(0,1)} &\leq C h (\|v\|_{H^2(0,c)} + \|v\|_{H^2(c,1)}) \quad \forall v : \begin{array}{l} v|_{(0,c)} \in H^2(0,c) \\ v|_{(c,1)} \in H^2(0,c) \end{array} \end{aligned}$$

The above proves that

$$\begin{aligned} \|(u - u_h, w - w_h)\|_{\mathbf{H}_2} &\leq C h \|u - i_h(u)\|_{H_0^1(0,1)} + \|w - i_h(w)\|_{H_0^1(0,1)} \\ &\leq C h [\sqrt{|u|_{H^2(0,1)}^2} + \sqrt{|w|_{H^2(0,c)}^2 + |w|_{H^2(c,1)}^2}]. \end{aligned}$$

□

Again, clearly the right hand side goes to zero when  $h$  tends to zero, this is when the mesh gets refined.

**Remark 20.** In both weak formulation  $S_2$  and  $S'_2$ , we assumed that the parameter  $\alpha$  is a constant. It is worth noting that similar formulations hold true when

$$\alpha = \alpha(x) : [0, 1] \rightarrow \mathbb{R}^+.$$

For example  $S'_2$  will become

$$(S'_3) \left\{ \begin{array}{l} \int_0^1 w(x)v(x) dx + \int_0^1 u'(x)v'(x) dx = 0 \quad \forall v \in H_0^1(0,1), \quad (S'_{3a}) \\ \gamma \int_0^1 w'(x)z'(x) dx + \int_0^1 w(x)z(x) dx - \int_0^1 \alpha(x) u(x)z(x) dx = 2z(c) \\ \forall z \in H_0^1(0,1). \quad (S'_{3b}) \end{array} \right.$$

## 4.5 Conclusion

This chapter was devoted to set the mathematical framework of our numerical methods. In particular, we started by proving a useful equivalence between a setup which is almost identical to our problem, except for one missing condition ( $S_1$ ), and weak formulation which can be approximated numerically ( $S_2$ ). As a matter of fact, we were able to develop two such equivalences, each one derived by dropping one of the following assumptions:  $u(c-) = u(c+)$  and  $u'(c-) = u'(c+) = 0$ . That is, we first created the weak formulation of the (4.2.1) by first dropping the continuity condition from the list of (4.2.2) and then created an alternate weak formulation of the (4.2.1) by dropping one of the derivative conditions of (4.2.2) (see Lemma 4 and Lemma 6). This allowed us to approach the problem numerically and find approximate solutions (see Sections 4.3 and 4.4).

Moreover, using ideas from functional analysis (i.e. the Lax-Millgram theorem) we showed that both weak formulations  $S_2$  and  $S'_2$  have a unique solution. This is important, because such a solution can be shown to satisfy the original problem (see Subsections 4.3.1 and 4.4.1).

In particular, we were first able to describe the weak formulations using a convenient equation involving (bi)linear functionals (4.3.11) and (4.4.4). From there, we used the Lax-Millgram theorem to establish existence and uniqueness in the solution spaces of the corresponding weak formulations (see Theorems 15 and 18). Next, by using the Finite Element Method approach we were able to first define appropriate solution subspaces (of piecewise linear functions for progressively finer mesh) and then show that both weak formulations (represented by (4.3.14) and (4.4.5)) have unique solutions within those solution subspaces for any given mesh (see Theorems 16 and 19). This is important, since finding solutions within these new subspaces is possible numerically and it can be done with the use of MATLAB. Crucially, by using Galerkin orthogonality we were also able to show that as we refine the mesh, the unique solution of the discrete problem can be arbitrarily close to the unique solution of the continuous problem (see Theorems 17 and 20). This allows us to efficiently and accurately approximate the

## CHAPTER FOUR

unique exact solution of our problem.

Last but not least, we illustrated the power of the method by showing that it can be applied to the generalized case where the parameter  $\alpha$  is not a constant function of  $x$ . This is useful, as in those cases we do not yet have a way of calculating the exact solutions analytically.

## Chapter 5

# The Finite Element Method for the Model Problem

### 5.1 Introduction

In the previous Chapter 4 we showed a way to express our main Euler-Lagrange equation into an equivalent weak formulation. This convenient formulation can be used as a tool for applying numerical methods which can help us find approximate solutions without having to solve the Euler-Lagrange equation directly. In particular, we will use a combination of two such numerical methods, namely the Finite Elements Method (F.E.M) and the Derivative-Free Optimization (D.F.O), see Section 5.5. FEM will allow us to solve the problem as a system of linear equations, where our target solution  $u$  is approximated by an element of a finite dimensional space. For a fixed value of  $c$ , this method allows us to approximate the solution. Now, the optimal value for  $c$  is also unknown, and then it needs to be approximated. For this purpose we will use Derivative-Free Optimization (D.F.O) method. This, in conjunction with the FEM, will give us an approximate location of the jump and an approximate solution to the Euler-Lagrange equation.

To test the performance of the method we first approximate a problem with a known

## CHAPTER FIVE

analytical solution. In particular, we choose a lap 2 case where the theory guarantees the existence of non-symmetric solutions ( $1 - 4\alpha\gamma < 0$ ). We show that both the approximate solution and the location of the jumps converge to the exact ones. From there, we expand the construction to solutions of higher lap numbers, using a lap 2 solution as a “building block”.

Finally, we solve a problem from which we do not know the analytical solution. For this, we let one of the parameter to depend on  $x$  (in this case, we let  $\alpha$  depends on  $x$ ). This further illustrates the potency of the numerical methods which can now approximate a solution to a problem that otherwise cannot be easily solved analytically, if at all.

### 5.2 The Finite Element Method (for the first weak formulation)

In the previous chapter we established two weak formulations, which are equivalent to our main Euler-Lagrange equation, each one of them dropped one of the conditions. The first of those formulations is determined by dropping the continuity condition and it is formally given by the following expressions: Find  $u \in \tilde{V}, w \in H_0^1(0, 1)$  such that

$$\begin{cases} \int_0^1 w(x)v(x) dx + \int_0^1 u'(x)v'(x) dx = 0 \quad \forall v \in \tilde{V}, \\ \gamma \int_0^1 w'(x)z'(x) dx + \int_0^1 w(x)z(x) dx - \alpha \int_0^1 u(x)z(x) dx = 2z(c) \quad \forall z \in H_0^1(0, 1). \end{cases}$$

Next, as was done in Chapter 2, we divide the interval  $[0, 1]$  as follows

$$0 = x_0 < x_1 < x_2 < \dots < x_{N-1} < x_N = 1$$

with  $h = \frac{1}{N} = (x_k - x_{k-1})$  for  $k = 1, \dots, N$ . This is, we divide  $[0, 1]$  into equidistant points. Over this partition we define a basis function for the space of continuous,

## CHAPTER FIVE

piecewise linear functions. In particular, we define  $\varphi_1, \varphi_2, \dots, \varphi_N$  as follows:

$$\varphi_i(x_j) = \begin{cases} 1 & j = i \\ 0 & \text{otherwise} \end{cases} \quad (5.2.1)$$

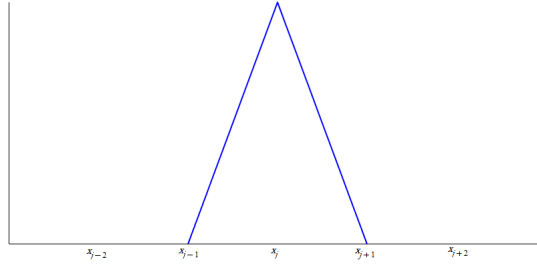


**Figure 5.1:** The basis function  $\varphi_i$

Now we define

$$H_h = \text{span} \{ \varphi_1, \varphi_2, \dots, \varphi_j, \varphi_{j+1}, \dots, \varphi_N \}. \quad (5.2.2)$$

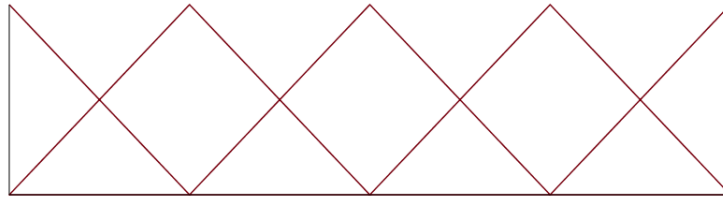


**Figure 5.2:** Basis of  $H_h$

To approximate  $u$  we need to take care of the location of the jump  $c$ . If the jump is located at  $c \in (0, 1)$  then there exists a unique  $j \in \{0, \dots, N\}$  such that

$$x_{j-1} \leq c < x_j.$$

Outside  $(x_{i-1}, x_j)$  the finite element functions remain unchanged, but inside this interval we introduce a major modification to this. More precisely, we replace the two functions  $\varphi_{j-1}$  and  $\varphi_j$  by four functions that are discontinuous at  $x = c$  and are defined

CHAPTER FIVE

as follow

$$l_{j-1} = \begin{cases} \frac{1}{h}(x - x_{j-2}), & x \in (x_{j-2}, x_{j-1}) \\ \frac{1}{h}(x_j - x), & x \in (x_{j-1}, c) \end{cases}$$

$$r_{j-1} = \frac{1}{h}(x_j - x), \quad x \in (c, x_j)$$

$$l_j = \frac{1}{h}(x - x_j), \quad x \in (x_{j-1}, c)$$

$$r_j = \begin{cases} \frac{1}{h}(x - x_{j-1}), & x \in (c, x_j) \\ \frac{1}{h}(x_j - x), & x \in (x_j, x_{j+1}) \end{cases}$$

We let

$$\psi_i = \begin{cases} \varphi_i & i \leq j-2 \\ l_{j-1} & i = j-1 \\ r_{j-1} & i = j \\ l_j & i = j+1 \\ r_j & i = j+2 \\ \varphi_{i-2} & i \geq j+3 \end{cases}$$

Finally, we introduce  $\tilde{V}_h$ , the finite element subspace of  $\tilde{V}$ , given by

$$\tilde{V}_h = \text{span} \{\psi_1, \psi_2, \dots, \psi_{N+2}\}.$$

CHAPTER FIVE

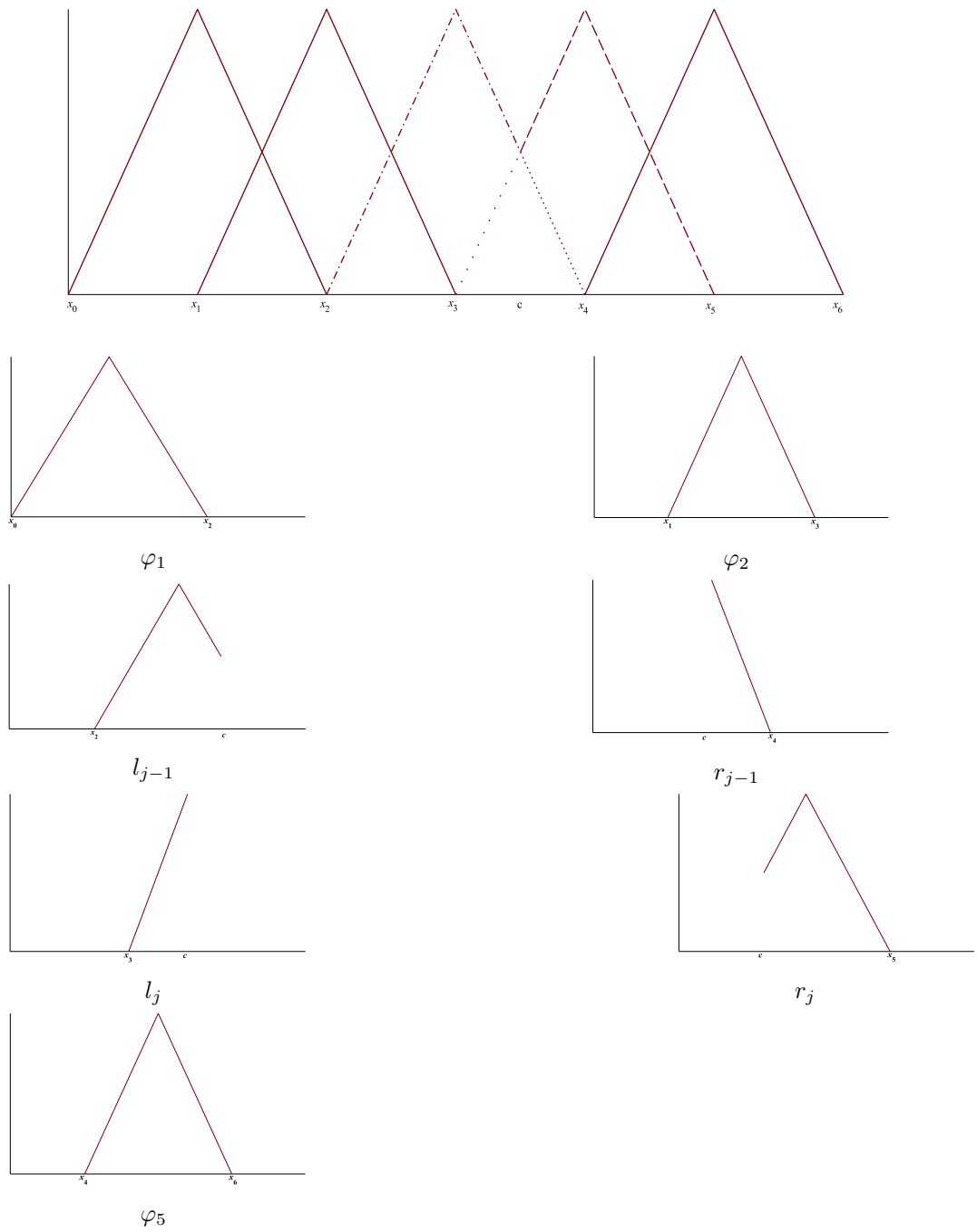


**Figure 5.4:** Basis of  $\tilde{V}_h$ .

This is the full setup for the Finite Element method and we are now ready to describe the method.

## CHAPTER FIVE

The finite element method reads as follow: Find  $u_h \in \tilde{V}_h$  and  $w_h \in H_h$  such that

$$(S_2)_h \begin{cases} \int_0^1 w_h(x)v_h(x) dx + \int_0^1 u'_h(x)v'_h(x) dx = 0 \quad \forall v_h \in \tilde{V}_h, \\ \gamma \int_0^1 w'_h(x)z'_h(x) dx + \int_0^1 w_h(x)z_h(x) dx - \alpha \int_0^1 u_h(x)z_h(x) dx = 2z(c) \quad \forall z_h \in H_h. \end{cases}$$

We look for approximation for  $u_h$  and  $w_h$  in the form

$$u_h = \sum_{i=1}^{N+2} \xi_i \psi_i(x) \quad \text{and} \quad w_h = \sum_{i=1}^N \zeta_i \varphi_i(x).$$

The above characterization allows us to describe elements  $v_h \in \tilde{V}_h$  as a linear combination of the above functions, for example if  $v_h \in \tilde{V}_h$ , then  $v_h = \sum_{i=1}^{N+2} \xi_i \psi_i(x)$ . This linear combinations allows us to calculate the inner products from above easier. For example:

$$\int_0^1 w_h(x)v_h(x) dx = \int_0^1 \left( \sum_{i=1}^N \zeta_i \varphi_i(x) \right) \left( \sum_{k=1}^{N+2} a_k \psi_k(x) \right) dx = \sum_{i=1}^N \sum_{k=1}^{N+2} \zeta_i a_k \int_0^1 \varphi_i(x) \psi_k(x) dx.$$

This leads us to two crucial observations.

1. It is enough to calculate all inner products of the form

$$\int_0^1 \varphi_i(x) \psi_k(x) dx, \quad \int_0^1 \varphi_i(x) \varphi_m(x) dx, \quad \int_0^1 \varphi'_i(x) \varphi'_m(x) dx, \quad \int_0^1 \psi'_i(x) \psi'_k(x) dx.$$

2. We can write the system  $(S_2)_h$  above in a matrix form, as follows:

$$\begin{bmatrix} \gamma \mathbb{A} + \mathbb{B} & \tilde{\mathbb{B}} \\ \tilde{\mathbb{B}}^T & \tilde{\mathbb{A}} \end{bmatrix} \cdot \mathbf{X} = \mathbf{b},$$

CHAPTER FIVE

where

$$\mathbb{A} = \left[ (\varphi'_i, \varphi'_m) \right]_{(i,m) \in N \times N} \in \mathbb{R}^{N \times N} \quad (5.2.3)$$

$$\mathbb{B} = \left[ (\varphi_i, \varphi_m) \right]_{(i,m) \in (N+2) \times N} \in \mathbb{R}^{N \times N} \quad (5.2.4)$$

$$\tilde{\mathbb{A}} = \left[ (\psi'_i, \psi'_k) \right]_{(i,k) \in (N+2) \times (N+2)} \in \mathbb{R}^{(N+2) \times (N+2)} \quad (5.2.5)$$

$$\tilde{\mathbb{B}} = \left[ (\varphi_i, \psi_k) \right]_{(i,k) \in N \times (N+2)} \in \mathbb{R}^{N \times (N+2)} \quad (5.2.6)$$

$$\mathbf{b} \in \mathbb{R}^{2N+1} \quad \text{s.t.} \quad \left[ \mathbf{b} \right]_i = \begin{cases} 2(1 - \theta) & i = N + j - 1 \\ 2\theta & i = N + j \\ 0 & \text{otherwise} \end{cases}, \theta = \frac{c - x_{j-2}}{x_j - x_{j-1}}. \quad (5.2.7)$$

Finally,  $\mathbf{X} = [\zeta_1, \zeta_2, \dots, \zeta_N, \xi_1, \xi_2, \dots, \xi_{N+2}]^T \in \mathbb{R}^{2N+2}$ , which is the unknown in our system, and thus the value we are solving for.

Before we proceed, it is worth mentioning that the matrices are sparse (most entries of the matrix are zero). More precisely:

$$\int_0^1 \varphi'_i(x) \varphi'_m(x) dx = \begin{cases} \frac{2}{h} & i = m, \\ \frac{-1}{h} & |i - m| = 1, \\ 0 & \text{otherwise.} \end{cases}$$

$$\int_0^1 \varphi_i(x) \varphi_m(x) dx = \begin{cases} \frac{2h}{3} & i = m, \\ \frac{h}{6} & |i - m| = 1, \\ 0 & \text{otherwise} \end{cases}$$

$$\int_0^1 \psi'_i(x) \psi'_k(x) dx = \begin{cases} \frac{2}{h} & \text{if } i = k \neq j-1, j, j+1, j+2 \\ \frac{-1}{h} & \text{if } |i-k|=1, i, k \neq j-1, j, j+1, j+2 \\ \frac{-1}{h} & \text{if } i = j-1, k = j-2 \text{ or } i = j-2, k = j-1 \\ \frac{1+\theta}{h} & \text{if } i = k = j-1 \\ \frac{-\theta}{h} & \text{if } i = j-1, k = j+1 \text{ or } i = j+1, k = j-1 \\ \frac{1-\theta}{h} & \text{if } i = k = j \\ \frac{\theta-1}{h} & \text{if } i = j, k = j+2 \text{ or } i = j+2, k = j \\ \frac{\theta}{h} & \text{if } i = j+1, k = j+1 \\ \frac{2-\theta}{h} & \text{if } i = j+2, k = j+2 \\ 0 & \text{otherwise} \end{cases}$$

where  $\theta$  is defined in (5.2.7) and  $j$  is the unique index s.t.  $x_{j-1} \leq c \leq x_j$ . In addition

$$\int_0^1 \varphi_i(x) \psi_k(x) dx = \begin{cases} \frac{2h}{3} & \text{if } i = k \neq j-1, j, j+1 \\ \frac{h}{6} & \text{if } |k-i|=1, i, k \neq j-1, j, j+1 \\ \frac{h}{3}(1+\beta) & \text{if } i = k = j-1 \\ \frac{h}{3}(1-\beta) & \text{if } i = j-1, k = j \\ \frac{h}{6}\delta & \text{if } k = j-1, i = j+1 \text{ or } i = j, k = j-1 \\ \frac{h}{6}(1-\delta) & \text{if } i = j-1, k = j+2 \text{ or } i = k = j \\ \frac{h}{3}\theta & \text{if } , i = j, k = j+1 \\ \frac{h}{3}(2-\theta) & \text{if } , i = j, k = j+2 \\ \frac{h}{6} & \text{if } i = j, k = j+3 \\ 0 & \text{otherwise} \end{cases}$$

CHAPTER FIVE

where  $\beta = \theta^3 - 3\theta^2 + 3\theta$  and  $\delta = 3\theta^2 - 2\theta^3$ .

Visually the matrices look as follows:

$$\mathbb{A} = \begin{bmatrix} (\varphi'_1, \varphi'_1) & (\varphi'_1, \varphi'_2) & 0 & 0 & \dots & \dots & 0 \\ (\varphi'_2, \varphi'_1) & (\varphi'_2, \varphi'_2) & (\varphi'_2, \varphi'_3) & 0 & \dots & \dots & 0 \\ 0 & (\varphi'_3, \varphi'_2) & (\varphi'_3, \varphi'_3) & (\varphi'_3, \varphi'_4) & 0 & \dots & 0 \\ \dots & \dots & \dots & \dots & \dots & \dots & \dots \\ 0 & 0 & 0 & \dots & \dots & (\varphi'_m, \varphi'_{m-1}) & (\varphi'_m, \varphi'_m) \end{bmatrix}$$

$$\mathbb{B} = \begin{bmatrix} (\varphi_1, \varphi_1) & (\varphi_1, \varphi_2) & 0 & 0 & \dots & \dots & 0 \\ (\varphi_2, \varphi_1) & (\varphi_2, \varphi_2) & (\varphi_2, \varphi_3) & 0 & \dots & \dots & 0 \\ 0 & (\varphi_3, \varphi_2) & (\varphi_3, \varphi_3) & (\varphi_3, \varphi_4) & 0 & \dots & 0 \\ \dots & \dots & \dots & \dots & \dots & \dots & \dots \\ 0 & 0 & 0 & \dots & \dots & (\varphi_m, \varphi_{m-1}) & (\varphi_m, \varphi_m) \end{bmatrix}$$

$$\tilde{\mathbb{A}} = \begin{bmatrix} (\psi'_1, \psi'_1) & (\psi'_1, \psi'_2) & 0 & \dots & 0 \\ (\psi'_2, \psi'_1) & (\psi'_2, \psi'_2) & (\psi'_2, \psi'_3) & 0 & \dots & \dots & \dots & \dots & \dots & 0 & 0 \\ \dots & \dots \\ 0 & \dots & (\psi'_{j-1}, \psi'_{j-2}) & (\psi'_{j-1}, \psi'_{j-1}) & 0 & (\psi'_{j-1}, \psi'_{j+1}) & 0 & 0 & \dots & \dots & \dots \\ 0 & \dots & 0 & 0 & (\psi'_j, \psi'_j) & 0 & (\psi'_j, \psi'_{j+2}) & 0 & \dots & \dots & \dots \\ 0 & \dots & 0 & (\psi'_{j+1}, \psi'_{j-1}) & 0 & (\psi'_{j+1}, \psi'_{j+1}) & 0 & 0 & \dots & \dots & \dots \\ 0 & \dots & \dots & 0 & (\psi'_{j+2}, \psi'_j) & 0 & (\psi'_{j+2}, \psi'_{j+2}) & (\psi'_{j+2}, \psi'_{j+3}) & 0 & \dots & \dots \\ 0 & \dots & \dots & \dots & \dots & 0 & (\psi'_{j+3}, \psi'_{j+2}) & (\psi'_{j+3}, \psi'_{j+3}) & (\psi'_{j+3}, \psi'_{j+4}) & 0 & \dots \\ \dots & \dots \\ 0 & \dots & \dots & \dots & \dots & \dots & 0 & \dots & 0 & (\psi'_m, \psi'_{m-1}) & (\psi'_m, \psi'_m) \end{bmatrix}$$

CHAPTER FIVE

$$\tilde{\mathbb{B}} = \begin{bmatrix} (\varphi_1, \psi'_1) & (\varphi_1, \psi'_2) & 0 & \dots & 0 \\ (\varphi_2, \psi'_1) & (\varphi_2, \psi'_2) & (\varphi_2, \psi'_3) & 0 & \dots & \dots & \dots & \dots & \dots & \dots & 0 \\ \dots & \dots \\ 0 & \dots & 0 & (\varphi_{j-1}, \psi'_{j-2}) & (\varphi_{j-1}, \psi'_{j-1}) & (\varphi_{j-1}, \psi'_j) & (\varphi_{j-1}, \psi'_{j+1}) & (\varphi_{j-1}, \psi'_{j+2}) & 0 & \dots & \dots \\ 0 & \dots & \dots & 0 & (\varphi_j, \psi'_{j-1}) & (\varphi_j, \psi'_j) & (\varphi_j, \psi'_{j+1}) & (\varphi_j, \psi'_{j+2}) & (\varphi_j, \psi'_{j+3}) & 0 & \dots \\ 0 & \dots & \dots & \dots & \dots & \dots & 0 & (\varphi_{j+1}, \psi'_{j+2}) & (\varphi_{j+1}, \psi'_{j+3}) & (\varphi_{j+1}, \psi'_{j+4}) & \dots \\ \dots & \dots \\ 0 & \dots & \dots & \dots & \dots & \dots & 0 & \dots & 0 & (\varphi_m, \psi'_{m-1}) & (\varphi_m, \psi'_m) \end{bmatrix}.$$

For example, for  $N = 6$ , and  $j = 4$  we have:

$$\mathbb{A} = \begin{bmatrix} 14 & -7 & 0 & 0 & 0 & 0 \\ -7 & 14 & -7 & 0 & 0 & 0 \\ 0 & -7 & 14 & -7 & 0 & 0 \\ 0 & 0 & -7 & 14 & -7 & 0 \\ 0 & 0 & 0 & -7 & 14 & -7 \\ 0 & 0 & 0 & 0 & -7 & 14 \end{bmatrix},$$

$$\mathbb{B} = \begin{bmatrix} 0.952 & 0.0238 & 0 & 0 & 0 & 0 \\ 0.0238 & 0.952 & 0.0238 & 0 & 0 & 0 \\ 0 & 0.0238 & 0.952 & 0.0238 & 0 & 0 \\ 0 & 0 & 0.0238 & 0.952 & 0.0238 & 0 \\ 0 & 0 & 0 & 0.0238 & 0.952 & 0.0238 \\ 0 & 0 & 0 & 0 & 0.0238 & 0.952 \end{bmatrix},$$

$$\tilde{\mathbb{A}} = \begin{bmatrix} 14 & -7 & 0 & 0 & 0 & 0 & 0 & 0 \\ -7 & 14 & -7 & 0 & 0 & 0 & 0 & 0 \\ 0 & -7 & 10.5 & 0 & -3.5 & 0 & 0 & 0 \\ 0 & 0 & 0 & 3.5 & 0 & -3.5 & 0 & 0 \\ 0 & 0 & -3.5 & 0 & 3.5 & 0 & 0 & 0 \\ 0 & 0 & 0 & -3.5 & 0 & 10.5 & -7 & 0 \\ 0 & 0 & 0 & 0 & 0 & -7 & 14 & -7 \\ 0 & 0 & 0 & 0 & 0 & 0 & -7 & 14 \end{bmatrix},$$

$$\tilde{\mathbb{B}} = \begin{bmatrix} 0.0952 & 0.0238 & 0 & 0 & 0 & 0 & 0 & 0 \\ 0.0238 & 0.0952 & 0.0238 & 0 & 0 & 0 & 0 & 0 \\ 0 & 0.0238 & 0.0893 & 0.006 & 0.0119 & 0.0119 & 0 & 0 \\ 0 & 0 & 0.0119 & 0.0119 & 0.0238 & 0.0714 & 0.0238 & 0 \\ 0 & 0 & 0 & 0 & 0 & 0.0238 & 0.0952 & 0.0238 \\ 0 & 0 & 0 & 0 & 0 & 0 & 0.0238 & 0.0952 \end{bmatrix}.$$

### 5.2.1 A Numerical Experiment

As first numerical experiment we consider the Euler-Lagrange equation with  $\alpha = 93$ ,  $\gamma = 0.05$ , which we know results in 3 solutions, one symmetric and two non symmetric, since  $1 - 4\alpha\gamma < 0$  (see Appendix A.3). For the symmetric one, the analytical solution is given by:

$$u_l(x) = \begin{cases} 0.002326 e^{5.1540x} \cos(4.0698x) + 0.005023 e^{5.1540x} \sin(4.0698x) \\ -0.002326 e^{-5.154x} \cos(4.0698x) + 0.005023 e^{-5.1540x} \sin(4.0698x) \end{cases}, \quad 0 \leq x \leq 0.5,$$

$$u_r(x) = \begin{cases} -0.000015 e^{5.1540x} \cos(4.0698x) + 0.000028 e^{5.1540x} \sin(4.0698x) \\ -0.93762 e^{-5.1540x} \cos(4.0698x) + 0.19876 e^{-5.1540x} \sin(4.0698x) \end{cases}, \quad 0.5 \leq x \leq 1,$$

where exact location of the jump is  $c = 0.5$ .

We use different values for  $N$  and see how increases the dimension of the finite elements

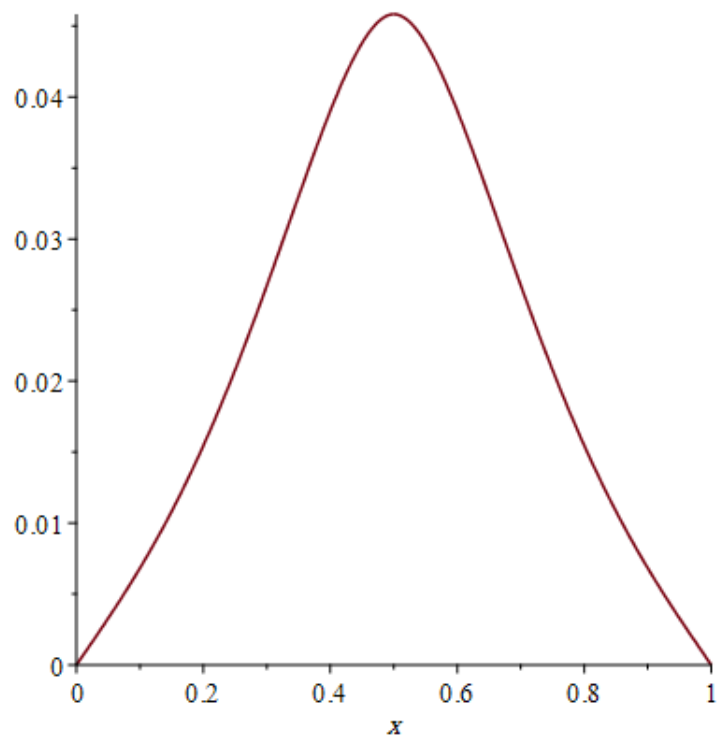


**Figure 5.5:** Exact symmetric solution when  $\alpha = 93, \gamma = 0.05$ .

space gives a better approximation of the exact solution. We know  $c$ , and introduce it in our code and refine the mesh. We see from (Figures 5.6 - 5.9) that refining the mesh produces a more and more accurate solution. In what follows, we use  $N$  to describe the size of the mesh. Also, to avoid confusion and since we are interested in the location of the jump for different types of solutions, we let  $j_1$  be the index of  $\{0, 1, 2, \dots, N\}$  corresponding to the jump location of the symmetric solution, while  $j_2$  and  $j_3$  are the jump indices corresponding to the two non-symmetric solutions.

To begin, let  $N = 10$  then we find  $j_1 = 6$ . Hence,  $u_h$  is depicted now:

## CHAPTER FIVE

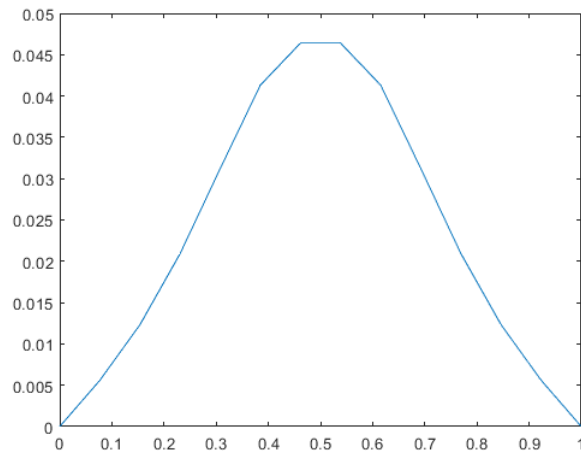


**Figure 5.6:** Numerical solution with  $\alpha = 93, \gamma = 0.05$  and  $N = 10$ .

We next try  $N = 40$ . In that case  $j_1 = 21$ , which leads to the following approximate  $u_h$

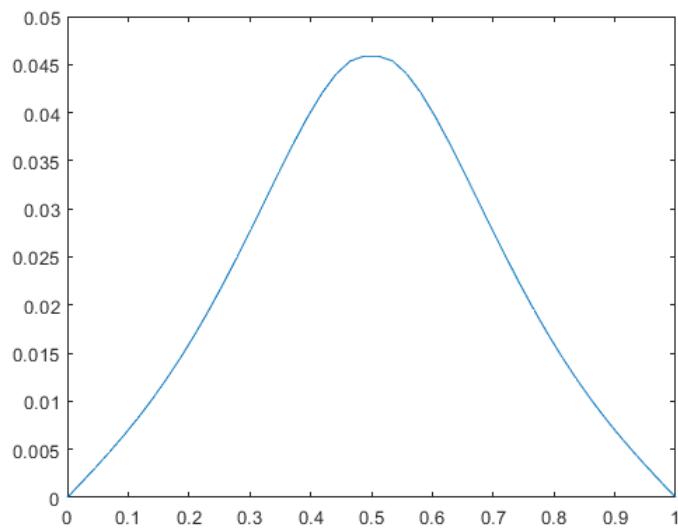


**Figure 5.7:** Numerical solution with  $\alpha = 93, \gamma = 0.05$  and  $N = 40$ .

Increasing the size of the mesh even further ( $N = 100$ ) we get  $j_1 = 51$  which gives:

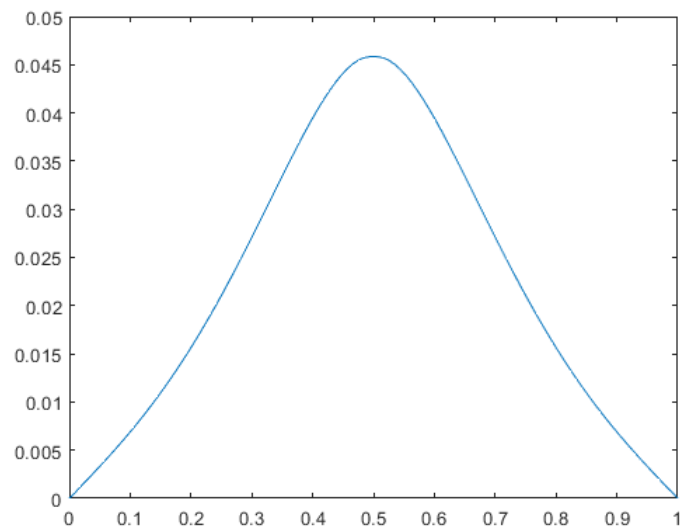


**Figure 5.8:** Numerical solution with  $\alpha = 93, \gamma = 0.05$  and  $N = 100$ .

Finally we set  $N = 1000$ , in which case  $j_1 = 501$  and  $u_h$  is presented below.

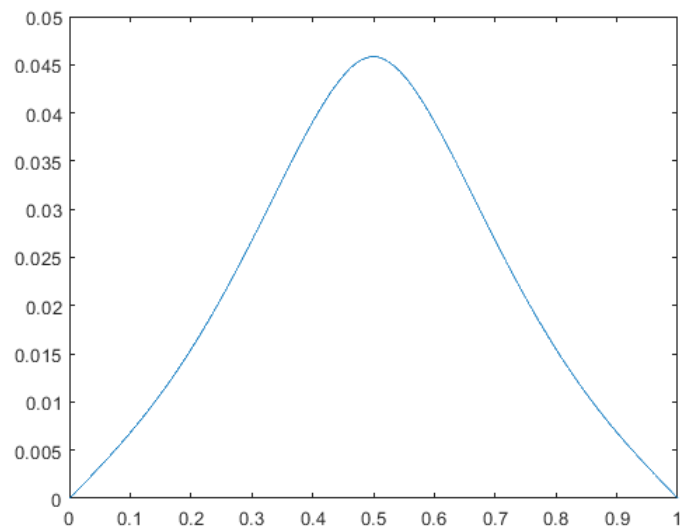


**Figure 5.9:** Numerical solution with  $\alpha = 93, \gamma = 0.05$  and  $N = 1000$ .

This last approximation is very close to the exact solution. To give a more quantitative measure of the error, we start measuring the errors between the exact and approximate

CHAPTER FIVE

energies. The exact energy given by

$$E(u) = \int_0^1 [\gamma u_{xx}^2 + W(u_x) + \alpha u^2] dx, \quad (5.2.8)$$

is for this example

$$E = 0.9083414738.$$

The approximate energy is given by

$$E(u_h) = \int_0^1 [\gamma w_h^2 + W(u_h)_x + \alpha u_h^2] dx. \quad (5.2.9)$$

Table 5.1 below shows the evolution of  $|E - E_h|$  as  $h \rightarrow 0$ , where we see that the error tends to zero as  $h \rightarrow 0$ , thus confirming the result from Theorem 17.

N	$E_h$	$ E - E_h $
10	0.7954545670	0.1128869068
20	0.8448342719	0.0635072019
40	0.8746563144	0.0336851594
80	0.8909991153	0.0173423585
160	0.8995436360	0.0087978378
320	0.9039107076	0.0044307662
640	0.9061181082	0.0022233656
1280	0.9072277929	0.0011136809
2560	0.9077841335	0.0005573403
5120	0.9080626786	0.0002787952
10240	0.9082020449	0.0001394289
20480	0.9082717515	0.0000697223
40960	0.9083066106	0.0000348632

**Table 5.1:** FEM numerical solutions for  $c = 0.5$  and various  $N$ , and the exact energy is  $E = 0.9083414738$ .

The log-log plot of the above error table is given by the following:

CHAPTER FIVE

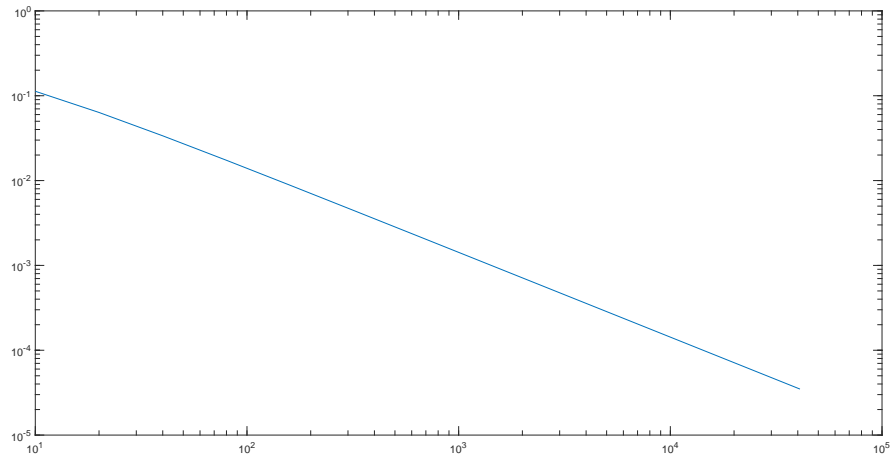


**Figure 5.10:** Log-log plot of the error estimate of the energy  $u$  for  $\alpha = 93, \gamma = 0.05$  and  $c = 0.5$ . The  $x$ -axis represents  $\log(N)$  while the  $y$ -axis represents  $\log|E - E_h|$ . Notice the linear pattern.

To assess the converges of  $u_h$  and  $w_h$  in Table 5.2, we report the error  $|u - u_h|_{\tilde{V}}$  and  $|w - w_h|_{H^1(0,1)}$ . We see that they tend to zero linearly as  $h \rightarrow 0$ , which again confirming the result of Theorem 17.

N	$ u - u_h _{\tilde{V}}$	$ w - w_h _{H^1_0(0,1)}$
10	0.003251291208095	0.0716300167
20	0.001301982412155	0.0385647033
40	0.0005951299405871450	0.0188128934
80	0.0002895590103471243	0.0091563540
160	0.0001437131863845694	0.0044986418
320	0.00007171915755099461	0.0022272376
640	0.00003584212183320310	0.0011078170
1280	0.00001791884341254925	0.0005524227
2560	0.000008959169650165406	0.0002758357
5120	0.000004479588318073530	0.0001378237
10240	0.000002239813841832357	0.0000688885
20480	0.000001119928629588577	0.0000344387
40960	0.0000005599862764760475	0.0000172183

**Table 5.2:** Errors generated for  $\alpha = 93$  and  $\gamma = 0.05$  and various  $N$ .

where the log-log plot of the above error table is given by the following:

CHAPTER FIVE

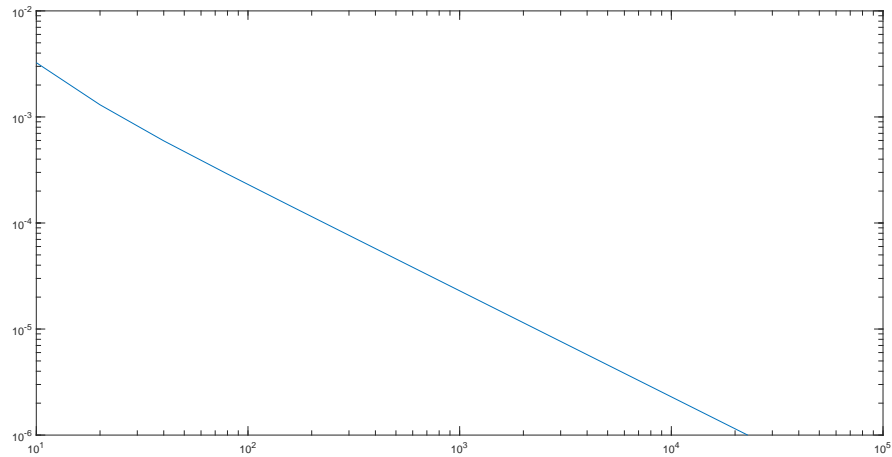


**Figure 5.11:** Log-log plot of the error estimate of the energy  $u$  for  $\alpha = 93, \gamma = 0.05$  and  $c = 0.5$ . The  $x$ -axis represents  $\log(N)$  while the  $y$ -axis represents  $\log |u - u_h|_{\tilde{V}}$ . Notice the linear pattern.

Note that dropping the continuity condition, allows us to always solve the matrix equation  $AX = B$  regardless of the value of  $c$ . In particular, if  $c$  is not the correct location of the jump, solving the matrix equation will result to discontinuous graph (which is of course not a solution to the Euler Lagrange equation). For example, let  $\alpha = 93, \gamma = 0.05$  and  $c = 0.2$ . Solving the matrix equation for these parameters yields the following graph

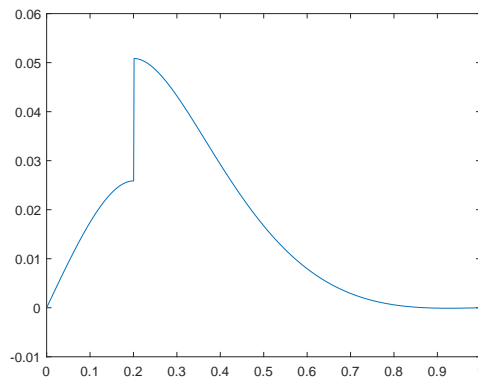


**Figure 5.12:** Plot of a discontinuous graph for an incorrect location of the jump. Here  $\alpha = 93$  and  $\gamma = 0.05$ , but  $c = 0.2$  as opposed to  $c = 0.5$  (which would be the correct value).

## CHAPTER FIVE

Similarly, we follow the same procedure from above, to construct plots/tables for the other two non-symmetric solutions. The location of their jumps are  $c = 0.40214$  and  $c = 0.59785$  respectively. Their precise (exact) solutions are given by:

$$u_l(x) = \begin{cases} 0.006766 e^{5.1540 x} \cos(4.0698 x) + 0.006133 e^{5.1540 x} \sin(4.0698 x) \\ -0.006766 e^{-5.1540 x} \cos(4.0698 x) + 0.006133 e^{-5.1540 x} \sin(4.0698 x) \end{cases}, \quad 0 \leq x \leq 0.40214,$$

$$u_r(x) = \begin{cases} -0.000015 e^{5.1540 x} \cos(4.0698 x) + 0.000012 e^{5.154 x} \sin(4.0698 x) \\ -0.48202 e^{-5.1540 x} \cos(4.0698 x) + 0.33302 e^{-5.154 x} \sin(4.0698 x) \end{cases}, \quad 0.40214 \leq x \leq 1.$$

$$u_l(x) = \begin{cases} 0.0001283 e^{5.1540 x} \cos(4.0698 x) + 0.003381 e^{5.1540 x} \sin(4.0698 x) \\ -0.0001283 e^{-5.1540 x} \cos(4.0698 x) + 0.003381 e^{-5.1540 x} \sin(4.0698 x) \end{cases}, \quad 0 \leq x \leq 0.59785,$$

$$u_r(x) = \begin{cases} -0.0000049 e^{5.1540 x} \cos(4.0698 x) + 0.000052 e^{5.1540 x} \sin(4.0698 x) \\ -1.5520 e^{-5.1540 x} \cos(4.0698 x) - 0.30151 e^{-5.1540 x} \sin(4.0698 x) \end{cases}, \quad 0.59785 \leq x \leq 1.$$

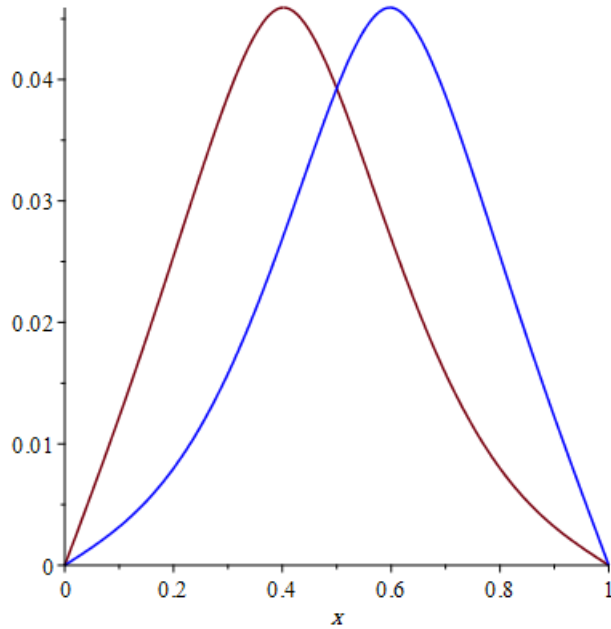


**Figure 5.13:** Exact (non-symmetric) solutions

First, let  $N = 10$  then we find  $j_2 = 5, j_3 = 7$ .

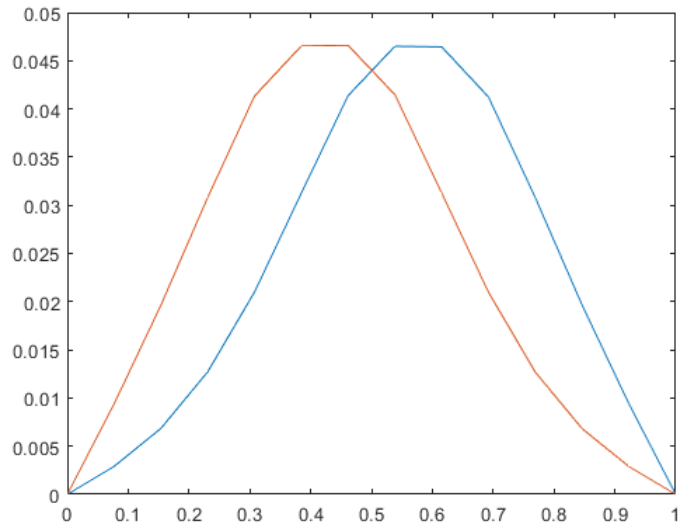


**Figure 5.14:** Numerical (non-symmetric) solutions for  $\alpha = 93, \gamma = 0.05$  and  $N = 10$ .

Again, this is already a good approximation, but we can do better. We try  $N = 40$ . In that case  $j_2 = 17, j_3 = 25$ , which leads to the following:

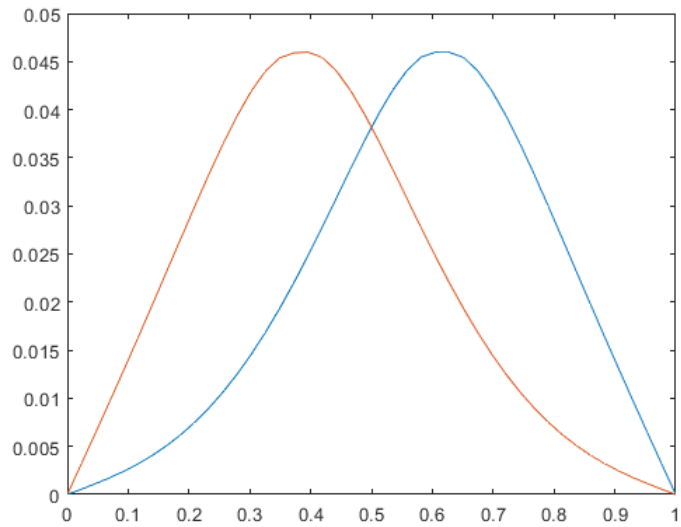


**Figure 5.15:** Numerical (non-symmetric) solutions for  $\alpha = 93, \gamma = 0.05$  and  $N = 40$ .

Increasing the size of the mesh ( $N = 100$ ) we get  $j_2 = 41, j_3 = 61$  which gives:

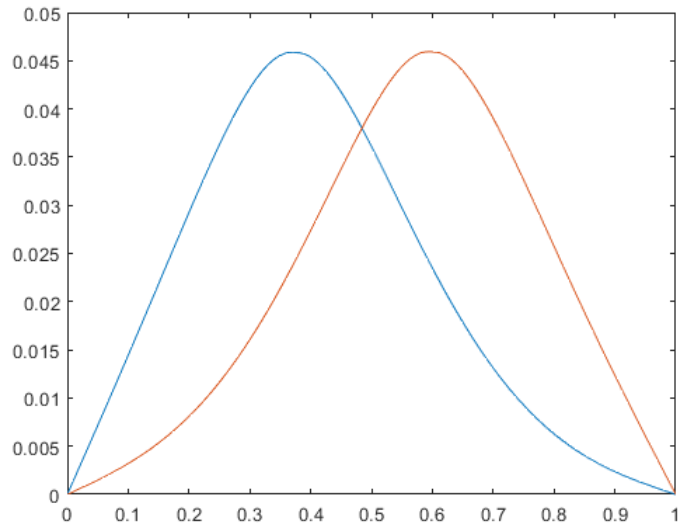


**Figure 5.16:** Numerical (non-symmetric) solutions for  $\alpha = 93, \gamma = 0.05$  and  $N = 100$ .

Finally we choose  $N = 1000$ , in which case  $j_2 = 401, j_3 = 601$ :

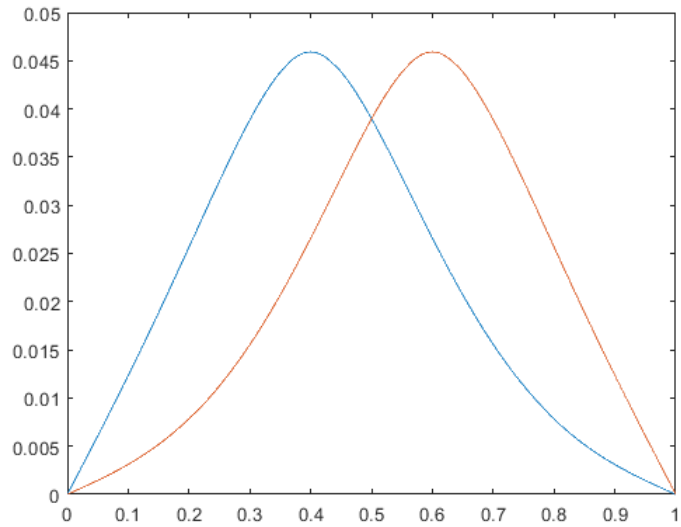


**Figure 5.17:** Numerical (non-symmetric) solutions for  $\alpha = 93, \gamma = 0.05$  and  $N = 1000$ .

Again, this last approximation is very close to the exact solution. Below in Table 5.3, we give a more quantitative measure of the error between exact and approximate energies where the exact energy is  $E = 0.9081601666$  and  $c = 0.40214$ . Also, we see

CHAPTER FIVE

that the error tends to zero as  $h \rightarrow 0$ , which again confirms the result from Theorem 17.

N	$E_h$	$ E - E_h $
10	0.7936323664	0.1145278002
20	0.8448534391	0.0633067275
40	0.8747851382	0.0333750284
80	0.8910294777	0.0171306889
160	0.8995058747	0.0086542919
320	0.9037738319	0.0043863347
640	0.9059733696	0.0021867970
1280	0.9070578431	0.0011023235
2560	0.9076134775	0.0005466891
5120	0.9078843626	0.0002758040
10240	0.9080222092	0.0001379574
20480	0.9080911668	0.0000689998
40960	0.9081256715	0.0000344951

**Table 5.3:** FEM numerical solutions for  $\alpha = 91, \gamma = 0.05, c = 0.40214$  and various  $N$ , and the exact energy is  $E = 0.9081601666$ .

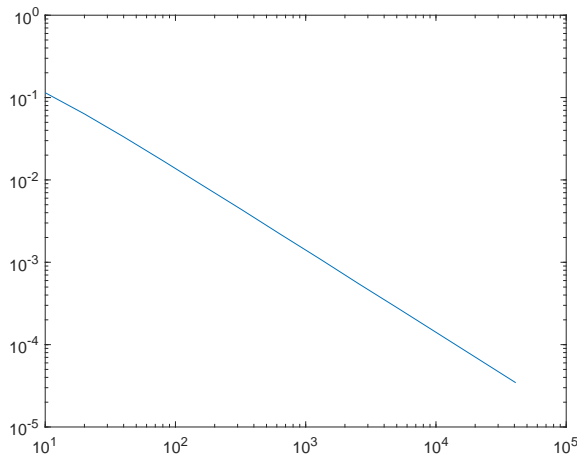


**Figure 5.18:** Log-log plot of the error estimate of the energy  $u$  for  $\alpha = 93, \gamma = 0.05$  and  $c = 0.40214$ . The  $x$ -axis represents  $\log(N)$  while the  $y$ -axis represents  $\log|E - E_h|$ . Notice the linear pattern.

Finally, to assess the converges of  $u_h$  and  $w_h$  in Table 5.4, we report the error  $|u - u_h|_{\tilde{V}}$  and  $|w - w_h|_{H_0^1(0,1)}$ . We, again, see that they tend to zero linearly as  $h \rightarrow 0$ , which, again, confirming the result of Theorem 17.

N	$ u - u_h _{\tilde{V}}$	$ w - w_h _{H_0^1(0,1)}$
10	0.0058984678	0.1345821510
20	0.0029131737	0.0753832276
40	0.0014709532	0.0517241132
80	0.0007432482	0.0404002343
160	0.0003741723	0.0346776081
320	0.0001839107	0.0134049369
640	0.0000931058	0.0077355421
1280	0.0000463558	0.0042458197
2560	0.0000232506	0.0010312378
5120	0.0000116130	0.0008534800
10240	0.0000058072	0.0006429552
20480	0.0000029037	0.0000163258
40960	0.0000014519	0.0000059124

**Table 5.4:** Errors generated for  $\alpha = 93$  and  $\gamma = 0.05$ ,  $c = 0.40216$  and various  $N$ .

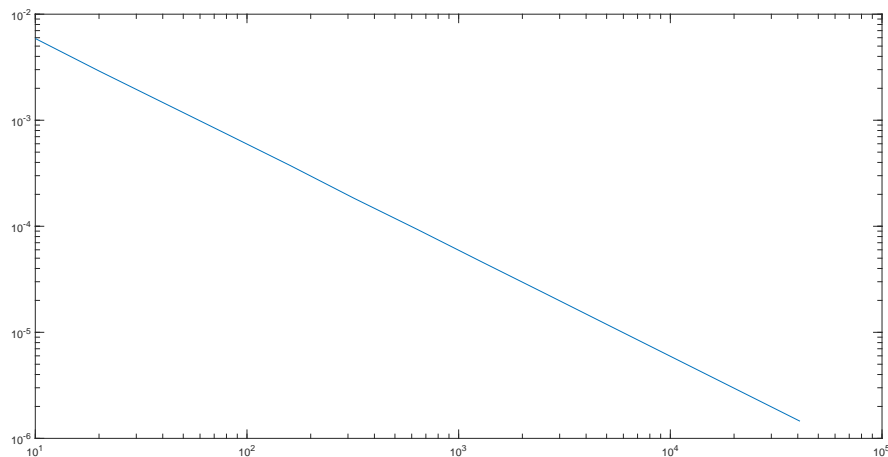


**Figure 5.19:** Log-log plot of the error estimate of the energy  $u$  for  $\alpha = 93, \gamma = 0.05$  and  $c = 0.40216$ . The  $x$ -axis represents  $\log(N)$  while the  $y$ -axis represents  $\log |u - u_h|_{\tilde{V}}$ . Notice the linear pattern.

**Remark 21.** Notice that up to this point we have been using examples where both the location of the jump (and consequently the corresponding solution of the Euler Lagrange equation) can be found analytically. This is to illustrate using the error estimate that FEM does indeed produce good approximations compared to the exact ones. As we will see later on, a priori analytical results are not necessary for us to find approximations to

the locations of the jumps. Instead we will employ methods like DFO to find those jumps, even for cases where it is hard (or even impossible) to do so analytically. Of course, without the knowledge of an exact solution we can never have numerical verification that this approximation is a good one. Fortunately, Theorem 17 from Chapter 4 already guarantees that for us. As a matter of fact, no such verification is technically necessary in the first place, we present it here for emphasis, completeness and to illustrate the rate of convergence.

### 5.3 The Finite Element Method (for the second weak formulation)

Similarly to our work in the previous section, we now consider the second weak formulation, namely the one where we drop one of the derivative conditions. The Finite Element Method reads as follow: Find  $u_h, w_h \in H_h$  such that

$$(S'_2)_h \begin{cases} \int_0^1 w_h(x)v_h(x) dx + \int_0^1 u'_h(x)v'_h(x) dx = 0 \quad \forall v_h \in H_h, \\ \gamma \int_0^1 w'_h(x)z'_h(x) dx + \int_0^1 w_h(x)z_h(x) dx - \alpha \int_0^1 u_h(x)z_h(x) dx = 2z(c) \quad \forall z_h \in H_h, \end{cases}$$

where  $H_h$  is defined in (5.2.2).

Since now we are working within the  $H_h$  space, we will be looking for approximations in the form:

$$u = \sum_{i=1}^N \xi_i \varphi_i(x) \quad \text{and} \quad w = \sum_{i=1}^N \zeta_i \varphi_i(x).$$

Other than that, the process is identical to the one used in Section 5.2, with only small algebraic changes. In particular, the matrix form will be given by

$$\begin{bmatrix} \gamma \mathbb{A} + \mathbb{B} & \mathbb{B} \\ \mathbb{B}^T & \mathbb{A} \end{bmatrix} \cdot \mathbf{X} = \mathbf{b}.$$

### 5.3.1 A Numerical Experiment

To illustrate how the method works, we once again consider the case  $\alpha = 93, \gamma = 0.05$  (see Appendix A.4). For the symmetric solution the exact location of the jump is  $c = 0.5$ , when  $N = 10$  we have

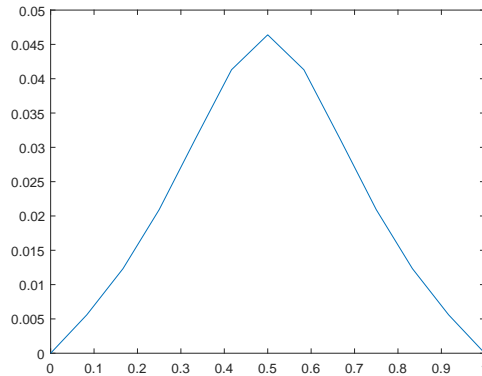


**Figure 5.20:** Numerical solution (for the second weak formulation) with  $\alpha = 93, \gamma = 0.05$  and  $N = 10$ .

Comparing the above to our finding from the first weak formulation, we see that their graphs are close to one another, with the numerical solution of the first weak formulation being higher.

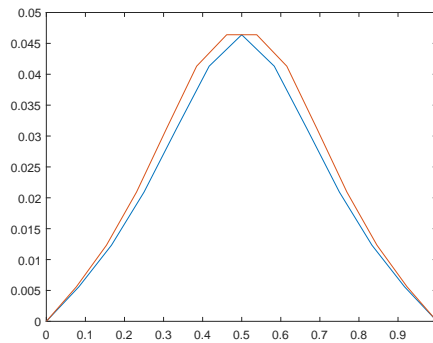


**Figure 5.21:** Comparison of the solutions corresponding to the two weak formulations. The red graph on top corresponds to the first weak formulation,  $\alpha = 91, \gamma = 0.05, c = 0.5$  and  $N = 10$ .

CHAPTER FIVE

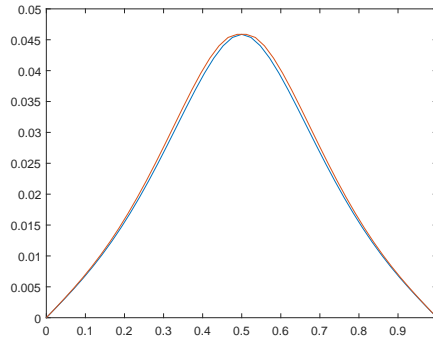


**Figure 5.22:** Comparison of the solutions corresponding to the two weak formulations. The red graph on top corresponds to the first weak formulation,  $\alpha = 91, \gamma = 0.05, c = 0.5$  and  $N = 40$ .

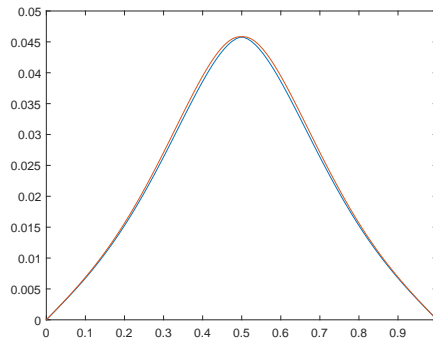


**Figure 5.23:** Comparison of the solutions corresponding to the two weak formulations. The red graph on top corresponds to the first weak formulation,  $\alpha = 91, \gamma = 0.05, c = 0.5$  and  $N = 100$ .

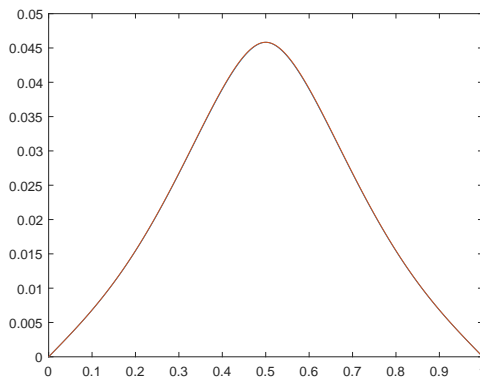


**Figure 5.24:** Comparison of the solutions corresponding to the two weak formulations. The red graph on top corresponds to the first weak formulation,  $\alpha = 91, \gamma = 0.05, c = 0.5$  and  $N = 1000$ .

CHAPTER FIVE

Again, Table 5.5 below shows the evolution of  $|E - E_h|$  as  $h \rightarrow 0$ , where we see that the error tends to zero as  $h \rightarrow 0$ , thus confirming the result from Theorem 20.

N	$E_h$	$ E - E_h $
10	0.7657982263	0.1425432475
20	0.8297645960	0.0785768778
40	0.8669465710	0.0413949028
80	0.8870767103	0.0212647635
160	0.8975617754	0.0107796984
320	0.9029140827	0.0054273911
640	0.9056183020	0.0027231718
1280	0.9069775073	0.0013639665
2560	0.9076588939	0.0006825799
5120	0.9080000345	0.0003414393
10240	0.9081707167	0.0001707571
20480	0.9082560858	0.0000853880
40960	0.9083071555	0.0000343183

**Table 5.5:** FEM numerical solutions for  $c = 0.5$  and various  $N$ , and the exact energy is  $E = 0.9083414738$ .

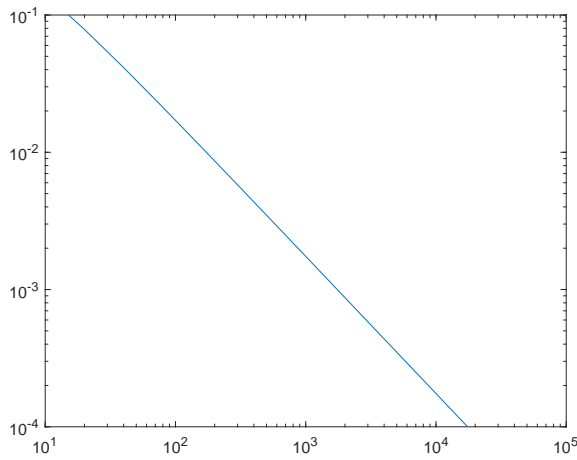


**Figure 5.25:** Log-log plot of the error estimate of the energy  $u$  for  $\alpha = 93, \gamma = 0.05$  and  $c = 0.5$ . The  $x$ -axis represents  $\log(N)$  while the  $y$ -axis represents  $\log|E - E_h|$ . Notice the linear pattern.

To assess the converges of  $u_h$  and  $w_h$  in Table 5.6, we report the error  $|u - u_h|_{\tilde{V}}$  and  $|w - w_h|_{H_0^1(0,1)}$ . We see that they tend to zero linearly as  $h \rightarrow 0$ , which, again, confirms

CHAPTER FIVE

the result of Theorem 20.

N	$ u - u_h _{\tilde{V}}$	$ w - w_h _{H_0^1(0,1)}$
10	0.0028539224	0.0688686853
20	0.0012318576	0.0353650051
40	0.0005851146	0.0177843626
80	0.0002882316	0.0088754925
160	0.0001435427	0.0044257548
320	0.0000716976	0.0022087002
640	0.0000358394	0.0011031443
1280	0.0000179185	0.0005512498
2560	0.0000089591	0.0002755419
5120	0.0000044795	0.0001377502
10240	0.0000022397	0.0000688701
20480	0.0000011198	0.0000344341
40960	0.0000005598	0.0000172171

**Table 5.6:** Errors generated for  $\alpha = 93$  and  $\gamma = 0.05$  and various  $N$ .

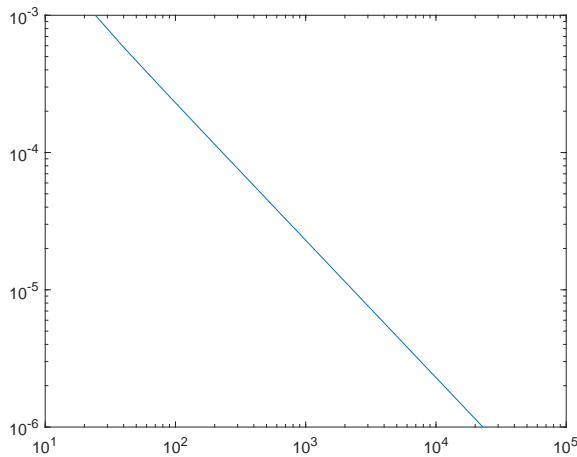


**Figure 5.26:** Log-log plot of the error estimate of the energy  $u$  for  $\alpha = 93, \gamma = 0.05$ . The  $x$ -axis represents  $\log(N)$  while the  $y$ -axis represents  $\log|u - u_h|_{\tilde{V}}$ . Notice the linear pattern.

**Remark 22.** *After reviewing both methods (namely dropping the  $[u(c)] = 0$  condition vs dropping the  $u'(c^-) = u'(c^+) = 0$  condition) it is worth summarizing their advantages and drawbacks.*

*Dropping the  $[u(c)] = 0$  condition seems to be the most intuitive approach as it produces a lot of obviously discontinuous solutions/graphs which can be easily rejected. The cost*

for this is the introduction of the more complicated space  $\tilde{V}_h$  and thus the need to distinguish between matrices such as  $\mathbb{A}$  and  $\tilde{\mathbb{A}}$ .

Dropping the derivative condition on the other hand, seems to be more convenient, as we no longer need the introduction of the  $\tilde{V}_h$  space (we can simply work on  $H_h$  instead) and we can write system  $(S'_2)_h$  above in a simpler matrix form. However, this makes all the candidate solutions/graph continuous and thus arguably visually harder to decide which of them have a local extremum at  $x = c$ .

In the Table 5.7 below we are comparing the errors (difference between the actual and the approximate solution) of the two formulations, for various choices of parameters. We use  $N = 500$  for the approximate solution. Notice that the errors in the second formulation are always smaller and no significant difference is observed if the mesh changes, or different solutions are used. We therefore conclude that the second method is better on to use since it produces more accurate results.

$\alpha$	$\gamma$	$ u - u_h _{\tilde{V}}$	$ u - u_h _{H_0^1(0,1)}$
1	0.1	0.0004059995137234233	0.000405910634606206
55	0.02	0.0000657440098026757	0.000064921486060296
9	0.01	0.0003335475178106126	0.000332107223063766
110	0.01	0.0000094017150117650	0.000009385133443203
93	0.05	0.0000458770984422224	0.000045877097072104
5	0.4	0.0001582018341075732	0.000158201795306649
150	0.1	0.0000315256348241931	0.000031525633627172
12	0.003	0.0002539429514240264	0.0002539429389922499

**Table 5.7:** Errors generated by the different formulations for various parameter pairs  $(\alpha, \gamma)$  and  $N = 500$ .

## 5.4 The Finite Element Method (Construct periodic solution of lap $> 2$ )

Now that we have established two concrete ways to approximate all solutions of lap 2, we can use those results to construct periodic solutions of higher lap number. This is possible due to the fact that any periodic solution can be thought of as an odd-even

## CHAPTER FIVE

extension of a lap 2 solution,

More specifically, we can use the methods described in the previous sections to find a solution in the interval  $[0, \frac{1}{n}]$ , and then “copy” it oddly- evenly for the remaining  $[0, 1]$  interval.

For example, for lap 3,  $n = 2$ . This means that we can solve the Euler-Lagrange equation on the  $[0, \frac{1}{2}]$  interval and then extend the result oddly in  $[\frac{1}{2}, 1]$ .

### 5.4.1 A Numerical Experiment

In the graphs below we give examples of the numerical approximations of several periodic solutions for  $\alpha = 1, \gamma = 0.1$  and  $N = 1000$ .

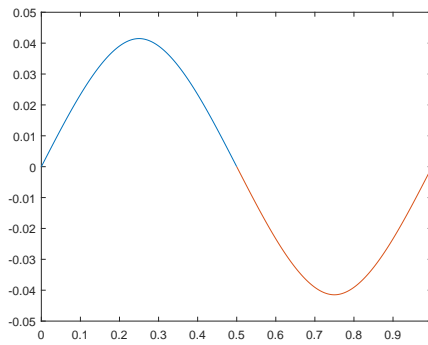


**Figure 5.27:** symmetric periodic solution of lap 3, where  $\alpha = 1, \gamma = 0.1, c_1 = \frac{1}{4}$  and  $c_2 = \frac{3}{4}$ .

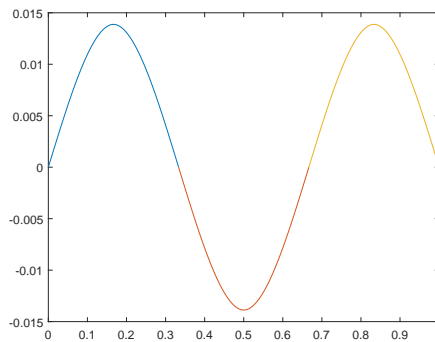


**Figure 5.28:** symmetric periodic solution of lap 4, where  $\alpha = 1, \gamma = 0.1, c_1 = \frac{1}{6}, c_2 = \frac{1}{2}$ , and  $c_3 = \frac{5}{6}$ .

CHAPTER FIVE

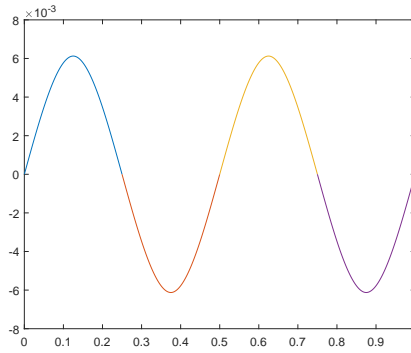


**Figure 5.29:** symmetric periodic solution of lap 5, where  $\alpha = 1, \gamma = 0.1, c_1 = \frac{1}{8}, c_2 = \frac{3}{8}, c_3 = \frac{5}{8}$  and  $c_4 = \frac{7}{8}$ .

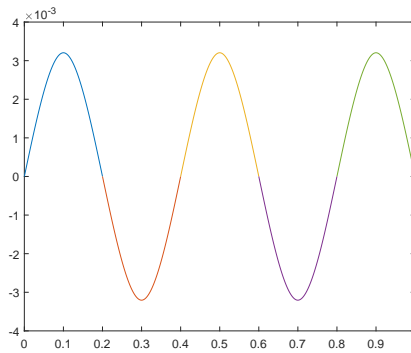


**Figure 5.30:** symmetric periodic solution of lap 6, where  $\alpha = 1, \gamma = 0.1, c_1 = \frac{1}{10}, c_2 = \frac{3}{10}, c_3 = \frac{1}{2}, c_4 = \frac{7}{10}$  and  $c_5 = \frac{9}{10}$ .

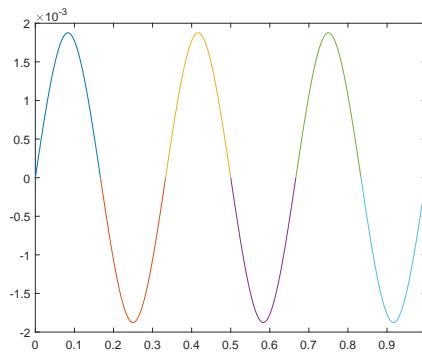


**Figure 5.31:** symmetric periodic solution of lap 7, where  $\alpha = 1, \gamma = 0.1, c_1 = \frac{1}{12}, c_2 = \frac{1}{4}, c_3 = \frac{5}{12}, c_4 = \frac{7}{12}, c_5 = \frac{3}{4}$  and  $c_6 = \frac{11}{12}$ .

**Remark 23.** *As we can see, the numerical approximation is leveraging the fact that the lap 2 solution (for different parameters) acts as a “building block”, but without*

*making an a priori assumption on those parameters change. This is another benefit of the method, since it does not depend on any theoretical properties or formulas.*

## 5.5 Derivative-Free Optimization

Next we analyze another numerical method for finding solutions to the Euler Lagrange equation, by utilizing the fact that those solutions are of minimal energy. In other words, we are interested in finding the correct location of the jump, leveraging the fact that for each candidate location we can compute its corresponding energy, namely

$$E(u(c)) = \int_0^1 \gamma u_{xx}^2(c) + W(u_x(c)) + \alpha u^2(c) dx,$$

where  $u(c)(x)$  is a function that has a jump at  $x = c$  and satisfies all but the derivative condition ( $u_x(c^-) = u_x(c^+) = 0$ ) as in the second weak formulation.

Clearly,  $E(u(c))$  is the smallest when  $c$  is the correct jump location. For that reason it is enough to minimize  $E(u(c))$ .

We can do this using the Derivative-Free Optimization (DFO) approach, an iterative method that improves the answer in each iteration without the use of derivatives (see [25], [35]). Instead, we replace the function by a quadratic approximation as indicated below.

### 5.5.1 The Algorithm

The steps of the algorithm are as follows.

step 0 (Initialization): We choose three arbitrary distinct points  $c_1, c_2, c_3 \in (0, 1)$  to act as our first candidates for the jump.

step 1 (Main phase): We calculate the energies  $E_i = E(u(c_i)) \quad i = 1, 2, 3$ .

step 2 (Main phase): Find a parabola  $P : [0, 1] \rightarrow \mathbb{R}$ ,  $P(x) = ax^2 + bx + c$  such that

CHAPTER FIVE

$P(c_i) = E_i$   $i = 1, 2, 3$ . In other words, find a parabola that goes through these three points.

In particular it is enough to find  $a, b, c$  where

$$\begin{bmatrix} a \\ b \\ c \end{bmatrix} = \begin{bmatrix} c_1^2 & c_1 & 1 \\ c_2^2 & c_2 & 1 \\ c_3^2 & c_3 & 1 \end{bmatrix}^{-1} \begin{bmatrix} E(u(c_1)) \\ E(u(c_2)) \\ E(u(c_3)) \end{bmatrix}.$$

step 3 (Main phase): Minimize the parabola  $P$  from above by finding its vertex  $c_4 = \frac{-b}{2a}$ , and calculate  $E_4 = E(u(c_4))$ .

step 4 (Main phase): Choose the lowest energies among  $E_1, E_2, E_3, E_4$  as well as the corresponding  $c_i$ 's. More specifically:

$$\{E_1, E_2, E_3\} \leftarrow \{E_1, E_2, E_3, E_4\} \setminus \max \{E_1, E_2, E_3, E_4\},$$

and the new  $\{c_1, c_2, c_3\}$  are the ones corresponding to the new  $\{E_1, E_2, E_3\}$ .

step 5 (Main phase): Go to step 1.

step 6 (Termination condition): Repeat until  $\max \{E_1, E_2, E_3\} - \min \{E_1, E_2, E_3\} < \epsilon$  where  $\epsilon$  is our chosen threshold.

step 7 (Final result) When the termination condition is met, return the  $c_i$  corresponding to the  $\min \{E_1, E_2, E_3\}$ .

After the algorithm terminates we will have access to a  $c$  that approximately minimizes the energy functional, and thus is a very good approximation to the exact location of one of the jumps (see Appendix A.2). This will further give us access to a solution of the Euler Lagrange equation.

## CHAPTER FIVE

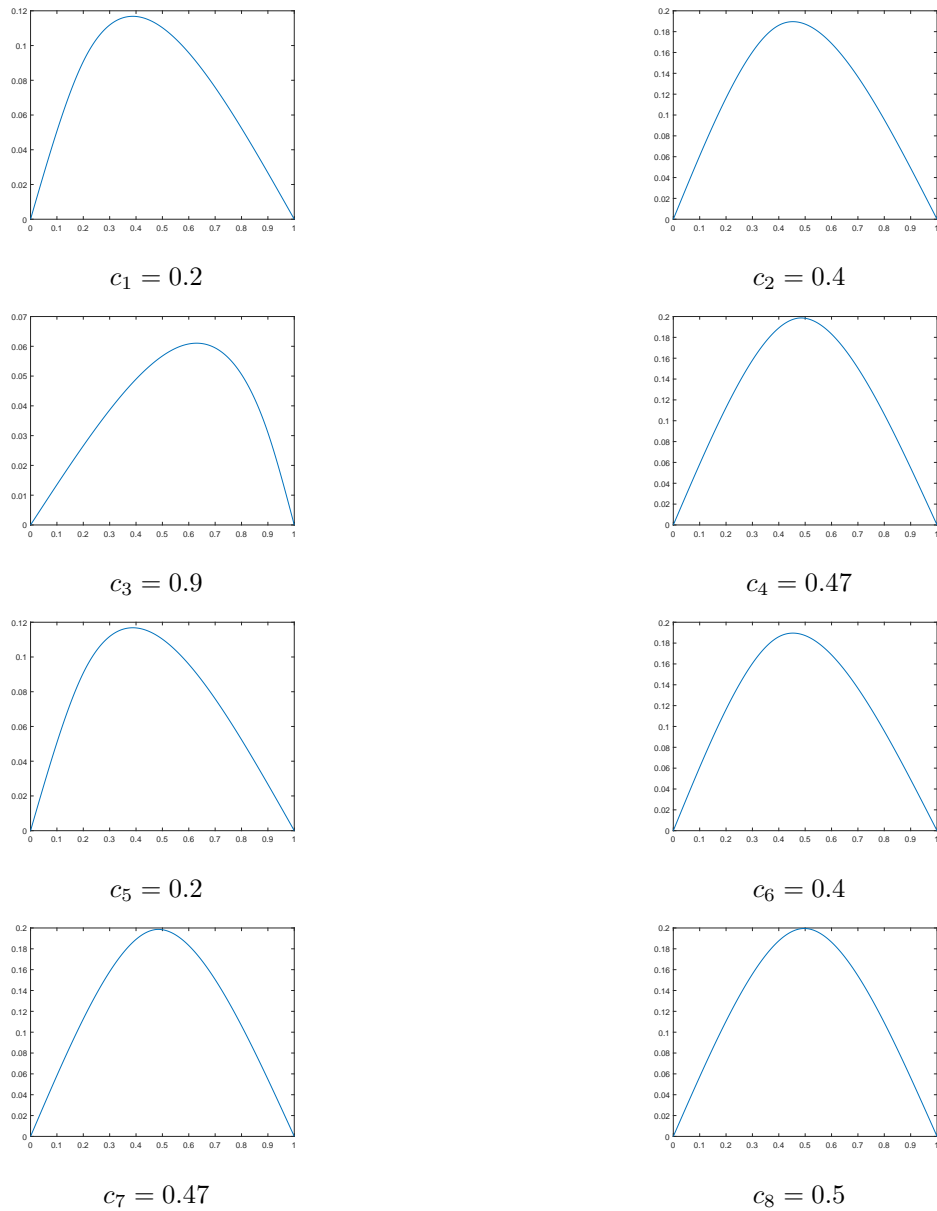


**Figure 5.33:** Successive iterations of DFO plotting solutions with a new location of the jump in each step where  $\alpha = 1$ ,  $\gamma = 0.1$ ,  $N = 1000$  and the starting points are  $c_1 = 0.2$ ,  $c_2 = 0.4$ ,  $c_3 = 0.9$ .

### 5.5.2 Numerical results

We apply the algorithm above, to different examples. The first with  $(\alpha, \gamma) = (50, 0.02)$  where we know from the analytical methods that the exact location of the jump is  $c = 0.5$  while the exact energy is  $E = 0.8935833875$

CHAPTER FIVE

In the table below we summarize the prediction of DFO for  $c$  and  $E$  under various number of iterations. Our three arbitrary distinct points are  $c_0 = 0.1$ ,  $c_1 = 0.4$  and  $c_2 = 0.7$ . Notice that as  $N$  grows large, the values  $c, E$  given by DFO correctly approach the exact value  $c = 0.5$  and  $E = 0.8935833875$ .

N	$c_{DFO}$	$E_{DFO}$	$ c - c_{DFO} $	$ E - E_{DFO} $
40	0.5260270042	0.8602881256	0.0260270043	0.0332952619
80	0.5110626832	0.8761136517	0.0110626833	0.0174697358
160	0.5051458119	0.8845699232	0.0051458119	0.0090134643
320	0.5025652106	0.8890008182	0.0025652107	0.0045825693
640	0.5001155429	0.8912739430	0.0001155429	0.0023094445
1280	0.5000676253	0.8924240649	0.0000676254	0.0011593226
2560	0.5000362768	0.8930026088	0.0000362769	0.0005807787
5120	0.5000187545	0.8932926977	0.0000187545	0.0002906898
10240	0.5000095312	0.8934379608	0.0000095313	0.0001454267
20480	0.5000051810	0.8935106586	0.0000051810	0.0000727289

**Table 5.8:** DFO numerical prediction for  $c = 0.5$  and  $E = 0.8935833875$ .

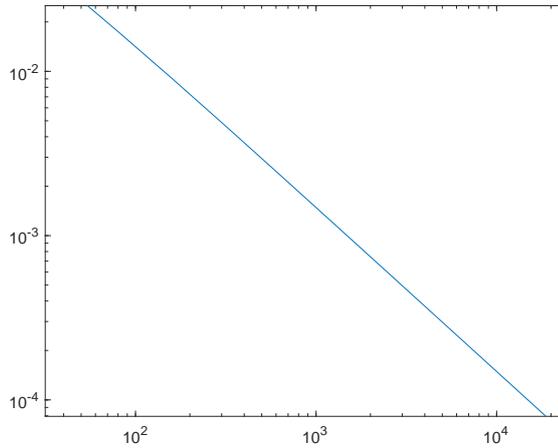


**Figure 5.34:** Log-log plot of the error estimate of the energy  $u$  for  $E = 0.8935833875$  and  $c = 0.5$ . The  $x$ -axis represents  $\log(N)$  while the  $y$ -axis represents  $\log |E - E_{DFO}|$ . Notice the linear pattern.

The second example is with  $(\alpha, \gamma) = (108, 0.05)$  where exact location of the jump is  $c = 0.3743602663$  and the exact energy is  $E = 0.917355785$ . We choose our three arbitrary distinct points to be  $c_0 = 0.1$ ,  $c_1 = 0.3$  and  $c_2 = 0.4$ . we summarize the

CHAPTER FIVE

prediction of DFO for  $c$  and  $E$  in the table below:

N	$c_{DFO}$	$E_{DFO}$	$ c - c_{DFO} $	$ E - E_{DFO} $
80	0.4299301593	0.8955977938	0.0555698930	0.0217579912
160	0.3909558692	0.9062859869	0.0165956029	0.0110697981
320	0.3868837807	0.9117485855	0.0125235144	0.0056071995
640	0.3827112935	0.9145319655	0.0083510272	0.0028238195
1280	0.3790152381	0.9159407327	0.0046549718	0.0014150523
2560	0.3766298522	0.9166470462	0.0022695859	0.0007087388
5120	0.3754507112	0.9170009554	0.0010904449	0.0003548296
10240	0.3746989419	0.9171780994	0.0003386756	0.0001776856
20480	0.3746037820	0.9172667241	0.0002435157	0.0000890609
40960	0.3745164746	0.9173110474	0.0001562083	0.0000447376

**Table 5.9:** DFO numerical prediction for  $c = 0.3743602663$  and  $E = 0.917355785$ .

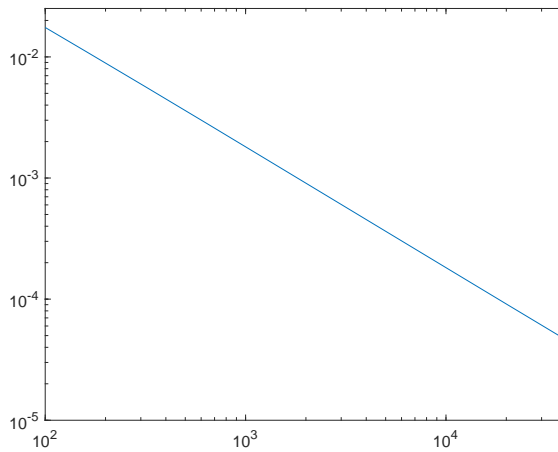


**Figure 5.35:** Log-log plot of the error estimate of the energy  $u$  for  $E = 0.917355785$  and  $c = 0.3743602663$ . The  $x$ -axis represents  $\log(N)$  while the  $y$ -axis represents  $\log|E - E_{DFO}|$ . Notice the linear pattern.

Next, in the Tables (5.10 - 5.12) we present a full DFO process for different  $\alpha$  and  $\gamma$  with different exact location of the jump. In particular, we keep track of all the  $c_i$ 's for every iteration. Notice again, that as we are going through the iterations, we converge to the correct value of  $c$ .

CHAPTER FIVE

Iteration	$c_1$	$c_2$	$c_3$	$c_4$
1	0.11	0.12	0.13	0.2564189682
2	0.12	0.13	0.2564189682	0.2878852633
3	0.13	0.2564189682	0.2878852633	0.3192688312
4	0.2564189682	0.2878852633	0.3192688312	0.3507970419
5	0.2878852633	0.3192688312	0.3507970419	0.3532388834
6	0.3192688312	0.3507970419	0.3532388834	0.3597824859
7	0.3507970419	0.3532388834	0.3597824859	0.3619350512
8	0.3532388834	0.3597824859	0.3619350512	0.3623508185

**Table 5.10:** Full DFO process with detailed iterations when  $(\alpha, \gamma) = (190, 0.1)$  and  $N = 1000$  and where the exact  $c = 0.3623549804$ .

Iteration	$c_1$	$c_2$	$c_3$	$c_4$
1	0.91	0.92	0.93	0.7529011875
2	0.92	0.93	0.7529011875	0.6694035449
3	0.93	0.7529011875	0.6694035449	0.5611388507
4	0.7529011875	0.6694035449	0.5611388507	0.4930445220
5	0.6694035449	0.5611388507	0.4930445220	0.4978671246
6	0.5611388507	0.4930445220	0.4978671246	0.5001351766
7	0.4930445220	0.4978671246	0.5001351766	0.5000282733

**Table 5.11:** Full DFO process with detailed iterations when  $(\alpha, \gamma) = (1, 0.1)$  and  $N = 1000$  and where the exact  $c = 0.5$ .

Iteration	$c_1$	$c_2$	$c_3$	$c_4$
1	0.1	0.4	0.7	0.5021125227
2	0.4	0.7	0.5021125227	0.4995094199
3	0.7	0.5021125227	0.4995094199	0.4999990724
4	0.5021125227	0.4995094199	0.4999990724	0.5000141110

**Table 5.12:** Full DFO process with detailed iterations when  $(\alpha, \gamma) = (33, 0.01)$  and  $N = 1000$  and where the exact  $c = 0.5$ .

Also, it is worth seeing the DFO as a function of  $h = \frac{1}{N}$ . As the following illustrates, as  $h$  goes to zero, the approximate value of  $c$  and  $E$  converge to the values of the exact solution. Here  $\alpha = 60, \gamma = 0.1, c = 0.5$  and  $E = 0.8891382917$ .

CHAPTER FIVE

$h$	$c$ (given by DFO)	Energy (given by DFO)
0.025	0.49842496	0.85464934
0.0125	0.50228775	0.87063314
0.00625	0.50252113	0.87953131
0.003125	0.50164962	0.88423681
0.001562	0.50093139	0.88666420
0.000781	0.50049379	0.88789532
0.000390	0.50025412	0.88851531
0.000195	0.50012889	0.88882642
0.000097	0.50006491	0.88898226
0.000048	0.50003257	0.88906025
0.000024	0.50001631	0.889099267
0.000012	0.50000816	0.889118778

**Table 5.13:** DFO predictions as a function of  $h = \frac{1}{N}$  where  $(\alpha, \gamma) = (60, 0.1)$  and the exact values are  $c = 0.5$  and  $E = 0.8891382917$ .

Last but not least, In the table below we summarize the prediction of DFO for  $c$  and  $E$  for different values of  $\alpha$  and  $\gamma$ .

$\alpha$	$\gamma$	$c$ (given by DFO)	Energy (given by DFO)	exact $c$	exact energy
55	0.02	0.50007949	0.84547658	0.5	0.84571172
140	0.02	0.27492439	0.91580915	0.27498612	0.91596674
7	0.1	0.50001902	0.68841462	0.5	0.68847220
140	0.03	0.50008207	0.92475010	0.5	0.92495885
130	0.1	0.44142490	0.93655715	0.44072196	0.93674129
1	0.5	0.50002595	0.86324115	0.5	0.86335026
92	0.06	0.56495795	0.91044042	0.56483294	0.91048682
73	0.08	0.50008754	0.89922490	0.5	0.89939575
12	0.09	0.50001945	0.72688605	0.5	0.72695694
32	0.01	0.50006148	0.75911134	0.5	0.75902964

**Table 5.14:** DFO numerical prediction for for various parameter pairs  $(\alpha, \gamma)$  and  $N = 5000$ .

As evidenced by all the tables above, the Derivative-Free-Optimization method, provides an efficient tool to accurately approximate the location of the jump, when the latter is not known a priori. The power of the method comes from the fact that it can rapidly locate (i.e. requires few iterations) the neighbourhood within which the energy functional has a local minimum and thus reveal it to us. As all of the examples above illustrate, not only does the method converge quickly to the exact solution but also it

does so with remarkable accuracy. All in all, DFO is a great way to approximate the location of the jump, an unknown which is otherwise hard to pin down analytically.

**Remark 24.** *Note that although the figures above are taken from examples where we have access their corresponding analytical solutions, DFO can be applied to far more general setting. In particular, for lap number higher than 3, MAPLE fails to solve the equation required by the Fredholm Alternative and thus we have no access to the locations of the jump nor their corresponding solutions to the Euler Lagrange equation. In contrast, DFO can be generalized to an arbitrary amount of jumps (i.e. an arbitrary lap number).*

## 5.6 The Finite Element Method for a problem with non-constant parameters

So far we only considered cases where the parameters are always constant and independent of the “space” variable  $x$ . In general, when  $\alpha$  or  $\gamma$  are non-constant, we can not solve the Euler-Lagrange equation analytically, and then numerical methods become essential.

Fortunately, the FEM is not affected by the complexity of the functions as it can always replace them with piecewise-linear counterparts. This allows for an additional freedom when choosing the parameters, provided that they are reasonably smooth.

In this section we set  $\alpha(x) = x + 1$  and we show that the FEM (coupled with the DFO for the jump) can give an approximate lap 2 solution to an otherwise non-tractable problem.

In what follows we work with the second weak formulation (as described in Section 5.3) due to the simplicity of the solution space. In that case, the Finite Element Method

CHAPTER FIVE

reads as follow: Find  $u_h, w_h \in H_h$  such that

$$\begin{cases} \int_0^1 w_h(x)v_h(x) dx + \int_0^1 u_h'(x)v_h'(x) dx = 0 \quad \forall v_h \in H_h, \\ \gamma \int_0^1 w_h'(x)z_h'(x) dx + \int_0^1 w_h(x)z_h(x) dx - \int_0^1 u_h(x)\alpha(x)z_h(x) dx = 2z(c) \quad \forall z_h \in H_h. \end{cases}$$

Since we are working in  $H_0^1(0, 1)$ , we can assume as earlier that

$$u_h = \sum_{i=1}^N \xi_i \varphi_i(x) \quad \text{and} \quad w_h = \sum_{i=1}^N \zeta_i \varphi_i(x).$$

Notice that (like in Section 5.3) we can use the same basis for both  $u_h$  and  $w_h$ , since they belong to the same space. This will significantly simplify our calculations. As a matter of fact, the only difference with the matrix form of Section 5.3 will be the part where  $\alpha$  is involved, namely the top-right block of the matrix. We can calculate this precisely by considering:

$$\int_0^1 u_h(x) \alpha(x) \varphi_j(x) dx = \int_0^1 u_h(x) (x+1) \varphi_j(x) dx = \sum_{i=1}^N \sum_{i=1}^N \xi_i \zeta_i \int_0^1 \varphi_i(x) (x+1) \varphi_j(x) dx.$$

Thus the new top-right block matrix  $\mathbb{B}_\alpha$  should have entries  $\int_0^1 \varphi_i(x) (x+1) \varphi_j(x) dx$ .

That is

$$\mathbb{B}_\alpha = \left[ \int_0^1 \varphi_i(x) (x+1) \varphi_j(x) dx \right]_{(i,j) \in N \times N}.$$

In particular, we have the following cases:

- $[\mathbb{B}_\alpha]_{(i-1,i)} = \int_{x_{i-1}}^{x_i} \left(-\frac{x}{h} + i\right)(x+1)\left(\frac{x}{h} - i + 1\right) dx = \frac{h^2(2i-1)}{12} + \frac{h}{6}.$
- $[\mathbb{B}_\alpha]_{(i,i)} = \int_{x_{i-1}}^{x_i} \left(\frac{x}{h} - i + 1\right)^2(x+1) + \int_{x_i}^{x_{i+1}} \left(-\frac{x}{h} + i + 1\right)^2(x+1) dx = \frac{2h(ih+1)}{3}.$
- $[\mathbb{B}_\alpha]_{(i,i+1)} = \int_{x_i}^{x_{i+1}} \left(-\frac{x}{h} + i + 1\right)(x+1)\left(\frac{x}{h} - i\right) dx = \frac{h^2(2i+1)}{12} + \frac{h}{6}.$
- $[\mathbb{B}_\alpha]_{(i,j)} = 0$  for all  $|i - j| > 1$ .

## CHAPTER FIVE

Note that, with a non-constant choice of  $\alpha$ , the entries of  $\mathbb{B}_\alpha$  are also non-constant and depends on  $i$  in general. This leads to the following form:

$$\begin{bmatrix} \gamma \mathbb{A} + \mathbb{B} & -\mathbb{B}_\alpha \\ \mathbb{B}^T & \mathbb{A} \end{bmatrix} \cdot \mathbf{X} = \mathbf{b}$$

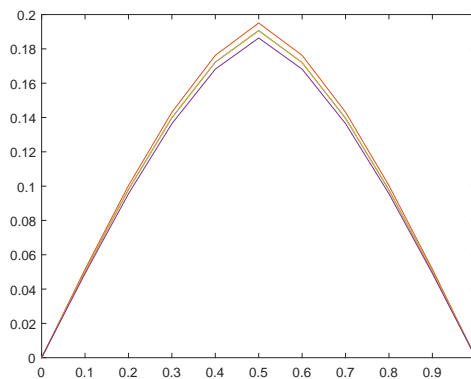
where  $\mathbf{X}, \mathbb{A}, \mathbb{B}, \mathbf{b}$  are exactly as before and  $\gamma$  is constant.

### 5.6.1 A Numerical Experiment

To advance our understanding of the above calculations, let us define  $u^1$  to be the solution corresponding to  $\alpha = 1$ ,  $u^2$  be the solution corresponding to  $\alpha = 2$  and  $u^{x+1}$  be the solution corresponding to  $\alpha(x) = x + 1$ . Since  $1 \leq x + 1 \leq 2$  for all  $x \in [0, 1]$  and the fact that the larger the stiffness parameter the closer the solution would be to zero, we would expect that:

$$u^2 \leq u^{x+1} \leq u^1.$$

This is exactly what we observe as the following figures illustrate (see Appendix A.1). Notice also that as we refine the mesh (i.e. as  $N$  goes to infinity) the energy of the middle solution (i.e. the one corresponding to  $\alpha(x) = x + 1$ ) converges to a fixed amount. We show this clearly in Table 5.6.1 where we compare the energies with mesh  $N = 10^{2n}$  for successive values  $n$ .



## CHAPTER FIVE

**Figure 5.36:** Comparison to numerical solutions with constant parameters when  $N = 10$ . Here we have  $1 \leq x + 1 \leq 2$  for all  $x \in [0, 1]$ .

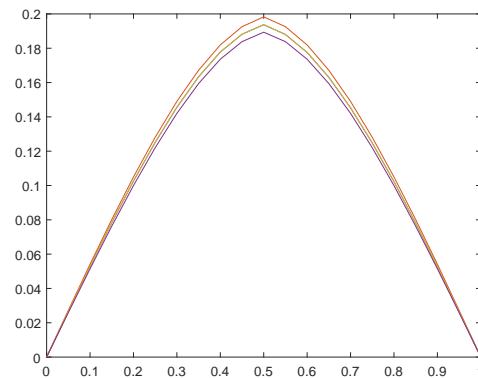


**Figure 5.37:** Comparison to numerical solutions with constant parameters when  $N = 20$ . Here we have  $1 \leq x + 1 \leq 2$  for all  $x \in [0, 1]$ .

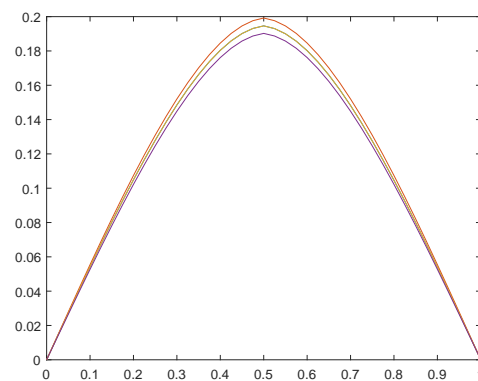
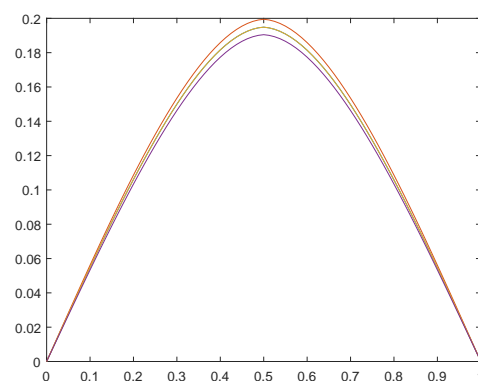


**Figure 5.38:** Comparison to numerical solutions with constant parameters when  $N = 40$ . Here we have  $1 \leq x + 1 \leq 2$  for all  $x \in [0, 1]$ .



## CHAPTER FIVE

**Figure 5.39:** Comparison to numerical solutions with constant parameters when  $N = 80$ . Here we have  $1 \leq x + 1 \leq 2$  for all  $x \in [0, 1]$ .

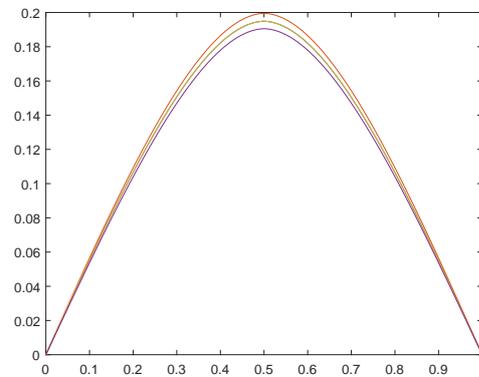


**Figure 5.40:** Comparison to numerical solutions with constant parameters when  $N = 160$ . Here we have  $1 \leq x + 1 \leq 2$  for all  $x \in [0, 1]$ .

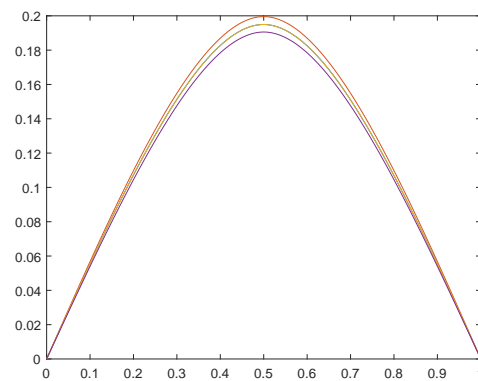


**Figure 5.41:** Comparison to numerical solutions with constant parameters when  $N = 1000$ . Here we have  $1 \leq x + 1 \leq 2$  for all  $x \in [0, 1]$ .

N	$E_{\frac{1}{10 \cdot 2^n}}$	$ E_{\frac{1}{10 \cdot 2^n}} - E_{\frac{1}{10 \cdot 2^{n+1}}} $
10	0.6803162658	-
20	0.6323789877	0.0479372780
40	0.6160299612	0.0163490265
80	0.6114050728	0.0046248885
160	0.6102796222	0.0011254506
320	0.6100592940	0.0002203281
640	0.6100557338	0.0000035602

**Table 5.15:** Numerical values (according to FEM) for energies corresponding to the solution with  $\alpha(x) = x + 1$  and  $c = 0.5$  for various values of  $N$ . On the left of the table we calculate the difference between successive levels of Energy in a logarithmic scale.

## 5.7 Conclusion

In this chapter we showed that both the Finite Element Method (FEM) and the Derivative-Free Optimization (DFO) method can be used in combination with one another to yield arbitrarily close approximations to the exact solution of our main Euler Lagrange equation. The proximity of those approximations was later verified by comparing the numbers produced by the FEM and the DFO methods to those given by MAPLE from the exact solutions.

Since we already established a concrete theoretical framework for the numerical methods in the previous chapter, we gave specific examples in the current one. In particular, we start with the Finite Element Method (FEM) and give a precise algorithmic process for how this method will work in practice for a given jump location  $c$ . The most important derivation is that of representing each weak formulation with a convenient matrix form (see (5.2.3) - (5.2.7)) which can then be solved efficiently using a simple Gauss-Jordan process.

To evaluate the accuracy of some of these numerical approximations, we compare them to their analytical solutions and graph them side by side. On top of that, we also consider both symmetric and non-symmetric solutions for various parameters  $\alpha$  and  $\gamma$ . We also calculated the corresponding energies both of the exact and the numerical

## CHAPTER FIVE

solutions. We accompany all of the above calculations with error tables, which indeed confirm that as the mesh gets more refined the error (between the exact and approximate energies) converges to zero (see Sections 5.2 and 5.3). Last but not least we apply the FEM to find periodic solutions of lap greater than 2 (see Section 5.4) and also solutions for when the parameter  $\alpha$  is not a constant function of  $x$  (see Section 5.6).

In Section 5.5, we introduced an approach that uses the Derivative-Free Optimization (DFO) method to find the location of the jump (which can then be used to construct a piecewise linear solution using the FEM - as described earlier). The algorithm approximates the location of the point of minimal energy in the discrete problem by constructing a sequence of approximations without the need of computing the derivative of the energy functional.

Moreover, we showed experimentally the convergence of the DFO method using specific examples and their corresponding energy tables for different and progressively finer partitions. As expected, the numerical values for the energies converge to the exact values as the mesh gets finer.

We conclude that both DFO and FEM should be used in combination in order to numerically find an efficient and accurate approximation to each weak formulation and by extension to the original Euler-Lagrange equation.

## Chapter 6

# Conclusion and future work

In Chapter 3, we reformulated Grinfeld and Lord's conjecture for Müller's problem to match Yip's problem (see Conjecture 10). We allow for a parameter  $\alpha > 0$  which will help us better study bifurcations and thus answer the conjecture.

First of all, we start with Yip's functional and Müller's boundary conditions (see Definition (3.2.2)). The functional gives rise to an Euler-Lagrange equation which we then solved. There were 3 cases to be considered for the solution of the Euler Lagrange equation, depending on the relationship between  $\alpha$  and  $\gamma$  (see Section 3.2).

In Section 3.3, we work in the simplest case with lap 2. We found that for given  $\alpha, \gamma$ , there exists a unique symmetric solution (see Theorem 11). This Theorem disproved the conjecture for Yip's problem, since we know that there is a solution without internal zeroes regardless of how large  $\alpha$  is. Also, we show that using solutions of lap 2, we can construct solutions of higher lap number (see Theorem 12).

Next, we show the existence of non-symmetric solutions. These extra non symmetric solutions bifurcate from pitchfork bifurcation curve where we go from one symmetric solution splits into three solutions (one symmetric and two non-symmetric); see Figure 3.21.

In the following Section 3.4, we calculate various energies corresponding to different

## CHAPTER SIX

Euler Lagrange solutions. Moreover, we present a formula that calculates the energies of higher lap number from those with lap number 2 (see Lemma 3). We also calculated specific energy curves like the  $E_{1,2}$  curve where  $E(u_1) = E(u_2)$ . Most of our work (of lap 2) can be summarized in Figure 3.32.

In summary we have the following: below the  $E_{1,2}$  curve,  $u_1$  is a global minimizer. Above the bifurcation curve,  $u_1$  is not a minimizer and between the  $E_{1,2}$  and the bifurcation curve,  $u_1$  is a local minimizer.

In the following Section 3.5.1, we begin our investigation on the bifurcation diagrams of solutions of lap 3. Our work of lap 3 can be summarized in Figure 3.33. In particular, we found two types of bifurcation curves, one that gives rise to a fresh pair of non-periodic solutions ( $p$ -curves) and one that gives rise to a fresh pair of non-symmetric solutions ( $s_1$ -curve). Below the curve  $p_1$  we have a unique solution while above  $p_1$  we have more than 1 solutions. Below  $s_1$  we only have symmetric solutions while above  $s_1$  non-symmetric solutions start to appear.

Chapter 4 sets up the stage for the mathematical framework of our numerical methods. The core of our work revolves around an important equivalence between a version almost identical to our problem ( $S_1$ ) and a weak formulation which can be approximated numerically ( $S_2$ ). As a matter of fact we develop two equivalences. The first by dropping the continuity condition and the second by dropping a derivative condition. This permits us to approximate the problem numerically (see Sections 4.3 and 4.4).

We also were able to prove that both weak formulations have a unique solution using key ideas from functional analysis, namely the Lax-Milgram theorem and (bi)linear functionals (4.3.11) and (4.4.4). That, combined with the equivalences mentioned earlier can be shown to satisfy the original problem (see Subsections 4.3.1 and 4.4.1 and Theorems 15 and 18).

The major component of our numerical approach is based on the Finite Element method. We started by defining convenient solution subspaces (on piecewise linear functions) and then showed that both weak formulations achieve unique solutions within

## CHAPTER SIX

those subspaces for any given mesh (see Theorems 16 and 19). The idea is that finding solutions within these subspaces can be done sufficiently using MATLAB. Another critical step in the right direction is using Galerkin orthogonality that allows us to prove that the unique solution of the discrete problem can be arbitrarily close to the unique solution of the continuous problem (see Theorems 17 and 20). These two facts allowed us to approximate the unique solution of our problem both efficiently and accurately.

We concluded the section by illustrating the potency of our method by showing that it can also be used in the general case where the parameter  $\alpha$  is not a constant function ( $S'_3$ ). This is important because we do not yet have access to ways of calculating the exact solution analytically in those cases.

In Chapter 5, we introduce the second numerical method called The Derivative-Free optimization to help us approximate the location of the jump  $c$ . More precisely, DFO was used to approximate the location of the jump while the FEM is used to approximate the solution corresponding to that jump. In other words both the DFO and FEM were used as a combination with one another to produce arbitrary close approximations to the exact solution of the Euler Lagrange equation. We verified the accuracy of these results by comparing them to the exact solution given by MAPLE.

This chapter also includes several specific numerical examples. In particular, we present a precise algorithmic process on how this FEM method works in practice for a given jump location  $c$ . specifically we were able to present each weak formulation using a matrix form (see (5.2.3) - (5.2.7)) which can be solved efficiently via the Gauss-Jordan process.

To make a strong case for the accuracy of our numerical approximation we compare them graphically to their corresponding analytical solutions and illustrate them side by side. Our examples include several symmetric and non symmetric solutions for different  $\alpha$  and  $\gamma$ . Moreover we included the energies of both the exact and numerical solutions as well as their corresponding error table which acts as a confirmation that the error converges to zero as we refine the mesh (see Sections 5.2 and 5.3).

## CHAPTER SIX

Lastly, we apply the FEM to periodic solutions with lap greater than 2 (see Section 5.4) and also to solutions corresponding to a non constant parameter  $\alpha$  (see Section 5.6).

Section 5.5 deals with the details of DFO described earlier. In particular, we take advantage of the fact that the location of the jump  $c$  corresponds to a minimal energy which can be found numerically and without the use of derivatives (thus the name). The section would not be complete without the use of specific examples and energy tables for progressively finer partitions. The convergence of the DFO method is then verified experimentally since the energies converge to the correct exact value as we refine the mesh.

For future work, one can establish proper theoretical frame work which proves that the DFO method always converges to the desired jump location. Also, one can consider gradient flow of our functional in order to understand how interfaces are created. Moreover, one can consider local and non-local Cahn-Hilliard and Cahn-Allen equations with Yip's free energy to see if the fact that one can do explicit computations allows for a deeper insight into the mathematics of those equations. Last but not least, one can numerically generalize the above results by considering arbitrary lap numbers and also one can apply our numerical method on several generalizations of the problem in areas where the exact solutions are not yet tractable analytically.

## Appendix A

# MATLAB and MAPLE codes

### A.1 Matlab Code for The Finite Element Method for a problem with non-constant parameters

```
function y = energy(c)

gamma=0.1;
a=0;
b=1;
N=500;
h=(b-a)/(N+1);
format long;

j = floor(c*N)+1;
O = (c ((j-1)* h))/(h);

A=sparse(N,N);
B=sparse(N,N);

bb=sparse(2*N,1);
bb(j)= 2;

A(1,1)=2/(h);
```

Appendix A. MATLAB and MAPLE codes

```

A(1,2)= 1/(h);

for i=2:N - 1
    A(i,i-1)= -1/(h);
    A(i,i)=2/(h);
    A(i,i+1)= -1/(h);
end

A(N,N)=2/(h);
A(N,N - 1)= -1/(h);

B(1,1)=(2*h)/3;
B(1,2)=(h/6);

for i=2:N-1
    B(i,i-1)=(h/6);
    B(i,i)=(2*h)/3;
    B(i,i+1)=(h/6);
end

B(N,N)=(2*h)/3;
B(N,N-1)=(h/6);

Balpha=sparse(N,N);

Balpha(1,1)=0.2e1 / 0.3e1 * h * (1 * h + 1);
Balpha(1,2)=(h ^ 2 * (2 * 1 + 1)) / 0.12e2 + h / 0.6e1;

for i=2:N-1
    Balpha(i,i-1)=(h ^ 2 * (2 * i - 1)) / 0.12e2 + h / 0.6e1;
    Balpha(i,i)=0.2e1 / 0.3e1 * h * (i * h + 1);
    Balpha(i,i+1)=(h ^ 2 * (2 * i + 1)) / 0.12e2 + h / 0.6e1;
end

Balpha(N,N)=0.2e1 / 0.3e1 * h * (N * h + 1);
Balpha(N,N-1)=(h ^ 2 * (2 * N-1)) / 0.12e2 + h / 0.6e1;

```

## Appendix A. MATLAB and MAPLE codes

```
M2=[(gamma*A)+B , -(B*alpha); B ,A];

X2=M2\bb;

x=linspace(0,1,N+1);

F5= (X2(N+1:2*N));
F5(j) = [];
G5=[0 ; - F5 ; 0];

F1 = diff(F5)/h;
F1(N+1,1)=0;
F1(j) = [];

F2 = (X2(1:N+1));

FF= F5.^2;

E3= trapz(FF)*h;

FF2 = (F2).^2;
E1 = trapz(FF2)*h;

FF1 = (abs(F1)- 1).^2;
E2 = trapz(FF1)*h;
y = gamma*E1 + E2 + i*h*E3;

end
```

## A.2 Matlab Code for DFO

```
clear all
c1 = 0.1;
```

## Appendix A. MATLAB and MAPLE codes

```
c2 = 0.3;
c3 = 0.7;
format long;

E1= energy(c1);
E2= energy(c2);
E3= energy(c3);

M1 = min([E1,E2,E3]);
M2 = max([E1,E2,E3]);

k=1;
minenergy(k)=M1;
tol=1;

while tol > 0.0000001
    P = parabola([c1 c2 c3]);
    c4 =minpara(P);
    E4 = energy(c4);

    A= [E1 E2 E3 E4; c1 c2 c3 c4];
    A= delete_max_column(A);

    c1= A(2,1);
    c2= A(2,2);
    c3= A(2,3);

    E1 = A(1,1);
    E2 = A(1,2);
    E3 = A(1,3);

    M1 = min([E1,E2,E3]);
    M2 = max([E1,E2,E3]);
    k=k+1;
    minenergy(k)=M1;
    tol=abs(minenergy(k)-minenergy(k-1))/minenergy(k);
end
```

## Appendix A. MATLAB and MAPLE codes

A  
M1

```
function y = parabola (c)

    p=sparse(3,3);

    p(1,1)= c(1)*c(1);
    p(1,2)= c(1);
    p(1,3)= 1;

    p(2,1)= c(2)*c(2);
    p(2,2)= c(2);
    p(2,3)= 1;

    p(3,1)= c(3)*c(3);
    p(3,2)= c(3);
    p(3,3)= 1;

    Z=sparse(3,1);
    Z(1,1)= energy(c(1));
    Z(2,1)= energy(c(2));
    Z(3,1)= energy(c(3));

    MM=p\Z;

    y = MM;

end
```

```
function y = minpara(p)

    aa= p(1);
    bb = p(2);

    y = -bb/(2*(aa));

end
```

```
function y = delete_max_column(A)

    R = A(1,:);

    [~, col] = max(R);

    A(:, col) = [];

    y = A;

end
```

### A.3 Matlab Code for The Finite Element Method (for the first weak formulation)

```
clear all
gamma=0.1;
alpha=1;
a=0;
b=1;
N=101;
c=0.5;
h=(b-a)/(N+1);
format short;

j = floor(c*N)+1;

O = (c-((j-1)* h))/(h);
beta = (O^3)-(3*O^2)+(3*O);
delta = (3*O^2)-(2*O^3);

A=sparse(N,N);
B=sparse(N,N);
```

## Appendix A. MATLAB and MAPLE codes

```
AA=zeros(N+2,N+2);
BB=zeros(N,N+2);
bb=sparse(2*N+2,1);
xx=linspace(a,b,N);

A(1,1)=2/(h);
A(1,2)=-1/(h);

for i=2:N-1
    A(i,i-1)=-1/(h);
    A(i,i)=2/(h);
    A(i,i+1)=-1/(h);
end

A(N,N)=2/(h);
A(N,N-1)=-1/(h);

B(1,1)=(2*h)/3;
B(1,2)=(h/6);

for i=2:N-1
    B(i,i-1)=(h/6);
    B(i,i)=(2*h)/3;
    B(i,i+1)=(h/6);
end

B(N,N)=(2*h)/3;
B(N,N-1)=(h/6);

AA(1,1)=2/(h);
AA(1,2)=-1/(h);

BB(1,1)=(2*h)/3;
BB(1,2)=h/6;

AA(N+2,N+2)=2/(h);
AA(N+2,N+1)=-1/(h);
```

Appendix A. MATLAB and MAPLE codes

```

BB(N,N+2)=(2*h)/3;
BB(N,N+1)=h/6;

for i=2:j-2
    AA(i,i-1)=-1/(h);
    AA(i,i)=2/(h);
    AA(i,i+1)=-1/(h);
end

AA(j-1,j-2)=-1/(h);
AA(j-1,j-1)=(1+O)/h;
AA(j-1,j)=0;
AA(j-1,j+1)=(-O)/h;

AA(j,j)=(1-O)/h;
AA(j,j+2)=(O-1)/h;

AA(j+1,j-1)=(-O)/h;
AA(j+1,j)=0;
AA(j+1,j+1)=O/h;

AA(j+2,j)=(O-1)/h;
AA(j+2,j+2)=(2-O)/h;
AA(j+2,j+3)=-1/(h);

for i=j+3:N+1 %j+2
    AA(i,i-1)=-1/(h);
    AA(i,i)=2/(h);
    AA(i,i+1)=-1/(h);
end

for i=2:j-2 %j-2
    BB(i,i-1)=h/6;
    BB(i,i)=(2*h)/3;
    BB(i,i+1)=h/6;
end

```

## Appendix A. MATLAB and MAPLE codes

```

BB(j-1,j-2)=h/6;
BB(j-1,j-1)=(h/3)*(1+beta);
BB(j-1,j)=(h/3)*(1-beta);
BB(j-1,j+1)=(h/6)*delta;
BB(j-1,j+2)=(h/6)*(1-delta);

BB(j,j-1)=(h/6)*delta;
BB(j,j)=(h/6)*(1-delta);
BB(j,j+1)=(h*O)/3;
BB(j,j+2)=(h*(2-O))/3;
BB(j,j+3)=h/6;

for i=j+1:N-1

    BB(i,i+1)=h/6;
    BB(i,i+2)=(2*h)/3;
    BB(i,i+3)=h/6;
end

T = transpose(BB);

    bb(j-1)=(1-O);
    bb(j)=(O);
    bb(j+1)=(O);
    bb(j+2)=(1-O);

M=[(gamma*A)+B , -(alpha*BB); T ,AA];

X=M\bb;
x=linspace(0,1,N+3);
F=(X(N+1:2*N+2));

F1 = diff(F)/h;
    F1(N+1,1)=0;
F2 = (X(1:N+1));
FF= F.^2;

```

## Appendix A. MATLAB and MAPLE codes

```
E3= trapz(FF)*h;  
FF2 = (F2).^2;  
E1 = trapz(FF2)*h;  
  
FF1 = (abs(F1)-1).^2;  
E2 = trapz(FF1)*h;  
y = gamma*E1 + E2 + alpha*E3;
```

### A.4 Matlab Code for The Finite Element Method (for the second weak formulation)

```
gamma=0.1;  
alpha=60;  
a=0;  
b=1;  
N=1000 ;  
h=(b-a)/(N+1);  
format long;  
  
j = floor(c*N)+1;  
O = (c-((j-1)* h))/(h);  
  
A=sparse(N,N);  
B=sparse(N,N);  
  
bb=sparse(2*N,1);  
bb(j)= 2;  
  
A(1,1)=2/(h);  
A(1,2)=-1/(h);  
  
for i=2:N-1  
A(i,i-1)=-1/(h);  
A(i,i)=2/(h);
```

## Appendix A. MATLAB and MAPLE codes

```

    A(i , i+1)=-1/(h) ;
end

    A(N,N)=2/(h) ;
    A(N,N-1)=-1/(h) ;

    B(1 , 1)=(2*h) /3;
    B(1 , 2)=(h/6) ;

for i =2:N-1
    B(i , i -1)=(h/6) ;
    B(i , i)=(2*h) /3;
    B(i , i+1)=(h/6) ;
end

    B(N,N)=(2*h) /3;
    B(N,N-1)=(h/6) ;

M=[(gamma*A)+B , -(alpha*B); B ,A];

    X=M\b;

    x=linspace(0 , 1 , N+2);
    F= (X(N+1:2*N)) ;

    F1 = diff(F)/h;
    F1(N+1,1)=0;

    F2 = (X(1:N+1)) ;

    FF= F.^ 2;

    E3= trapz(FF)*h;

    FF2 = (F2).^ 2;
    E1 = trapz(FF2)*h;

```

Appendix A. MATLAB and MAPLE codes

```

FF1 = (abs(F1)-1).^2;
E2 = trapz(FF1)*h;
y = gamma*E1 + E2 + alpha*E3;

```

## A.5 MAPLE code for the Fredholm Alternative (with lap 2)

*with(LinearAlgebra):*

$$A = \begin{bmatrix}
 \Lambda^3 e^{\Lambda c} & -\Lambda^3 e^{-\Lambda c} & \lambda^3 e^{\lambda c} & -\lambda^3 e^{-\lambda c} & -\Lambda^3 e^{\Lambda c} & \Lambda^3 e^{-\Lambda c} & -\lambda^3 e^{\lambda c} & \lambda^3 e^{-\lambda c} \\
 \Lambda^2 & \Lambda^2 & \lambda^2 & \lambda^2 & 0 & 0 & 0 & 0 \\
 \Lambda e^{\Lambda c} & -\Lambda e^{-\Lambda c} & \lambda e^{\lambda c} & -\lambda e^{-\lambda c} & 0 & 0 & 0 & 0 \\
 0 & 0 & 0 & 0 & e^{\Lambda} & e^{-\Lambda} & e^{\lambda} & e^{-\lambda} \\
 0 & 0 & 0 & 0 & \Lambda^2 e^{\Lambda} & \Lambda^2 e^{-\Lambda} & \lambda^2 e^{\lambda} & \lambda^2 e^{-\lambda} \\
 0 & 0 & 0 & 0 & \Lambda e^{\Lambda c} & -\Lambda e^{-\Lambda c} & \lambda e^{\lambda c} & -\lambda e^{-\lambda c} \\
 e^{\Lambda c} & e^{-\Lambda c} & e^{\lambda c} & e^{-\lambda c} & -e^{\Lambda c} & -e^{-\Lambda c} & -e^{\lambda c} & -e^{-\lambda c} \\
 \Lambda^2 e^{\Lambda c} & \Lambda^2 e^{-\Lambda c} & \lambda^2 e^{\lambda c} & \lambda^2 e^{-\lambda c} & -\Lambda^2 e^{\Lambda c} & -\Lambda^2 e^{-\Lambda c} & -\lambda^2 e^{\lambda c} & -\lambda^2 e^{-\lambda c} \\
 1 & 1 & 1 & 1 & 0 & 0 & 0 & 0
 \end{bmatrix}$$



Appendix A. MATLAB and MAPLE codes

$$b := \begin{bmatrix} \frac{2}{\varepsilon} \\ 0 \\ 0 \\ 0 \\ 0 \\ 0 \\ 0 \\ 0 \\ 0 \\ 0 \end{bmatrix}$$

*LinearSolve* (*A*, *b*)

$$A1 := -\frac{(e^{0.5\lambda} + e^{-0.5\lambda})((\Lambda - \lambda)e^{-0.5\Lambda - 0.5\lambda} + (\Lambda + \lambda)e^{-0.5\Lambda + 0.5\lambda} + (-\Lambda - \lambda)e^{0.5\Lambda - 0.5\lambda} - e^{0.5\Lambda + 0.5\lambda}(\Lambda - \lambda))}{\left( \begin{array}{l} (-1.0\Lambda + \lambda)e^{-1.0\Lambda - 1.0\lambda} + (-1.0\Lambda - 1.0\lambda)e^{-1.0\Lambda + 1.0\lambda} + (\Lambda + \lambda)e^{1.0\Lambda - 1.0\lambda} \\ + (\Lambda - 1.0\lambda)e^{\Lambda + \lambda} + 2.0\Lambda e^{\Lambda} - 2.0\Lambda e^{-1.0\Lambda} + 2.0e^{-1.0\lambda}\lambda - 2.0e^{\lambda}\lambda \end{array} \right) \varepsilon \Lambda (\Lambda^2 - 1.0\lambda^2)}$$

$$A2 := \frac{(e^{0.5\lambda} + e^{-0.5\lambda})((\Lambda - \lambda)e^{-0.5\Lambda - 0.5\lambda} + (\Lambda + \lambda)e^{-0.5\Lambda + 0.5\lambda} + (-\Lambda - \lambda)e^{0.5\Lambda - 0.5\lambda} - e^{0.5\Lambda + 0.5\lambda}(\Lambda - \lambda))}{\left( \begin{array}{l} (-1.0\Lambda + \lambda)e^{-1.0\Lambda - 1.0\lambda} + (-1.0\Lambda - 1.0\lambda)e^{-1.0\Lambda + 1.0\lambda} + \\ (\Lambda + \lambda)e^{1.0\Lambda - 1.0\lambda} + (\Lambda - 1.0\lambda)e^{\Lambda + \lambda} + 2.0\Lambda e^{\Lambda} - 2.0\Lambda e^{-1.0\Lambda} + 2.0e^{-1.0\lambda}\lambda - 2.0e^{\lambda}\lambda \end{array} \right) \varepsilon \Lambda (\Lambda^2 - 1.0\lambda^2)}$$

$$A3 := \frac{(\Lambda - 1.0\lambda)e^{-0.5\lambda - \Lambda} + (\Lambda + \lambda)e^{0.5\lambda - \Lambda} + (-1.0\Lambda - 1.0\lambda)e^{-0.5\lambda + \Lambda} + (-1.0\Lambda + \lambda)e^{0.5\lambda + \Lambda} + 2.0\lambda e^{0.5\lambda} - 2.0\lambda e^{-0.5\lambda}}{\left( \begin{array}{l} (-1.0\Lambda + \lambda)e^{-1.0\Lambda - 1.0\lambda} + (-1.0\Lambda - 1.0\lambda)e^{-1.0\Lambda + 1.0\lambda} + (\Lambda + \lambda)e^{1.0\Lambda - 1.0\lambda} \\ + (\Lambda - 1.0\lambda)e^{\Lambda + \lambda} + 2.0\Lambda e^{\Lambda} - 2.0\Lambda e^{-1.0\Lambda} + 2.0e^{-1.0\lambda}\lambda - 2.0e^{\lambda}\lambda \end{array} \right) \lambda \varepsilon (\Lambda^2 - 1.0\lambda^2)}$$

$$A4 := \frac{(-1.0\Lambda + \lambda)e^{-0.5\lambda - \Lambda} + (-1.0\Lambda - 1.0\lambda)e^{0.5\lambda - \Lambda} + (\Lambda + \lambda)e^{-0.5\lambda + \Lambda} + (\Lambda - 1.0\lambda)e^{0.5\lambda + \Lambda} - 2.0\lambda e^{0.5\lambda} + 2.0\lambda e^{-0.5\lambda}}{\left( \begin{array}{l} (-1.0\Lambda + \lambda)e^{-1.0\Lambda - 1.0\lambda} + (-1.0\Lambda - 1.0\lambda)e^{-1.0\Lambda + 1.0\lambda} + (\Lambda + \lambda)e^{1.0\Lambda - 1.0\lambda} \\ + (\Lambda - 1.0\lambda)e^{\Lambda + \lambda} + 2.0\Lambda e^{\Lambda} - 2.0\Lambda e^{-1.0\Lambda} + 2.0e^{-1.0\lambda}\lambda - 2.0e^{\lambda}\lambda \end{array} \right) \lambda \varepsilon (\Lambda^2 - 1.0\lambda^2)}$$

$$A5 := \frac{e^{-1.0\Lambda}(e^{0.5\lambda} + e^{-0.5\lambda})((\Lambda - \lambda)e^{-0.5\Lambda - 0.5\lambda} + (\Lambda + \lambda)e^{-0.5\Lambda + 0.5\lambda} + (-\Lambda - \lambda)e^{0.5\Lambda - 0.5\lambda} - e^{0.5\Lambda + 0.5\lambda}(\Lambda - \lambda))}{\left( \begin{array}{l} (-1.0\Lambda + \lambda)e^{-1.0\Lambda - 1.0\lambda} + (-1.0\Lambda - 1.0\lambda)e^{-1.0\Lambda + 1.0\lambda} + (\Lambda + \lambda)e^{1.0\Lambda - 1.0\lambda} + (\Lambda - 1.0\lambda)e^{\Lambda + \lambda} \\ + 2.0\Lambda e^{\Lambda} - 2.0\Lambda e^{-1.0\Lambda} + 2.0e^{-1.0\lambda}\lambda - 2.0e^{\lambda}\lambda \end{array} \right) \varepsilon \Lambda (\Lambda^2 - 1.0\lambda^2)}$$

Appendix A. MATLAB and MAPLE codes

$$A6 := -\frac{(e^{0.5\lambda} + e^{-0.5\lambda})((\Lambda - \lambda)e^{-0.5\Lambda - 0.5\lambda} + (\Lambda + \lambda)e^{-0.5\Lambda + 0.5\lambda} + (-\Lambda - \lambda)e^{0.5\Lambda - 0.5\lambda} - e^{0.5\Lambda + 0.5\lambda}(\Lambda - \lambda))e^\Lambda}{\left( \begin{array}{l} (-1.0\Lambda + \lambda)e^{-1.0\Lambda - 1.0\lambda} + (-1.0\Lambda - 1.0\lambda)e^{-1.0\Lambda + 1.0\lambda} + (\Lambda + \lambda)e^{1.0\Lambda - 1.0\lambda} \\ + (\Lambda - 1.0\lambda)e^{\Lambda + \lambda} + 2.0\Lambda e^\Lambda - 2.0\Lambda e^{-1.0\Lambda + 2.0} e^{-1.0\lambda} \lambda - 2.0 e^{\lambda} \lambda \end{array} \right) \varepsilon \Lambda (\Lambda^2 - 1.0\lambda^2)} :$$

$$A7 := -\frac{e^{-1.0\lambda}(e^{-0.5\Lambda} + e^{0.5\Lambda})((\Lambda - \lambda)e^{-0.5\Lambda - 0.5\lambda} + (\Lambda + \lambda)e^{-0.5\Lambda + 0.5\lambda} + (-\Lambda - \lambda)e^{0.5\Lambda - 0.5\lambda} - e^{0.5\Lambda + 0.5\lambda}(\Lambda - \lambda))}{\left( \begin{array}{l} (-1.0\Lambda + \lambda)e^{-1.0\Lambda - 1.0\lambda} + (-1.0\Lambda - 1.0\lambda)e^{-1.0\Lambda + 1.0\lambda} + (\Lambda + \lambda)e^{1.0\Lambda - 1.0\lambda} \\ + (\Lambda - 1.0\lambda)e^{\Lambda + \lambda} + 2.0\Lambda e^\Lambda - 2.0\Lambda e^{-1.0\Lambda + 2.0} e^{-1.0\lambda} \lambda - 2.0 e^{\lambda} \lambda \end{array} \right) \lambda \varepsilon (\Lambda^2 - 1.0\lambda^2)} :$$

$$A8 := \frac{e^\lambda(e^{-0.5\Lambda} + e^{0.5\Lambda})((\Lambda - \lambda)e^{-0.5\Lambda - 0.5\lambda} + (\Lambda + \lambda)e^{-0.5\Lambda + 0.5\lambda} + (-\Lambda - \lambda)e^{0.5\Lambda - 0.5\lambda} - e^{0.5\Lambda + 0.5\lambda}(\Lambda - \lambda))}{\left( \begin{array}{l} (-1.0\Lambda + \lambda)e^{-1.0\Lambda - 1.0\lambda} + (-1.0\Lambda - 1.0\lambda)e^{-1.0\Lambda + 1.0\lambda} + (\Lambda + \lambda)e^{1.0\Lambda - 1.0\lambda} \\ + (\Lambda - 1.0\lambda)e^{\Lambda + \lambda} + 2.0\Lambda e^\Lambda - 2.0\Lambda e^{-1.0\Lambda + 2.0} e^{-1.0\lambda} \lambda - 2.0 e^{\lambda} \lambda \end{array} \right) \lambda \varepsilon (\Lambda^2 - 1.0\lambda^2)} :$$

$$eq1 := A1 e^{\Lambda x} + A2 e^{-\Lambda x} + A3 e^{\lambda x} + A4 e^{-\lambda x}$$

$$-0.093007 e^{2.9787 x} + 0.093007 e^{-2.9787 x} + 0.53139 e^{1.0616 x} - 0.53139 e^{-1.0616 x}$$

$$eq2 := A5 e^{\Lambda x} + A6 e^{-\Lambda x} + A7 e^{\lambda x} + A8 e^{-\lambda x}$$

$$0.0047299 e^{2.9787 x} - 1.8288 e^{-2.9787 x} - 0.18381 e^{1.0616 x} + 1.5362 e^{-1.0616 x}$$

$$plots : -display(plot(eq1, x = 0 \dots c), plot(eq2, x = c \dots 1))$$

## A.6 MAPLE code for the Fredholm Alternative (with lap 3)

*with(LinearAlgebra) :*

*with(plots) :*

$$M = \begin{bmatrix} \Lambda^3 e^{\Lambda c l} & -\Lambda^3 e^{-\Lambda c l} & \lambda^3 e^{\lambda c l} & -\lambda^3 e^{-\lambda c l} & -\Lambda^3 e^{\Lambda c l} & \Lambda^3 e^{-\Lambda c l} & -\lambda^3 e^{\lambda c l} & \lambda^3 e^{-\lambda c l} & 0 & 0 & 0 & 0 \\ 0 & 0 & 0 & 0 & \Lambda^3 e^{\Lambda c 2} & -\Lambda^3 e^{-\Lambda c 2} & \lambda^3 e^{\lambda c 2} & -\lambda^3 e^{-\lambda c 2} & -\Lambda^3 e^{\Lambda c 2} & \Lambda^3 e^{-\Lambda c 2} & -\lambda^3 e^{\lambda c 2} & \lambda^3 e^{-\lambda c 2} \\ 1 & 1 & 1 & 1 & 0 & 0 & 0 & 0 & 0 & 0 & 0 & 0 \\ \Lambda e^{\Lambda c l} & -\Lambda e^{-\Lambda c l} & \lambda e^{\lambda c l} & -\lambda e^{-\lambda c l} & 0 & 0 & 0 & 0 & 0 & 0 & 0 & 0 \\ \Lambda^2 & \Lambda^2 & \lambda^2 & \lambda^2 & 0 & 0 & 0 & 0 & 0 & 0 & 0 & 0 \\ 0 & 0 & 0 & 0 & \Lambda e^{\Lambda c l} & -\Lambda e^{-\Lambda c l} & \lambda e^{\lambda c l} & -\lambda e^{-\lambda c l} & 0 & 0 & 0 & 0 \\ 0 & 0 & 0 & 0 & \Lambda e^{\Lambda c 2} & -\Lambda e^{-\Lambda c 2} & \lambda e^{\lambda c 2} & -\lambda e^{-\lambda c 2} & 0 & 0 & 0 & 0 \\ 0 & 0 & 0 & 0 & 0 & 0 & 0 & 0 & e^{\Lambda} & e^{-\Lambda} & e^{\lambda} & e^{-\lambda} \\ 0 & 0 & 0 & 0 & 0 & 0 & 0 & 0 & \Lambda e^{\Lambda c 2} & -\Lambda e^{-\Lambda c 2} & \lambda e^{\lambda c 2} & -\lambda e^{-\lambda c 2} \\ 0 & 0 & 0 & 0 & 0 & 0 & 0 & 0 & \Lambda^2 e^{\Lambda} & \Lambda^2 e^{-\Lambda} & \lambda^2 e^{\lambda} & \lambda^2 e^{-\lambda} \\ e^{\Lambda c l} & e^{-\Lambda c l} & e^{\lambda c l} & e^{-\lambda c l} & -e^{\Lambda c l} & -e^{-\Lambda c l} & -e^{\lambda c l} & -e^{-\lambda c l} & 0 & 0 & 0 & 0 \\ \Lambda^2 e^{\Lambda c l} & \Lambda^2 e^{-\Lambda c l} & \lambda^2 e^{\lambda c l} & \lambda^2 e^{-\lambda c l} & -\Lambda^2 e^{\Lambda c l} & -\Lambda^2 e^{-\Lambda c l} & -\lambda^2 e^{\lambda c l} & -\lambda^2 e^{-\lambda c l} & 0 & 0 & 0 & 0 \\ 0 & 0 & 0 & 0 & e^{\Lambda c 2} & e^{-\Lambda c 2} & e^{\lambda c 2} & e^{-\lambda c 2} & -e^{\Lambda c 2} & -e^{-\Lambda c 2} & -e^{\lambda c 2} & -e^{-\lambda c 2} \\ 0 & 0 & 0 & 0 & \Lambda^2 e^{\Lambda c 2} & \Lambda^2 e^{-\Lambda c 2} & \lambda^2 e^{\lambda c 2} & \lambda^2 e^{-\lambda c 2} & -\Lambda^2 e^{\Lambda c 2} & -\Lambda^2 e^{-\Lambda c 2} & -\lambda^2 e^{\lambda c 2} & -\lambda^2 e^{-\lambda c 2} \end{bmatrix}$$

$M1 := Transpose(M)$

$N := NullSpace(M1)$

$N := NullSpace(M1)$

$a1 := N[1]$

$a2 := N[2]$



Appendix A. MATLAB and MAPLE codes

$$\begin{aligned}
LL = & ((\Lambda \cosh(\lambda) \sinh(\Lambda) - \lambda \cosh(\Lambda) \sinh(\lambda)) \cosh(\lambda c2) - \sinh(\lambda c2)(\Lambda \sinh(\Lambda) \sinh(\lambda) \\
& - \lambda \cosh(\Lambda) \cosh(\lambda))) \cosh(\Lambda c2) + ((-\Lambda \cosh(\Lambda) \cosh(\lambda) + \lambda \sinh(\Lambda) \sinh(\lambda)) \cosh(\lambda c2) \\
& + \sinh(\lambda c2)(\Lambda \cosh(\Lambda) \sinh(\lambda) - \lambda \cosh(\lambda) \sinh(\Lambda))) \sinh(\Lambda c2)(\Lambda - \lambda)(\Lambda + \lambda)(\sinh(\lambda) \sinh(\lambda c2) \\
& - \cosh(\lambda) \cosh(\lambda c2))(\sinh(\Lambda c2) \sinh(\Lambda) - \cosh(\Lambda c2) \cosh(\Lambda))
\end{aligned}$$

$$eq2 := \frac{-2}{\varepsilon} \left( \frac{C}{D} \right)$$

$$\begin{aligned}
C = & (-\cosh(\Lambda c2))^2 \Lambda \cosh(\Lambda) \sinh(\lambda) + \cosh(\Lambda c2) \sinh(\Lambda c2) \Lambda \sinh(\Lambda) \sinh(\lambda) \\
& + \cosh(\lambda c2) \lambda \sinh(\Lambda)(\cosh(\lambda) \cosh(\lambda c2) - \sinh(\lambda) \sinh(\lambda c2))(\cosh(\Lambda c1))^2 \\
& + (\cosh(\Lambda c2))^2 \sinh(\Lambda c1) \Lambda \sinh(\Lambda) \sinh(\lambda) + \cosh(\Lambda) \Lambda (\cosh(\lambda c2) \sinh(\lambda c1) \cosh(\lambda) \\
& + \sinh(\lambda)(\sinh(\Lambda c1) \sinh(\Lambda c2) - \sinh(\lambda c1) \sinh(\lambda c2))) \cosh(\Lambda c2) - (\cosh(\lambda c2))^2 \sinh(\Lambda c1) \lambda \cosh(\Lambda) \cosh(\lambda) \\
& + (\sinh(\Lambda c1) \sinh(\lambda c2) \lambda \cosh(\Lambda) \sinh(\lambda) - \sinh(\Lambda c2) \sinh(\lambda c1) \Lambda \cosh(\lambda) \sinh(\Lambda)) \cosh(\lambda c2) \\
& + \Lambda \sinh(\Lambda) \sinh(\lambda)(\sinh(\Lambda c2) \sinh(\lambda c1) \sinh(\lambda c2) + \sinh(\Lambda c1)) \cosh(\Lambda c1) \\
& + (\Lambda \cosh(\Lambda)(\cosh(\lambda c1) \sinh(\lambda) - \sinh(\lambda c1) \cosh(\lambda))(\cosh(\Lambda c2))^2 + (-\cosh(\lambda c1) \sinh(\Lambda c2) \Lambda \sinh(\Lambda) \sinh(\lambda) \\
& + \cosh(\lambda c2) \sinh(\Lambda c1) \lambda \cosh(\Lambda) \cosh(\lambda) - \sinh(\Lambda c1) \sinh(\lambda c2) \lambda \cosh(\Lambda) \sinh(\lambda) \\
& + \sinh(\Lambda c2) \sinh(\lambda c1) \Lambda \cosh(\lambda) \sinh(\Lambda)) \cosh(\Lambda c2) - (\cosh(\lambda c2)(\cosh(\lambda) \cosh(\lambda c2) \\
& - \sinh(\lambda) \sinh(\lambda c2)) \cosh(\lambda c1) + (\cosh(\lambda c2))^2 \sinh(\lambda c1) \sinh(\lambda) + \cosh(\lambda)(\sinh(\Lambda c1) \sinh(\Lambda c2) \\
& - \sinh(\lambda c1) \sinh(\lambda c2)) \cosh(\lambda c2) - \sinh(\lambda)(\sinh(\Lambda c1) \sinh(\Lambda c2) \sinh(\lambda c2) \\
& + \sinh(\lambda c1))) \sinh(\Lambda) \lambda \cosh(\lambda c1) \Lambda (\Lambda - \lambda)(\Lambda + \lambda) \lambda (\cosh(\lambda c1) \cosh(\Lambda c2) \\
& - \cosh(\Lambda c1) \cosh(\lambda c2))(\cosh(\lambda) \cosh(\lambda c2) - \sinh(\lambda) \sinh(\lambda c2))(\cosh(\Lambda c2) \cosh(\Lambda) - \sinh(\Lambda c2) \sinh(\Lambda)).
\end{aligned}$$

$$\begin{aligned}
D = & ((\Lambda \cosh(\Lambda) \sinh(\lambda) - \lambda \cosh(\lambda) \sinh(\Lambda)) \cosh(\lambda c2) \\
& - \sinh(\lambda c2)(\Lambda \cosh(\Lambda) \cosh(\lambda) - \lambda \sinh(\Lambda) \sinh(\lambda))) \cosh(\Lambda c2) \\
& + ((-\Lambda \sinh(\Lambda) \sinh(\lambda) + \lambda \cosh(\Lambda) \cosh(\lambda)) \cosh(\lambda c2) \\
& + \sinh(\lambda c2)(\Lambda \cosh(\lambda) \sinh(\Lambda) - \lambda \cosh(\Lambda) \sinh(\lambda))) \sinh(\Lambda c2) + \Lambda (\Lambda - \lambda)(\Lambda + \lambda) \lambda (\sinh(\lambda) \sinh(\lambda c2) \\
& - \cosh(\lambda) \cosh(\lambda c2))(\sinh(\Lambda c2) \sinh(\Lambda) - \cosh(\Lambda c2) \cosh(\Lambda))
\end{aligned}$$

## A.7 Optimizing Energy (pseudo code)

```
epsilon = 0.01
for gamma=0.01:10 (step epsilon)

Initialize alpha=0.01
Calculate u1, u2, E(u1), E(u2)

while |E(u1)-E(u2)| > 10^-6
alpha= alpha +epsilon
end
plot(alpha,1 \ gamma)
end
```

# Bibliography

- [1] D. N. Arnold. Lecture notes on numerical analysis of partial differential equations. <http://www-users.math.umn.edu/~arnold//8445/notes.pdf>. [Online; accessed 27, November 2019].
- [2] F. Auricchio, L. B. da Veiga, F. Brezzi, and C. Lovadina. Mixed finite element methods. In *Encyclopedia of Computational Mechanics*, pages 1–53. Wiley, Philadelphia, 2004.
- [3] I. Babuška. The finite element method with Lagrangian multipliers. *Numer. Math.*, 20:179–192, 1973.
- [4] J. Ball, P. J. Holmes, R. James, R. Pego, and P. Swart. On the dynamics of fine structure. *Journal of Nonlinear Science*, 1:17–70, 1991.
- [5] J. M. Ball. Some open problems in elasticity. In *Geometry, Mechanics, and Dynamics*, pages 3–59. Springer, New York, 2002.
- [6] F. Baumgart. Stiffness-an unknown world of mechanical science? *Injury*, 31(2):14–23, 2000.
- [7] K. Bhattacharya. Theory of martensitic microstructure and the shape-memory effect. *Available from author: bhatta@co.caltech.edu*, 1998.
- [8] D. Boffi, F. Brezzi, and M. Fortin. *Mixed Finite Element Methods and Applications*, volume 44. Springer, Berlin, Heidelberg, 2013.

## Bibliography

- [9] D. Brandon and R. C. Rogers. Nonlocal regularization of L.C. Young's tacking problem. *Applied Mathematics and Optimization*, 25:287–301, 1992.
- [10] H. Brezis. *Functional Analysis, Sobolev Spaces and Partial Differential Equations*. Springer-Verlag New York, 2010.
- [11] F. Brezzi. On the existence, uniqueness and approximation of saddle-point problems arising from Lagrangian multipliers. *RAIRO Numerical Analysis*, 8:129–151, 1974.
- [12] F. Brezzi. A survey of mixed finite element methods. In *Finite Elements*, pages 34–49. Springer, New York, 1988.
- [13] M. C. Calderer and P. Palffy-Muhoray. Ericksen's bar and modeling of the smectic a–nematic phase transition. *SIAM Journal on Applied Mathematics*, 60(3):1073–1098, 2000.
- [14] C. Carstensen and G. Dolzmann. Convergence of adaptive finite element methods for a nonconvex double-well minimization problem. *Mathematics of Computation*, 84(295):2111–2135, 2015.
- [15] M. Chaplin. Water structure and science. [www1.lsbu.ac.uk/water/water\\_structure\\_science.html](http://www1.lsbu.ac.uk/water/water_structure_science.html). [Online; accessed 29, June 2018].
- [16] S. Z. Cheng. *Phase Transitions in Polymers: The Role of Metastable States*. Elsevier, Amsterdam, 2008.
- [17] M. Chipot. Numerical analysis of oscillations in nonconvex problems. *Numer. Math.*, 59:747–767, 1991.
- [18] M. Chipot and C. Collins. Numerical approximations in variational problems with potential wells. *SIAM J. Numer. Anal.*, 29(4):1002–1019, 1992.
- [19] M. Chipot, C. Collins, and D. Kinderlehrer. Numerical analysis of oscillations in multiple well problems. *Numer. Math.*, 70:259–282, 1995.

## Bibliography

- [20] J.-Y. Cho. *Finite element modeling of martensitic phase transformation*. PhD thesis, Texas Tech University, 2009.
- [21] P. G. Ciarlet. *The Finite Element Method for Elliptic Problems*. Siam, Philadelphia, 2002.
- [22] F. Clément and V. Martin. The Lax-Milgram Theorem. A detailed proof to be formalized in Coq. *[Research Report] RR-8934, Inria Paris.*, 2016. URL <https://hal.inria.fr/hal-01344090>.
- [23] C. Collins, D. Kinderlehrer, and M. Luskin. Numerical approximation of the solution of a variational problem with a double well potential. *SIAM J. Numer. Anal.*, 28(2):321–332, 1991.
- [24] C. Collins and M. Luskin. Optimal-order error estimates for the finite element approximation of the solution of a nonconvex variational problem. *Math. Comp.*, 57(196):621–637, 1991.
- [25] A. R. Conn, K. Scheinberg, and P. L. Toint. On the convergence of derivative-free methods for unconstrained optimization. *Approximation Theory and Optimization: Tributes to M.J.D. Powell*, pages 83–108, 1997.
- [26] J. B. Conway. *A Course in Functional Analysis*. Springer-Verlag, New York, 1990.
- [27] R. Courant. Variational methods for the solution of problems of equilibrium and vibrations. *Bull. Amer. Math. Soc.*, 49(1):1–23, 1943.
- [28] R. Courant and D. Hilbert. *Methods of Mathematical Physics*. John Wiley & Sons, New York, 2008.
- [29] B. Dacorogna. *Introduction to the Calculus of Variations*. World Scientific Publishing Company, 2014.
- [30] R. Dautray and J.-L. Lions. *Mathematical Analysis and Numerical Methods for Science and Technology: Volume 2 Functional and Variational Methods*. Springer, New York, 1988.

## Bibliography

- [31] N. Dunford and J. Schwartz. *Linear Operators Part I: General Theory*. Interscience, New York, 1958.
- [32] J. Ericksen. Equilibrium of bars. *Journal of elasticity*, 5(3):191–201, 1975.
- [33] A. Ern and J. Guermond. *Theory and Practice of Finite Elements*. Springer, New-York, 2004.
- [34] R. Falk and J. Osborn. Error estimates for mixed methods. *RAIRO. Anal. Numér.*, 14(3):249–277, 1980.
- [35] A. Flores. *Towards fully computable error bounds for the incompressible Navier-Stokes equations*. PhD thesis, University of Strathclyde, 2012.
- [36] G. Friesecke and J. McLeod. Dynamic stability of non-minimizing phase mixtures. *Proc. Royal Soc. London A*, 453:2427–2436, 1997.
- [37] D. Gao and R. W. Ogden. Multiple solutions to non-convex variational problems with implications for phase transitions and numerical computation. *Quart. J. Mech. Appl. Math.*, 61(4):497–522, 2008.
- [38] G. Gatica. *A simple Introduction to the Mixed Finite Element Method: Theory and Applications*. Springer Briefs in Mathematics, Springer, Cham, 2014.
- [39] P.-A. Gremaud. Numerical analysis of a nonconvex variational problem related to solid-solid phase transitions. *SIAM journal on numerical analysis*, 31(1):111–127, 1994.
- [40] M. Grinfeld and G. Lord. Bifurcations in the regularized ericksen bar model. *Journal of Elasticity*, 90(2):161–173, 2008.
- [41] M. E. Gurtin. *Topics in Finite Elasticity*. SIAM, Philadelphia, 1981.
- [42] C. Johnson. *Numerical Solution of Partial Differential Equations by the Finite Element Method*. Cambridge University Press, Cambridge, 1987.

## Bibliography

- [43] P. Kelly. Solid mechanics part i: An introduction to solid mechanics. [http://homepages.engineering.auckland.ac.nz/~pkel015/SolidMechanicsBooks/Part\\_II/index.html](http://homepages.engineering.auckland.ac.nz/~pkel015/SolidMechanicsBooks/Part_II/index.html). [Online; accessed 1, February 2019].
- [44] R. Kohn and S. Müller. Branching of twins near an austenite / twinned-martensite interface. *Philos. Mag. Ser. A*, 66:697–715, 1992.
- [45] R. Kohn and S. Müller. Surface energy and microstructure in coherent phase transitions. *Comm. Pure Appl. Math.*, 47:405–435, 1994.
- [46] S. J. Malham. An introduction to Lagrangian and Hamiltonian mechanics. <https://www.macs.hw.ac.uk/~simonm/mechanics.pdf>. [Online; accessed 20, December 2017].
- [47] S. Müller. Singular perturbations as a selection criterion for periodic minimizing sequences. *Calc. Var.*, 1(2):169–204, 1993.
- [48] S. Müller. Variational models for microstructure and phase transitions. In *Calculus of variations and geometric evolution problems. Lecture Notes in Mathematics*, volume 1713, pages 85–210. Springer, Berlin, 1999.
- [49] Z. Nishiyama. *Martensitic Transformation*. Academic Press, New York, 1978.
- [50] R. Ogden. Elements of the theory of finite. *Nonlinear Elasticity: Theory and Applications*, 283:1–57, 2001.
- [51] P. J. Olver and C. Shakiban. *Applied Linear Algebra*. Prentice Hall, Upper Saddle River, NJ, 2006.
- [52] P. Pedregal. *Variational Methods in Nonlinear Elasticity*. SIAM, Philadelphia, 2000.
- [53] G. Pelosi. The finite-element method, part i: R. l. courant [historical corner]. *IEEE Antennas and Propagation Magazine*, 49(2):180–182, 2007.

## Bibliography

- [54] I. Pinelis. L'Hospital type rules for monotonicity, with applications. *J. Ineq. Pure Appl. Math.*, 3(1), 2002.
- [55] X. Ren and L. Truskinovsky. Finite scale microstructures in nonlocal elasticity. *Journal of elasticity*, 59:319–355, 2000.
- [56] X. Ren and J. Wei. On the multiplicity of solutions of two nonlocal variational problems. *SIAM J. Math. Anal.*, 31(4):909–924, 2000.
- [57] X. Ren and J. Wei. On energy minimizers of the diblock copolymer problem. *Interfaces and Free Boundaries*, 5(2):193–238, 2003.
- [58] E. Süli. A brief excursion into the mathematical theory of mixed finite element methods. *Lecture Notes*, University of Oxford, 2013.
- [59] L. Truskinovsky and G. Zanzotto. Ericksen's bar revisited: Energy wiggles. *J. Mech. Phys. Solids*, 44:1371–1408, 1996.
- [60] A. Vainchtein. Dynamics of phase transitions and hysteresis in a viscoelastic ericksen's bar on an elastic foundation. *Journal of elasticity*, 57(3):243–280, 1999.
- [61] A. Vainchtein, T. Healey, P. Rosakis, and L. Truskinovsky. The role of the spinodal region in one-dimensional martensitic phase transitions. *Physica D*, 115(1-2):29–48, 1998.
- [62] P. Wriggers. Mixed finite element methods-theory and discretization. In *Mixed finite element technologies*, pages 131–177. CISM, Courses and Lectures, Springer-Verlag, Wien, 2009.
- [63] N. K. Yip. Structure of stable solutions of a one-dimensional variational problem. *ESAIM: Control, Optimisation and Calculus of Variations*, 12(4):721–751, 2006.
- [64] L. C. Young. *Lectures on the Calculus of Variations and Optimal Control Theory*. Chelsea Publishing Company, New York, 1980.
- [65] E. Zeidler. *Applied Functional Analysis: Applications to Mathematical Physics*. Springer-Verlag, New York, 1995.